DETECTION OF SMOKE IMPACT IN AEROSOL SAMPLES IN THE EASTERN AND SOUTHEASTERN UNITED STATES DURING LATE SPRING AND SUMMER

Elizabeth M. Zarovy

Sonia M. Kreidenweis

Department of Atmospheric Science

Colorado State University

Spring 2003

ABSTRACT

DETECTION OF SMOKE IMPACT IN AEROSOL SAMPLES IN THE EASTERN AND SOUTHEASTERN UNITED STATES DURING LATE SPRING AND SUMMER

Biomass burning, including forest fires, is a major global source for CO, aerosols and other pollutants. Much focus has been given to biomass burning in the tropics, but recently more attention has been given to the emissions of CO from boreal forest fires in Canada and Russia. Smoke from these fires can have important local and long-range effects on trace gas and particle concentrations. This work focuses on fires in North and Central America and their effects on particulate matter concentrations in the eastern and southeastern U.S.

Non-soil potassium (K_{NON}) was investigated as a tracer for smoke impact from biomass burning in aerosol samples in the eastern and southeastern U.S. during late spring and summer (15-April through 31-July). Aerosol data from eight ground-based sites in the Interagency Monitoring of Protected Visual Environments (IMPROVE) monitoring network were examined. Two years were selected for establishing and testing a criterion indicating smoke impact in an aerosol sample, 1995 and 1998. Back trajectories using the HYSPLIT trajectory model were calculated for each site, on every IMPROVE sample day from 15-April through 31-July 1995 and 1998. The back

trajectories were then compared to maps of fire locations and satellite detected hot spots to identify source regions and determine whether fires were within those regions.

The general utility of K_{NON} as an indicator of significant smoke impact in an aerosol sample was confirmed. Using a criterion of the median K_{NON} concentration over all available data at each site plus two standard deviations, K_{NON} was able to capture cases seen in gas phase data by Wotawa and Trainer (2000) during July 1995 in the aerosol data. In addition, smoke impact from the intense fires in Mexico and Central America during May 1998 were identified in the aerosol data.

The sites investigated in this study frequently have transport from the Gulf of Mexico and the Atlantic and are impacted by North African dust in the summer. Thus, it was necessary to modify the K_{NON} formula to account for contributions to aerosol potassium from sea salt and the lower K/Fe ratio in Saharan dust. When the K/Fe ratio was adjusted to account for Saharan dust it appeared that the two-part criterion used by Perry et al. (1997) to indicate the presence of Saharan dust on an aerosol sample was too strict for the sites examined. Hence, modifications were also made to the criterion indicating Saharan dust impact in aerosol samples.

Overall source contributions and source contributions on days with high K_{NON} were investigated at three of the eight sites for 1995 and 1998. Results show that in addition to source contributions from the U.S., source contributions from Canada and Mexico/Central America are important in the eastern and southeastern U.S. during late spring and summer. A correlation between acreage burned in Mexico/Central America and Canada and source contributions on high K_{NON} days is suggested.

Elizabeth M. Zarovy
Colorado State University
Department of Atmospheric Science, Spring 2003

ACKNOWLEDGEMENTS

This research was funded by DOC-NOAA NA17RJ1228 and the Ronald E. McNair Fellowship. I would like to thank Kristi Gebhart of the National Park Service's Air Resources Division at CIRA for numerous hours of assistance with trajectories and source contributions and for the programs to run the data. I would also like to thank Rodger Ames of the National Park Service's Air Resources Division at CIRA for the National Fire Occurrence Database and assistance with processing the data.

I would like to express my gratitude to Dr. Ken Carlson from the Department of Civil Engineering at Colorado State University, Graham Feingold from NOAA and Dr. Jeff Collett, Jr. for their contributions to this work as my committee members and to my advisor, Dr. Sonia Kreidenweis for her guidance and patience.

TABLE OF CONTENTS

LIST OF FIGURES

LIST OF TABLES

Chapter 1. Introduction and Problem Statement

1.1 Introduction

Biomass burning, including forest fires, is a major global source for CO, aerosols and other pollutants. Smoke from fires affects human health, visibility and climate. Much focus has been given to biomass burning in the tropics, primarily because about 80% of the global burned biomass is there (Kaufman et al., 1998; Hao and Liu, 1994). Recently, more attention has been given to emissions of CO and particulate carbon from boreal forest fires in Canada and Russia (Wotawa and Trainer, 2000; Forster et al., 2001; Lavoue et al., 2000). Smoke from these fires can have important local and long-range effects. This work focuses on fires in North and Central America and their effects on particulate matter concentrations in the southeastern U.S.

In an average year forest fires in Canada, the United States and Mexico consume over 11.7 million acres of forest, over 7.4 million acres of which are in the boreal forests of Canada (Table 1.1.1). Canada and Mexico had more than twice the yearly average areas burned in 1995 and 1998, respectively.

Table 1.1.1 Forest Coverage and Area Burned Yearly in North and Central America

Country	Forests (Million acres)	Average Area Burned (Million acres)	Area Burned (Million acres)		Source
			1995	1998	
USA	630.0	3.7 (1990-1999)	2.3	2.3	FAO (2002)
Mexico	135.8	0.6 (1990-1999)	0.8	2.1	FAO (2002)
Canada	1027.7	7.4 (1920-1996)	16.1	9.0	Canadian Forest Service (1997) FAO (2002)

Smoke from forest fires contains fine particles and gases including: carbon monoxide, organic and elemental carbon, sulfur dioxide, sulfates, nitrates, elemental S, Cl, and K, ionic Cl^- and K^+, and to a lesser extent elemental Na, Mg, Al, Si and Fe (Watson et al., 2001). Plumes of smoke from fires can be transported over substantial distances of hundreds or thousands of miles. For example, smoke plumes from fires in Canada are known to affect gas and particulate matter concentrations in Europe (Forster et al., 2001) and the southeastern United States (Wotawa and Trainer, 2000). By scattering and absorbing light, these smoke plumes have an adverse affect on visibility and can influence vast regions because of the potential long-range transport. The fine particles in smoke are also dangerous to humans and animals because they are able to penetrate deep into the respiratory system (Finlayson-Pitts and Pitts, 2000 and Prospero, 1999).

In addition to smoke from forest fires, emissions from vehicles, industries and power plants contribute to poor visibility conditions. In 1977, in Amendments to the Clean Air Act, Congress addressed the issue of degrading visibility in many national parks and wilderness areas in the United States. The goal of the Amendments was to resolve current and prevent future visibility impairment caused by manmade pollution (USDA Forest Service, 1978). Shortly thereafter the EPA issued regulations relating to visibility in Federal Class I areas, but held off issuing regulations on regional haze until more information could be obtained about the sources and composition of the pollution causing the haze.

To obtain the information needed for regional haze regulations the Interagency Monitoring of Protected Visual Environments (IMPROVE) program was implemented in

1988. In 1999, the EPA issued the first regulations regarding regional haze. The regulations required States to set goals for improving visibility in national parks and wilderness areas and to develop long-term strategies for controlling emissions of the pollutants that cause visibility impairment (UC-Davis, 1995). In addition, National Ambient Air Quality Standards (NAAQS) limit the concentrations of particulate matter less than 2.5 μm (PM2.5) allowed in the atmosphere in a 24-hour period. Thus, strategies will require assessment of the contributions of smoke emissions from forest fires to regional haze and PM2.5.

1.2 Problem Statement

Wotawa and Trainer (2000) were able to identify CO from Canadian forest fires as a major contributor to the CO concentrations in the eastern and southeastern U.S. during the summer of 1995. This suggests long-range transport has an important contribution to the summertime trace gas concentrations in the eastern and southeastern U.S. This study examines whether the influence of these fires can be detected in aerosol data from the southeastern U.S. To identify smoke plumes from the Canadian fires (20-June through 10-July 1995) IMPROVE aerosol data from eight parks in and around the region Wotawa and Trainer (2000) investigated are used to find a tracer unique to smoke and establish a criterion which indicates smoke is present in the aerosol measurements. For smoky and non-smoky events, back trajectories are calculated using the HYSPLIT model version 4.5 (HYSPLIT4 Model, 1997 and Draxler and Hess, 1998) to identify source regions, e.g. regions where an air parcel arriving at the site have crossed. If the 1995 smoke-impacted events can be successfully identified, the criterion will then be

applied to the entire database to establish the frequency of occurrence and spatial extent of smoke plumes in the eastern and southeastern U.S.

1.2.1 Summary of Findings By Wotawa and Trainer (2000)

During a field measurement campaign in the summer of 1995 (SOS95), Wotawa and Trainer (2000) observed episodically elevated CO concentrations over a two-week period in the eastern and southeastern United States. To determine the source of the elevated CO concentrations, Wotawa and Trainer (2000) conducted a modeling study. CO measurements from four background stations in the SOS95 region and two outside stations near the East Coast (Table 1.2.1) and back trajectories using the FLEXTRA trajectory model (Stohl et al., 1995) were used to make reconstructed source regions.

Table 1.2.1 Site Locations (* indicates sites used in model calculations)

SOS95 Sites	Longitude (degrees)	Latitude (degrees)
Giles County, TN*	-86.85	35.00
Cove Mountain, TN (GRSM)*	-83.94	35.63
Mammoth Cave, KY (MACA)*	-86.15	37.13
Land Between the Lakes, KY*	-88.27	37.03
Coastal Sites		
Arendtsville, PA*	-77.30	39.92
Harvard Forest, MA*	-72.17	42.54
Wye River, MD	-76.20	38.83
Shenandoah, VA (SHEN)	-78.43	38.52

Wotawa and Trainer (2000) used a redistributed concentration field method to attribute the measured CO concentrations at the ground stations to grid cells crossed by trajectories from the stations. This method involves calculating average, residence-time weighted concentrations for each cell a trajectory crossed. Elevated concentrations in a cell imply a source of CO within that cell. In addition to the anthropogenic CO emissions in the eastern U.S., a large source of CO was identified in the Northwest Territories. Strong CO source regions were also identified in the Yucatan Peninsula and Cuba (Figure

1.2.1, Fig. 1 from Wotawa and Trainer, 2000). From this figure it can also be seen that contributions from the forest fires in Canada appear to exceed those from anthropogenic sources in the eastern U.S. during the study period.

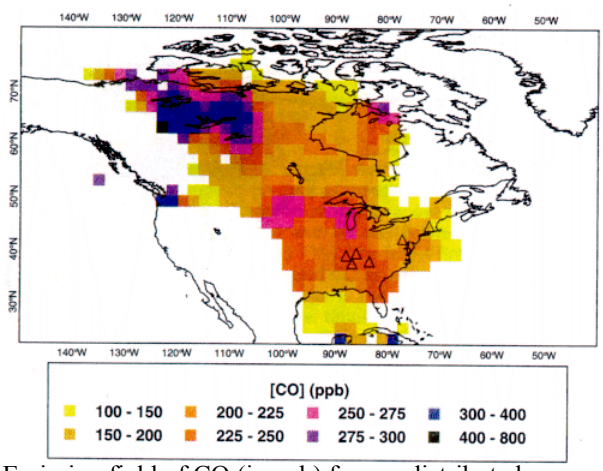

Figure 1.2.1 Emission field of CO (in ppb) from redistributed concentration field method during the summer of 1995. Triangles indicate measurement sites. (Fig. 1. from Wotawa and Trainer (2000), scanned without permission)

Model simulations of anthropogenic and forest fire CO transport were then performed using the FLEXPART particle diffusion model (Stohl and Thompson, 1999). The model simulated CO emissions from forest fires and anthropogenic sources separately to examine the contributions from each source. From Figure 1.2.2 (Fig. 2 from Wotawa and Trainer, 2000) it can be seen that in the afternoon of 1-July CO emissions from the Canadian fires greatly exceeded emissions from anthropogenic sources.

Three episodes of smoke plumes were identified from the model simulations, the largest behind a cold front on 1-July. Two other episodes were identified on 27-30 June and 7-10 July (Figure 1.2.3, Fig. 3 from Wotawa and Trainer, 2000).

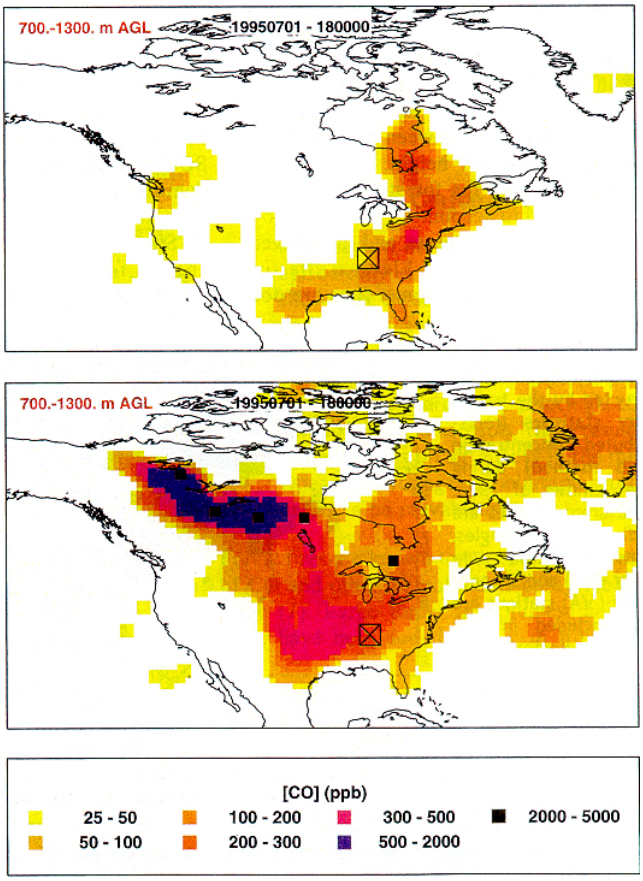

Figure 1.2.2 Calculated CO concentrations (in ppb) from anthropogenic emissions (top) and forest fires (bottom) for 1-July 1995, 18 UTC. Black filled square mark forest fire release locations and the open square indicates the SOS95 region. (Fig. 2. from Wotawa and Trainer (2000), scanned without permission)

The model results were compared to observations in the SOS95 region and four sites on the East Coast (Table 1.2.1). While the anthropogenic contribution had a clear diurnal cycle, the forest fire contribution occurred in multi-day episodes. Both forest fires and anthropogenic sources are needed to explain the observations. At Giles County, Tennessee 74% of the variance in afternoon CO concentrations was explained by the forest fires (Figure 1.2.3). Although forest fires accounted for at least 50% of the variance in the afternoon CO concentrations at all sites, the coastal sites had a larger

unexplained variance. The smoke plume episodes were not as well defined at these sites as the episodes at the sites within the SOS95 region. It was concluded that over the two weeks, CO measurements within the SOS95 region were dominated by forest fire emissions from Canada.

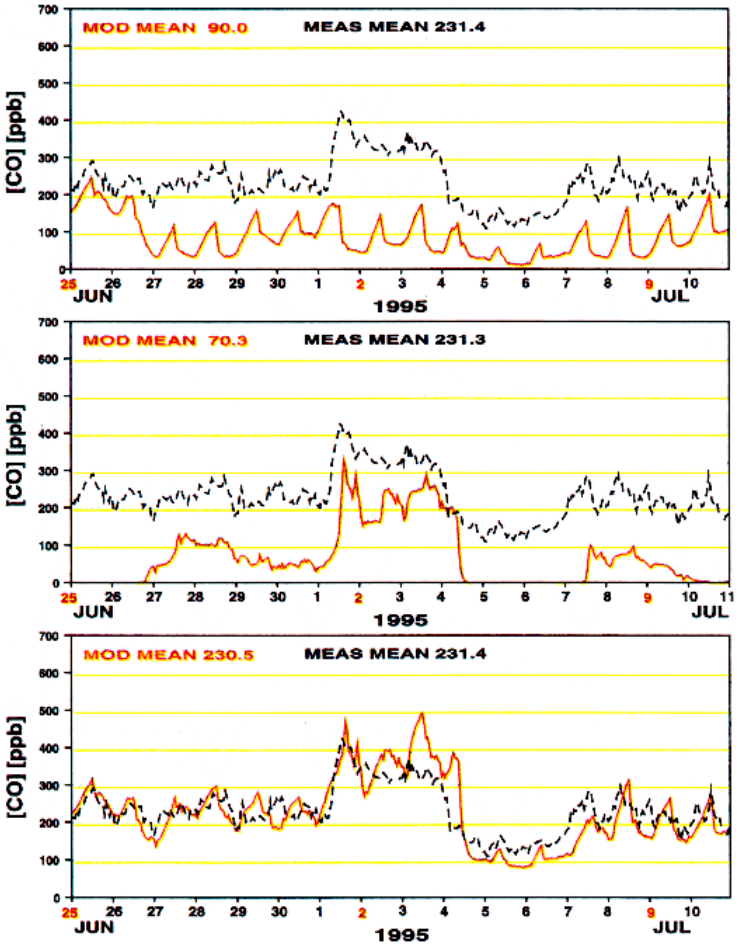

Figure 1.2.3 Hourly measured (dashed line) and simulated (solid line) CO concentrations (ppb) from anthropogenic (top), forest fires (middle), and both sources plus a 70 ppb background concentration (bottom) at Giles County, Tennessee. (Fig. 3. from Wotawa and Trainer (2000), scanned without permission)

1.3 Data Sets Used in This Study

1.3.1 IMPROVE Aerosol Data

The IMPROVE monitoring program began operation in 1988 as a cooperative effort between the National Park Service (NPS), the U.S. Forest Service (USFS), the Bureau of Land Management, the Fish and Wildlife Services, the Environmental Protection Agency (EPA) and other state organizations. Monitoring sites have been established at Class I areas, primarily national parks and wilderness areas, across the conterminous U.S., Alaska, Hawaii and the Virgin Islands since 1988. Figure 1.3.1 is a map of all sites as of August 1995 (UC-Davis, 1995).

Figure 1.3.1 Map of all IMPROVE monitoring sites as of August 1995 from http://vista.cira.colostate.edu/improve/Publications/OtherDocs/IMPROVEDataGuide/IMPROVEDataGuide.htm

All sites measure the chemical composition and concentrations of fine aerosols and some measure aerosol scattering or extinction using nephelometers or transmissometers. Samples were taken twice weekly, Wednesday and Saturday, from midnight to midnight at each site until spring of 2000 when an every third day schedule was adopted.

The standard IMPROVE sampler has instrumentation that deposits samples on four separate filters, which are called modules. Modules A through C measure fine particles less than 2.5 micrometers in diameter (PM2.5) and module D measures the total mass of all particles less than 10 micrometers (PM10). All sites have Module A and most also have Modules B through D. Filters are changed weekly by on-site personnel and shipped to UC-Davis for analysis. The module A Teflon filter is the primary filter at all sites and is analyzed for PM2.5 mass, H, and elements Na through Pb. Gravimetric analysis is used to obtain the mass; Particle Induced X-ray Emission (PIXE) and X-ray Fluorescence (XRF) are used for elements Na through Pb and Proton Elastic Scattering Analysis (PESA) is used for H. Module D also consists of a Teflon filter and gravimetric analysis is used to obtain the PM10 mass. Module B has a nylon filter preceded by a denuder that removes acidic gases. Ion Chromatography (IC) is used to analyze the nylon filter for nitrate, sulfate and chloride. Module C has a quartz filter that is used to measure carbon (elemental and organic) in eight temperature fractions using a Thermal Optical Reflectance (TOR) combustion method. Some sites have an additional quartz filter, impregnated with K_2CO_3, following the Module A or D Teflon filter for measuring SO_2.

Composite variables, such as soil, can be derived from the measured variables. The composite variables used in this study are listed in Table 1.3.1. Total organic carbon (OC) is the sum of the four organic carbon fractions (OC1-OC4) and pyrolized organic carbon (OP). Total elemental carbon (EC) is the sum of the three elemental carbon fractions (EC1-EC3) minus OP. Total carbon (TC) is the sum of OC and EC. For fine soil (SOIL) it is assumed the elements present in soil (Al, Si, Ca, Fe, and Ti) exist in their normal oxide states. The elements are multiplied by the appropriate factor and summed. The calculation of non-soil potassium, K_{NON}, is discussed in Section 2.1.2. It is assumed that all sulfate on the Teflon filter is fully neutralized ammonium sulfate (AMMSULF), the mass of which is calculated by multiplying the sulfur concentration (S) by 4.125. Similarly, the nitrate present is assumed to be fully neutralized ammonium nitrate (AMMNITR), with a mass calculated by multiplying the nitrate concentration (NO_3^-) by 1.29. The reconstructed fine mass (FMSUM) is the sum of AMMSULF, AMMNITR, OC, EC, and SOIL.

Table 1.3.1 Derived Variables

OC	Total Organic Carbon	1.4*(OC1 + OC2 + OC3 + OC4 + OP)
EC	Total Elemental Carbon	EC1 + EC2 + EC3 – OP
TC	Total Organic Carbon	EC + OC
SOIL	Fine Soil	2.20*Al + 2.49*Si + 1.63*Ca + 2.42*Fe + 1.94*Ti
K_{NON}	Non-Soil Potassium	K – 0.6*Fe
AMMSULF	Ammonium Sulfate	4.125*S
AMMNITR	Ammonium Nitrate	1.29*NO_3^-
FMSUM	Reconstructed Fine Mass	AMMSULF + AMMNITR + OC + EC + SOIL

1.3.2 Fire Data

1.3.2.1 National Fire Occurrence Database (United States)

Fires in the conterminous United States were identified using the National Fire Occurrence Database (Prescribed Fire and Fire Effects Research Work Unit, 1999). The database contains information on fire locations from 1986-1996 provided by federal and

state agencies. States reported data either as GIS coverages, latitude-longitude coordinates, legal descriptions or a county as the finest location. All states report a day of discovery; some report any or all of the following: time discovered, day contained, time contained and acreage burned. Prescribed burns, assist fires, and false alarms were not included in the database. In 1995 there were 918,300 acres treated by prescribed burns in the U.S. in addition to the 2.3 million acres of wildfires (National Interagency Fire Center, 2002). GIS state boundaries were overlaid on the fire data to examine whether the fire occurred within that state. If a fire was located more than ten kilometers from the reporting state boundary or was within ten kilometers and was not reported by the adjacent state the data were thrown out. Table 1.3.2 summarizes the data reported for each state, including whether data were available for 1995 or not. Three states did not report data for 1995: Pennsylvania, South Carolina and Virginia. The lack of data on prescribed burns and no fire data at all for these three states near the study region are important limitations to the work reported here.

Table 1.3.2 State provided information for the National Fire Occurrence Database.

State	1995 Data	Month	Day	Time	Month	Day	Time	Acres Burned
		Discovered			Contained			
Alabama	Y	Y	Y	N	N	N	N	N
Arkansas	Y	Y	Y	Y	N	N	N	Y
Arizona	Y	Y	Y	Y	Y	Y	Y	Y
California	Y	Y	Y	Y	Y	Y	Y	Y
Colorado	Y	Y	Y	N	N	N	N	Y
Connecticut	Y	Y	Y	Y	N	N	N	Y
Delaware	Y	Y	Y	N	N	N	N	N
Florida	Y	Y	Y	Y	Y	Y	Y	Y
Georgia	Y	Y	Y	Y	Y	N	N	Y
Iowa	Y	Y	Y	N	N	N	N	N
Idaho	Y	Y	Y	Y	Y	Y	Y	Y
Illinois	Y	Y	Y	N	N	N	N	N
Indiana	Y	Y	Y	N	N	N	N	Y
Kansas	Y	Y	Y	Y	N	N	N	Y
Kentucky	Y	Y	Y	N	N	N	N	N
Louisiana	Y	Y	Y	N	N	N	N	N
Massachusetts	Y	Y	Y	Y	N	N	N	Y
Maryland	Y	Y	Y	N	N	N	N	Y

Table 1.3.2 Continued

Maine	Y	Y	Y	Y	Y	Y	Y	Y
Michigan	Y	Y	Y	Y	Y	Y	Y	Y
Minnesota	Y	Y	Y	Y	Y	Y	Y	Y
Missouri	Y	Y	Y	Y	Y	Y	Y	Y
Mississippi	Y	Y	Y	Y	N	N	Y	Y
Montana	Y	Y	Y	Y	Y	Y	Y	Y
North Carolina	Y	Y	Y	Y	Y	Y	N	Y
North Dakota	Y	Y	Y	N	N	N	N	Y
Nebraska	Y	Y	Y	N	N	N	N	Y
Nevada	No State Record							
N. Hampshire	Y	Y	Y	N	N	N	N	N
New Jersey	Y	Y	Y	N	N	N	N	Y
New Mexico	Y	Y	Y	Y	Y	Y	Y	Y
New York	Y	Y	Y	N	Y	Y	N	Y
Ohio	Y	Y	Y	N	N	N	N	Y
Oklahoma	Y	Y	Y	Y	Y	Y	Y	Y
Oregon	Y	Y	Y	Y	Y	Y	Y	Y
Pennsylvania	N	Y	Y	N	N	N	N	Y
Rhode Island	Y	Y	Y	N	N	N	N	N
South Carolina	N	Y	Y	N	N	N	N	Y
South Dakota	Y	Y	N	N	N	Y	Y	Y
Tennessee	Y	Y	Y	Y	Y	Y	Y	Y
Texas	Y	Y	Y	Y	N	N	Y	Y
Utah	Y	Y	Y	N	N	N	N	Y
Virginia	N	Y	Y	N	N	N	N	Y
Vermont	Y	Y	Y	Y	N	N	N	Y
Washington	Y	Y	Y	Y	Y	Y	Y	Y
Wisconsin	Y	Y	Y	Y	Y	Y	Y	Y
West Virginia	Y	Y	Y	N	N	N	N	N
Wyoming	Y	Y	Y	N	N	N	N	Y

1.3.2.2 Canadian Fire Maps

The locations of fires in Canada during 1995 were identified using maps of hot spots from the Fire Monitoring Mapping and Modeling (FIREM3) website (Canadian Forest Service, 2002). The maps are made available by the Canadian Forest Service and the Canada Centre for Remote Sensing. Daily maps of hot spots, detected using the NOAA-AVHRR satellite, are available from 1994-present. Note that satellite detected hot spots are limited to nighttime, cloud-free views, so some fires may be missed, and there is also no information on the size of the fire from this source.

1.3.2.3 Mexico and Central America

There are no data on locations or sizes of fires in Mexico and Central America for 1995. It is assumed that burning during 1995 was similar to the average from 1995-2000 for this region, occurring primarily in April and May (General Directorate for Forestry, Forest Protection Office, 2001).

1.3.2.4 1998 Fire Data

Global satellite detected hot spot maps were available for 1998 from the ATSR World Fire Atlas (European Space Agency – ESA/ESRIN, 2002). Again, note that satellite detected hot spots are limited to nighttime, cloud-free views, so some fires may be missed, and there is also no information on the size of the fire from this source.

1.3.3 HYSPLIT (Hybrid Single-Particle Lagrangian Integrated Trajectory) Model

The National Oceanic and Atmospheric Association's (NOAA) HYSPLIT model has many applications from calculating trajectories to complex puff and particle dispersion and deposition modeling. The model is able to use meteorological data, archived or forecast, from various sources including the Nested Grid Model (NGM), Eta Data Assimilation System (EDAS), Medium Range Forecast Model (MRF), NCEP/NCAR Reanalysis Data and others. The meteorological data are gridded and converted to sigma (terrain-following) coordinates prior to use by HYSPLIT. The model requires, at minimum, the U and V components of the wind, temperature, height or pressure, and the surface pressure. Other variables, such as rainfall or moisture, may be required for deposition or dispersion modeling.

Back trajectories are an approximation of where an air parcel arriving at a location has traveled. Each point along a trajectory has error associated with it and thus

not only the points on the trajectory influence the air parcels arriving at a site. As time and distance from the site increase, the error surrounding a point on the trajectory also increases. Draxler (1991) estimated the error at any point along a trajectory from a site as approximately 20 to 30 percent of the distance traveled from the site. Hence, the trajectories are a good indication of the region air came from, but aren't an exact trace of the path the air traveled.

For the purpose of this study NGM data were used to calculate trajectories in 1995. Actually, the data are from the Regional Analysis and Forecast System (RAFS), but are called NGM data because RAFS uses the Nested Grid Model for forecasts (Rolph, 1997). For each model run, observations are assimilated with forecast data from the previous run. Dynamic discrepancies in the data are reduced and the new forecast is made. The resulting data, after assimilation and reduction of dynamic errors, provides better spatial and temporal coverage than observations alone. Figure 1.3.2 is the domain for the NGM meteorological data.

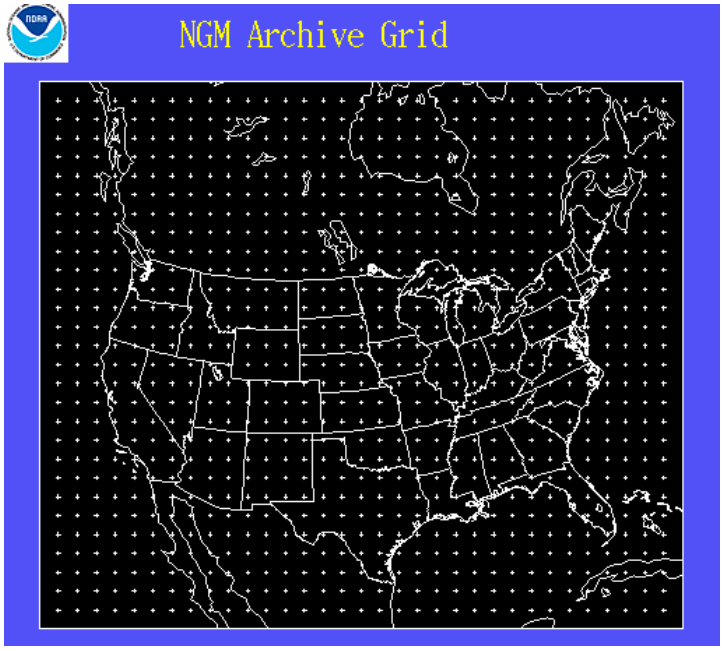

Figure 1.3.2 Map of the NGM grid domain from: http://arl.noaa.gov/ss/transport/ngmgrid.gif

For days that had trajectories ending near the lower boundary of the NGM grid trajectories were recomputed over a larger domain to clarify source regions. In those cases global NCEP/NCAR reanalysis data were used in HYSPLIT. The horizontal resolution of the reanalysis data is not as fine as the NGM data and thus these data were not used exclusively for the 1995 trajectories.

For the 1998 cases considered here, FNL and EDAS data were used. Data from the National Centers for Environmental Prediction's (NCEP) Global Data Assimilation System (GDAS) is used to produce the FNL data (Stunder, 1997). The resulting data fields cover the Northern Hemisphere. The horizontal and vertical resolution of the FNL data are not as fine as the resolution of data from the Eta Data Assimilation System (EDAS). However, during the study period (April – July) much of the EDAS data was missing and it was necessary to supplement with the FNL data. Table 1.3.3 illustrates the differences between the various types of meteorological data used in this study (additional information is available on the ARL website at: http://www.arl.noaa.gov). Figures 1.3.3 and 1.3.4 are the grid domain maps for FNL and EDAS data, respectively.

Table 1.3.3 Meteorological Data Details

Data Archive	Year Used	Vertical Levels	Projection	Area Covered	Source
NGM	1995	Surface + 10 sigma levels	33 X 28 Polar Stereographic	United States	Rolph, 1997
Reanalysis	1995	Surface + 17 pressure levels	144 X 73 Global Grid	Global	ARL, 2001
FNL	1998	Surface + 13 pressure levels	129 X 129 Polar Stereographic	Northern Hemisphere	Stunder, 1997
EDAS	1998	Surface + 22 pressure levels	79 X 55 Lambert Conformal	United States	Rolph, 2002

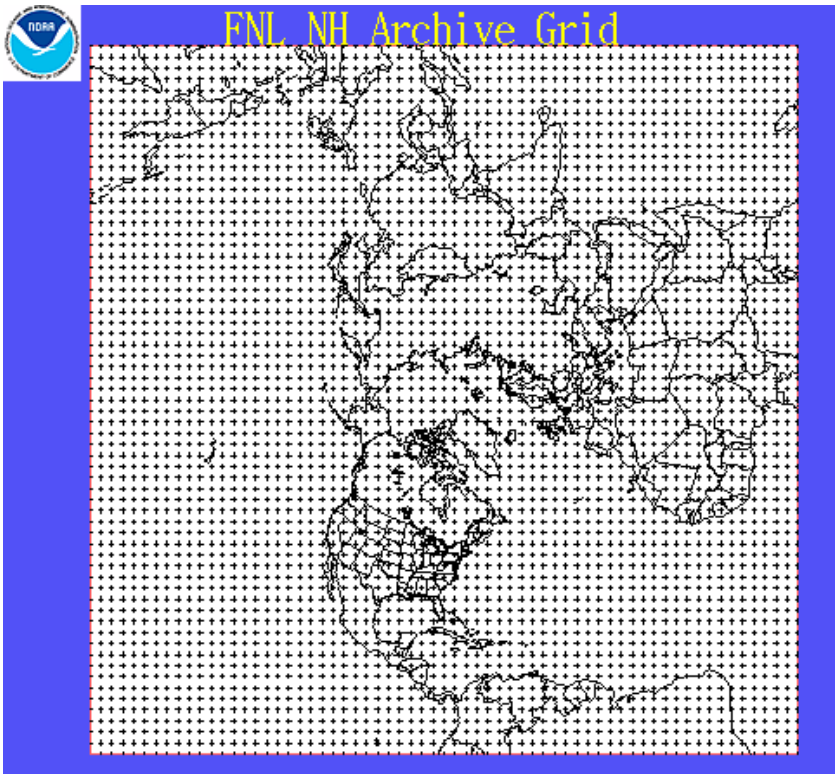

Figure 1.3.3 Map of the FNL grid domain from: http://arl.noaa.gov/ss/transport/ngmgrid.gif

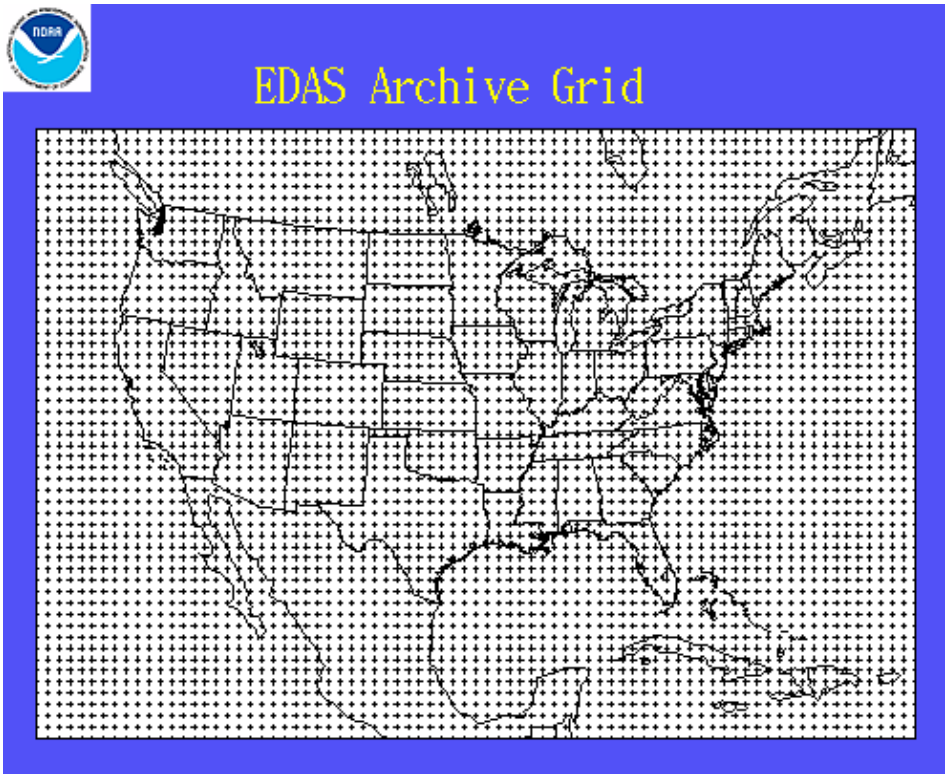

Figure 1.3.4 Map of the EDAS grid domain from: http://arl.noaa.gov/ss/transport/ngmgrid.gif

Chapter 2. Methodology

2.1 Selection of Parks

There were a total of eight parks within the IMPROVE network examined for this study. Four sites were chosen to represent the SOS95 region (Wotawa and Trainer, 2000). The parks near or within the SOS95 region (SOS parks) are: Great Smoky Mountains National Park, TN (GRSM); Mammoth Cave National Park, KY (MACA); Sipsey Wilderness, AL (SIPS); and Shining Rock Wilderness, NC (SHRO). Data from four sites outside the SOS95 region were also examined: Dolly Sods/Otter Creek Wilderness, WV (DOSO); Jefferson/James River Face Wilderness, VA (JEFF); Shenandoah N. P., VA (SHEN); and Upper Buffalo Wilderness, AR (UPBU) (Figure 2.1.1).

DOSO, SHEN and JEFF were chosen to represent the coastal stations examined by Wotawa and Trainer (2000) and UPBU was chosen to examine the spatial extent of the July 1995 smoke event. Table 2.1.1 details the locations and data available for the selected sites. Three of the eight sites selected are identical to the sites used by Wotawa and Trainer (2000) (Figure 2.1.1). GRSM and MACA were part of the SOS95 region and SHEN was one of the coastal sites used for the model comparisons (Section 1.2.1).

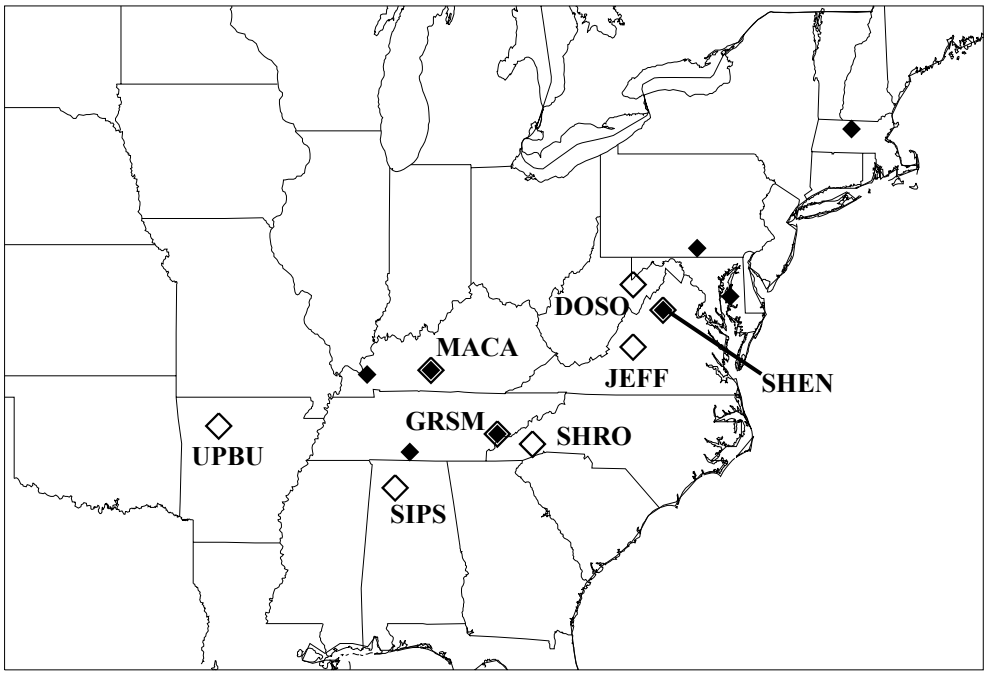

Figure 2.1.1 Map of sites used by Wotawa and Trainer (2000) (small, solid diamonds) and IMPROVE sites used for this study (large, open diamonds).

Table 2.1.1 Site Metadata

Site Code	Site Name	Longitude (degrees)	Latitude (degrees)	Elevation (meters)	Years	Sponsor	Measurements
DOSO	Dolly Sods/Otter Creek Wilderness, WV	-79.43	39.11	1158	1992-present	USFS	Channels A,B,C,D Nephelometer
GRSM	Great Smoky Mountains National Park, TN	-83.94	35.63	815	1988-present	NPS	Channels A,B,C,D Nephelometer SO_2
JEFF	Jefferson/James River Face Wilderness, VA	-79.51	37.63	299	1995-present	USFS	Channels A,B,C,D
MACA	Mammoth Cave National Park, KY	-86.15	37.13	248	1992-present	NPS	Channels A,B,C,D Nephelometer SO_2
SHEN	Shenandoah National Park, VA	-78.43	38.52	1098	1988-present	NPS	Channels A,B,C,D Transmissometer SO_2
SHRO	Shining Rock Wilderness, NC	-82.77	35.39	1621	1994-present	USFS	Channels A,B,C,D Nephelometer
SIPS	Sipsey Wilderness, AL	-87.34	34.34	279	1992-present	USFS	Channels A,B,C,D
UPBU	Upper Buffalo Wilderness, AR	-93.20	35.83	723	1992-present	USFS	Channels A,B,C,D Nephelometer

2.2 Selection of a Tracer

Non-soil potassium was investigated as a smoke tracer for this study. The primary sources of potassium in aerosols are soil and smoke with additional contributions from sea salt. Organic matter emits potassium vapor when burned, which converts to fine particles during transport. The particles resulting from smoke are generally smaller than soil particles, but soil, sea salt and smoke-derived potassium may be present in the PM2.5 aerosol fraction. In order to estimate the contribution to aerosol potassium from smoke some assumptions need to be made about the soil contribution.

Cahill et al. (1980) observed a ratio K/Fe=0.6 in resuspended soil samples taken from eight states in the western U.S. (Section 2.2.1). Assuming that the same ratio is present in fine particles, the ratio can be used along with the measured concentration of iron to estimate the non-soil contribution (K_{NON}) as:

$$K_{NON} = K - 0.6*Fe \quad \text{(Eq. 1)}$$

Another known source of aerosol potassium is sea salt. The average ratio of potassium to sodium in sea salt is 0.036. So, it is necessary to modify the Eq. 1 by further subtracting the fraction of potassium associated with sea salt:

$$K_{NON} = K - 0.6*Fe - 0.036*Na \quad \text{(Eq. 2)}$$

The resulting quantity, K_{NON}, is not a quantitative measure of the amount of smoke present at the given location, but it was chosen as a potentially useful indicator of the presence of significant smoke impact.

2.2.1 Soil Composition and Calculation of K_{NON}

Cahill et al. (1980) compared resuspended soil samples to ambient aerosol samples at 40 sites in eight states in the western U.S.: Montana, North and South Dakota,

Wyoming, Utah, Colorado, Arizona, and New Mexico. Over 100 soil samples were taken at or near the aerosol collection sites, sieved into five fractions and particles less than 50 microns were then resuspended. The resuspended samples were collected in a five stage Lundgren impactor with size ranges of 50 to 25 microns, 25 to 8 microns, 8 to 3 microns, 3 to 0.8 microns and less than 0.8 microns. The fractions of soil mass that were resuspended into particles less than 15 microns were used for comparison to ambient aerosol samples at each site. Ambient and soil samples were then analyzed by PIXE for elements sodium and heavier. Soil particles are dominated by silicon, aluminum, calcium, iron, potassium, titanium, and manganese with contributions from sodium, strontium, and zirconium in smaller amounts (Cahill et al., 1980).

For the resuspended soil particle samples there was little variation in elemental concentration in the fine versus coarse particle sizes. The elemental composition of the ambient aerosol closely resembled the elemental composition of the resuspended soil with the exception of the ratio K/Fe that was higher in the ambient aerosol than the resuspended soil. This elemental ratio is also the only one that exhibits a difference between the fine and coarse mode in the ambient aerosol (Cahill et al., 1980). The excess potassium was attributed to smoke sources. Cahill et al. (1980) calculated a mean ratio of K/Fe=0.6 over the 40 sites, however there was site-to-site variation in the observed values of nearly an order of magnitude. The site-to-site variation in the observed K/Fe ratio suggests that to accurately represent the soil contribution to the potassium concentration at a given site, site-specific information about the soil composition around the monitoring site is needed.

A similar study has not been done for sites in the eastern U.S. Thus, it must be assumed that the ratio calculated by Cahill et al. (1980) will represent the soil contribution to fine aerosol potassium concentrations in the eastern U.S. However, it is known that Saharan dust impacts the eastern and southeastern U.S. during the summer months (Perry et al., 1997). The summer of 1995 was no exception with two episodes of Saharan dust transport identified. Thus, the soil composition of Saharan dust must be taken into consideration when calculating K_{NON} at the sites in the eastern and southeastern U.S.

Using the criterion established by Perry et al. (1997), further discussed in Chapter 6, aerosol data at each park (for all years) on days impacted by Saharan dust were isolated. Next, the ratio K/Fe was calculated for each of the Saharan days at each park. For comparison, the same was done at Virgin Islands National Park (VIIS) since it is frequently affected by Saharan dust (Perry et al., 1997). The mean K/Fe ratio at VIIS was calculated to be 0.45 on the Saharan days. Each of the parks selected for this study was within one standard deviation of the ratio at VIIS. Thus, on days that pass the modified Saharan dust criterion (Chapter 6) Eq. 3 is used:

$$K_{NON} = K - 0.45*Fe - 0.036*Na \quad \text{(Eq. 3)}$$

Sensitivity to the assumptions made for calculating K_{NON} are explored in Chapter 6.

2.3 Trajectories

Backward trajectories starting at 500 meters above each site were calculated using HYSPLIT (Section 1.2.3). The trajectories were calculated using model vertical velocity for a duration of five days. A trajectory was calculated once every hour for every day.

Four representative times were selected for analysis; all times are local standard time (LST): 1 A.M., 7 A.M., 1 P.M., and 7 P.M. The trajectory maps used in this study are presented in Appendix A. The trajectory maps were then compared to fire maps to determine whether transport was from regions where fires were for all parks on every IMPROVE sample day from 15-April through 31-July in 1995 and 1998. By comparing the trajectories to fire maps, days can be separated based on whether smoke impact is likely, transport is from a fire region, and smoke impact not likely, transport not from a fire region. This process is time consuming and requires a large amount of data, thus it was only applied in 1995 and 1998 to test K_{NON} as an indicator of smoke impact in aerosol samples.

2.4 Selection of a Smoke Criterion

There are several uncertainties in the calculation of K_{NON} that need to be taken into consideration when selecting a criterion to indicate the presence of smoke in an aerosol sample. These uncertainties include variations in soil composition, variations in the smoke contributions to aerosol K, and elemental concentrations near the minimum detection limits, all of which occassionally, result in negative K_{NON} values. Keeping these uncertainties in mind, a minimum value of K_{NON} associated with significant smoke impact needed to be selected for each park.

As mentioned in Section 2.3, back-trajectory maps were compared to fire maps to determine all sample days in 1995 and 1998 that were not likely to be smoke impacted based on whether the transport was from regions where fires were not occurring. A frequency plot of KNON for these non-smoky days was then constructed. Figure 2.4.1 is

the frequency plot for GRSM. Also shown in Figure 2.4.1 are the K_{NON} values for the days likely to be smoke impacted. Clearly, the smoky and non-smoky K_{NON} values overlap. Thus, selecting a criterion above the highest non-smoky value would result in many smoky days not being identified by the criterion (false negatives). Conversely, selecting the criterion to be below the lowest smoky value would result in many non-smoky days being identified as smoky by the criterion (false positives). The goal when selecting the criterion was to minimize both the false positive and false negative identifications. Three potential criteria were explored: the 90^{th} and 95^{th} percentile values for the non-smoky days in 1995 and 1998 and the median value of K_{NON} over all months and all years of available data (through 1999), plus two standard deviations. The median was selected rather than the mean due to the occassional computation of negative K_{NON} values. The resulting K_{NON} values at GRSM are shown in Figure 2.4.1 as vertical lines. In all cases, including the median plus two standard deviations, K, Fe and Na concentrations below the minimum detection limit were set at the minimum detection limit. Negative data points were not removed from the calculations and no assumptions were made about the distribution of the data.

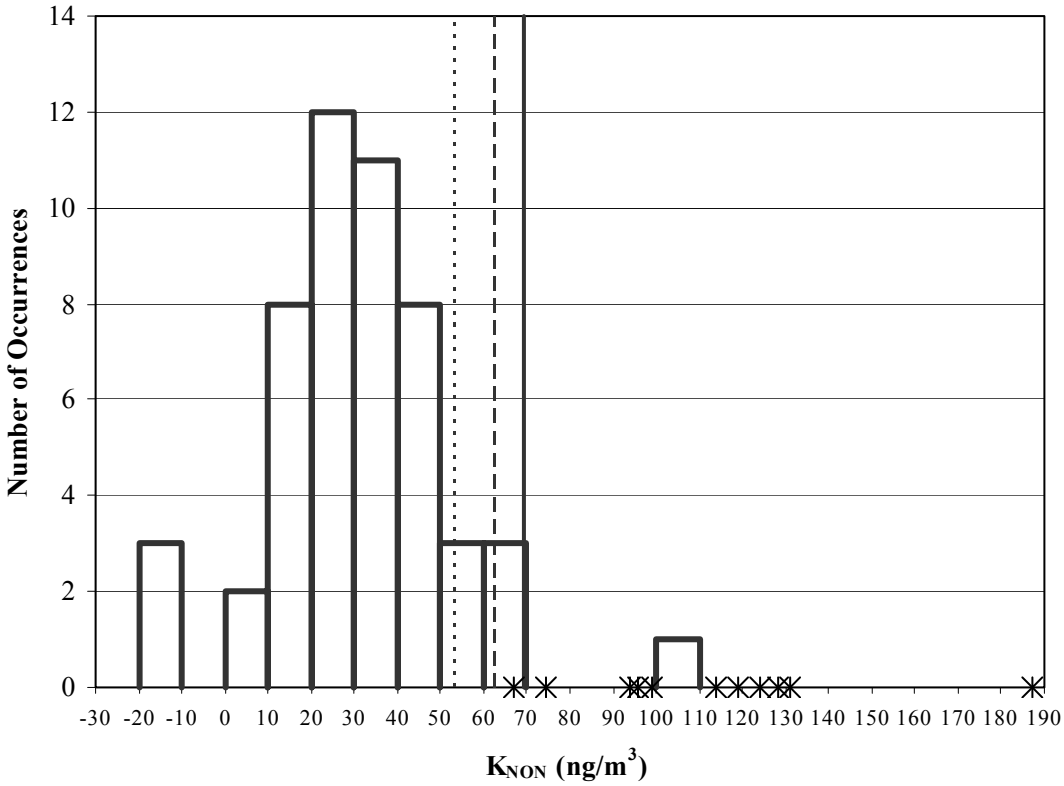

Figure 2.4.1 Non-smoky (bars) and smoky days (stars along axis) at GRSM from 15-April through 31-July 1995 and 1998. Vertical lines represent criterion tested: 90th percentile – dotted line, 95th percentile – dashed line, and median plus two standard deviations – solid line.

The same plots were constructed for each park (not shown). The desired criterion will minimize the overall number of false positives and false negatives. Table 7.3.1 details the results over all parks using the three different criteria, median plus two standard deviations, 95th percentile and 90th percentile. The false positive rate is the number of false positives divided by the total number of observations passing the criterion. The false negative rate is the number of false negatives divided by the number of observations not passing the criterion. The number passing is the total number of smoky observations determined by comparing back-trajectories and fire maps (70) plus the false positives minus the false negatives. The number not passing the criterion is the

total number of observations (475) minus the number passing the criterion. Since the goal is to minimize both false positives and false negatives, it can be seen from Table 7.3.1 that the selected criterion, median plus two standard deviations, performed the best with 15.2% false positives while keeping a minimal number of false negatives (3.4%).

Table 2.4.1 Results for all parks using three different criteria.

Criterion	Number Non-smoky	Number Smoky	Number False Positive	Number False Negative	Number Passing Criterion	Number Not Passing	Percent False Positive	Percent False Negative
Median + 2σ	405	70	10	14	66	409	15.2%	3.4%
95%	405	70	24	10	84	391	28.6%	2.6%
90%	405	70	46	5	111	364	41.4%	1.4%

Thus, it is concluded that using the median plus two standard deviations is the best criterion for indicating the presence of smoke impact in aerosol samples. The medians, standard deviations and resulting smoke criteria for each park are presented in Table 2.4.2. It is worth noting the exceptionally high standard deviation and resulting smoke criterion at JEFF.

Table 2.4.2 K_{NON} medians, standard deviations and smoke criteria (ng/m^3) for each park.

Park	Median	Standard Deviation	Smoke Criterion
DOSO	14.92	17.15	49.22
GRSM	21.94	23.72	69.38
JEFF	38.90	44.95	128.81
MACA	21.05	26.37	73.79
SHEN	12.10	18.05	48.20
SHRO	14.77	18.65	52.07
SIPS	26.04	30.66	87.35
UPBU	20.56	33.58	87.71

Chapter 3. Results for 1995

3.1 K_{NON} and 1995 Smoke Impacted Days

The medians, smoke criteria and values of K_{NON} for 15-April through 31-July 1995 are shown in Figure 3.1.1a and Figure 3.1.1b. It is worth reiterating that K_{NON} is not a quantitative measure of the amount of smoke present, but indicates significant smoke impact. The smoke criteria were calculated, as discussed in Section 2.2.2, as the median of K_{NON} plus two standard deviations.

From 15-April through 31-July there were a total of 236 observations in the region of consideration of which 34 observations were flagged as smoke impacted (Table 3.1.1). Days that were flagged smoky, but could not be confirmed by comparing trajectory maps to fire maps are considered false positive for smoke impact. A park that had transport from a known fire region on a given day or a trajectory crossing a large fire, but was not flagged as smoke impacted is considered a false negative for smoke impact on that day. Of the 34 smoke impacted observations five were concluded to be false positives and eight false negatives. Possible reasons for false positive and false negative findings are discussed in Section 3.4.

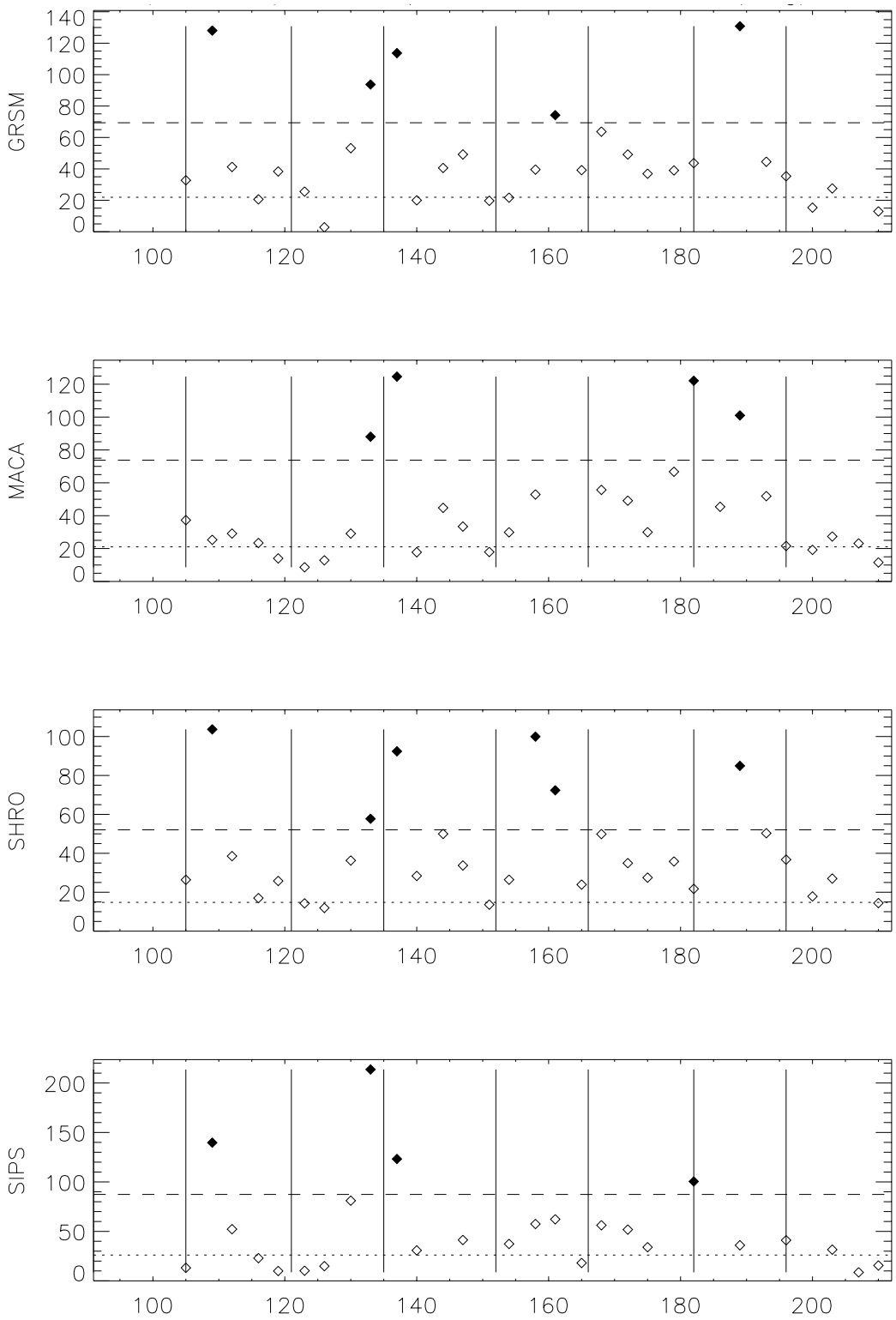

Figure 3.1.1a 4/15 through 7/31 1995 K_{NON} (ng/m^3) values for parks in the SOS95 region. Numbers along x-axis indicate Julian day where 105 is 15-April. Dotted lines indicate median value; dashed lines indicate smoke criteria and filled diamonds smoke impacted days. Vertical lines indicate the first and fifteenth of each month, April through July.

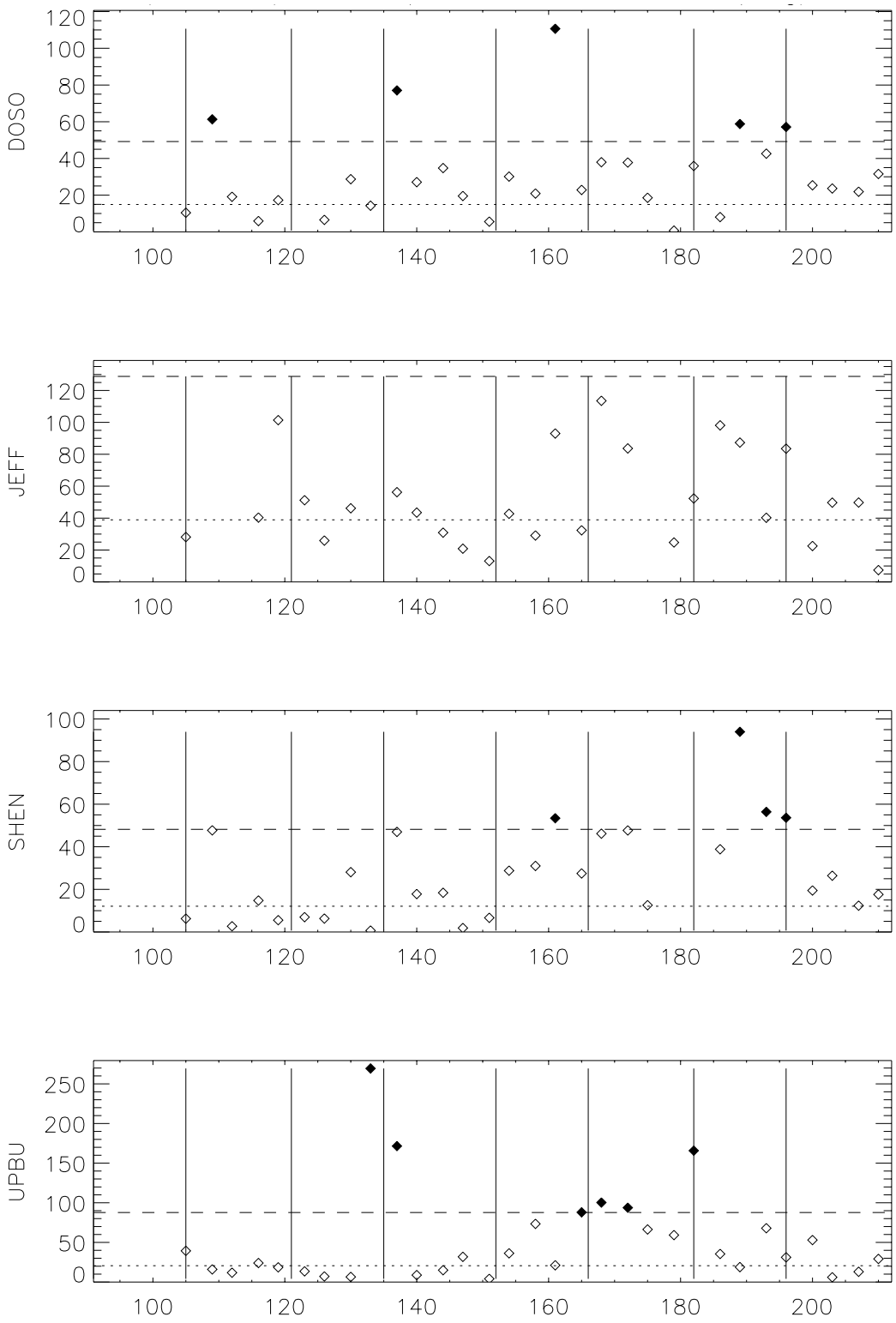

Figure 3.1.1b 4/15 through 7/31 1995 K_{NON} (ng/m^3) values for parks outside the SOS95 region. Numbers along x-axis indicate Julian day where 105 is 15-April. Dotted lines indicate median value; dashed lines indicate smoke criteria and filled diamonds smoke impacted days. Vertical lines indicate the first and fifteenth of each month, April through July.

Table 3.1.1 Number of Observations, Smoky Flags and False Flags.

Park	Number of Observations 4/15/95 - 7/31/95					Park	Number of Days Flagged Smoky 4/15/95 - 7/31/95				
	April	May	June	July	Total		April	May	June	July	Total
DOSO	5	8	8	9	30	DOSO	1	1	1	2	5
GRSM	5	9	8	9	31	GRSM	1	2	1	1	5
JEFF	5	8	8	9	30	JEFF	0	0	0	0	0
MACA	5	9	6	9	29	MACA	0	2	0	2	4
SHEN	5	9	7	8	29	SHEN	0	0	1	3	4
SHRO	5	9	8	9	31	SHRO	1	2	2	1	6
SIPS	5	7	7	6	25	SIPS	1	2	0	1	4
UPBU	5	9	8	9	31	UPBU	0	2	3	1	6
Total	40	68	60	68	236	Total	4	11	8	11	34
Park	Number of False Positives 4/15/95 - 7/31/95					Park	Number of False Negatives 4/15/95 - 7/31/95				
	April	May	June	July	Total		April	May	June	July	Total
DOSO	0	0	0	1	1	DOSO	0	0	0	0	0
GRSM	0	0	0	0	0	GRSM	0	0	0	0	0
JEFF	0	0	0	0	0	JEFF	1	1	1	1	4
MACA	0	0	0	0	0	MACA	0	0	0	0	0
SHEN	0	0	0	2	2	SHEN	1	1	0	0	2
SHRO	0	0	1	0	1	SHRO	0	0	0	0	0
SIPS	0	0	0	0	0	SIPS	0	0	1	0	1
UPBU	0	0	1	0	1	UPBU	0	0	1	0	1
Total	0	0	2	3	5	Total	2	2	3	1	8

There were two false positives at SHEN, the highest number of any park. They were on 12-July and 15-July. It is possible that prescribed burns, which are not reported in the National Fire Occurrence Database, or fires in states without data in 1995, Virginia or Pennsylvania, impacted the observations at SHEN on those days. Similarly, prescribed burns or fires in Pennsylvania could have influenced the day determined to be false positive at DOSO, 15-July. SHRO was false positive for smoke impact on 7-June. A prescribed burn could be the reason for the false positive at SHRO. Another possibility is an elevated smoke plume from Mexico as will be discussed in the results for 1998 in Chapter 4. SHRO has the highest elevation of all parks in the study region, thus it is quite likely an elevated smoke plume would impact SHRO and no other parks. JEFF,

SHEN, SIPS and UPBU all had days determined to be false negative for smoke impact. These days will be discussed in detail later in this chapter.

3.2 Canadian Smoke Events

Wotawa and Trainer (2000) identified three plumes of CO from fires in Canada, one in late June, the second on 1-July and the third from 7 to 10-July. There was one IMPROVE sample day during each of the events. Smoke impact in the aerosol data was seen on 1-July and 8-July. Back trajectories were compared to hot spot maps from FIREM3 and the calculated CO concentrations from forest fire emissions in Figure 1.1.2 to confirm the presence of fires in the aerosol source regions. Each of these events will now be examined separately.

On 1-July MACA, UPBU, and SIPS were flagged as smoky and SHEN was missing data (Figure 3.2.1).

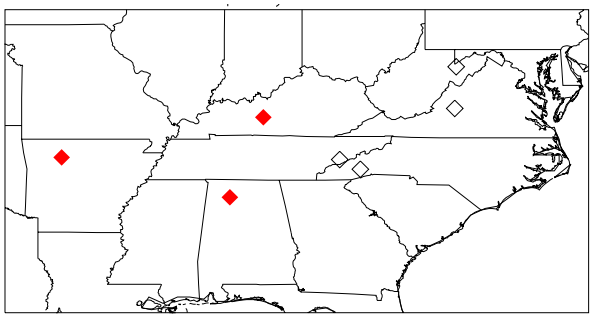

Figure 3.2.1 Smoke impacted parks (filled diamonds) and non-impacted parks (open diamonds) for 1-July.

A cold front moved through the southeast U.S. on this day passing MACA, SIPS and UPBU early in the sample period and GRSM, SHRO, DOSO and JEFF late in the sample period. After frontal passage transport to the sites was from regions where known fires were located (Figure 3.2.2).

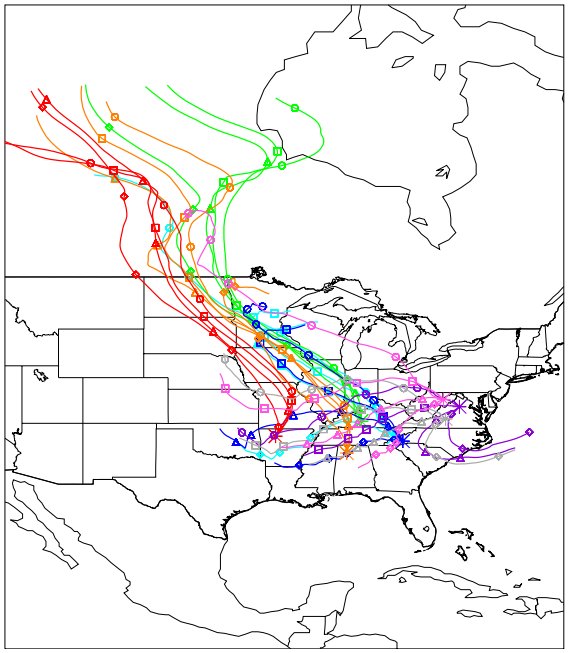

Figure 3.2.2 1-July trajectories calculated using NGM data. Red-UPBU, orange-SIPS, green-MACA, light blue-GRSM, dark blue-SHRO, gray-JEFF, pink-DOSO, purple-SHEN. Symbols mark the position of the air parcel at the end of each day for all five days back from the site. Four representative times are presented: 1 LST (diamonds), 7 LST (triangles), 13 LST (squares), and 19 LST (circles).

On 26 and 27-June several hot spots were detected in the Northwest Territories (Figures 3.2.3 and 3.2.4). Several large hot spots were also detected in Saskatchewan and Manitoba on 27-June (Figure 3.2.4). The fires in Manitoba and Saskatchewan were in the source region for MACA and SIPS for nearly the entire day since the front passed in early morning (Figures 3.2.4 and 3.2.2). The fires in Saskatchewan and the Northwest Territories impacted UPBU all day due to frontal passage early in the sample period (Figures 3.2.4, 3.2.3, and 3.2.2). Transport patterns for MACA, SIPS and UPBU were from known large fire regions and were consistent with the finding of smoke impact on the aerosol samples.

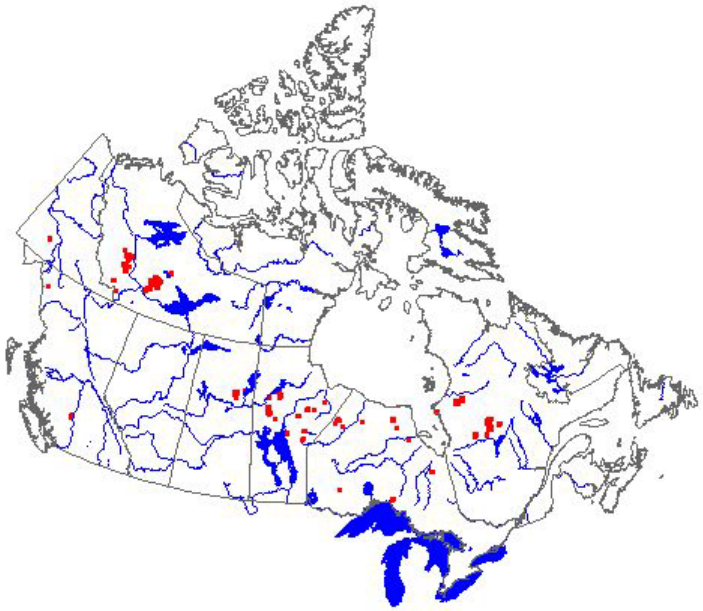

Figure 3.2.3 Hot Spots on 26-June (used without permission from fms.nofc.cfs.nrcan.gc.ca/firem3).

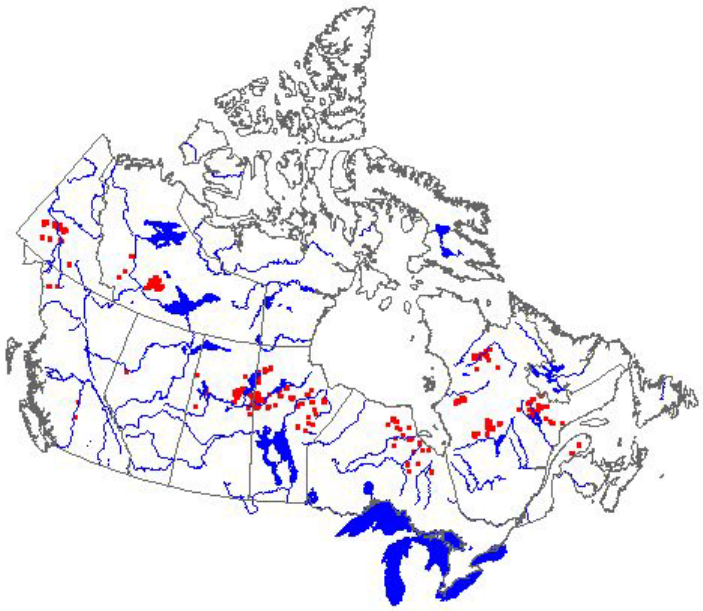

Figure 3.2.4 Hot Spots on 27-June (used without permission from fms.nofc.cfs.nrcan.gc.ca/firem3).

Transport to GRSM and SHRO early in the day was from Oklahoma east to the sites. After frontal passage, the source region was central Minnesota southeast to the

sites. Near the end of the sample period GRSM did have transport from Saskatchewan, but trajectories passed southwest of the hot spots (Figures 3.2.2 and 3.2.3). Early in the day JEFF and SHEN had transport from the Atlantic turning southwest to west throughout the day. The source regions for DOSO, JEFF and SHEN were primarily from Missouri and Arkansas east to the sites (Figure 3.2.2). Transport to GRSM, SHRO, DOSO, SHEN and JEFF was from regions in the U.S. in which no known large fires were burning (data not shown), which is consistent with the finding of no smoke impact on the aerosol samples. On 30-June there was a fire reported on the border of Kentucky and Tennessee north of MACA, but the size and duration are unknown. Based on transport patterns (Figure 3.2.2), if the fire were of substantial size it could have impacted the samples at GRSM, MACA, SHRO and SIPS.

On 8-July the final smoke plume identified by Wotawa and Trainer (2000) was detected in the aerosol data. MACA, GRSM, SHRO, DOSO and SHEN were flagged as smoke impacted on this day (Figure 3.2.5). As identified by Wotawa and Trainer (2000) transport to the smoke impacted parks and JEFF was from Canada (Figure 3.2.6).

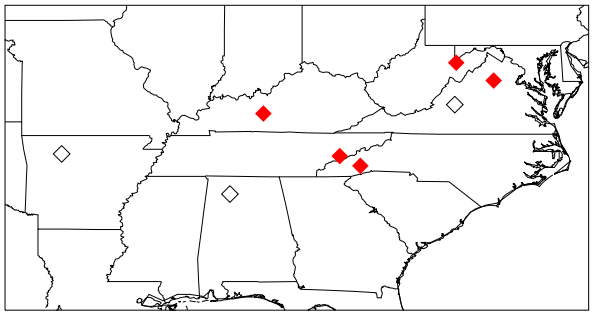

Figure 3.2.5 Smoke impacted parks (filled diamonds) and non-impacted parks (open diamonds) for 8-July.

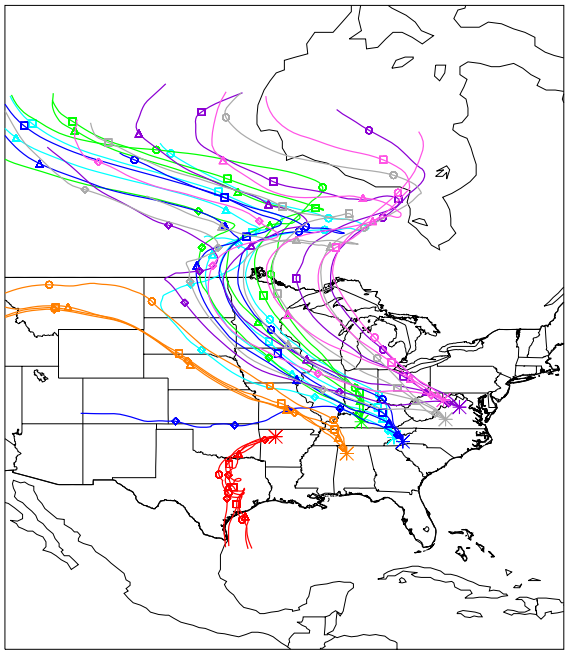

Figure 3.2.6 8-July trajectories calculated using NGM data.

Hot spots detected in Manitoba and Saskatchewan on 4-July (Figure 3.2.7) and 5-July (Figure 3.2.8) were in the source regions for DOSO, SHEN, JEFF, MACA, GRSM and SHRO. In addition, hot spots detected in the Northwest Territories were in the source regions for MACA, GRSM and SHRO on 3-July (Figure 3.2.9) and 4-July (Figure 3.2.7). Transport patterns for MACA, GRSM, SHRO, DOSO and SHEN (Figure 3.2.6) were thus from known fire regions in Canada and consistent with the finding of smoke impact on the aerosol samples. Transport to JEFF was also from known fire regions in Canada, which was not consistent with the finding of no smoke impact on the aerosol sample. Thus, this day was concluded a false negative for smoke impact at JEFF. It is possible that elevation played a role in the finding of no smoke impact at JEFF as well. The elevation of JEFF is 299m above sea level in the Appalachian Mountains. SHEN and DOSO are both located at over 1000m. It is possible the smoke plume was elevated

above the IMPROVE sampler located at JEFF which would be consistent with the finding of no smoke impact there.

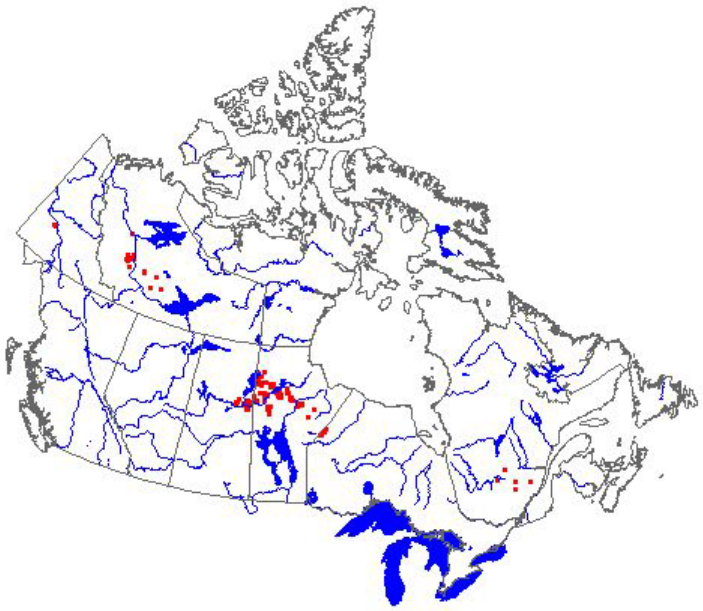

Figure 3.2.7 Hot Spots on 4-July (used without permission from fms.nofc.cfs.nrcan.gc.ca/firem3).

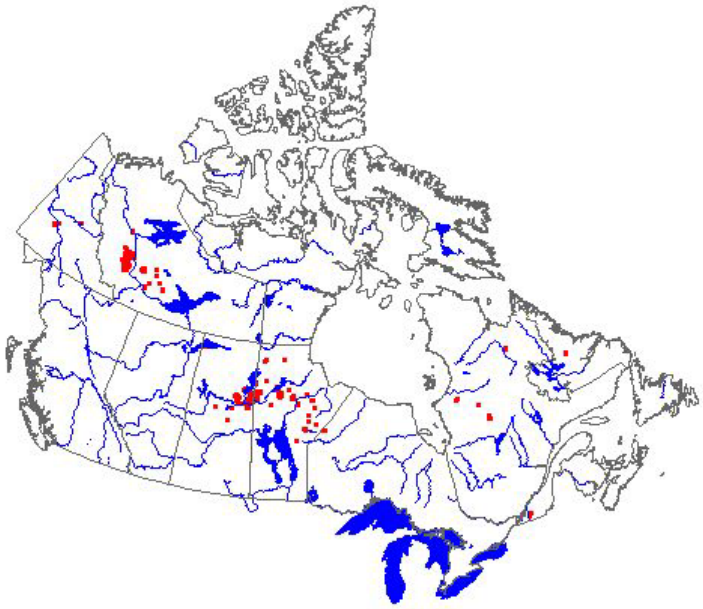

Figure 3.2.8 Hot Spots on 5-July (used without permission from fms.nofc.cfs.nrcan.gc.ca/firem3).

Figure 3.2.9 Hot Spots on 3-July (used without permission from fms.nofc.cfs.nrcan.gc.ca/firem3).

One trajectory from SHEN, DOSO and JEFF passes near large fires in Northern Minnesota on 7-July (Figure 3.2.10). Over the period 9-June to 3-August one fire burned over 3,000 acres, which would mean an average of about 55 acres per day burned, and the other over 1,200 acres from 20-June to 29-July, which is an average of about 32 acres per day. It is possible that these fires contributed to the smoke impact on the aerosol sample at SHEN and DOSO.

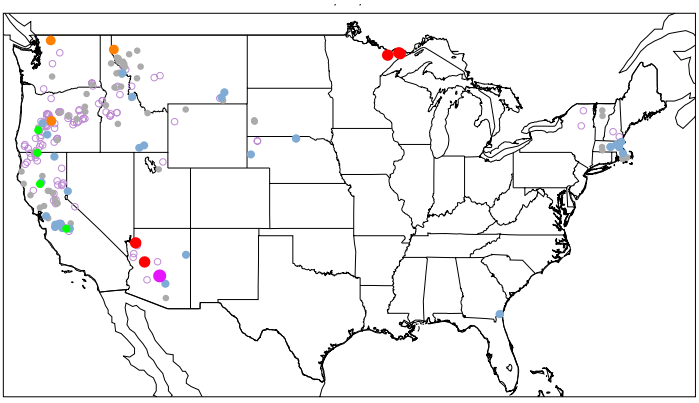

Figure 3.2.10 Wildfires reported on 7-July. Colored dots represent acreage burned by each fire: open purple circles-0 or unknown acreage, gray filled dots-0 to 1 acre, blue-1 to 10 acres, green-10 to 50 acres, orange-100 to 1,000 acres, red-1,000 to 10,000 acres, solid purple-greater than 10,000 acres.

Transport to SIPS was from the Pacific Northwest through Montana and the Central Plains (Figure 3.2.6). On the 4th several small fires were near the trajectories from SIPS, all less than ten acres. One trajectory did pass over a larger fire in Montana on the 4th that burned 395 acres from 30-May through 19-July. Due to the small areas burned by these fires, it is unlikely smoke from them had a measurable impact on SIPS. Transport to UPBU was from the Gulf of Mexico through Texas and Oklahoma (Figure 3.2.6). The fire season in Mexico is usually less active by this time and there were no fires reported in Texas and Oklahoma. Therefore, no known large fires in the source regions for SIPS and UPBU confirmed the finding of no smoke impact on the aerosol samples.

The late June event, identified by Wotawa and Trainer (2000), was not clearly detected in the aerosol data. There was one IMPROVE sample day during this event, which was 28-June. SHEN and SIPS were both missing data on this day. Transport to the sites supports the finding of no smoke impact for this day (Figure 3.2.11).

Transport to DOSO, SHEN and JEFF was east from the Atlantic, which supports the finding of no smoke impact at these parks as there were no fire data for Virginia. MACA and SIPS had trajectories reaching Canada, but they did not reach the hot spots detected on 23-June (Figure 3.2.12). The K_{NON} value at MACA was close to passing the criterion, which might be expected from the CO data reported by Wotawa and Trainer (2000). The K_{NON} values at GRSM and SHRO were not close to passing their criteria and primarily had transport from the Gulf Coast. There were no fires reported in the U.S. that were near the sites or their trajectories at this time, which further supports the finding of no smoke impact in the region.

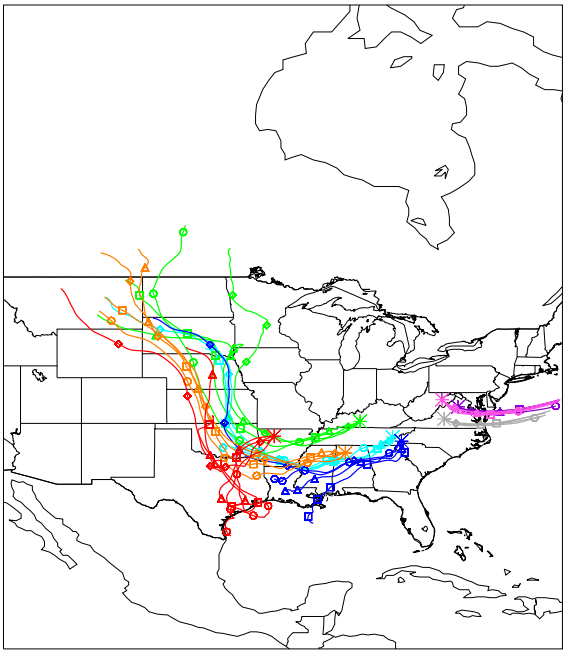

Figure 3.2.11 28-June trajectories calculated using NGM data.

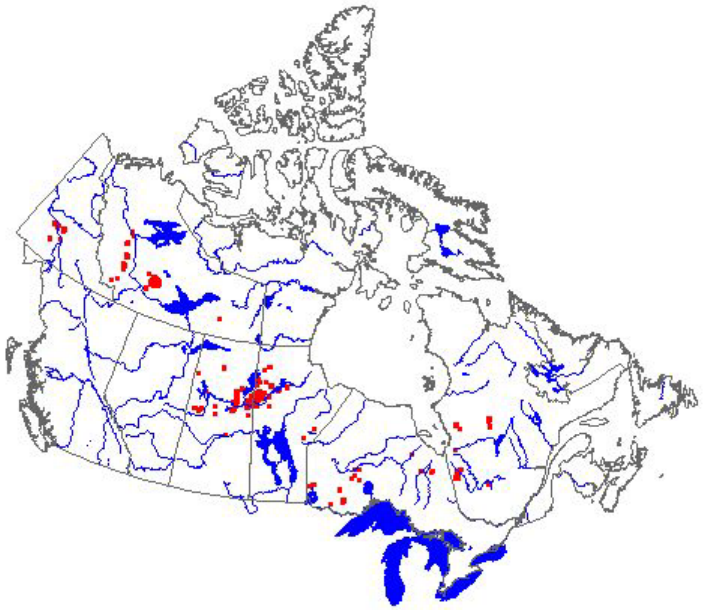

Figure 3.2.12 Hot Spots on 23-June (used without permission from fms.nofc.cfs.nrcan.gc.ca/firem3).

14-June and 17-June were flagged smoke impacted at UPBU. Transport patterns on both days suggest Canada and Northern Minnesota as the sources for the smoke impact (Figures 3.2.13 and 3.2.14).

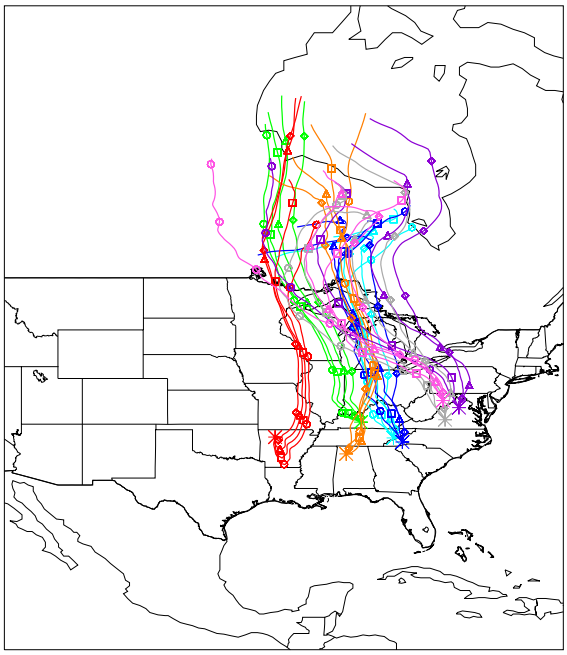

Figure 3.2.13 14-June trajectories calculated using NGM data.

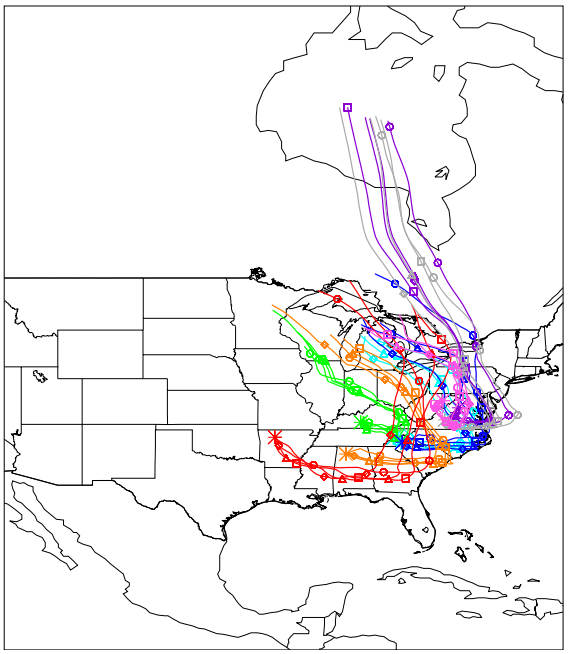

Figure 3.2.14 17-June trajectories calculated using NGM data.

On 14-June UPBU was the only park with high K_{NON}. Both UPBU and MACA had multiple trajectories near the large fire in Minnesota on 11-June (Figure 3.2.15), unfortunately MACA was missing data for 14-June. Over the period 9-June to 3-August the fire burned over 3,000 acres, which would mean an average of about 55 acres per day burned. In addition, UPBU and MACA had trajectories near a few hot spots in Manitoba on 10-June (Figure 3.2.16). SHEN, DOSO and JEFF each had one trajectory near the fires in Minnesota and Canada near the end of the sample period, which is not thought to be enough to result in significant smoke impact at these parks. Thus, DOSO, SHEN and JEFF are not considered false negative for smoke impact on 14-June.

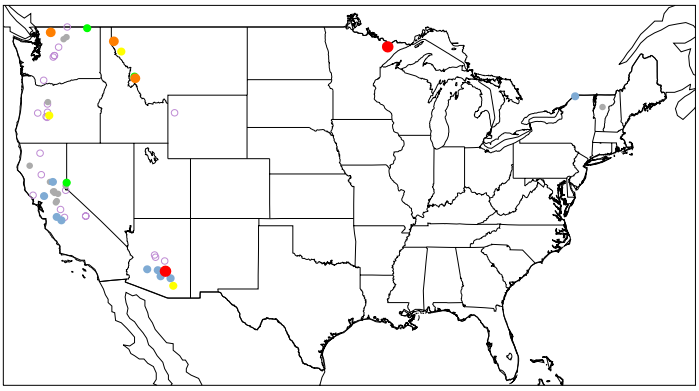

Figure 3.2.15 Wildfires reported on 11-June.

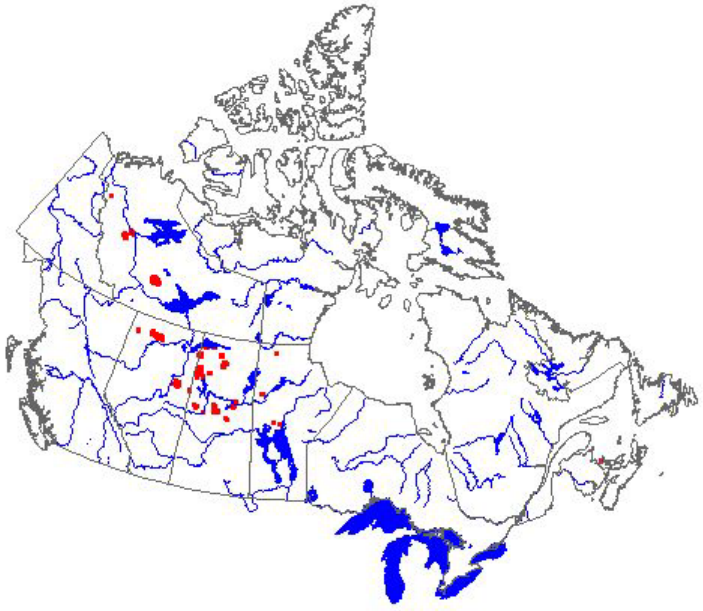

Figure 3.2.16 Hot Spots on 10-June (used without permission from fms.nofc.cfs.nrcan.gc.ca/firem3).

Based on the transport patterns, U.S. fire map and hot spots the smoke impact at UPBU is consistent. GRSM, SHRO and SIPS did not have any trajectories near fires in the U.S. or hot spots in Canada, which is consistent with the finding of no smoke impact at these parks.

Although only UPBU passed the criterion on 17-June, SHEN, GRSM and SHRO were all close to passing and JEFF had the highest K_{NON} for the study period. Trajectories indicated Canada and the Great Lakes region as the source regions for all parks except MACA and SIPS. Transport to MACA and SIPS was from Wisconsin southeast turning due west to the sites. Several hot spots were detected on 12-June north of Lake Superior near the trajectories for UPBU, SHRO, SHEN and JEFF (Figure 3.2.17). In addition, trajectories for UPBU also ended near the fire in Northern Minnesota on 12-June (Figure 3.2.18). There were no other fires in the U.S. near the trajectories for any of the parks (see Appendix B for additional fire maps).

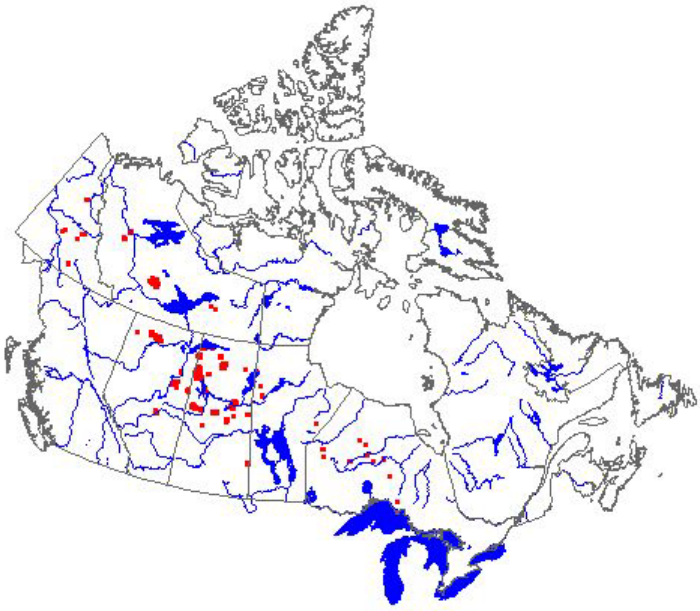

Figure 3.2.17 Hot Spots on 12-June (used without permission from fms.nofc.cfs.nrcan.gc.ca/firem3).

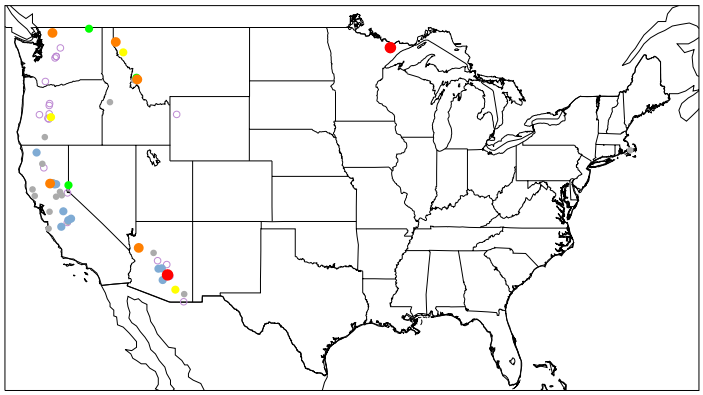

Figure 3.2.18 Wildfires reported on 12-June.

Although the individual hot spots in Canada on 12-June were not large in area, they were numerous. Thus, it is believed that smoke from the fires in Canada and Minnesota impacted the sample at UPBU. Trajectories and fire (hot spot) maps confirm the presence of smoke aerosols at UPBU and the findings of no smoke impact at all other parks.

3.3 Other 1995 Smoke Events

Three regional smoke events that are believed to be from fires in the Yucatan, Central America and Cuba were identified. The first event was in mid-April, followed by two in mid-May and one in early June. There were no fire data available for Mexico, Central America or Cuba that detailed the dates, locations or sizes of fires in 1995. However, it is known that biomass burning occurs in this region during late spring and early summer (Kreidenweis et al., 2001 and Figure 3.3.1).

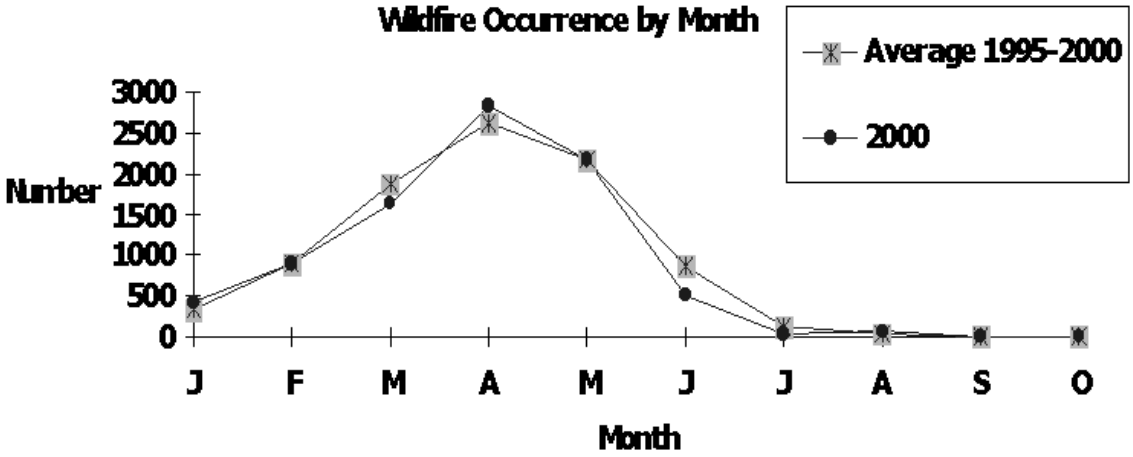

Figure 3.3.1 Wildfire Occurrence by Month in Mexico (used without permission from http://www.fire.uni-freiburg.de/inventory/stat/mx/mex2001.htm).

It is also suggested that there were sources of high CO in the Yucatan and Cuba during the summer of 1995 (Figure 1.1.1). Global reanalysis data were used to recalculate the trajectories for these days due to the grid domain of the NGM data ending too far north.

On 19-April GRSM, SHRO, DOSO and SIPS were flagged smoky (Figure 3.3.2). Trajectories indicate the Yucatan and Cuba as the primary source region for the smoky parks (Figures 3.3.3a and 3.3.3b). JEFF and SHEN also had transport from this region, which was not consistent with the finding of no smoke impact on the aerosol samples. Thus, this day was concluded to be a false negative for smoke impact at JEFF and SHEN.

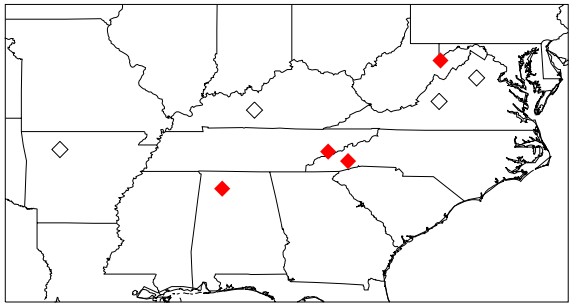

Figure 3.3.2 Smoke impacted parks (filled diamonds) and non-impacted parks (open diamonds) for 19-April.

It is also likely that fires near the sites influenced the parks flagged as smoke impacted on 19-April (Figure 3.3.4). There were two fires between DOSO and SHEN and two near SHRO and GRSM on the sample day.

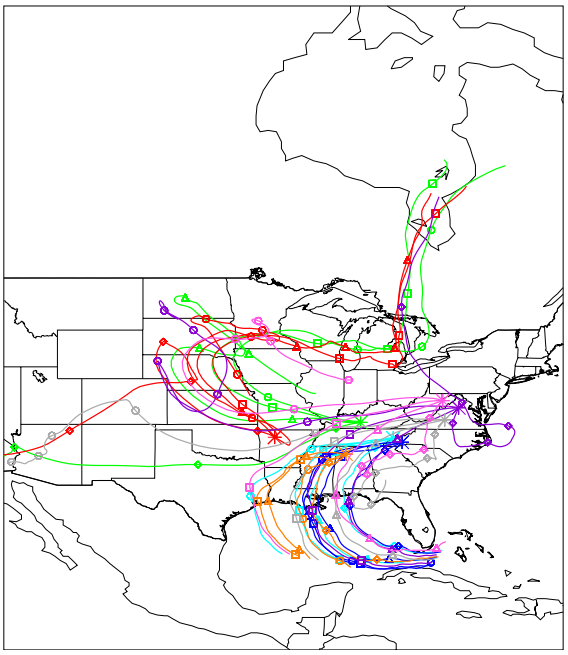

Figure 3.3.3a 19-April trajectories calculated using NGM data.

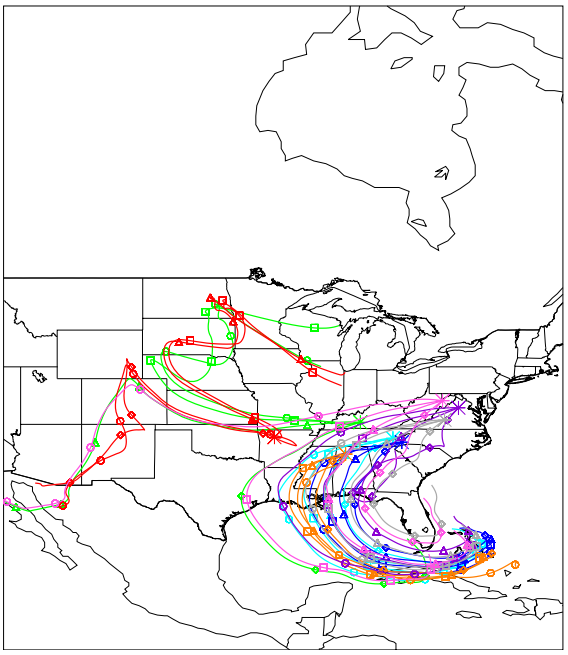

Figure 3.3.3b 19-April trajectories calculated using reanalysis data.

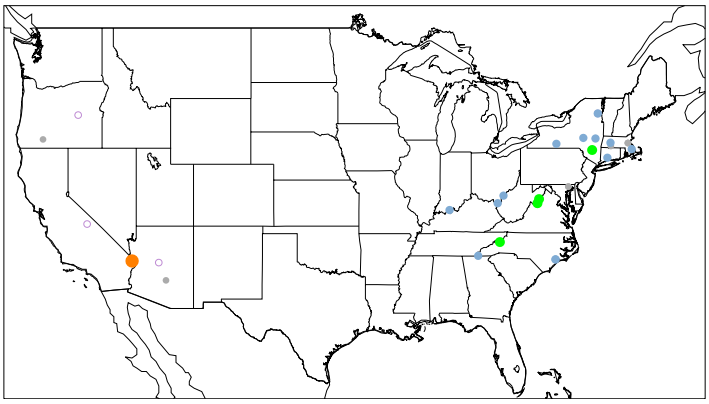

Figure 3.3.4 Wildfires reported on 19-April. Colored dots represent acreage burned by each fire: open purple circles-0 or unknown acreage, gray filled dots-0 to 1 acre, blue-1 to 10 acres, green-10 to 50 acres, orange-100 to 1,000 acres, red-1,000 to 10,000 acres, solid purple-greater than 10,000 acres.

Trajectories for the parks flagged as non-smoky, MACA and UPBU, extended northwest from the sites through the Central Plains, east to Michigan and for part of the day, north to James Bay (Figures 3.3.3a and b). Early in the sample period transport to MACA was from the Southwest U.S. Fires less than ten acres in Michigan and Arizona were near the trajectories for MACA, UPBU, DOSO and JEFF. No large fires near the trajectories for MACA and UPBU confirms the finding of no significant smoke impact on the aerosol data at these parks.

On 13-May GRSM, MACA, SHRO, SIPS and UPBU were flagged smoky and JEFF was missing data (Figure 3.3.5). Transport to MACA, SIPS and UPBU was from the Yucatan and Cuba for over half of the sample period (Figures 3.3.6a and 3.3.6b). GRSM and SHRO also had transport from this region later in the sample period.

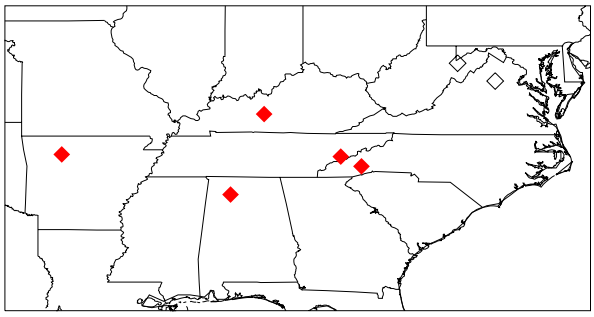

Figure 3.3.5 Smoke impacted parks (filled diamonds) and non-impacted parks (open diamonds) for 13-May.

The transport patterns for GRSM, SHRO, MACA, SIPS and UPBU and the understanding that biomass burning occurs in the region of the Yucatan and Cuba at this time of year were consistent with the finding of smoke impact on the aerosol samples at these sites.

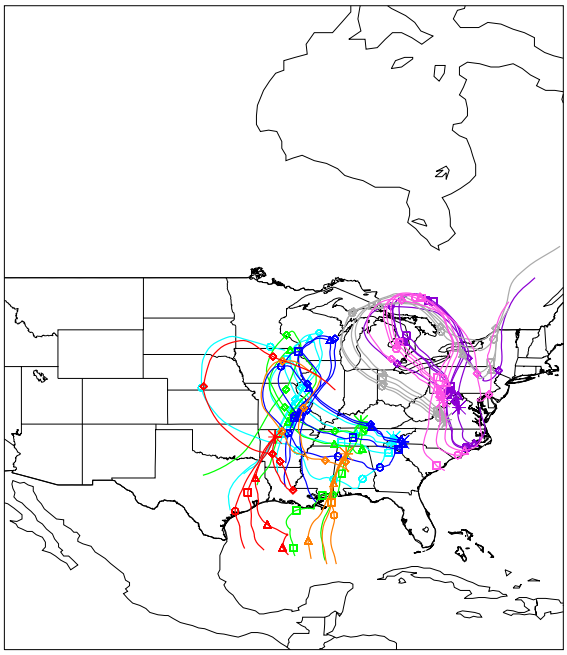

Figure 3.3.6a 13-May trajectories calculated using NGM data.

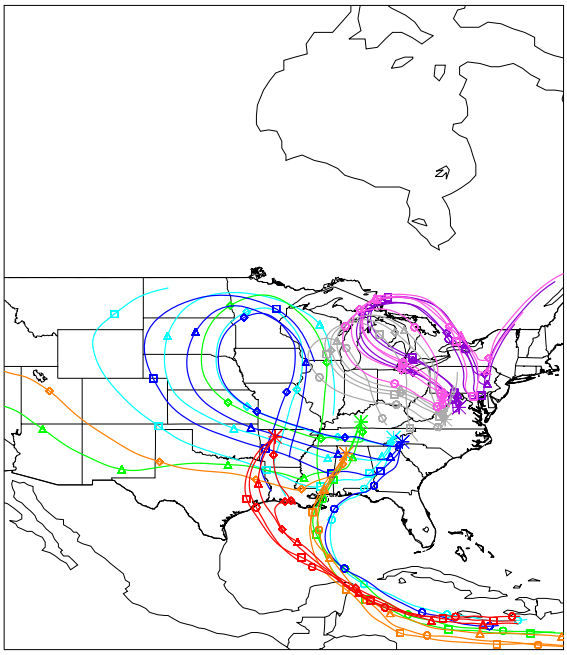

Figure 3.3.6b 13-May trajectories calculated using reanalysis data.

The source region for the non-smoky parks, DOSO and SHEN, was from Michigan east to Lake Ontario and south to the Carolinas (Figures 3.3.6a and b). There was a small fire between DOSO and SHEN that burned less than ten acres from the 7th through the 11th and another on the North Carolina coast from the 7th through the 9th that burned less than ten acres. There were no fires near the sites on 13-May, but DOSO, SHEN and JEFF had trajectories near fires in New England on 8 and 9-May (Figures 3.3.7 and 3.3.8). All fires near the trajectories were less than 50 acres and were likely too small to have a significant impact on the aerosol samples at all three parks. Thus, the transport patterns for DOSO and SHEN were consistent with the finding of no smoke impact in the aerosol data.

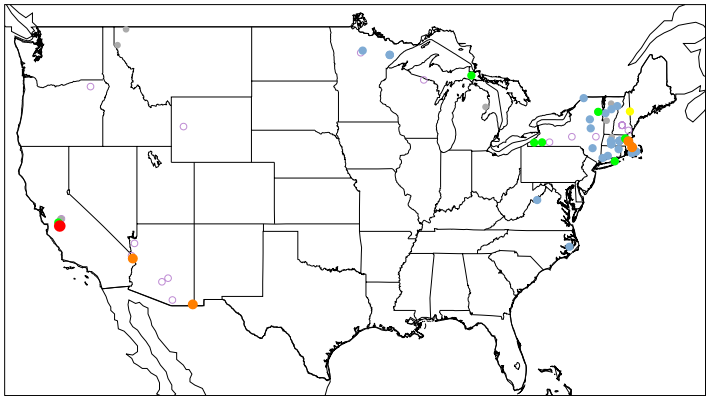

Figure 3.3.7 Wildfires reported on 8-May. Colored dots represent acreage burned by each fire: open purple circles-0 or unknown acreage, gray filled dots-0 to 1 acre, blue-1 to 10 acres, green-10 to 50 acres, yellow-50 to 100 acres, orange-100 to 1,000 acres, red-1,000 to 10,000 acres.

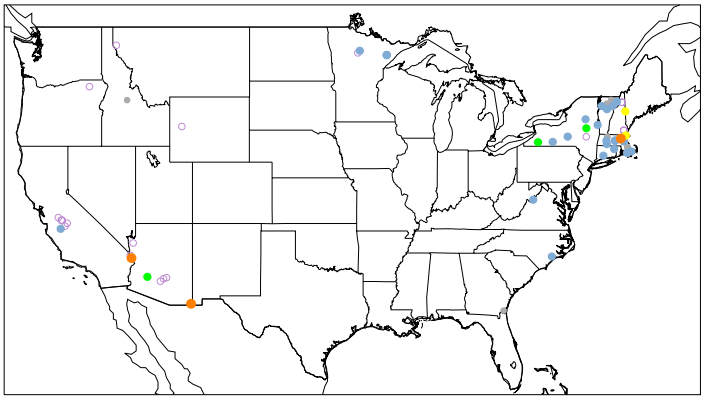

Figure 3.3.8 Wildfires reported on 9-May.

On 17-May DOSO, MACA, GRSM, SHRO, SIPS and UPBU were flagged smoky (Figure 3.3.9). Transport to GRSM, MACA, SHRO, SIPS and UPBU was from the Yucatan and Cuba with the exception of some early morning transport to GRSM and SHRO from the Central Plains (Figures 3.3.10a and 3.3.10b). Later in the sample period, transport to JEFF, DOSO and SHEN was also from the Yucatan and Cuba. The transport patterns for all parks except JEFF and SHEN support the finding of smoke impact on the

aerosol samples at these sites. Based on the trajectories, JEFF and SHEN should also have been flagged as smoke influenced, but were not. This day is considered false negative for smoke impact at JEFF and SHEN.

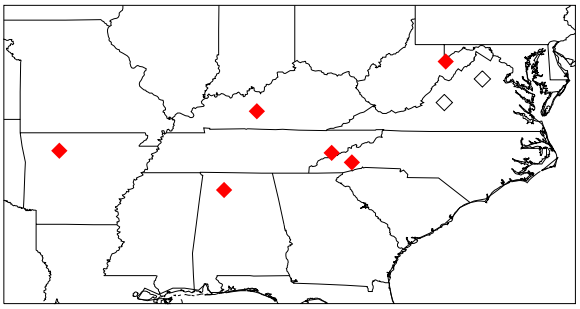

Figure 3.3.9 Smoke impacted parks (filled diamonds) and non-impacted parks (open diamonds) on 17-May.

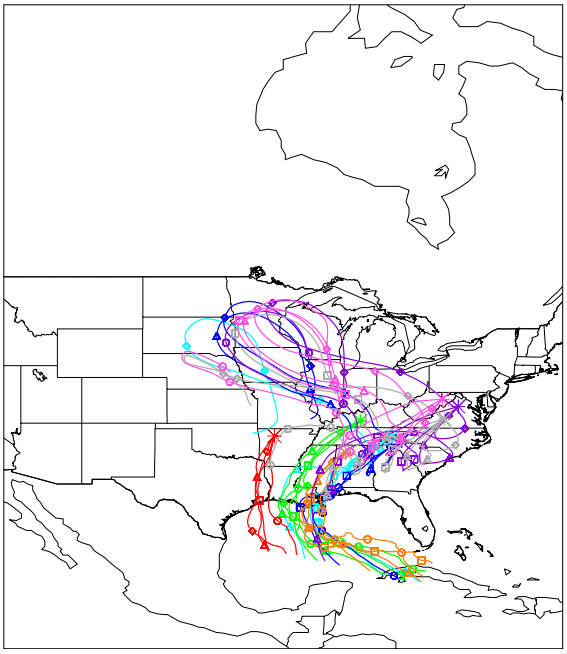

Figure 3.3.10a 17-May trajectories calculated using NGM data.

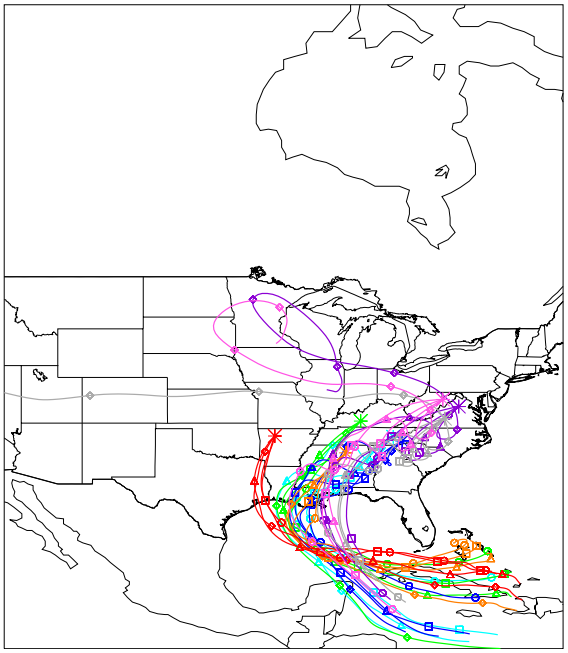

Figure 3.3.10b 17-May trajectories calculated using reanalysis data.

On 10-June GRSM, SHRO, DOSO and SHEN were flagged as smoke influenced and MACA was missing data (Figure 3.3.11). Based on reanalysis data, transport to all parks was primarily from the Gulf indicating Mexico or Central America as the source

for smoke impact (Figure 3.3.12b). Trajectories based on NGM data differ in that DOSO and SHEN had transport from Canada (Figure 3.3.12a). There were no fires near the sites on 10-June nor near the trajectories in the U.S. and Canada. Thus, it is concluded that the parks flagged smoky were such due to fires in Mexico and Central America and that JEFF, SIPS and UPBU were false negative for smoke impact on 10-June.

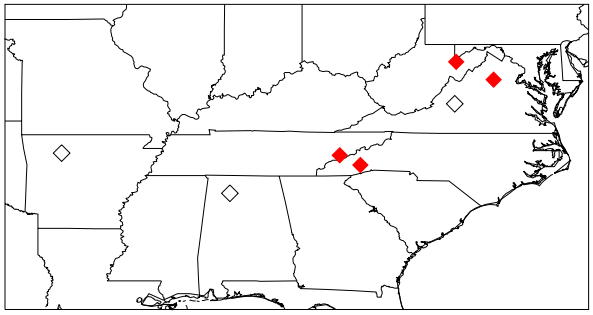

Figure 3.3.11 Smoke impacted parks (filled diamonds) and non-impacted parks (open diamonds) for 10-June.

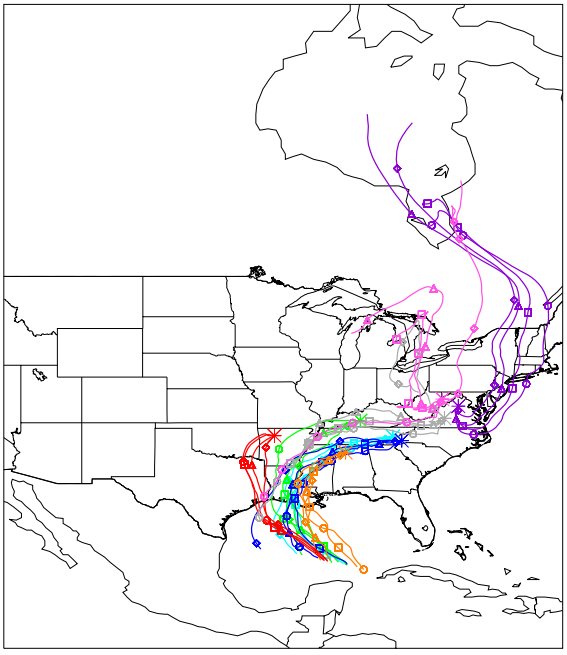

Figure 3.3.12a 10-June trajectories calculated using NGM data.

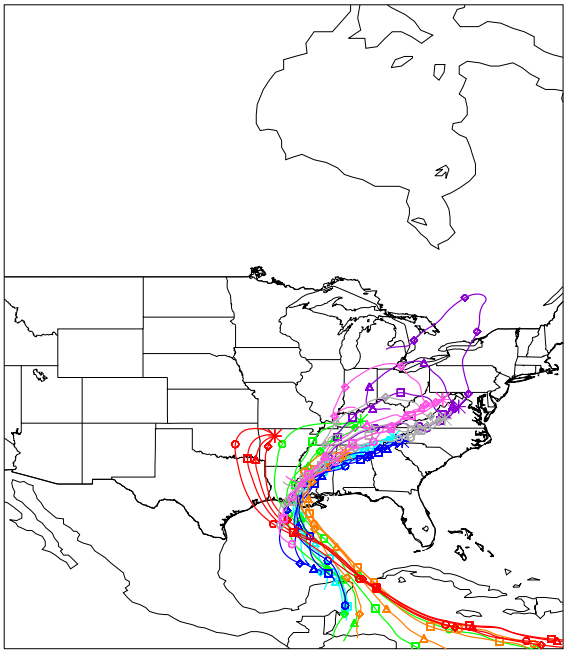

Figure 3.3.12b 10-June trajectories calculated using reanalysis data.

3.4 Summary of Findings for 1995

Table 3.4.3 summarizes the findings for 1995. Overall there were 26 aerosol samples determined to be influenced by smoke from fires in Mexico and Central America and six from fires in the U.S. Smoke from fires in Canada influenced a total of eleven aerosol samples. North African dust was indicated in a total of 22 samples. One of the 22 aerosol samples thought to be influenced by non-local dust were in April, two in May and 19 in July. Five samples were false positive for smoke impact and eight were false negative for smoke impact. A total of twelve observations were missing, six of which were at SIPS. Four of the eight false negatives were at JEFF, which also had the highest criterion of all eight parks. It is speculated that the location of JEFF in a valley between fairly high peaks in the Appalachian Mountains is a factor, either trapping smoke or with the trajectory model unable to properly handle the terrain effects.

Observations flagged as false positive could be inaccurately labeled as such due to a lack of fire data or inaccurate back-trajectories. The National Fire Occurrence Database does not contain information on prescribed burns and was missing data for Pennsylvania, South Carolina and Virginia in 1995. In addition, satellite detected hot spots are limited by clouds and nighttime detection. As stated earlier, there is error associated with the back-trajectories. Being that some sites investigated are located where there is complex terrain the model could inaccurately calculate the transport patterns. Similarly, it is possible that an elevated plume, which is not sampled at the ground station, or precipitation along a transport path (Section 3.5), which would remove smoke particles from the air, could cause an aerosol sample to not have signs of smoke impact and inaccurately be labeled as false negative for smoke impact.

Table 3.4.3 Summary of Results for 1995. 'MX'-Smoke impact from Mexico, 'Cen.A'-Smoke impact from Central America, 'US'-Smoke impact from the U.S., 'CA'-Smoke impact from Canada, 'False –' – False negative for smoke impact, 'False +' –False positive for smoke impact, 'NAD'-North African Dust impact, 'AD'-Asian Dust impact.

Date	DOSO	GRSM	JEFF	MACA	SHEN	SHRO	SIPS	UPBU
15-Apr								
19-Apr	MX/Cen.A /US	MX/Cen.A /US	False -		False -	MX/Cen.A/ US	MX/Cen.A/ US	
22-Apr							NAD	
26-Apr								
29-Apr								
3-May	Missing							
6-May								
10-May					NAD			
13-May		MX/Cen.A NAD	Missing	MX/Cen. A		MX/Cen.A	MX/Cen.A	MX/Cen.A
17-May	MX/Cen.A	MX/Cen.A	False -	MX/Cen. A	False -	MX/Cen.A	MX/Cen.A	MX/Cen.A
20-May								
24-May							Missing	
27-May								
31-May							Missing	
3-Jun								
7-Jun						False +		
10-Jun	MX/Cen.A	MX/Cen.A	False -	Missing	MX/Cen. A	MX/Cen.A	False -	False -
14-Jun				Missing				CA
17-Jun								CA
21-Jun								False +
24-Jun								
28-Jun					Missing		Missing	
1-Jul				CA	Missing		CA	CA
5-Jul	NAD	NAD	NAD	NAD	NAD	NAD	Missing	
8-Jul	CA	CA	False -	CA	CA	CA		NAD
12-Jul					False +		Missing	
15-Jul	False +				False +			
19-Jul							Missing	
22-Jul								
26-Jul	NAD	NAD	NAD	NAD	NAD	NAD	NAD	
29-Jul	NAD		NAD	NAD	NAD			NAD

3.5 Effects of Precipitation

Aerosol samples considered to be false negative for smoke impact could actually have had no smoke impact due to removal of particles by precipitation. Synoptic data, e.g. radar summaries, were not readily available for all years, but rainfall rates along the back trajectories are available if trajectories are run on the HYSPLIT website. One example is presented here for 10-June 1995. Rainfall rates for GRSM, which was flagged smoke impacted, and for SIPS, which was flagged as false negative for smoke impact, are compared (Figures 3.5.1 and 3.5.2).

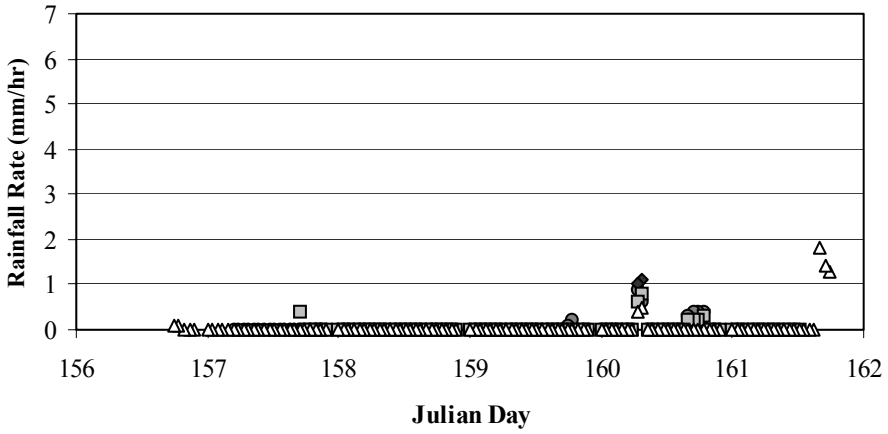

Figure 3.5.1 Rainfall rates (mm/hr) for GRSM using NGM data beginning on 10-June (Julian day 161). Circles – 1AM LST, diamonds – 7AM LST, squares – 1PM LST, and triangles – 7PM LST.

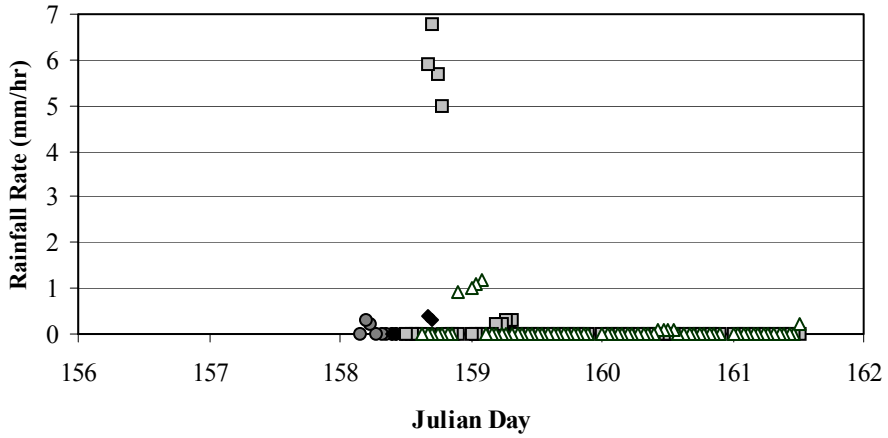

Figure 3.5.2 Rainfall rates (mm/hr) for SIPS using NGM data beginning on 10-June (161). Circles – 1AM LST, diamonds – 7AM LST, squares – 1PM LST, and triangles – 7PM LST.

Although both parks had transport from similar regions (Figure 3.3.12a) the K_{NON} value at SIPS did not pass the criterion. From Figure 3.5.2 it can be seen that there was heavy rainfall on 7-June (Julian day 158) along the afternoon back trajectory for SIPS. Rainfall rates were between 5 and 7 mm/hr for approximately four hours. In addition, along the evening back trajectory for SIPS there was another four hour period where rainfall rates were around 1 mm/hr. In contrast, rainfall rates along the GRSM back trajectories never exceed 2 mm/hr and did not persist as long as the rainfall along the SIPS back trajectories. The most persistent rainfall for GRSM was along the early morning trajectory, which had light rainfall on 9-June at a rate of about 0.4 mm/hr for about four hours. The heavy rainfall along the SIPS trajectories suggests that precipitation contributed to the finding of no smoke impact on the aerosol sample there, despite having transport from a region thought to be impacted by smoke. Based on the results for 10-June, rain along a trajectory that occurs after the parcel has passed through a fire-impacted region is a plausible explanation for a finding of no smoke impact on an aerosol sample when smoke impact was expected.

Chapter 4. Results for 1998 and Summary of All Years

4.1 K_{NON} and 1998 Smoke Impacted Days

The medians, smoke criteria and values of K_{NON} for 15-April through 31-July 1998 are shown in Figure 4.1.1a and Figure 4.1.1b. The same K_{NON} equations and smoke criteria were applied for 1998 as for 1995. Different meteorological data were used for HYSPLIT due to availability of data. Similarly, different fire data were used in 1998 because global satellite retrieved hot spots were available after 1997.

From 15-April through 31-July there were a total of 239 observations in the region of which 32 aerosol samples were flagged as smoke impacted (Table 4.1.1). As in 1995, trajectory maps were compared to the hot spot maps and days flagged smoke impacted that did not have trajectories near fires were considered false positive for smoke impact. Days not flagged smoke impacted that had transport from a known fire region or trajectories crossing large fire areas are considered false negative for smoke impact. Of the 32 smoke impacted observations five were concluded to be false positive and six false negative for smoke impact.

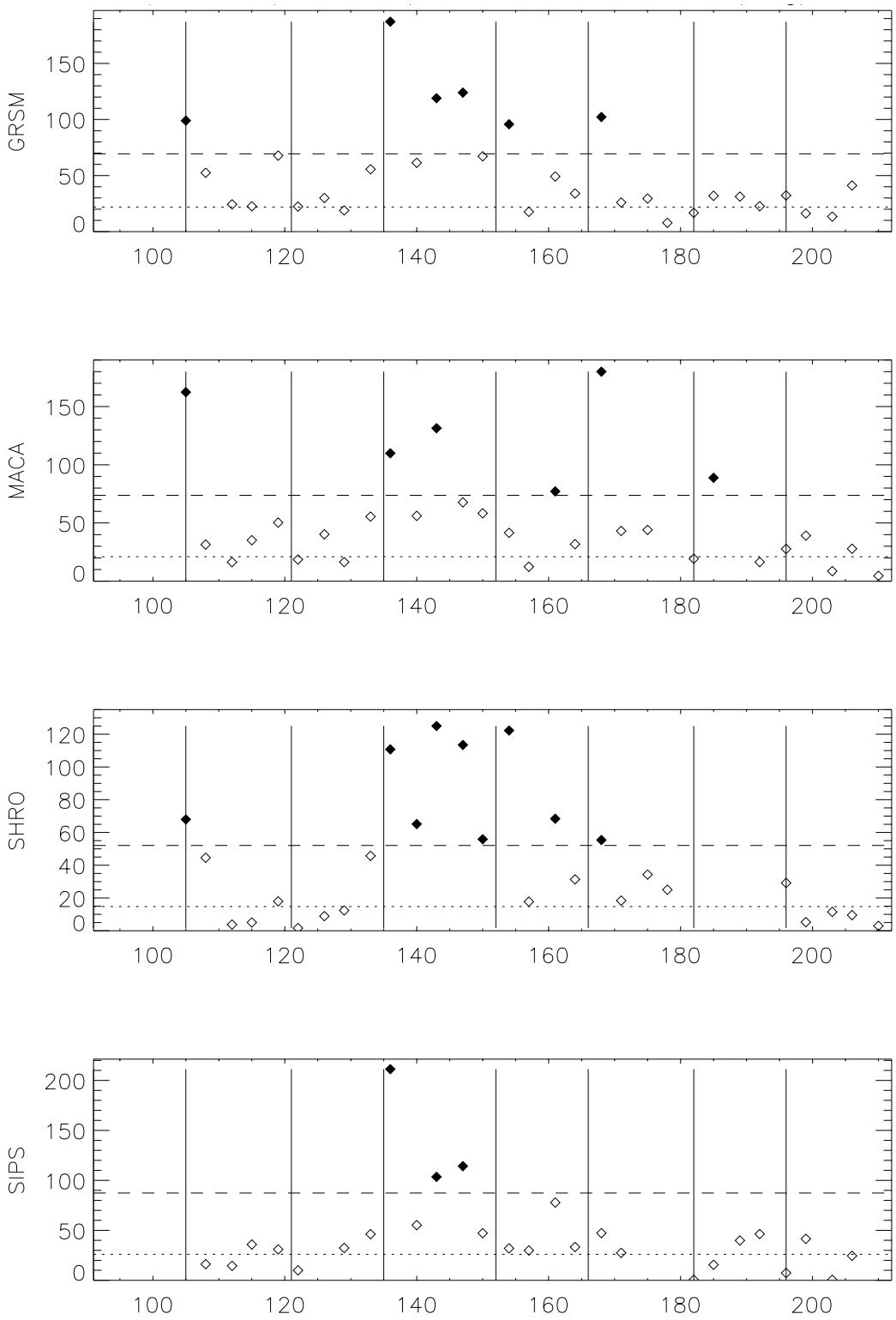

Figure 4.1.1a 4/15 through 7/31 1998 K_{NON} (ng/m^3) values for parks in the SOS95 region. Numbers along x-axis indicate Julian day where 105 is 15-April. Dotted lines indicate median value; dashed lines indicate background values and filled diamonds smoke impacted days. Vertical lines indicate the first and fifteenth of each month, April through July.

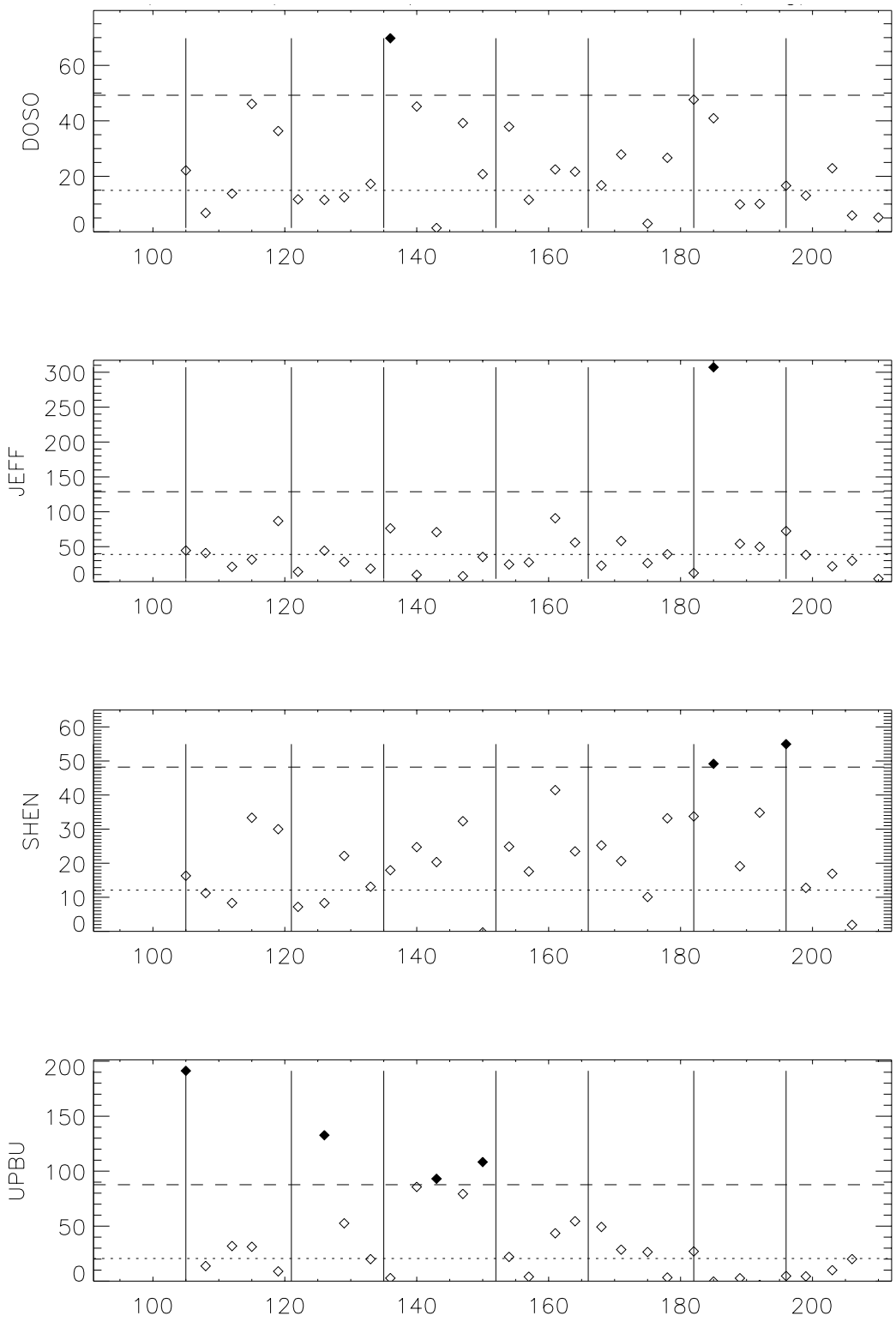

Figure 4.1.1b 4/15 through 7/31 1998 K_{NON} (ng/m^3) values for parks outside the SOS95 region. Numbers along x-axis indicate Julian day where 105 is 15-April. Dotted lines indicate median value; dashed lines indicate background values and filled diamonds smoke impacted days. Vertical lines indicate the first and fifteenth of each month, April through July.

Table 4.1.1 Number of Observations, Smoky Flags and False Flags.

Park	Number of Observations 4/15/98 - 7/31/98					Park	Number of Days Flagged Smoky 4/15/98 - 7/31/98				
	April	May	June	July	Total		April	May	June	July	Total
DOSO	5	9	8	9	31	DOSO	0	1	0	0	1
GRSM	5	9	8	9	31	GRSM	1	3	2	0	6
JEFF	5	9	8	9	31	JEFF	0	0	0	1	1
MACA	5	9	8	9	31	MACA	1	2	2	1	6
SHEN	5	9	8	9	31	SHEN	0	0	0	2	2
SHRO	5	9	8	5	27	SHRO	1	5	3	0	9
SIPS	4	8	7	8	27	SIPS	0	3	0	0	3
UPBU	5	8	8	9	30	UPBU	1	3	0	0	4
Total	39	70	63	67	239	Total	4	17	7	4	32
Park	Number of False Positives 4/15/98 - 7/31/98					Park	Number of False Negatives 4/15/98 - 7/31/98				
	April	May	June	July	Total		April	May	June	July	Total
DOSO	0	0	0	0	0	DOSO	0	0	0	1	1
GRSM	0	0	1	0	1	GRSM	0	1	0	0	1
JEFF	0	0	0	0	0	JEFF	0	1	0	0	1
MACA	0	0	1	1	2	MACA	0	1	0	0	1
SHEN	0	0	0	1	1	SHEN	0	1	0	0	1
SHRO	0	0	1	0	1	SHRO	0	0	0	0	0
SIPS	0	0	0	0	0	SIPS	0	0	0	0	0
UPBU	0	0	0	0	0	UPBU	0	1	0	0	1
Total	0	0	3	2	5	Total	0	5	0	1	6

There were three samples considered false positive for smoke impact in June. They were all on 17-June at GRSM, MACA and SHRO. Trajectories for these parks were not near any hot spots and are the reason for the false positive flags. The remaining two false positives were in July at MACA on 4-July and SHEN on 15-July. Again, trajectories on these days, at these parks, did not pass near hot spots. Of the six samples considered false negative for smoke impact five were in May and one in July. These days will be discussed later in this chapter. For 10-June MACA and SHRO were flagged as smoke impacted, but could not be confirmed because from 4-June through 8-June hot spot retrievals were missing from the data. This day is not considered false positive for either MACA or SHRO because of the missing fire data.

4.2 April, May and June Smoke Events

In 1999, International Forest Fire News (IFFN) reported the 1998 season was Mexico's worst fire season on record. Figure 4.2.1 compares the average area burned by month from 1992 through 1997 to the area burned in 1998. During April, May and June 1998 over 2.5 times the average area burned for each month, 1992-1997, was consumed by fire. July was over 3.5 times higher than average.

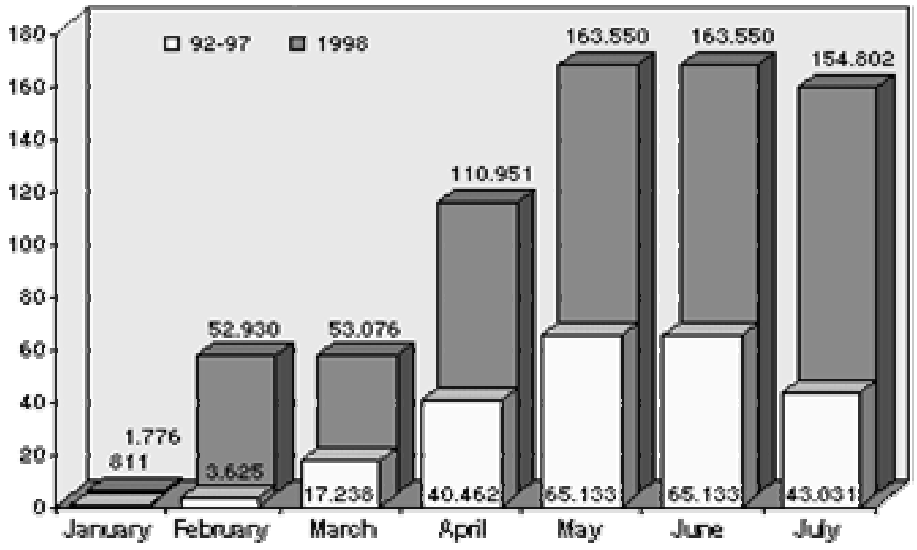

Figure 4.2.1 Mexico comparative burned area. (IFFN, 1999. Reprinted without permission from http://www.fire.uni-freiburg.de/iffn/country/mx/mx_3.htm)

In May 1998 images from the GOES-8 satellite clearly show smoke from the fires in Mexico covering the Gulf of Mexico and extending northward into the U.S. Smoke was transported into Texas and the southeastern U.S. containing high levels of particulate matter that resulted in the issuance of a public health alert in Texas (Kreidenweis et al., 2001).

On 15-April the first influence from fires in Mexico, Cuba and Central America was detected in the study region. GRSM, MACA, SHRO and UPBU were flagged as smoke impacted and SIPS was missing data (Figure 4.2.2).

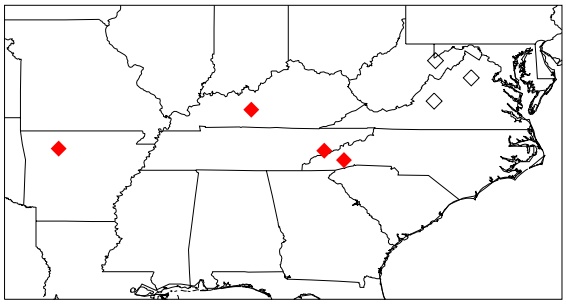

Figure 4.2.2 Smoke impacted parks (filled diamonds) and non-impacted parks (open diamonds) for 15-April.

Transport patterns differ slightly between FNL and EDAS data (Figures 4.2.3a and 4.2.3b). In both cases transport to DOSO and SHEN is different from the smoke impacted parks and JEFF. FNL and EDAS trajectories for UPBU pass near fires in Mexico on 11-April (Figure 4.2.4). FNL trajectories for MACA, GRSM and SHRO pass near fires in Mexico on 12-April and Cuba on 13-April (Figure 4.2.5 and 4.2.6). JEFF has similar patterns, according to the FNL trajectories, to MACA, GRSM and SHRO although the trajectories do not extend as far south. The EDAS trajectories for GRSM and SHRO do not extend as far south as the FNL trajectories and therefore do not pass over the fires in Cuba on 13-April.

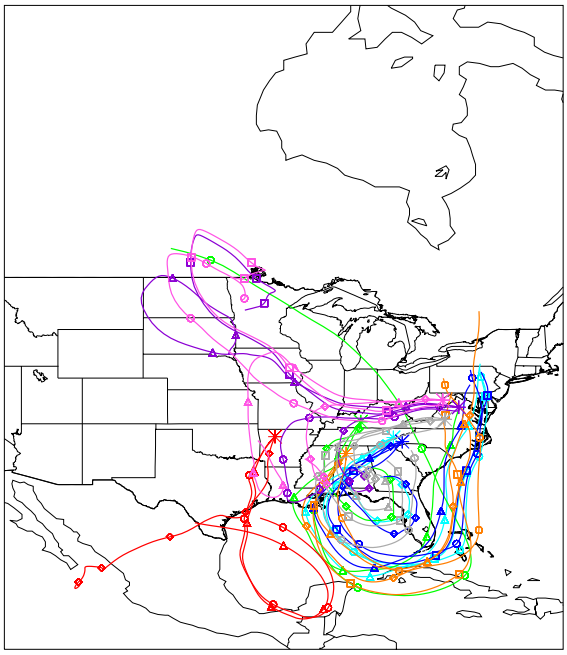

Figure 4.2.3a 15-April trajectories calculated using FNL data.

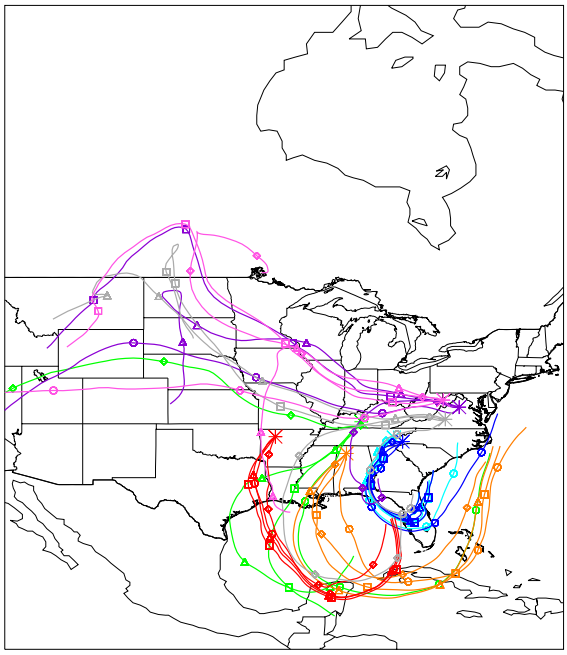

Figure 4.2.3b 15-April trajectories calculated using EDAS data.

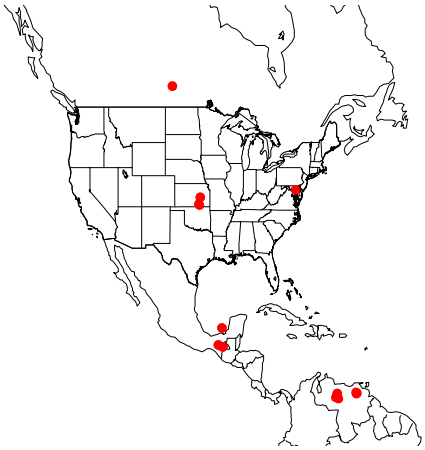

Figure 4.2.4 Hot spots detected on 11-April.

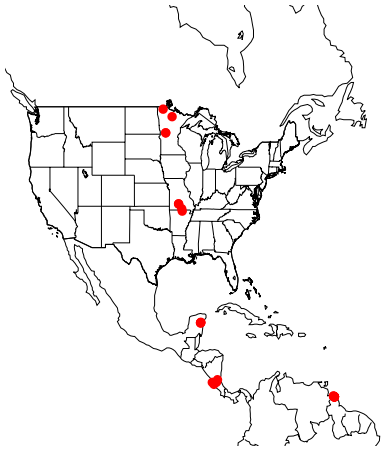

Figure 4.2.5 Hot spots detected on 12-April.

Figure 4.2.6 Hot spots detected on 13-April.

EDAS and FNL trajectories and hot spot maps confirm the finding of no smoke impact on the aerosol samples at DOSO, JEFF and SHEN. EDAS and FNL trajectories and hot spot maps also all confirm the finding of smoke impact on the aerosol sample at UPBU. FNL trajectories and hot spot maps confirm the finding of smoke impact on the aerosol samples at GRSM, MACA and SHRO.

After 15-April transport patterns were not favorable for smoke transport from Mexico and Central America again until 6-May at UPBU and SIPS and 16-May at all other parks. On 6-May UPBU was the only park flagged as smoke impacted and SIPS was missing data (Figure 4.2.7).

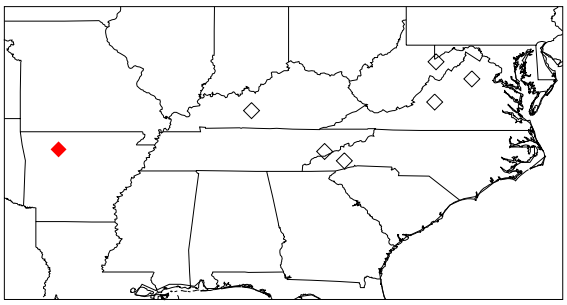

Figure 4.2.7 Smoke impacted parks (filled diamonds) and non-impacted parks (open diamonds) for 6-May.

Trajectories confirm that transport for the non-impacted parks was from the central U.S. and Canada whereas transport to UPBU was from the Gulf of Mexico and the Yucatan (Figures 4.2.8a and 4.2.8b). Although the FNL trajectories do not reach the fire regions indicated by the hot spot maps (Figures 4.2.9 and 4.2.10) it is known that the extreme drought and stagnant air mass over Mexico caused smoke to build up in the region and extend into the Gulf (Kreidenweis et al., 2001).

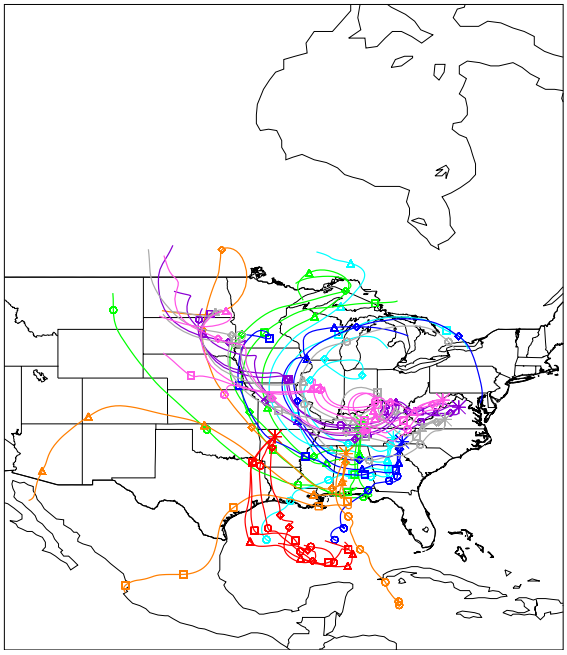

Figure 4.2.8a 6-May trajectories calculated using FNL data.

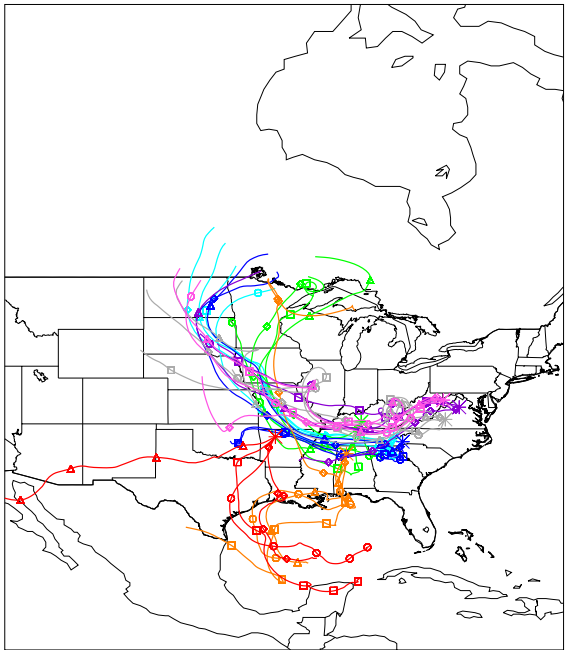

Figure 4.2.8b 6-May trajectories calculated using EDAS data.

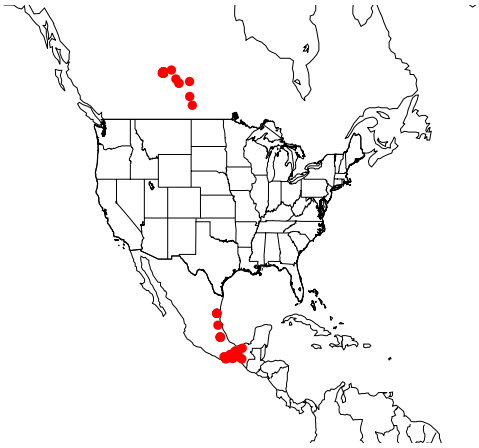

Figure 4.2.9 Hot spots detected on 3-May.

Figure 4.2.10 Hot spots detected on 4-May.

Trajectories from the parks flagged as non-impacted did not pass over or near any fires and thus confirm the finding of no smoke impact. UPBU had transport from a region where fires occurred and a large plume of smoke had developed, confirming the finding of smoke impact on the aerosol sample.

The next day impacted by smoke from the fires in Mexico and Central America was 16-May. The sample days prior to 16-May, 9-May and 13-May, did not have transport from the smoke-filled Gulf region, which is consistent with the finding of no smoke impact on those days. On 16-May DOSO, GRSM, MACA, SHRO and SIPS were flagged as smoke impacted (Figure 4.2.11).

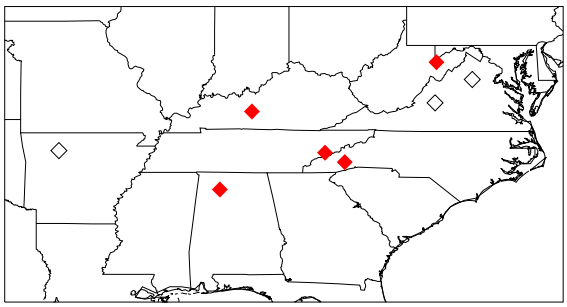

Figure 4.2.11 Smoke impacted parks (filled diamonds) and non-impacted parks (open diamonds) for 16-May.

After a frontal passage on 15-May and associated precipitation the transport to UPBU was from the Baja and southwest U.S. and fine mass concentrations were significantly lower. In contrast, parks not experiencing the frontal passage until late on 16-May had transport from the smoky Gulf region (Figure 4.2.12). The GOES-8 image for the early evening of 16-May clearly shows the plume of smoke extending from Mexico through the Gulf and along the front in the southeastern U.S. to Virginia (Figure 4.2.13). The clean air over Arkansas (UPBU) is also evident in this image. Smoke can also be seen in the Pacific Ocean southwest of Mexico. Hot spots on 12-May are an example of the fire areas influencing the 16-May aerosol samples (Figure 4.2.14).

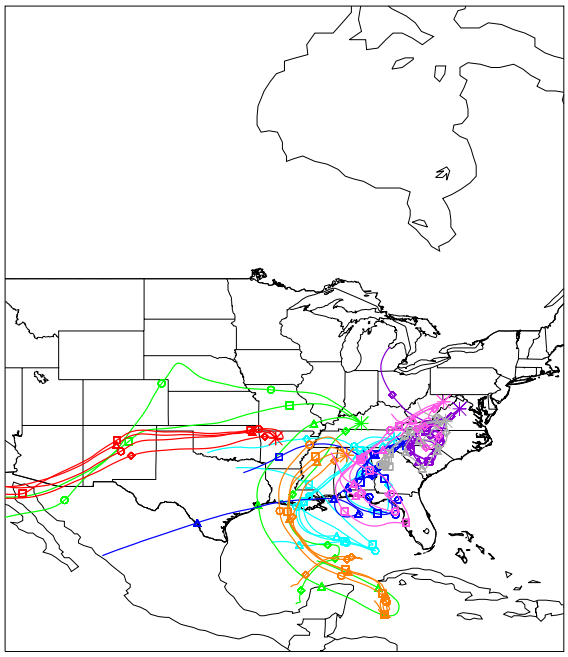

Figure 4.2.12 16-May trajectories calculated using FNL data.

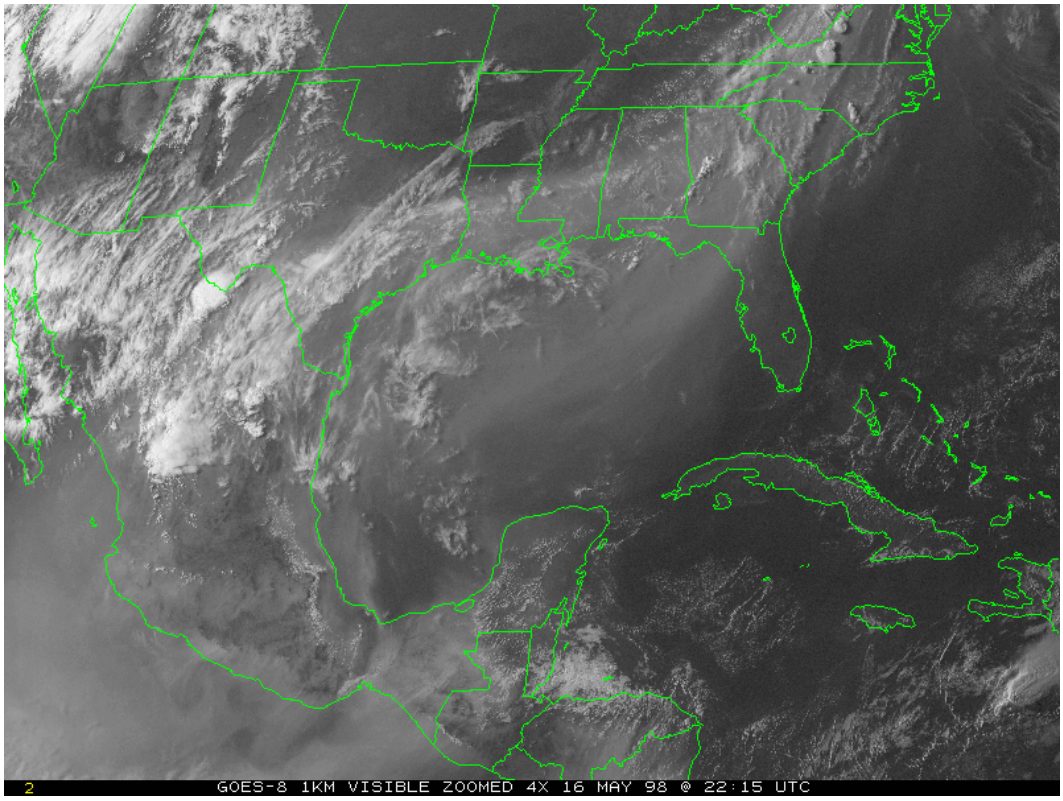

Figure 4.2.13 GOES-8 1KM visible satellite image for 22UTC on 16-May. (Reprinted without permission from http://capita.wustl.edu/Central-America/Resources/Images)

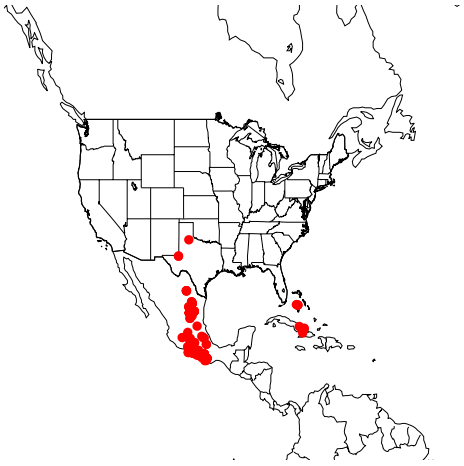

Figure 4.2.14 Hot spots detected on 12-May.

JEFF and SHEN were considered false negative for smoke impact on this day. However, a number of factors suggest that the finding of no smoke impact on the aerosol samples at these sites was not in error. The first factor to consider, especially at JEFF, is elevation. JEFF is located only 299m above sea level in the Appalachian Mountains. It is possible the smoke plume was located high enough above the monitoring site to not influence the surface aerosol sample. Another possibility is heavy rain near the site. Referring to the satellite image, Figure 4.2.13, two large convective clouds can be seen near JEFF and SHEN. Rain removes particulate matter from the air, which could affect the finding of no smoke impact. This is unlikely on this day considering the fine mass concentrations at JEFF and SHEN were over 20 $\mu g/m^3$. A final consideration is that the transport to JEFF and SHEN was confined primarily to the Mid-Atlantic States (Figure 4.2.12). This area is largely industrial and it is possible that an anthropogenic source for iron caused the K_{NON} values to be low.

Therefore, on 16-May trajectories, the satellite image and hot spot maps confirm the finding of no smoke impact at UPBU. The finding of smoke impact at DOSO, GRSM, MACA, SHRO and SIPS is also confirmed by the trajectories, satellite image and

hot spot maps. The conclusion for JEFF and SHEN, based on trajectories, the satellite image and fine mass, is that both are false negative for smoke impact.

Optical measurements from a site in Oklahoma suggest the smoke was in an elevated layer from 17-May through 19-May (Kreidenweis et al., 2001). This is consistent with the findings on 20-May when SHRO was the only park flagged as smoke impacted (Figure 4.2.15). SHRO has the highest elevation of all the sites selected for this study (Table 2.1.1) at 1621m above sea level.

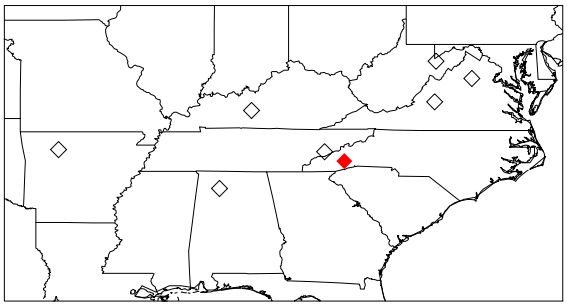

Figure 4.2.15 Smoke impacted parks (filled diamonds) and non-impacted parks (open diamonds) for 20-May.

DOSO, GRSM and UPBU all had elevated K_{NON}, nearly passing the criterion of the median plus two standard deviations (Figures 4.1.1a and 4.1.1b). Trajectories for SHRO did not reach the Gulf or the fire areas with the source region being primarily Alabama, Georgia and Tennessee (Figure 4.2.16). However, the GOES-8 satellite image for 20-May shows the smoke plume along the western Gulf coast north into Texas and east covering most of the southeastern U.S. (Figure 4.2.17). Although trajectories never reach the Gulf the satellite image for 20-May, along with park elevation and the elevated smoke plume support the finding of smoke impact only at SHRO.

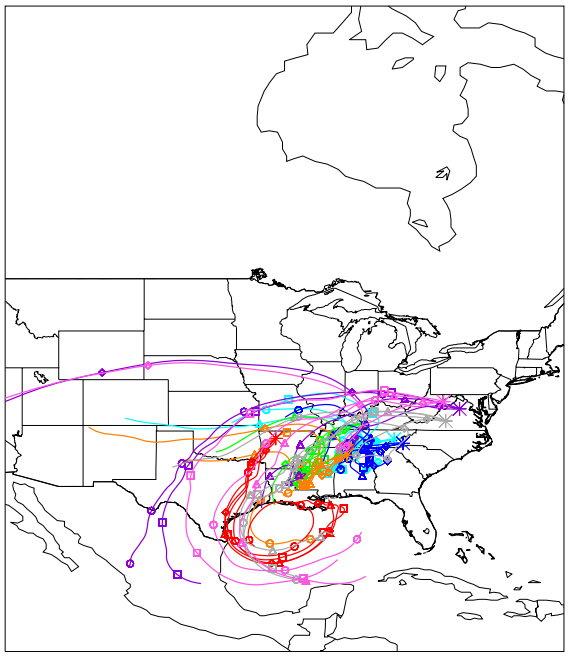

Figure 4.2.16 20-May trajectories calculated using FNL data.

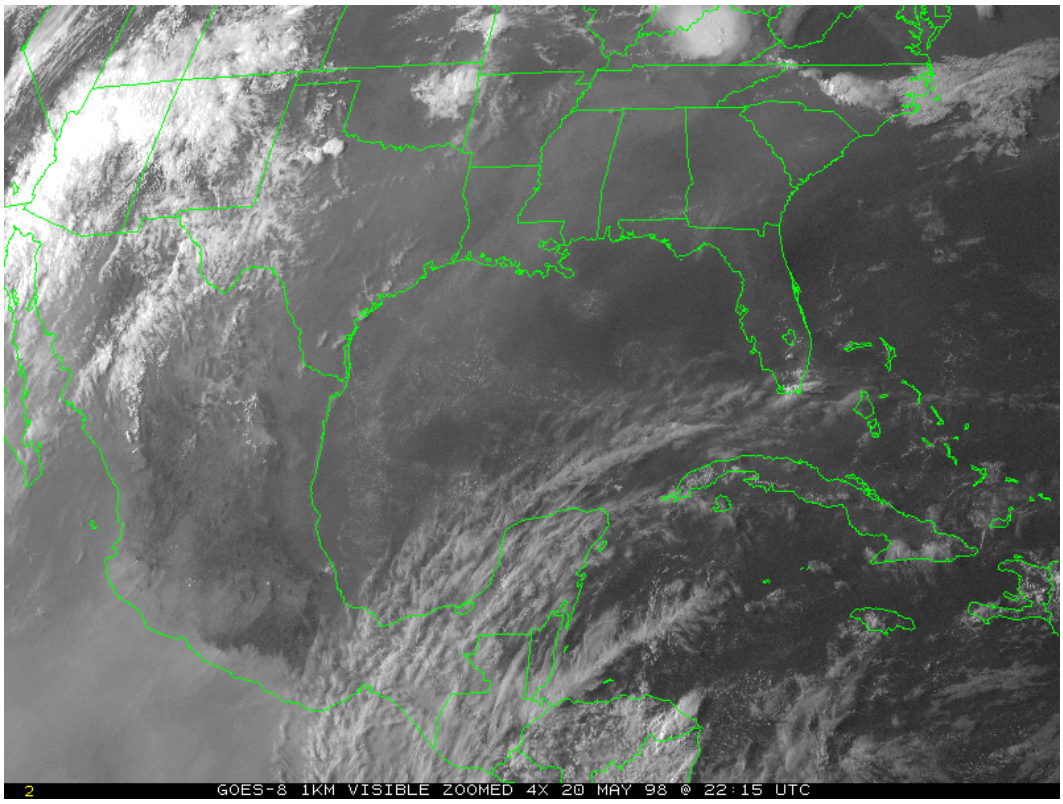

Figure 4.2.17 GOES-8 1KM visible satellite image for 22UTC on 20-May. (Reprinted without permission from http://capita.wustl.edu/Central-America/Resources/Images)

On 23-May GRSM, MACA, SHRO, SIPS and UPBU were flagged as smoke impacted (Figure 4.2.18). Transport to the parks not flagged as smoke impacted was from Canada and the upper Midwest (Figure 4.2.19). There were no hot spots detected near their trajectories nor did they have transport from a region with a large smoke plume. Fire activity persisted until the last week of May with the smoke plume still in the Gulf region. Transport to the smoke-impacted parks was from the Gulf for this day (Figure 4.2.19).

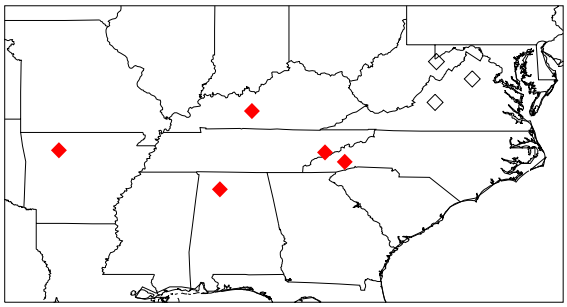

Figure 4.2.18 Smoke impacted parks (filled diamonds) and non-impacted parks (open diamonds) for 23-May.

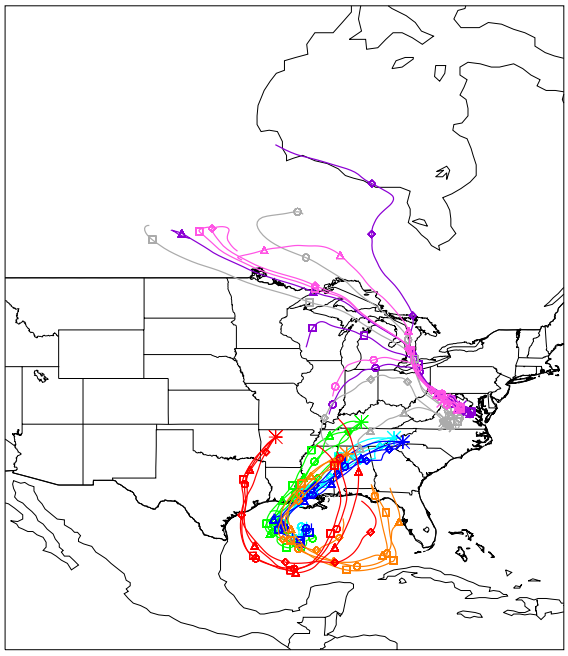

Figure 4.2.19 23-May trajectories calculated using FNL data.

There was intense fire activity from 18-May through 22-May in Mexico and Central America (Figures 4.2.20a-e). As previously discussed the smoke from these fires filled the Gulf region and thus transport did not need to reach the hot spots in order for smoke impact to be present on the aerosol samples.

Figure 4.2.20a Hot spots detected on 18-May.

Figure 4.2.20b Hot spots detected on 19-May.

Figure 4.2.20c Hot spots detected on 20-May.

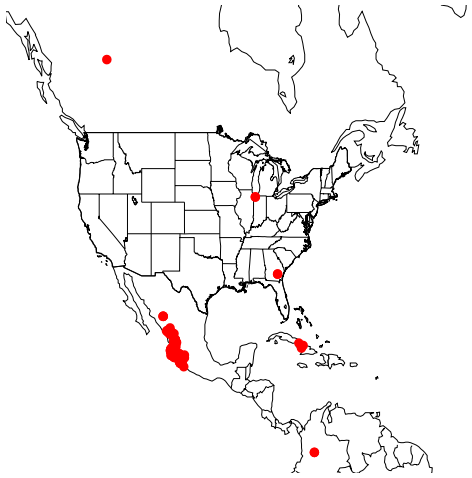

Figure 4.2.20d Hot spots detected on 21-May.

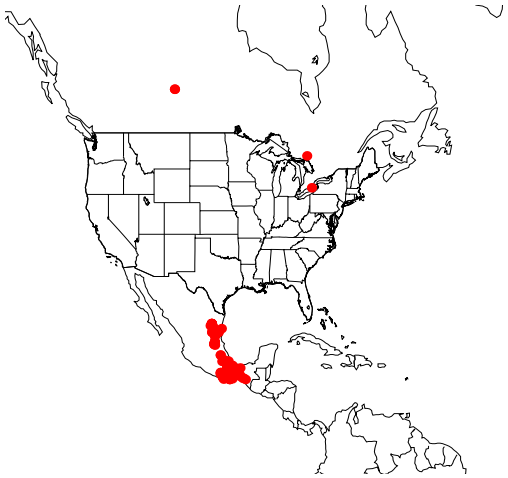

Figure 4.2.20e Hot spots detected on 22-May.

Transport patterns and hot spot maps confirm the finding of smoke impact on the aerosol samples at GRSM, MACA, SHRO, SIPS and UPBU. Similarly, the northerly transport to DOSO, SHEN and JEFF along with the absence of large fires or smoke plumes along their trajectories supports the finding of no smoke impact on the aerosol samples at these parks.

On 27-May GRSM, SHRO and SIPS were flagged as smoke impacted (Figure 4.2.21) and MACA and UPBU nearly passed the two standard deviation criterion (Figures 4.1.1a and b). Trajectories once again indicate the Gulf as the primary source region for the smoke impacted parks, MACA and UPBU (Figure 4.2.22). Trajectories for DOSO, SHEN and JEFF do not reach the smoky Gulf region (Figure 4.2.22).

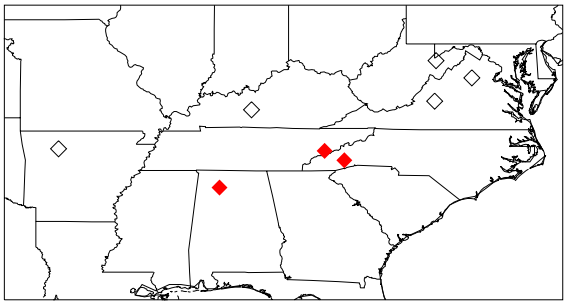

Figure 4.2.21 Smoke impacted parks (filled diamonds) and non-impacted parks (open diamonds) for 27-May.

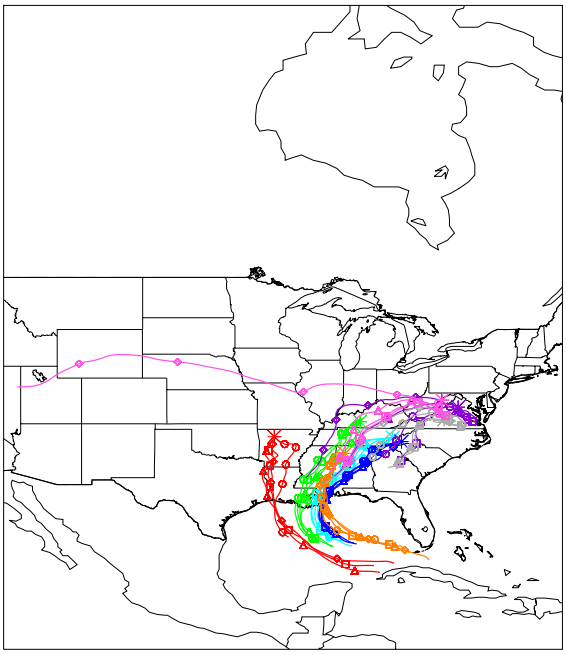

Figure 4.2.22 27-May trajectories calculated using FNL data.

MACA and UPBU have transport from a known smoky region and nearly pass their criterion, thus both are considered false negative for smoke impact. Transport patterns confirm the finding of smoke impact on the samples at SIPS, GRSM and SHRO. The finding of no smoke impact at SHEN, DOSO and JEFF is consistent with their transport patterns.

On 30-May UPBU and SHRO were flagged as smoke impacted (Figure 4.2.23). GRSM was close to passing the two standard deviation criterion also (Figure 4.1.1a).

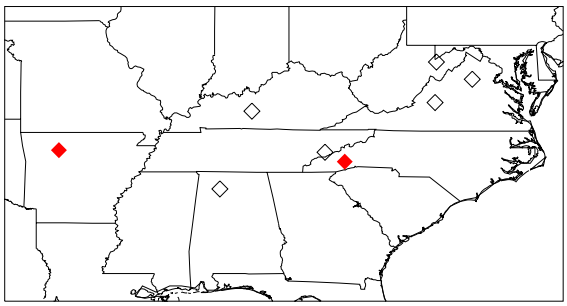

Figure 4.2.23 Smoke impacted parks (filled diamonds) and non-impacted parks (open diamonds) for 30-May.

Transport to GRSM, MACA, SHRO, SIPS and UPBU was southerly, whereas DOSO, JEFF and SHEN had west-southwesterly transport (Figures 4.2.24a and 4.2.24b). There was disagreement between the FNL and EDAS trajectories for SIPS, DOSO, JEFF, SHEN and UPBU. The EDAS trajectories have a stronger westerly component to the transport for DOSO, JEFF, SHEN and UPBU. The FNL data result in fast transport from the Atlantic north of Cuba, Haiti and the Dominican Republic for SIPS whereas EDAS trajectories result in slow transport primarily from the northern Gulf coast.

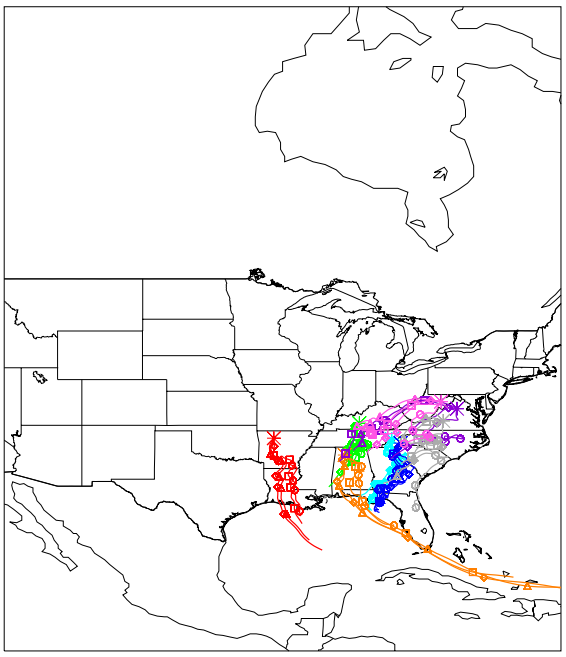

Figure 4.2.24a 30-May trajectories calculated using FNL data.

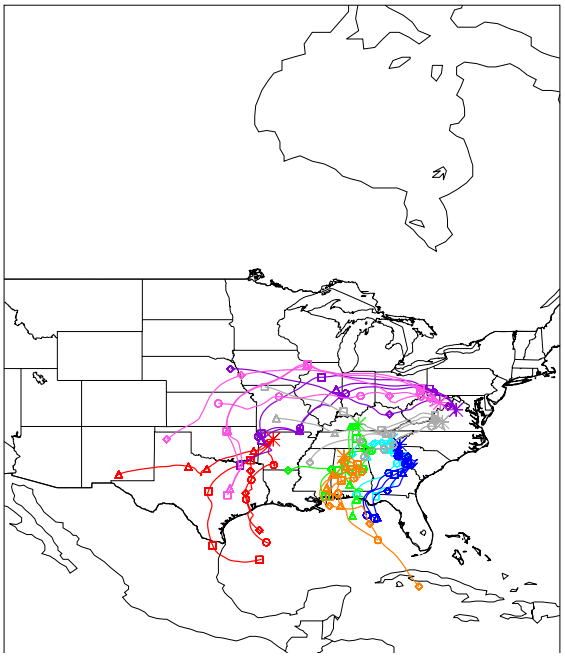

Figure 4.2.24b 30-May trajectories calculated using EDAS data.

Although transport to SIPS and MACA is from a similar region as SHRO and GRSM the difference in elevation is the likely cause for no smoke impact detected at SIPS and MACA. Both SIPS and MACA are less than 300m above sea level whereas GRSM is over 800m and SHRO over 1600m above sea level. Thus, the finding of no smoke impact at SIPS and MACA is considered valid. Since GRSM almost passed the

criterion and has a higher elevation than UPBU it is considered false negative for smoke impact.

Based on the FNL transport patterns it is possible a fire on 26-May in Louisiana influenced the sample at UPBU, in addition to the smoke pall from Mexico (Figure 4.2.25). Transport patterns for UPBU and SHRO are consistent with the finding of smoke impact on the aerosol samples. The finding of no smoke impact at DOSO, SHEN and JEFF is also consistent with the more westerly transport at these parks.

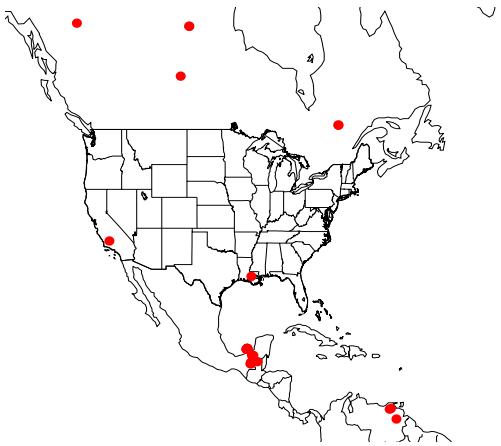

Figure 4.2.25 Hot spots detected on 26-May.

On 3-June, the last day influenced from the fires in Mexico and Central America, GRSM and SHRO were flagged as smoke impacted (Figure 4.2.26). Transport to GRSM and SHRO was from the southwest, but did not reach the Gulf (Figure 4.2.27). SIPS and UPBU did have transport from the Gulf with one trajectory for SIPS reaching Central America. Again, GRSM and SHRO are at higher elevations than UPBU and SIPS, which is a likely cause for smoke impact at those sites and not UPBU and SIPS. It is also possible that the smoke plume was located farther to the east, thus not impacting UPBU and SIPS. Transport to MACA was from Missouri and Arkansas, which supports the finding of no smoke impact on the aerosol sample. The finding of no smoke impact at

DOSO, SHEN and JEFF is supported by transport from the Pacific Northwest where there were no fires.

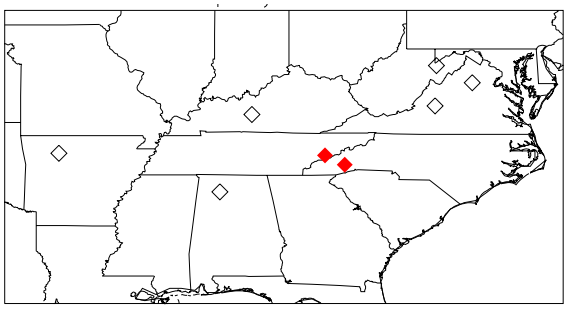

Figure 4.2.26 Smoke impacted parks (filled diamonds) and non-impacted parks (open diamonds) for 3-June.

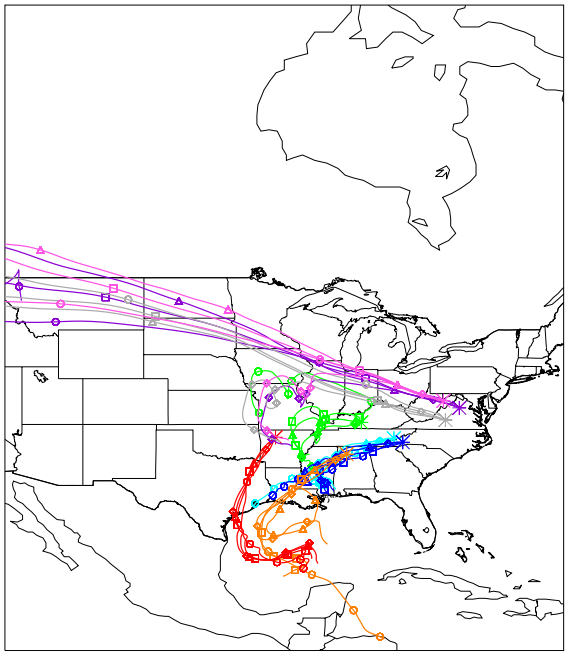

Figure 4.2.27 3-June trajectories calculated using FNL data.

4.3 July Smoke Event

4-July was the only day in July with confirmed smoke impact on the aerosol samples. MACA, JEFF and SHEN were flagged as smoke impacted and SHRO was missing data (Figure 4.3.1). The smoke impact at MACA could not be confirmed from hot spot maps and is considered false positive for smoke impact.

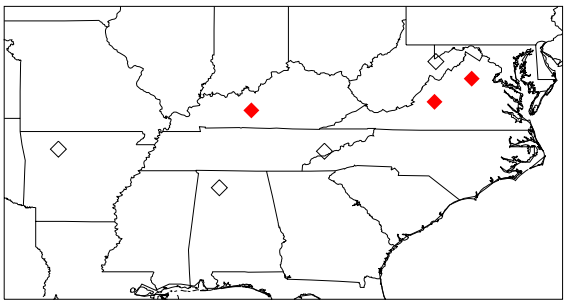

Figure 4.3.1 Smoke impacted parks (filled diamonds) and non-impacted parks (open diamonds) for 4-July.

Transport to DOSO, JEFF and SHEN was from Canada, Michigan, Indiana and Ohio (Figure 4.3.2). There were numerous hot spots detected near DOSO, JEFF and SHEN and near their trajectories on 2-July (Figure 4.3.3). In addition, hot spots in Canada on 30-June were near the trajectories for these parks (Figure 4.3.4). Transport to UPBU and SIPS was from the Gulf of Mexico with trajectories from UPBU extending through the Caribbean Sea. GRSM, MACA and SHRO had transport from the Midwest. MACA and SHRO each had one trajectory near hot spots on 30-June in Iowa and Illinois, respectively.

Trajectories for DOSO were near both the U.S. fires on 2-July and the fires in Canada on 30-June. Considering that DOSO was close to passing the two standard deviation criterion and had transport similar to JEFF and SHEN it is concluded to be false negative for smoke impact.

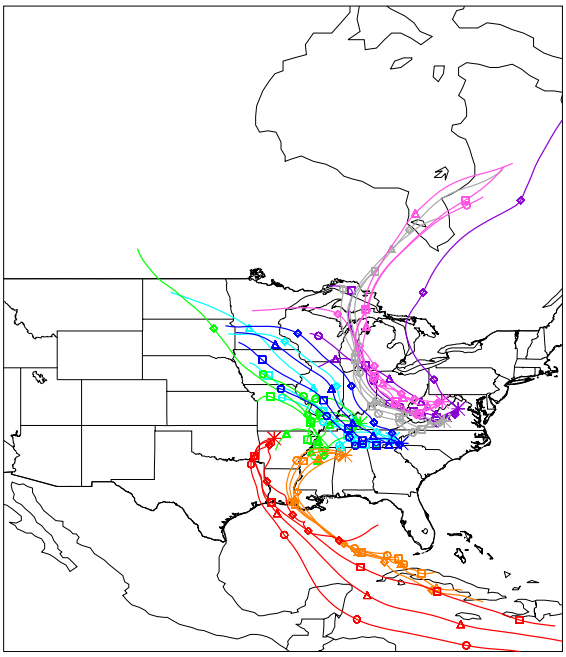

Figure 4.3.2 4-July trajectories calculated using FNL data.

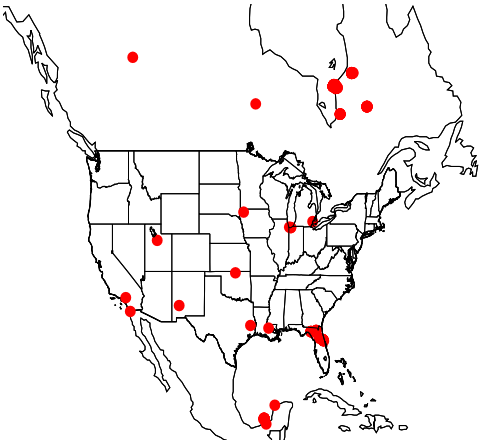

Figure 4.3.3 Hot spots detected on 30-June.

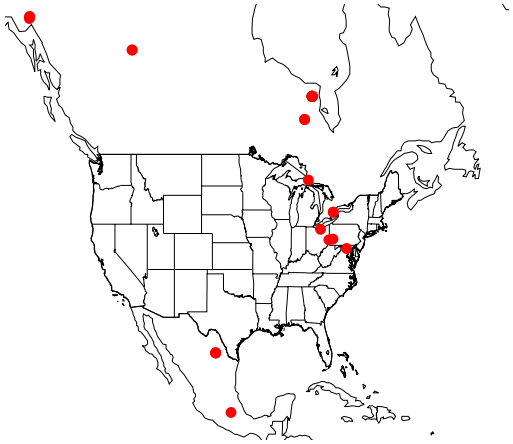

Figure 4.3.4 Hot spots detected on 2-July.

The finding of no smoke impact at GRSM, UPBU and SIPS is consistent with the transport patterns and hot spot maps. Although MACA had a trajectory near a fire in Iowa on 30-June, it is considered false positive for smoke impact due to the short amount of time transport was from that area. SHRO also had one trajectory near a fire in Illinois

on 30-June, but the finding of no smoke impact on the aerosol sample is consistent due to the short amount of time air was transport from that region to the site.

4.4 Summary of Findings for 1998

Table 4.4.1 summarizes the findings for 1998. Overall there were 28 aerosol samples determined to be influenced by smoke from fires in Mexico, Cuba and Central America. Three samples were impacted by fires in the U.S. and Canada and two were unable to be confirmed due to lack of fire data in June. A total of 23 samples indicated the presence of North African dust in the aerosol samples. Eight of the samples influenced by North African dust were in June and the remainder in July. Five samples were determined to be false positive for smoke impact and six false negative. Of the six false negative samples five were during the May smoke event from extreme fires in Mexico and Central America. A total of nine observations were missing, four of which were over two consecutive weeks at SHRO.

Table 4.4.1 Summary of Results for 1998. 'MX'-Smoke impact from Mexico, 'Cen.A'-Smoke impact from Central America, 'CB'-Smoke impact from Cuba, 'US'-Smoke impact from the U.S., 'CA'-Smoke impact from Canada, 'False –' –False negative for smoke impact, 'False +'-False positive for smoke impact, 'NAD'-North African dust impact.

Date	DOSO	GRSM	JEFF	MACA	SHEN	SHRO	SIPS	UPBU
15-Apr		MX/CB		MX/CB		MX/CB	Missing	MX/CB
18-Apr								
22-Apr								
25-Apr								
29-Apr								
2-May								Missing
6-May							Missing	MX/Cen.A
9-May								
13-May								
16-May	MX/CB/ Cen.A	MX/CB/ Cen.A	False -	MX/CB/ Cen.A	False -	MX/CB/ Cen.A	MX/CB/ Cen.A	
20-May						MX/CB/ Cen.A		
23-May		MX/CB/ Cen.A		MX/CB/ Cen.A		MX/CB/ Cen.A	MX/CB/ Cen.A	MX/CB/ Cen.A
27-May		MX/Cen.A		False -		MX/Cen.A	MX/Cen.A	False -
30-May		False -				MX/Cen.A		MX/Cen.A
3-Jun		MX/Cen.A				MX/Cen.A		
6-Jun								
10-Jun				Smoky (No Fire Data)		Smoky (No Fire Data)		
13-Jun		NAD				NAD		NAD
17-Jun		False +		False +		False +		
20-Jun								
24-Jun							Missing	
27-Jun				NAD	NAD		NAD	NAD
1-Jul						Missing	NAD	
4-Jul	False -		US/CA	False +	US/CA	Missing		NAD
8-Jul		NAD	NAD	NAD		Missing	NAD	NAD
11-Jul						Missing		NAD
15-Jul					False +		NAD	
18-Jul								
22-Jul		NAD					NAD	NAD
25-Jul								
29-Jul				NAD			Missing	NAD

4.5 Smoke Impact on Fine Mass Concentrations

Fine mass concentrations in the southeastern U.S. tend to be dominated by sulfates, which comprise over 50% of the fine mass (Eldred et al., 1987). In spite of this, it was thought that since forest fires are a source for particulate matter, during significant smoke events the fine mass concentrations would be higher than on days not impacted by smoke. During some of the smoke events the smoke did have an impact on fine mass concentrations; however, samples impacted by smoke were not always the ones with the highest fine mass concentrations (Figures 4.5.1a and 4.5.1b). In general, fine mass concentrations vary by a factor of three to four at all parks over the study period, 15-April through 31-July.

In general, fine mass concentrations at DOSO, JEFF, SHEN and MACA on smoke impacted days are not obviously different from the days not impacted by smoke. During April and May at MACA, the smoke impacted days were among the days with high fine mass concentrations, but later in the study period fine mass concentrations on days not impacted by smoke were as high or higher than the smoke impacted days. Similarly, the smoke impacted days at SHEN in July were among the days with the highest fine mass concentrations, but earlier smoke impacted days are not. The fine mass concentrations at SHRO and SIPS during the May 1998 smoke event are much higher than the concentrations during May 1995 and are among the highest fine mass concentrations over the entire study period. At UPBU and GRSM the fine mass concentrations on days flagged smoke impacted throughout the entire study period tend to be as high or higher than the concentrations on days not flagged smoke impacted.

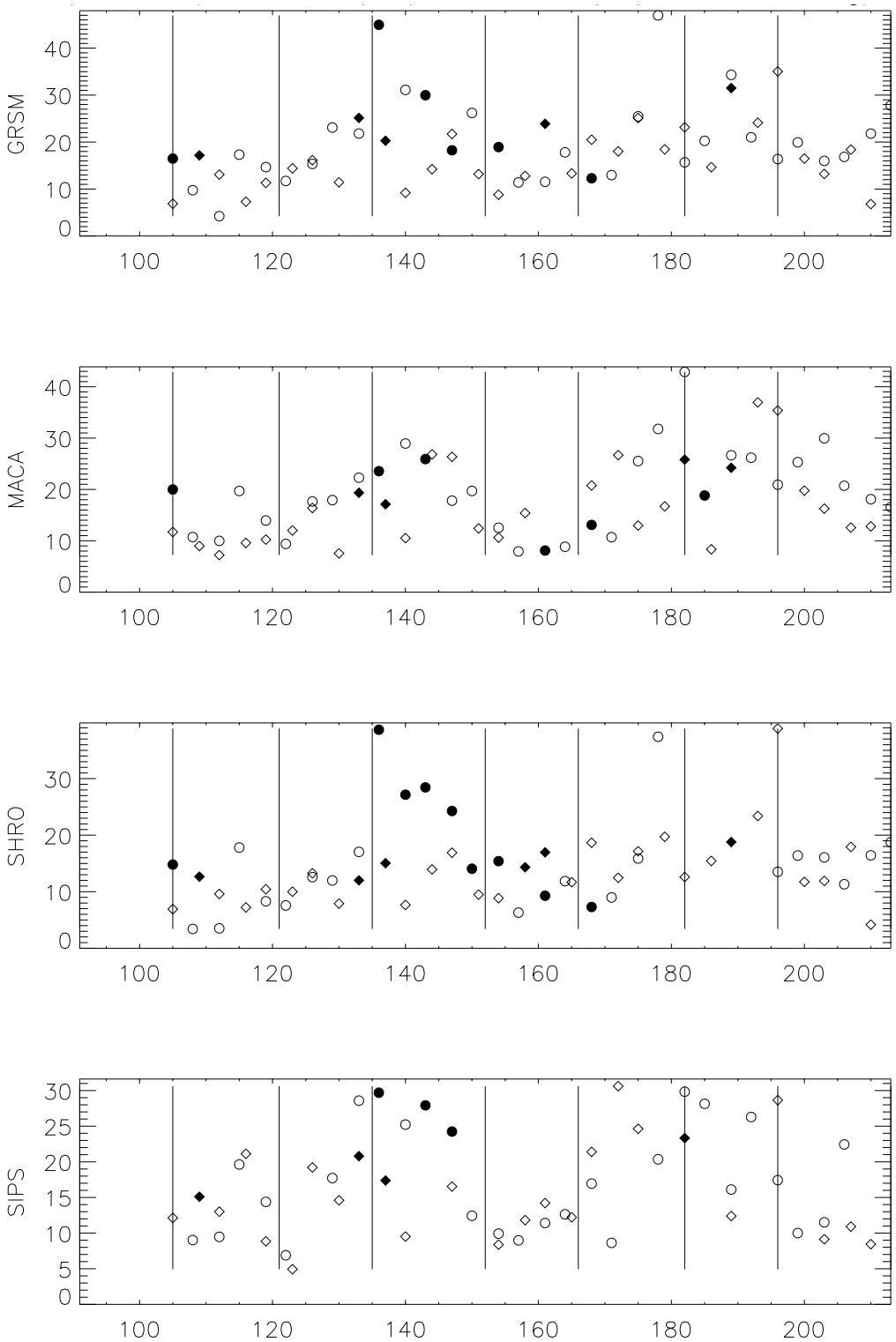

Figure 4.5.1a Fine mass concentrations (μg/m^3) for 4/15 through 7/31 1995 (diamonds) and 1998 (circles) for parks in the SOS95 region. Filled symbols indicate sample was flagged as smoke impacted, numbers along x-axis indicate Julian day where 105 is 15-April and vertical lines mark the first and fifteenth of each month, April through July.

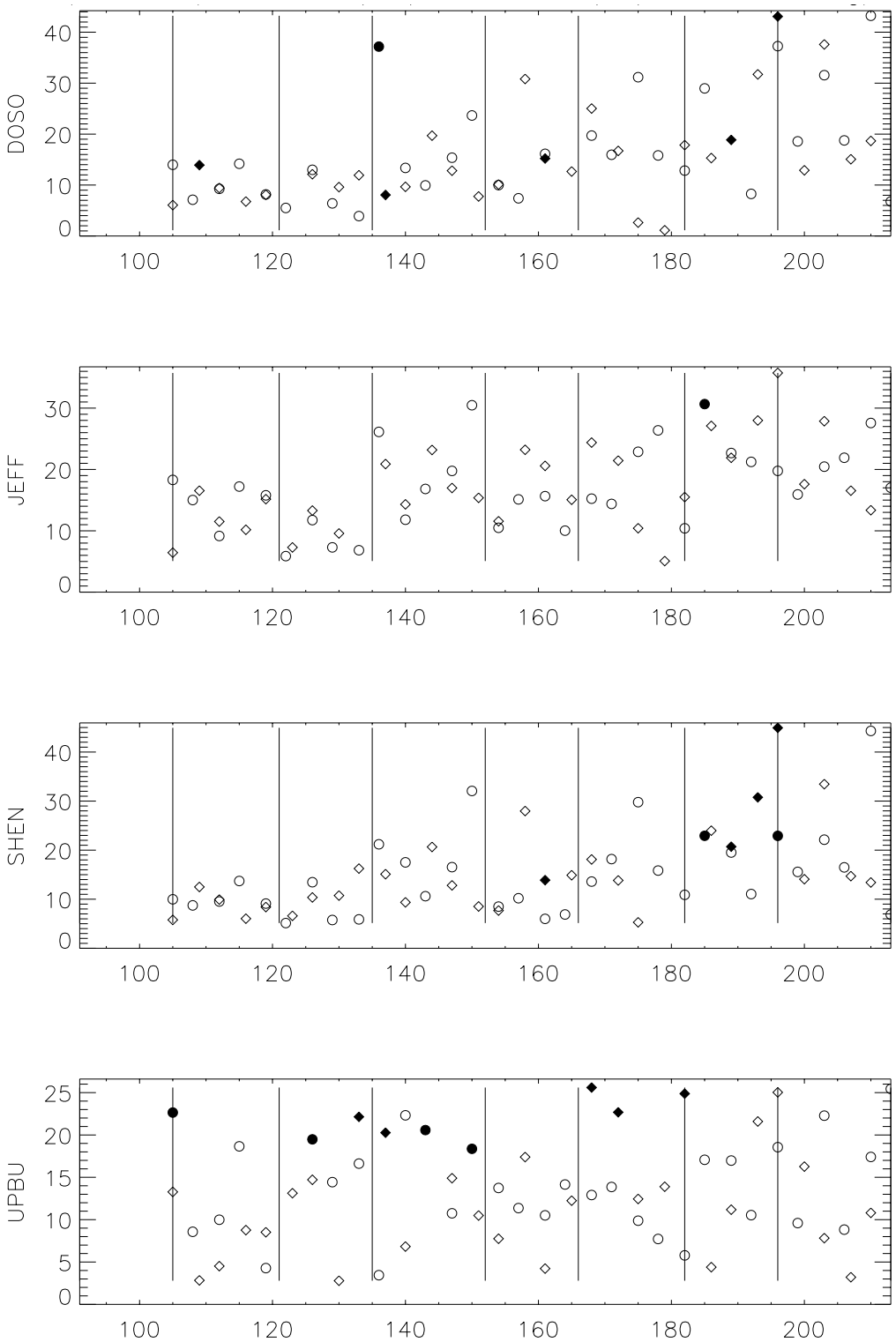

Figure 4.5.1b Fine mass concentrations (μg/m^3) for 4/15 through 7/31 1995 (diamonds) and 1998 (circles) for parks outside the SOS95 region. Filled symbols indicate sample was flagged as smoke impacted, numbers along x-axis indicate Julian day where 105 is 15-April and vertical lines mark the first and fifteenth of each month, April through July.

Based on the results for 1995 and 1998, fine mass concentrations on days flagged as smoke impacted tend to be high, but not consistently higher than days not impacted by smoke. Fine mass concentrations vary significantly from day to day due to variations in the source region, the weather, and aerosol emissions. So, although there is some evidence of smoke impact on the fine mass concentrations it is not consistent enough to be generalized into a criterion indicating smoke impact on an aerosol sample.

4.6 Summary of Smoke Impact for All Available Years

The same criteria for determining smoke impact on aerosol samples that were applied to 1995 and 1998 were applied to all years of available data from 15-April through 31-July of each year. There were a total of 1,901 observations from 1988 through 1999 at all parks combined (Table 4.6.1). Of the 1,901 observations 120 were flagged as smoke impacted (Table 4.6.2). Based on 1995 and 1998 results, 10/66 observations flagged as smoke impacted were assumed to be false positive for smoke impact. Applying this ratio to the overall results suggests 18 of the 120 observations flagged as smoke impacted might be expected to be false positive for smoke impact. Similarly, based on 1995 and 1998 results 14 of the 409 observations not flagged as smoke impacted were false negative for smoke impact. Applying this ratio to the overall results suggests approximately 61 of the 1,781 observations not flagged as smoke impacted might be false negative for smoke impact. Thus, the actual number of observations impacted by smoke can be estimated by subtracting the number of false positives and adding the number of false negatives to the number of observations passing

the criterion for smoke impact. This results in a total of 163 out of 1,901 observations being impacted by smoke from 15-April through 31-July from 1988 through 1999.

Table 4.6.3 details the results by year. 1995 and 1998 had the most smoke impacted days with 37 (15.6%) and 33 (13.9%), respectively. Over all years it is estimated that 8.6% of the observations were impacted by smoke from 15-April through 31-July. Out of the three and a half months examined, May and June have the highest percentage of smoke impacted observations and April and July are equivalent to each other (Table 4.6.4).

Table 4.6.1 Number of Observations from 4/15 – 7/31 1988 - 1999. 'ND'-No Data.

Year	Month	DOSO	GRSM	JEFF	MACA	SHEN	SHRO	SIPS	UPBU	Total
1988	April	ND	5	ND	ND	5	ND	ND	ND	10
	May	ND	8	ND	ND	6	ND	ND	ND	14
	June	ND	9	ND	ND	8	ND	ND	ND	17
	July	ND	7	ND	ND	9	ND	ND	ND	16
1989	April	ND	5	ND	ND	5	ND	ND	ND	10
	May	ND	9	ND	ND	9	ND	ND	ND	18
	June	ND	8	ND	ND	8	ND	ND	ND	16
	July	ND	8	ND	ND	7	ND	ND	ND	15
1990	April	ND	4	ND	ND	4	ND	ND	ND	8
	May	ND	9	ND	ND	9	ND	ND	ND	18
	June	ND	7	ND	ND	9	ND	ND	ND	16
	July	ND	8	ND	ND	8	ND	ND	ND	16
1991	April	ND	4	ND	ND	3	ND	ND	ND	7
	May	ND	9	ND	ND	9	ND	ND	ND	18
	June	ND	5	ND	ND	9	ND	ND	ND	14
	July	ND	9	ND	ND	6	ND	ND	ND	15
1992	April	5	5	ND	5	5	ND	5	5	30
	May	9	9	ND	9	9	ND	6	7	49
	June	8	8	ND	8	8	ND	5	8	45
	July	9	9	ND	9	9	ND	8	8	52
1993	April	4	4	ND	4	4	ND	4	4	24
	May	9	9	ND	9	9	ND	7	9	52
	June	9	9	ND	5	9	ND	9	9	50
	July	9	9	ND	9	9	ND	9	9	54
1994	April	5	3	ND	5	5	ND	4	5	27
	May	8	6	ND	8	7	ND	7	6	42
	June	8	5	ND	8	9	ND	5	4	39
	July	9	9	ND	3	9	4	9	9	52
1995	April	5	5	5	5	5	5	5	5	40
	May	8	9	8	9	9	9	7	9	68
	June	8	8	8	6	7	8	7	8	60
	July	9	9	9	9	8	9	6	9	68
1996	April	4	4	4	4	4	4	4	4	32
	May	9	9	9	9	9	9	3	8	65
	June	8	9	9	9	9	9	4	9	66
	July	9	9	9	9	9	9	9	9	72
1997	April	5	4	5	5	5	5	0	5	34
	May	9	9	7	9	9	9	0	9	61
	June	8	8	7	7	8	8	4	8	58
	July	9	9	9	9	9	7	9	9	70
1998	April	5	5	5	5	5	5	4	5	39
	May	9	9	9	9	9	9	8	8	70
	June	8	8	8	8	8	8	7	8	63
	July	9	9	9	9	9	5	8	9	67
1999	April	4	4	4	4	4	1	4	4	29
	May	9	9	9	9	9	6	9	7	67
	June	9	9	9	9	8	5	8	9	66
	July	9	9	9	9	5	4	8	9	62
Total Over All Years		245	353	151	234	354	138	192	234	1901

Table 4.6.2 Number of Observations Flagged Smoke Impacted from 4/15–7/31 1988-1999. 'ND'-No Data.

Year	Month	DOSO	GRSM	JEFF	MACA	SHEN	SHRO	SIPS	UPBU	Total
1988	April	ND	1	ND	ND	0	ND	ND	ND	1
	May	ND	0	ND	ND	0	ND	ND	ND	0
	June	ND	1	ND	ND	1	ND	ND	ND	2
	July	ND	0	ND	ND	0	ND	ND	ND	0
1989	April	ND	0	ND	ND	0	ND	ND	ND	0
	May	ND	1	ND	ND	2	ND	ND	ND	3
	June	ND	0	ND	ND	0	ND	ND	ND	0
	July	ND	0	ND	ND	1	ND	ND	ND	1
1990	April	ND	0	ND	ND	0	ND	ND	ND	0
	May	ND	1	ND	ND	1	ND	ND	ND	2
	June	ND	1	ND	ND	2	ND	ND	ND	3
	July	ND	0	ND	ND	0	ND	ND	ND	0
1991	April	ND	0	ND	ND	0	ND	ND	ND	0
	May	ND	1	ND	ND	0	ND	ND	ND	1
	June	ND	0	ND	ND	0	ND	ND	ND	0
	July	ND	0	ND	ND	0	ND	ND	ND	0
1992	April	0	0	ND	0	0	ND	0	0	0
	May	0	0	ND	0	0	ND	0	0	0
	June	0	1	ND	1	1	ND	1	0	4
	July	0	0	ND	0	0	ND	0	0	0
1993	April	0	0	ND	0	0	ND	0	0	0
	May	0	0	ND	0	0	ND	0	0	0
	June	2	1	ND	0	2	ND	1	1	7
	July	0	0	ND	0	0	ND	0	0	0
1994	April	0	0	ND	0	0	ND	1	2	3
	May	0	0	ND	0	0	ND	1	0	1
	June	0	0	ND	0	0	ND	0	2	2
	July	0	0	ND	0	0	ND	0	0	0
1995	April	1	1	0	0	0	1	1	0	4
	May	1	2	0	2	0	2	2	2	11
	June	1	1	0	0	1	2	0	3	8
	July	2	1	0	2	3	1	1	1	11
1996	April	0	0	0	0	0	0	0	1	1
	May	0	0	0	0	0	0	0	0	0
	June	1	0	0	1	2	0	0	3	7
	July	0	0	1	1	0	0	0	0	2
1997	April	0	0	0	0	0	0	0	0	0
	May	0	1	0	0	1	1	0	0	3
	June	0	0	0	0	0	0	0	0	0
	July	0	1	1	1	1	1	2	0	7
1998	April	0	1	0	1	0	1	0	1	4
	May	1	3	0	2	0	5	3	3	17
	June	0	2	0	2	0	3	0	0	7
	July	0	0	1	1	2	0	0	0	4
1999	April	0	0	0	0	0	0	0	0	0
	May	0	0	0	0	0	0	0	0	0
	June	0	0	0	1	0	2	0	1	4
	July	0	0	0	0	0	0	0	0	0
Total Over All Years		9	21	3	15	20	19	13	20	120

Table 4.6.3 Number of Observations, Observations Flagged Smoke Impacted, False Positives and False Negatives for Each Year.

Year	Number Of Observations	Number of Observations Flagged Smoke Impacted	Estimated Number of False Positives	Estimated Number of False Negatives	Estimated Number of Observations Impacted by Smoke	Percent of Observations Impacted by Smoke
1988	57	3	0	2	4	7.7%
1989	59	4	1	2	5	8.9%
1990	58	5	1	2	6	10.4%
1991	54	1	0	2	3	4.9%
1992	176	4	1	6	9	5.3%
1993	180	7	1	6	12	6.6%
1994	160	6	1	5	10	6.5%
1995	236	34	5	8	37	15.6%
1996	235	10	2	8	16	6.9%
1997	223	10	2	7	16	7.1%
1998	239	32	5	6	33	13.9%
1999	224	4	1	8	11	4.9%
Total	1901	120	18	61	163	8.6%

Table 4.6.4 Number of Observations and Smoke Impacted Days by Month.

Month	Number Of Observations	Number of Observations Flagged Smoke Impacted	Estimated Number of False Positives	Estimated Number of False Negatives	Estimated Number of Observations Impacted by Smoke	Percent of Observations Impacted by Smoke
April	290	13	2	9	21	7.1%
May	542	38	6	17	49	9.1%
June	510	44	7	16	53	10.4%
July	559	25	4	18	39	7.1%
Total	1901	120	18	61	163	8.6%

Chapter 5. Statistical Analysis of Transport Patterns

5.1 Residence Time and Source Contributions

The results from 1995 and 1998 indicate that high K_{NON} values in the southeastern U.S. tend to occur on days when transport is from Canada or Mexico, although contributions from U.S. sources along the trajectories may be important. For a more objective approach source contributions were examined for GRSM, SHEN and UPBU in 1995 and 1998. Source contributions are residence times (computed using the NGM and FNL trajectories discussed in Section 1.3.3) weighted by an equal probability surface such that a high value indicates transport to a site is more likely along that path rather than along a path with lower values. The reason for adjusting the residence times using an equal probability surface is purely geometric (Poirot and Wishinski, 1986). Every trajectory will contribute "residence time" to the grid cell containing the site creating a bull's-eye effect around the site with a maximum in the center and values decreasing radially. By multiplying the residence time by a distance factor, i.e. distance from the grid cell to the site, this artificial bull's-eye effect can be minimized. For more information on this type of calculation see Ashbaugh et al. (1985) and Poirot and Wishinski (1986).

Overall source contributions and source contributions on days passing the K_{NON} criterion (Section 2.2.2) were computed for GRSM, SHEN and UPBU for 15-April through 31-July 1995 and 1998. Calculations for 1995 were done using the NGM

trajectories and 1998 used the FNL trajectories. GRSM was chosen to represent the SOS95 region, SHEN to represent the coastal sites, and UPBU to investigate the spatial differences in source contributions at sites across the eastern and southeastern U.S.

5.2 Overall Source Contributions

Overall source contributions are source contributions calculated using trajectories from all IMPROVE sample days, 15-April through 31-July, and represent the general transport patterns over the time period. Figures 5.2.1 through 5.2.6 are the overall source contributions for GRSM, SHEN and UPBU for 1995 and 1998. Values greater than one suggest a higher than random probability for transport through that grid box. Differences are expected between the resulting source contributions for 1995 and 1998 at each site, primarily because of the different meteorological conditions present in 1995 and 1998, but also partly because of the different meteorological data used to calculate the trajectories. It is worth noting the primary difference between NGM and FNL data are the grid domains. NGM has a grid domain covering the U.S. whereas FNL has a grid domain covering the entire Northern Hemisphere.

At GRSM two primary source contribution patterns emerge in 1995 in addition to the source contributions from the U.S.; one from the Northwest Territories in Canada and the other from the Gulf of Mexico (Figures 5.2.1 and 5.2.2). During 1995 source contributions from Canada appear to be equivalent to contributions from the Gulf of Mexico/Mexico. In 1998 source contributions are primarily from the south-central U.S. and the Gulf of Mexico, indicating transport from Mexico and Central America, with no obvious pathway from Canada. In addition, the high source contributions near the site

during 1998 suggest it was under the influence of high pressure more often than in 1995. When an area of high pressure is present the air flow tends to be more stagnant and trajectories tend to loop around, potentially passing through the same grid cells multiple times, both of which would contribute to increased residence times in the area under high pressure. Since the source contributions are based on trajectories, this will result in high source contributions in an area influenced by high pressure. Due to the larger grid domain of the FNL data, source contributions from the eastern Pacific region can been seen in 1998 extending from Alaska and Canada south along the west coast of the U.S. This pattern indicates transport of Asian dust or smoke from fires in the Pacific Northwest, the Baja and northwest Mexico could contribute to the aerosol concentrations at GRSM.

The overall source contributions at SHEN are similar to the contributions at GRSM in that in addition to U.S. source contributions, there are high source contributions from Canada and the Gulf of Mexico. In 1995 source contributions from central Canada through the Upper Midwest seem to dominate over other regions (Figure 3.2.3). There are also high source contributions from a small area in northwest Mexico. 1998 source contributions are high from the Gulf of Mexico north through the east-central U.S. and into Canada (Figure 3.2.4). Similar to GRSM, there are high source contributions in the east-central U.S. during 1998, suggesting a persistent area of high pressure in the region. Source contributions were also present along the west coast of North America and into the Pacific during 1998. This suggests transport of Asian dust or smoke from fires along the west coast of North America could contribute to the aerosol concentrations at SHEN as well as GRSM.

The results at UPBU are similar to GRSM in 1995, with overall source contributions from Canada and the Gulf of Mexico being nearly equivalent (Figure 3.2.5). However, the source contributions at UPBU in 1998 are clearly dominant south of the site in the Gulf of Mexico and southeastward (Figure 3.2.6). This agrees well with the high number of observations impacted by North African dust in 1998 (Chapter 6). Source contributions from Canada in 1998 were not significant as in 1995. UPBU also had a large area of high source contributions throughout California and northwest Mexico in 1998.

Despite the different meteorological data used to calculate the trajectories similar source contributions were found in 1995 and 1998 at each park. Overall, the regions of high source contributions at SHEN and GRSM were similar. GRSM had higher source contributions in the Gulf region than SHEN and SHEN had higher source contributions from the Atlantic coast and eastern Canada than GRSM. In contrast, UPBU had higher overall source contributions from the Gulf region than SHEN and GRSM during both years. Thus, it would be expected that UPBU is more likely to have influence from fires in Mexico and Central America and impact from North African dust than GRSM and SHEN. Similarly, SHEN is more likely to have influence from fires in Quebec and Ontario than GRSM and UPBU.

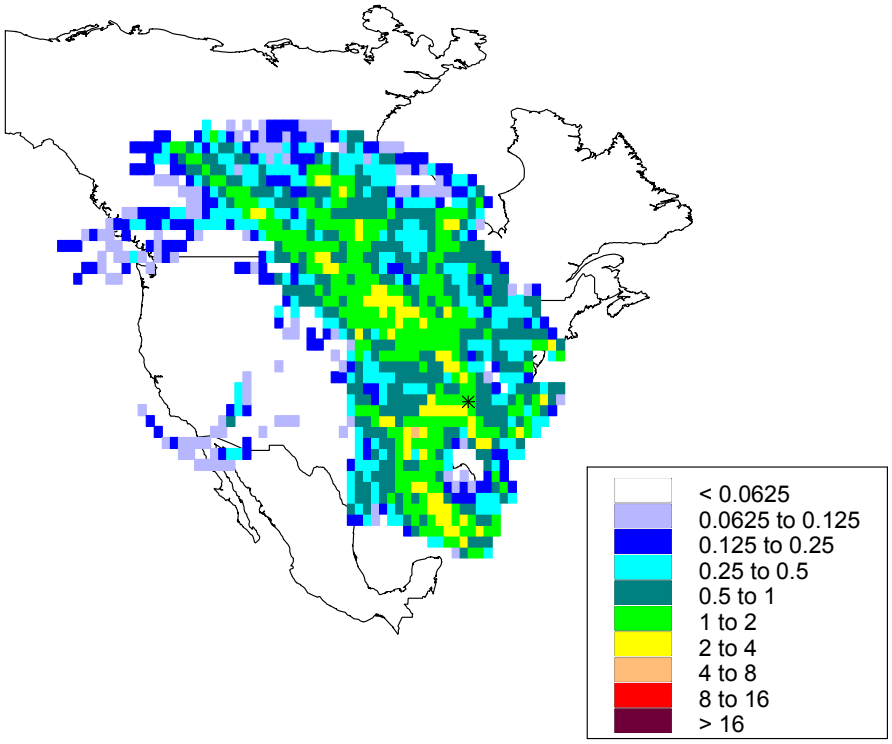

Figure 5.2.1 GRSM 1995 overall source contributions. Scale is residence time/equal probability surface. Computed over all IMPROVE sample days, 15-April through 31-July.

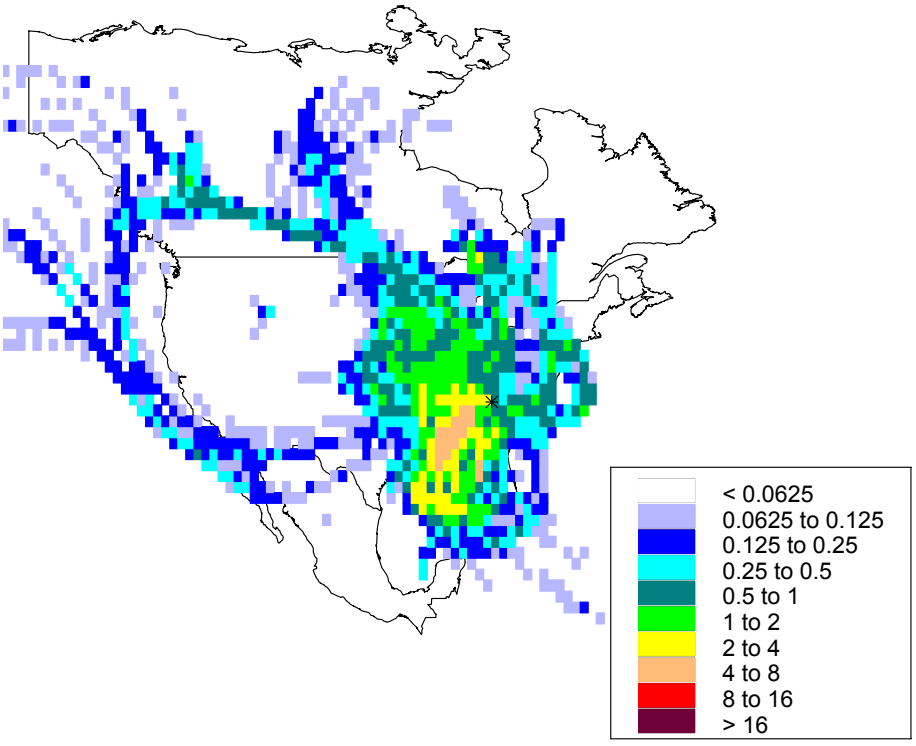

Figure 5.2.2 GRSM 1998 overall source contributions. Scale is residence time/equal probability surface. Computed over all IMPROVE sample days, 15-April through 31-July.

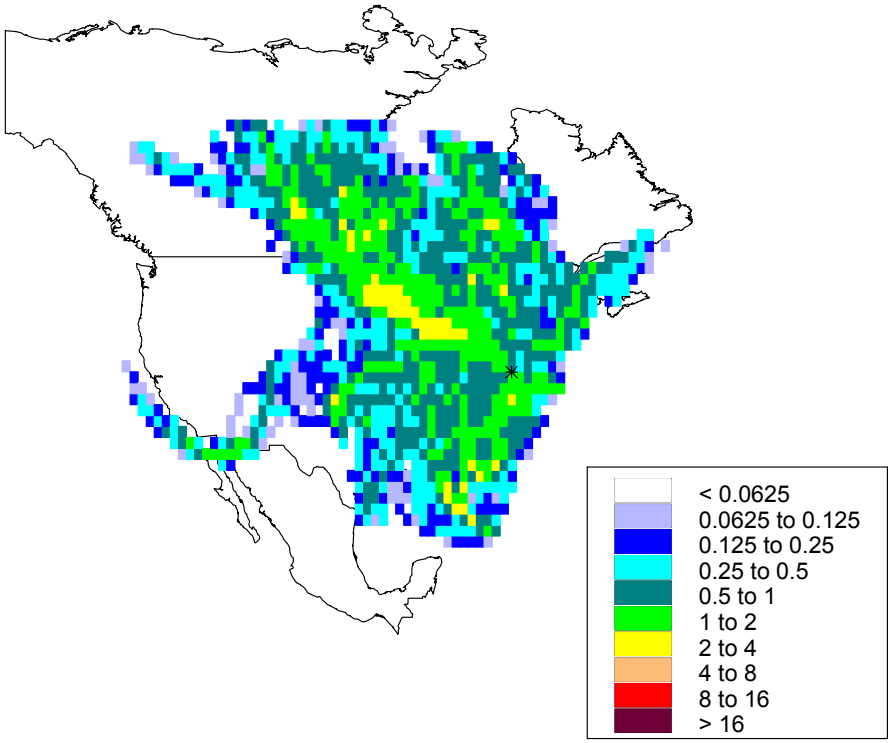

Figure 5.2.3 SHEN 1995 overall source contributions. Scale is residence time/equal probability surface. Computed over all IMPROVE sample days, 15-April through 31-July.

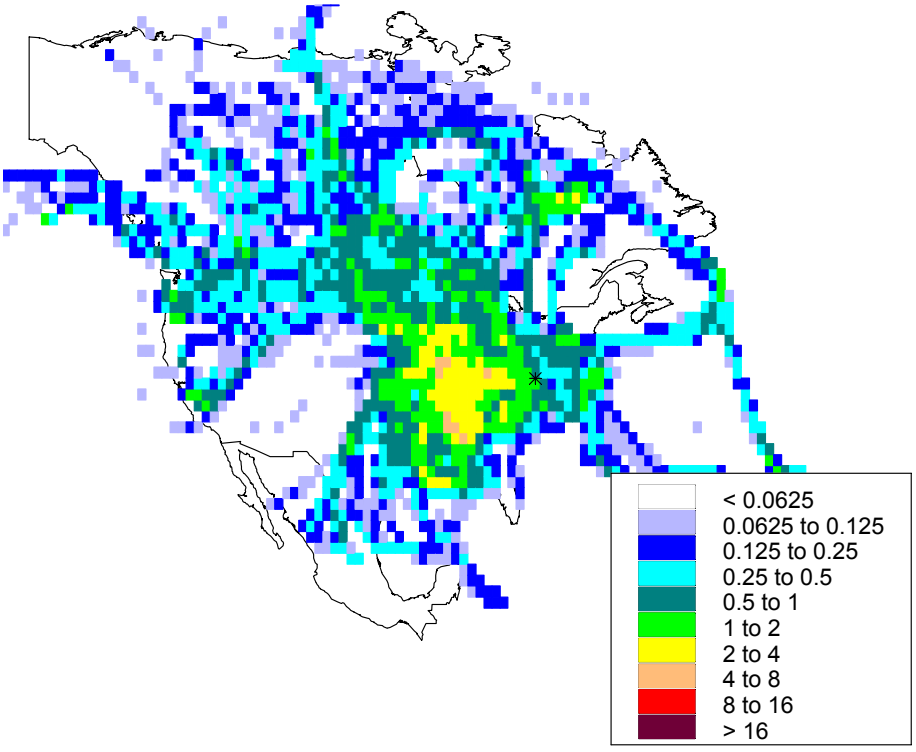

Figure 5.2.4 SHEN 1998 overall source contributions. Scale is residence time/equal probability surface. Computed over all IMPROVE sample days, 15-April through 31-July.

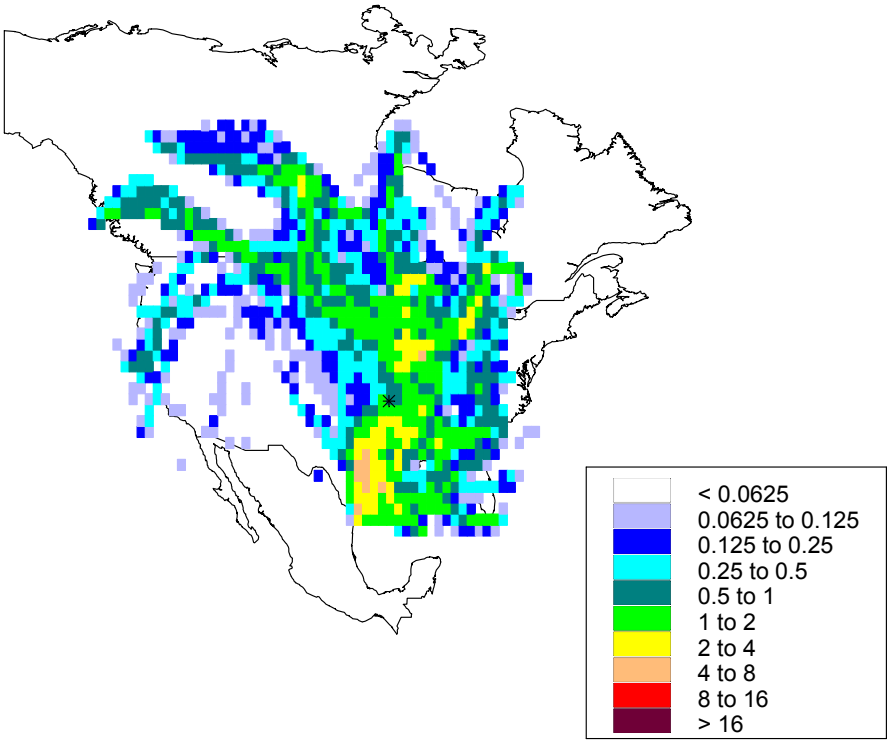

Figure 5.2.5 UPBU 1995 overall source contributions. Scale is residence time/equal probability surface. Computed over all IMPROVE sample days, 15-April through 31-July.

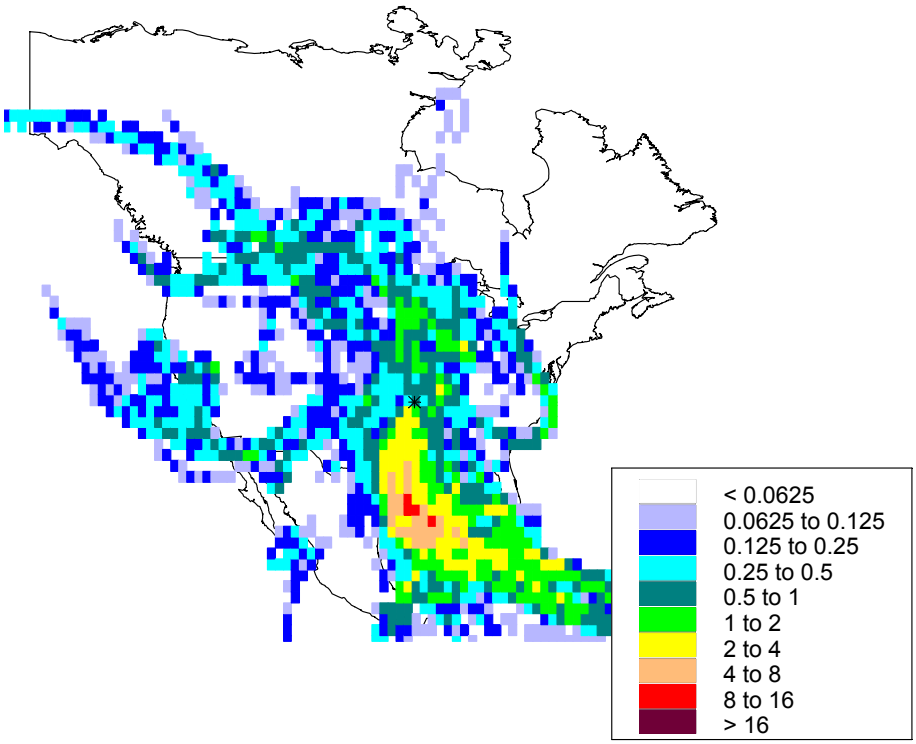

Figure 5.2.6 UPBU 1998 overall source contributions. Scale is residence time/equal probability surface. Computed over all IMPROVE sample days, 15-April through 31-July.

5.3 Source Contributions on High K_{NON} Days

Figures 5.3.1 through 5.3.6 are the source contributions calculated over days where K_{NON} passed the criterion at GRSM, SHEN and UPBU individually. Again, the time period of consideration was 15-April through 31-July of 1995 and 1998 and values greater than one suggest a higher than random probability for transport through that grid box. The patterns that emerge vary both from park to park and year to year. Based on the results in Chapter 3 and Chapter 4, it was expected that in 1995 source contributions from Canada would be higher than in 1998 at all three parks based on the larger area burned in Canada during 1995. Similarly, it was anticipated that in 1998 source contributions from Mexico would be higher in 1998 than 1995 at all three parks because the area burned in Mexico during 1998 was much larger than in 1995.

Two very distinct source contribution patterns are apparent on the high K_{NON} days at GRSM, one indicates source contributions primarily from the central U.S. northward into Canada and the other from the Gulf of Mexico/Mexico and Central America. As anticipated, at GRSM the source contributions from Canada in 1995 exceed the 1998 contributions. Also meeting expectations, the source contributions from Mexico in 1998 exceed the 1995 contributions.

At SHEN the high K_{NON} day's source contributions are very different from GRSM. For both 1995 and 1998 the primary source contributions are from the northeast U.S., the upper Midwest and Canada. The 1995 source contributions extend from Ontario west into Manitoba and Saskatchewan whereas in 1998 they are predominantly Quebec and Ontario. In 1995 SHEN also had high source contributions from the south-central U.S., but neither year indicated high source contributions from Mexico. This

corresponds with the overall source contributions in Section 5.2 in that contributions from Canada tend to exceed those from the Gulf of Mexico/Mexico and Central America at SHEN.

On the high K_{NON} days, UPBU had very different source contributions for 1995 and 1998. During 1995 the predominant source contributions were from the Northwest Territories, Manitoba, Ontario and Saskatchewan. High source contributions from Mexico were also present in 1995. Source contributions during 1998 were solely from Mexico and Central America. These results connect well with the overall source contributions in the previous section in that for both years the highest source contributions tend to be south of the site, especially in 1998.

As with the overall source contributions, UPBU and GRSM had higher source contributions from Mexico and Central America on high K_{NON} days in 1998 than in 1995. During 1995 the source contributions from central and western Canada were higher than during 1998 at all three parks. These results suggest that when K_{NON} values are high long-range transport of smoke from fires in Mexico, Central America or Canada is an important source contribution in the eastern and southeastern U.S. during late spring and early summer as well as transport of smoke from fires in the U.S.

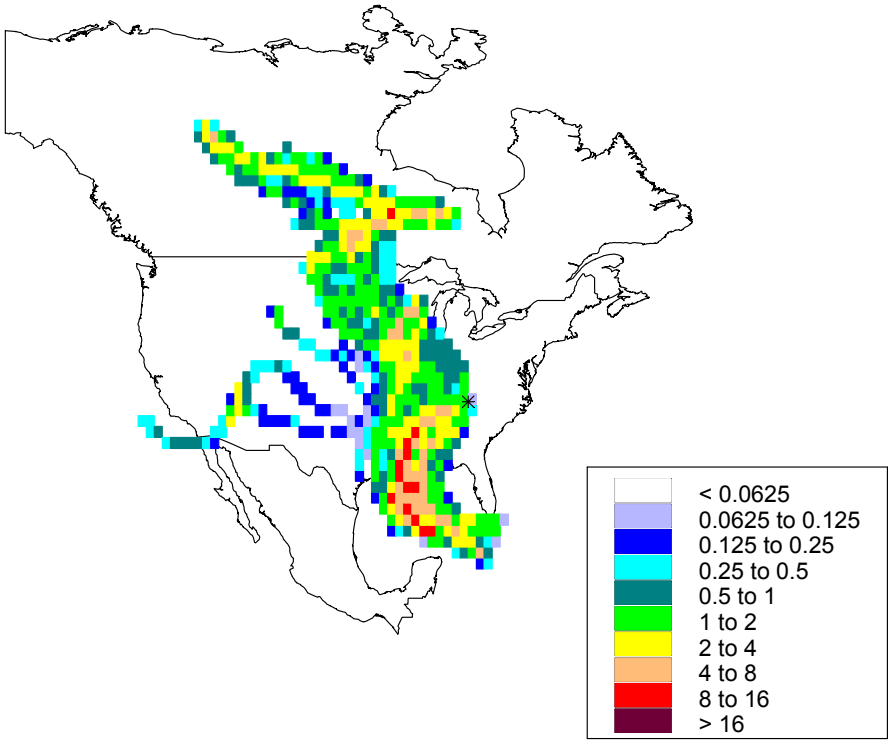

Figure 5.3.1 GRSM 1995 source contributions for days passing K_{NON} criterion. Scale is residence time/equal probability surface. Computed over all IMPROVE sample days, 15-April through 31-July.

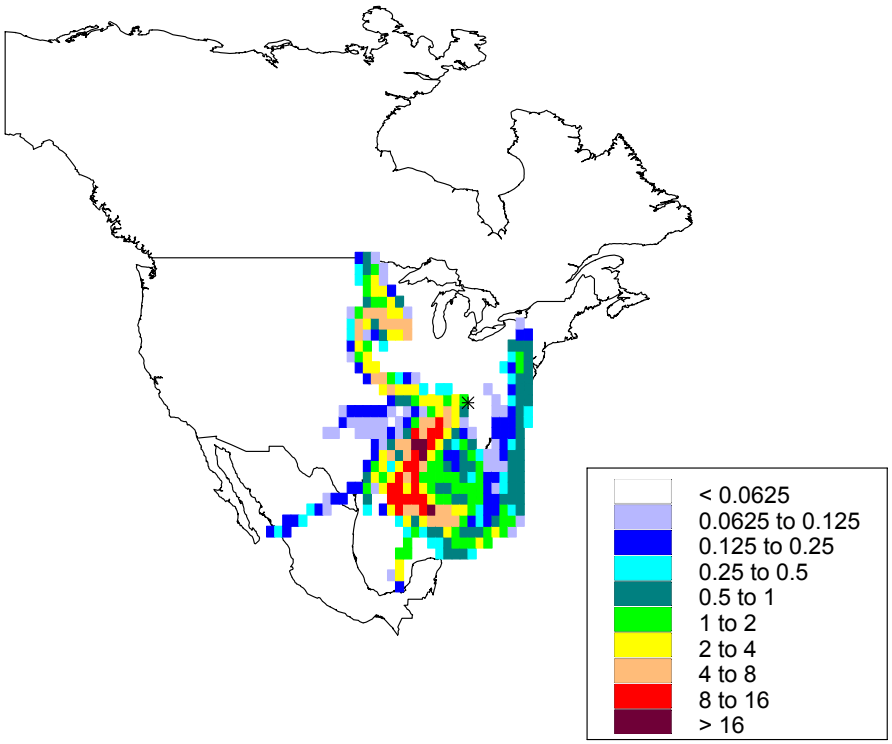

Figure 5.3.2 GRSM 1998 source contributions for days passing K_{NON} criterion. Scale is residence time/equal probability surface. Computed over all IMPROVE sample days, 15-April through 31-July.

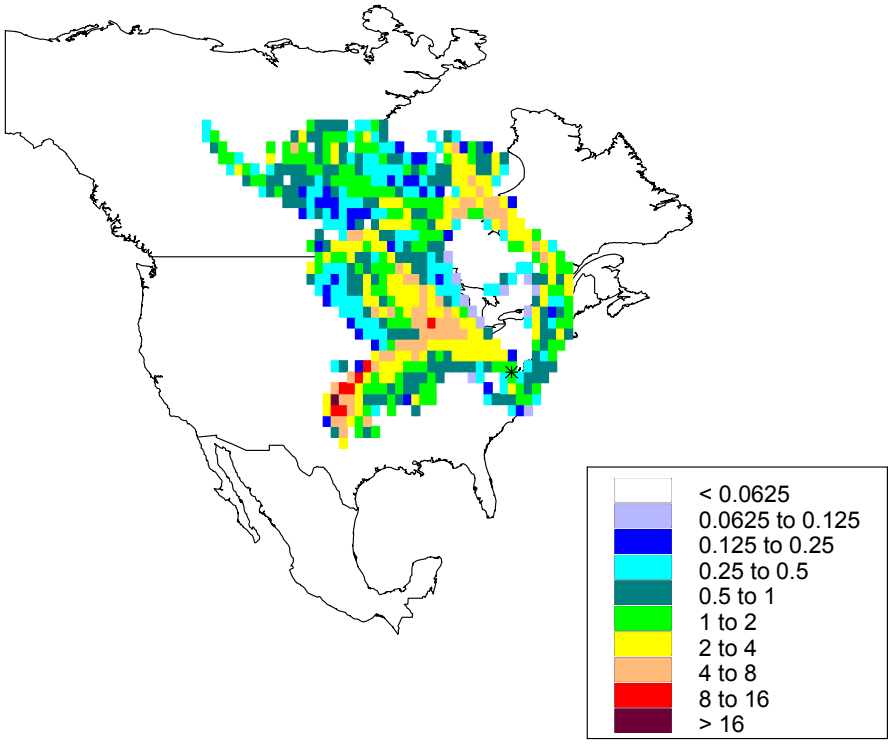

Figure 5.3.3 SHEN 1995 source contributions for days passing K_{NON} criterion. Scale is residence time/equal probability surface. Computed over all IMPROVE sample days, 15-April through 31-July.

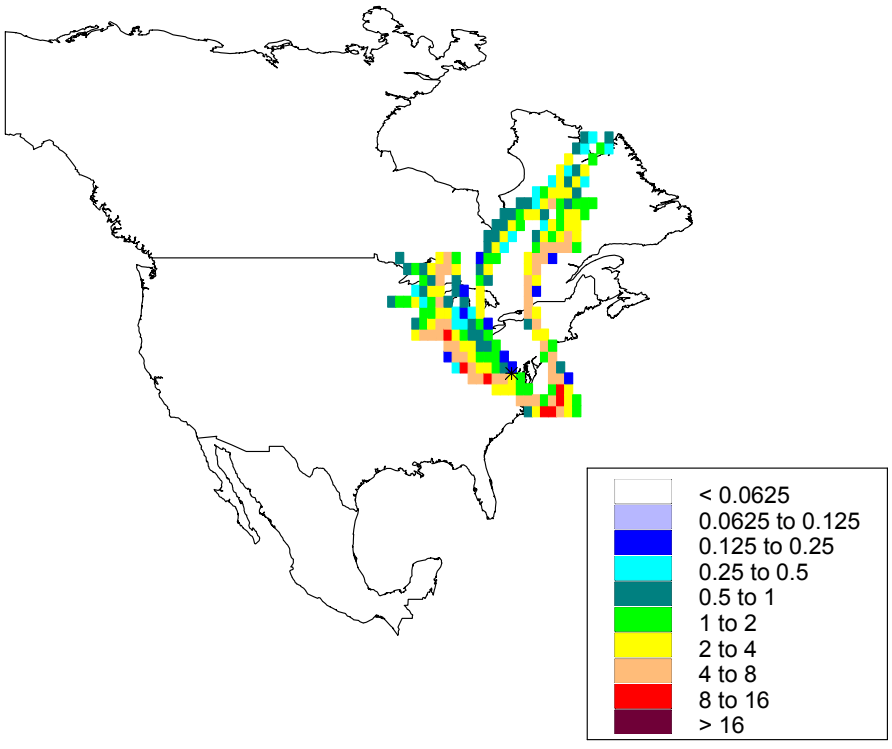

Figure 5.3.4 SHEN 1998 source contributions for days passing K_{NON} criterion. Scale is residence time/equal probability surface. Computed over all IMPROVE sample days, 15-April through 31-July.

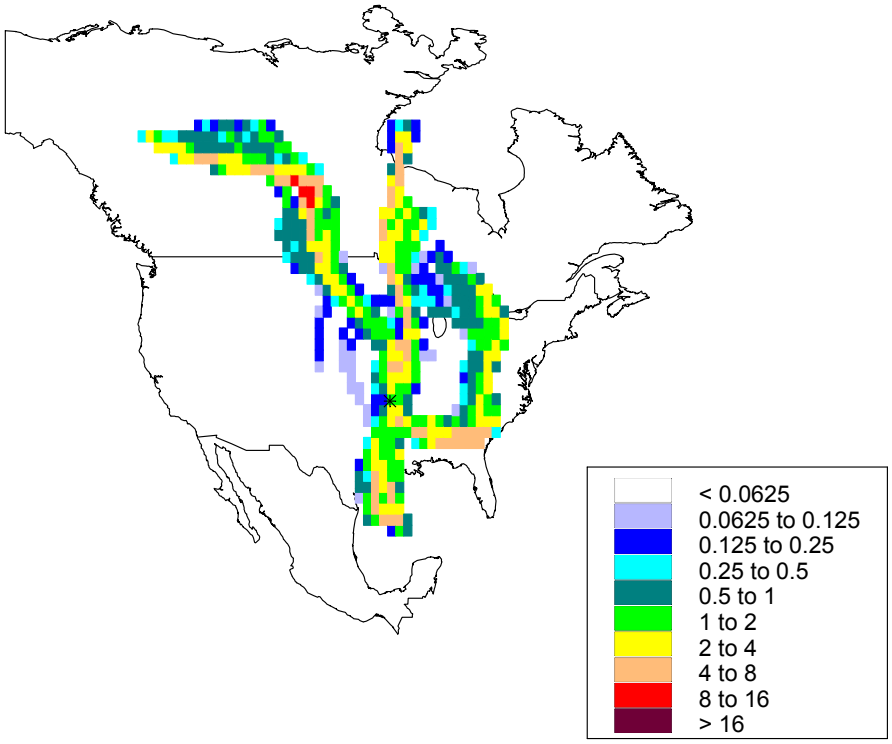

Figure 5.3.5 UPBU 1995 source contributions for days passing K_{NON} criterion. Scale is residence time/equal probability surface. Computed over all IMPROVE sample days, 15-April through 31-July.

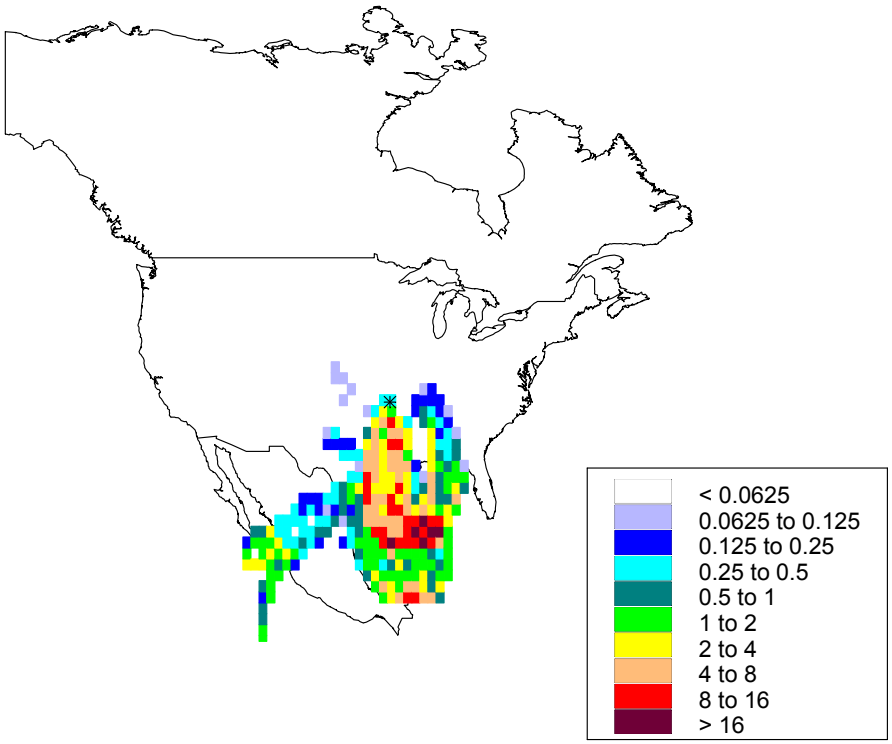

Figure 5.3.6 UPBU 1998 source contributions for days passing K_{NON} criterion. Scale is residence time/equal probability surface. Computed over all IMPROVE sample days, 15-April through 31-July.

Chapter 6. Saharan Dust Criteria and Events

6.1 Saharan Dust Criterion

During the summer months (June-August) the Bermuda high off the east coast of Florida provides favorable wind patterns for transport of dust from the Saharan Desert region to the southeastern and eastern United States (Perry et al., 1997). Dust plumes from North Africa affected the U.S., on average, three times per year from 1992 to 1995 and each event lasted about 10 days (Perry et al., 1997).

Perry et al. (1997) used IMPROVE data to establish a criterion in order to distinguish between dust from North Africa and dust from North America. Elemental ratios, e.g. Al/Ca, Si/Fe, at sites in the eastern U.S. were compared to the ratios at Virgin Islands National Park during a known Saharan dust event in 1993. Perry et al. (1997) found the elemental ratios in the eastern U.S. were nearly identical to the values at Virgin Islands during the dust event. However, when soil concentrations, calculated using the equation in Table 1.3.1, in the eastern U.S. were low the elemental ratios were significantly different from those at Virgin Islands. Thus, data from the Virgin Islands were used to establish a two-part criterion based on a high fine soil concentration and an elevated Al/Ca ratio (Perry et al., 1997). The Al/Ca ratio was chosen because it was significantly elevated at Virgin Islands during the Saharan dust event whereas other ratios exhibited a less significant difference.

Perry et al. (1997) chose fine soil concentrations over 3 $\mu g/m^3$ as the first part of the criterion based on the size distribution of the soil mass concentration at Virgin Islands. The value was chosen because it represents the 25th percentile of the portion of the size distribution dominated by Saharan dust. The second part of the criterion is an Al/Ca ratio greater than 3.8. This value represents the 25th percentile of the Al/Ca ratios at Virgin Islands when the fine soil concentration exceeded 3 $\mu g/m^3$. Using their criterion, Perry et al. (1997) found that Saharan dust events predominantly occur in July with the maximum frequency of events in the southeastern U.S. and decreasing northward and westward.

The two-part criterion used by Perry et al. (1997) was initially used to distinguish North African dust from local soils in this study. The final results presented are based on modifications to this criterion discussed in Section 6.2.

6.2 Modification of the Saharan Dust Criterion

The criterion used by Perry et al. (1997) of Al/Ca ratio greater than 3.8 and fine soil concentrations exceeding 3 $\mu g/m^3$ was initially applied to data from all parks in this study to identify Saharan dust. It was found that parks such as SHEN and JEFF rarely, if ever, actually fulfilled the criterion. As Saharan dust is transported northward and westward from the Gulf of Mexico or the Atlantic, local soil can mix with Saharan dust resulting in an Al/Ca ratio lower than the 3.8 value used by Perry et al. (1997). In addition, settling can remove some of the Saharan dust particles from the atmosphere such that the 3 $\mu g/m^3$ soil concentration is not satisfied. Thus, the two-part criterion indicating the presence of Saharan dust in aerosol samples was modified at each park.

Dust transported from North Africa to the southeastern U.S. reaches a maximum in June, July and August (Perry et al., 1997 and Prospero, 1999). Samples taken during these months were removed from the IMPROVE aerosol data to calculate the local contributions to fine soil concentrations and the Al/Ca ratio in local soil. By removing the summer months it is assumed all soil present in the aerosol samples is from local sources. The means and standard deviations of fine soil and Al/Ca were calculated using the remaining months of data over all years available (see Table 2.2.1 for years available at each park). Observations with Al or Ca concentrations below the minimum detection limits were not included in the calculation of the Al/Ca means or standard deviations. Table 6.2.1 details the results of these calculations. Saharan dust is considered present in a sample when the mean plus one standard deviation of the fine soil concentration and the mean plus one and a half standard deviations of the Al/Ca ratio are exceeded. One and a half standard deviations were used for the Al/Ca ratio to eliminate observations in April that had passed the criterion at one standard deviation and did not have transport from a region consistent with North African dust transport. The Al/Ca ratio is further discussed in Section 6.5. The two-part criterion used throughout this study to indicate the presence of Saharan dust for each park is detailed in Table 6.2.1.

Table 6.2.1 Fine soil concentration and Al/Ca ratio means, standard deviations and criteria used. Calculated using non-summer data.

Park	Al/Ca			Soil ($\mu g/m^3$)		
	Mean	Standard Deviation	Criterion Used	Mean	Standard Deviation	Criterion Used
DOSO	1.8	0.9	3.2	0.341	0.254	0.595
GRSM	1.8	1.1	3.5	0.409	0.335	0.744
JEFF	1.5	0.7	2.6	0.532	0.337	0.869
MACA	1.6	0.9	3.0	0.421	0.276	0.697
SHEN	1.7	0.9	3.1	0.385	0.323	0.708
SHRO	2.2	1.2	4.0	0.402	0.378	0.779
SIPS	1.5	0.7	2.6	0.531	0.404	0.935
UPBU	1.6	0.8	2.8	0.497	0.609	1.107

6.3 1995 Dust Events

Perry et al. (1997) identified two regional Saharan dust events in the eastern and southeastern U.S. during July 1995. The first was on 5-July and the second from 22 through 26-July; maximum spatial extents of the dust impact occurred on the 5th and 26th (Perry et al., 1997).

On 5-July all parks except UPBU and SIPS passed their modified Saharan dust criterion (Table 6.3.1). UPBU did not pass the soil portion of the criterion and the Al concentration was below the minimum detection limit. SIPS was missing data for this day. Trajectories for all parks were southerly from the Gulf of Mexico turning east toward Cuba (Figures 6.3.1a and 6.3.1b). These transport patterns are consistent with the Saharan dust transport patterns identified by Perry et al. (1997). SHEN and JEFF had some trajectories not reaching the Gulf within five days, but still passed their criterion.

Table 6.3.1 Fine soil concentrations and Al/Ca ratios for select days in 1995. Numbers in bold pass the criterion in Table 6.2.1. 'ND' indicates missing data and 'NaN' indicates that the Al or Ca concentrations were below the minimum detection limit or zero.

Date	Quantity	22-Apr	10-May	13-May	1-Jul	5-Jul	8-Jul	12-Jul	15-Jul	19-Jul	22-Jul	26-Jul	29-Jul
DOSO	Soil (μg/m^3)	**1.374**	**1.762**	**0.847**	0.291	**3.653**	0.324	0.478	**1.057**	0.387	0.520	**0.731**	**1.083**
	Al/Ca	2.60	2.80	3.03	1.61	**5.12**	1.02	1.55	1.35	1.24	1.98	**3.43**	**3.61**
GRSM	Soil (μg/m^3)	**2.249**	**1.073**	**0.880**	0.279	**8.538**	0.415	0.571	0.672	0.583	0.431	**6.826**	**0.997**
	Al/Ca	2.31	2.19	**3.77**	NaN	**5.83**	1.40	1.43	2.02	0.80	2.55	**5.70**	3.03
JEFF	Soil (μg/m^3)	**3.004**	**0.931**	ND	0.328	**1.328**	0.456	0.667	**1.073**	0.542	0.536	**0.980**	**1.562**
	Al/Ca	2.52	2.58	ND	NaN	**4.68**	0.96	0.63	1.64	0.77	1.12	**3.51**	**2.69**
MACA	Soil (μg/m^3)	0.479	**1.419**	0.689	0.370	**3.296**	0.272	0.419	0.565	0.613	0.423	**1.699**	**1.240**
	Al/Ca	2.14	1.90	2.88	1.80	**4.97**	1.03	1.54	1.71	1.34	1.70	**4.12**	**4.00**
SHEN	Soil (μg/m^3)	**2.199**	**0.964**	**0.888**	ND	**0.862**	0.378	0.488	**1.398**	0.427	0.513	**1.207**	**1.400**
	Al/Ca	2.95	**3.60**	3.06	ND	**5.08**	1.28	1.86	1.57	0.97	1.31	**4.79**	**3.76**
SHRO	Soil (μg/m^3)	**2.261**	**1.236**	**0.794**	0.323	**6.992**	0.343	0.654	0.706	0.495	0.376	**9.005**	0.233
	Al/Ca	1.93	2.21	2.67	1.71	**5.73**	1.10	2.22	2.57	1.66	2.20	**6.93**	3.13
SIPS	Soil (μg/m^3)	**1.362**	0.928	0.541	0.421	ND	0.222	ND	0.692	ND	0.652	**2.835**	0.719
	Al/Ca	**3.16**	2.45	NaN	1.29	ND	1.59	ND	1.30	ND	2.38	**5.19**	2.42
UPBU	Soil (μg/m^3)	0.424	0.361	**1.243**	0.356	0.397	**2.785**	**1.302**	0.918	0.755	0.958	0.776	**1.961**
	Al/Ca	2.39	2.39	2.28	NaN	NaN	**3.85**	1.67	**3.33**	1.34	2.41	**3.43**	**3.37**

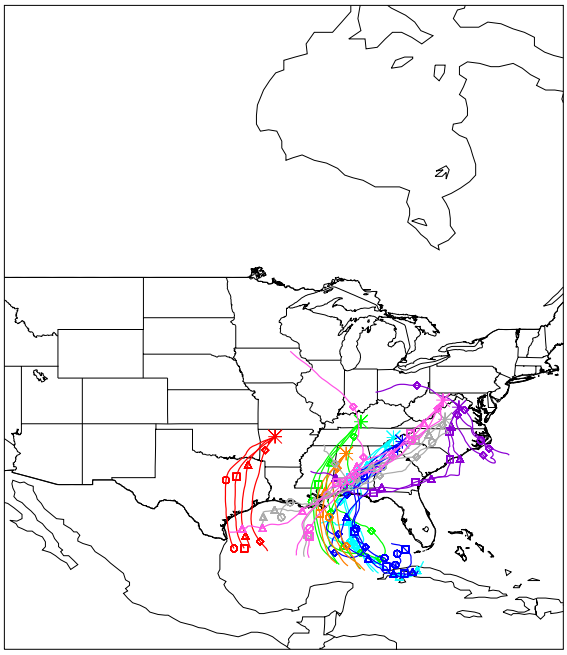

Figure 6.3.1a 5-July trajectories calculated using NGM data.

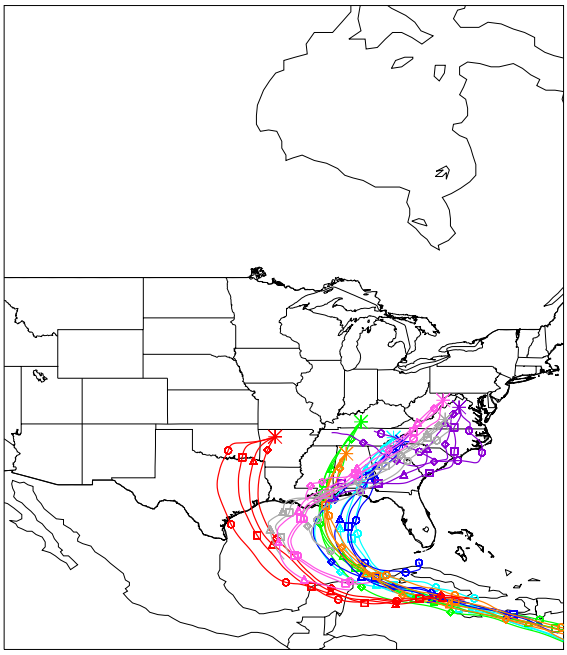

Figure 6.3.1b 5-July trajectories calculated using reanalysis data.

It is also interesting to note the difference in fine soil mass concentrations and Al/Ca ratio at DOSO, GRSM, JEFF, MACA, SHEN and SHRO from 5-July, during the dust event, to 8-July when the smoke plume from Canada was present. Fine soil concentrations on 8-July were less than 0.5 $\mu g/m^3$ and the ratio Al/Ca was less than 1.6 at all except UPBU, which was dust impacted. At DOSO, GRSM, MACA and SHRO fine mass concentrations on the 8th were less than one tenth the concentrations on the 5th.

On 26-July the second Saharan dust plume is evident at all parks. UPBU was the only park to not pass both parts of the criterion on this day. Transport was from the Gulf north to Missouri and east to the sites for all parks, except UPBU, which was north from the Gulf to the site (Figures 6.3.2a and 6.3.2b).

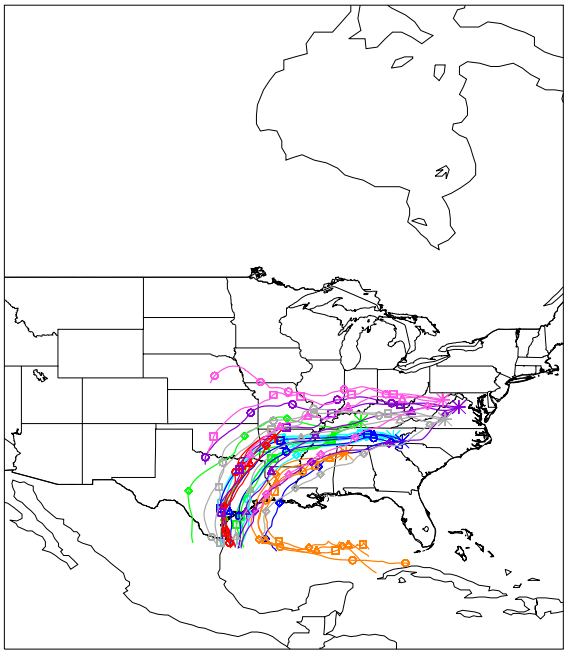

Figure 6.3.2a 26-July trajectories calculated using NGM data.

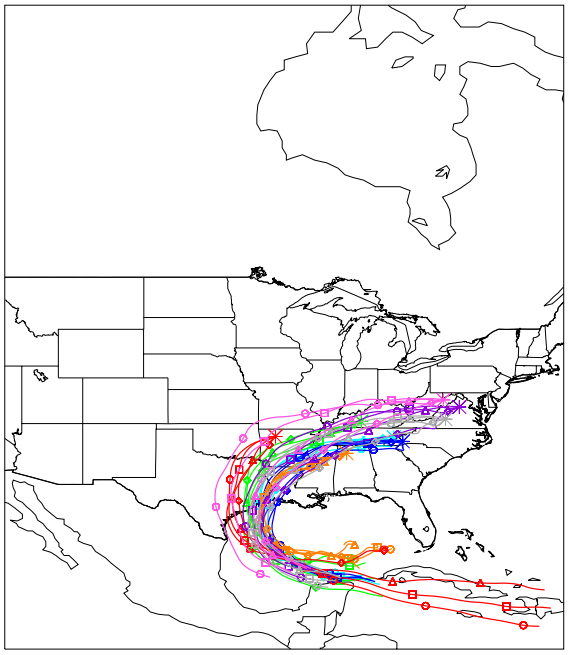

Figure 6.3.2b 26-July trajectories calculated using reanalysis data.

On 29-July DOSO, JEFF, MACA, SHEN and UPBU passed their criteria and GRSM had a high soil concentration. Transport patterns are consistent with the finding of North African dust impact at DOSO, JEFF, MACA, SHEN and UPBU. Transport to SIPS, GRSM and SHRO was from the same region as the dust impacted parks, but precipitation could have removed particles causing the fine soil to be low at these parks.

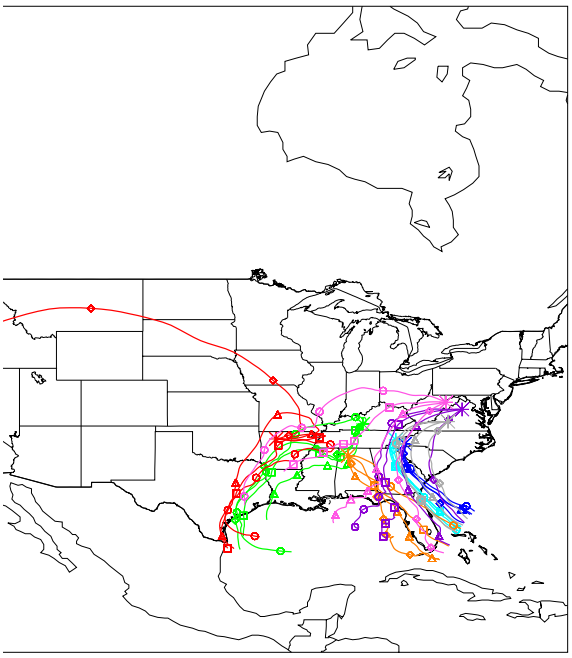

Figure 6.3.3a 29-July trajectories calculated using NGM data.

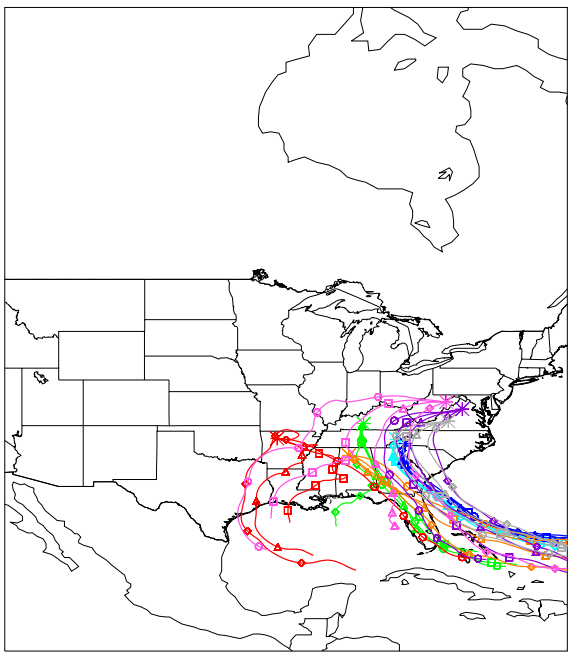

Figure 6.3.3b 29-July trajectories calculated using reanalysis data.

Although North African dust transport doesn't peak until summer, it has been observed in samples from Virgin Islands National Park in April and at Everglades National Park in Florida during May (Perry et al., 1997). On 22-April there were elevated soil concentrations at all parks except UPBU and MACA. SIPS also passed the Al/Ca criterion. SHEN passed the two-part criterion on 10-May. DOSO, GRSM, JEFF, MACA and SHRO also had high soil concentrations on 10-May, which supports the finding of North African dust at SHEN. Similarly, on 13-May the presence of North African dust was indicated at GRSM and there were fine soil concentrations exceeding the criteria at all parks except MACA and UPBU. Transport on all three days is consistent with North African dust transport patterns in July. See Appendix A for trajectories for 22-April, 10-May and 13-May.

6.4 1998 Dust Events

In 1998 the presence of North African dust was indicated in 21 observations, seven in June and 14 in July (Tables 6.4.1 and 6.4.2). In 1995 the maximum fine soil concentration during the time period of consideration was 9 μg/m^3 at SHRO in late July. In 1998 the highest observed fine soil concentration was over 14 μg/m^3 at SIPS on 27-June. During July, five out of nine observations at UPBU were impacted by Saharan dust (Table 6.4.2) with soil concentrations exceeding twice the criterion on all five days. SIPS also had substantial Saharan dust impact in July with four of eight observations passing the two-part criterion. In contrast, during 1995 one of six observations at SIPS and only two of nine at UPBU passed the criteria. Trajectories are presented here for days where multiple parks had dust impact. For the days where only UPBU or SIPS passed the North African dust criterion trajectories are in Appendix A.

Table 6.4.1 Fine soil concentrations and Al/Ca ratios for June 1998. Numbers in bold exceed the criterion in Table 6.2.1. 'ND' indicates data was missing and 'NaN' indicates that the Al or Ca concentrations were below the minimum detection limit or zero.

Park	Quantity	10-Jun	13-Jun	17-Jun	20-Jun	24-Jun	27-Jun
DOSO	Soil (μg/m^3)	0.244	0.339	0.122	0.357	0.474	**1.008**
	Al/Ca	NaN	NaN	NaN	NaN	1.95	NaN
GRSM	Soil (μg/m^3)	0.385	**2.801**	0.313	0.292	**0.878**	**2.209**
	Al/Ca	1.58	**5.09**	NaN	NaN	2.32	3.47
JEFF	Soil (μg/m^3)	0.261	0.681	0.436	0.430	0.514	**1.377**
	Al/Ca	0.94	NaN	NaN	0.73	0.75	2.13
MACA	Soil (μg/m^3)	0.445	**0.789**	0.456	0.364	0.619	**9.329**
	Al/Ca	NaN	NaN	NaN	NaN	NaN	**7.54**
SHEN	Soil (μg/m^3)	0.008	0.553	0.234	0.487	0.455	**1.844**
	Al/Ca	NaN	NaN	NaN	NaN	NaN	**3.48**
SHRO	Soil (μg/m^3)	0.470	**1.802**	0.265	0.236	0.606	**0.992**
	Al/Ca	NaN	**4.88**	NaN	NaN	2.00	2.18
SIPS	Soil (μg/m^3)	0.450	**1.433**	0.479	0.434	ND	**14.119**
	Al/Ca	NaN	NaN	NaN	NaN	ND	**8.56**
UPBU	Soil (μg/m^3)	0.679	**2.745**	0.640	0.841	0.492	**3.016**
	Al/Ca	NaN	**3.37**	2.10	NaN	NaN	**6.61**

Table 6.4.2 Fine soil concentrations and Al/Ca ratios for July 1998. Numbers in bold exceed the criterion in Table 6.2.1. 'ND' indicates data was missing and 'NaN' indicates that the Al or Ca concentrations were below the minimum detection limit or zero.

Park	Quantity	1-Jul	4-Jul	8-Jul	11-Jul	15-Jul	18-Jul	22-Jul	25-Jul	29-Jul
DOSO	Soil ($\mu g/m^3$)	0.211	0.081	**1.031**	0.317	0.318	0.454	**0.642**	0.446	0.241
	Al/Ca	NaN	NaN	NaN	1.25	2.82	NaN	NaN	NaN	NaN
GRSM	Soil ($\mu g/m^3$)	0.600	**1.108**	**3.233**	0.410	0.464	0.477	**1.066**	0.456	**1.629**
	Al/Ca	1.71	NaN	**6.32**	0.67	1.85	NaN	**3.67**	1.60	NaN
JEFF	Soil ($\mu g/m^3$)	0.300	0.379	**1.435**	0.144	0.429	0.460	0.665	0.505	0.733
	Al/Ca	NaN	NaN	**3.11**	NaN	NaN	0.66	NaN	0.97	NaN
MACA	Soil ($\mu g/m^3$)	0.425	**0.920**	**4.642**	0.420	0.081	0.583	**0.826**	0.520	**1.565**
	Al/Ca	0.65	NaN	**6.16**	NaN	NaN	NaN	2.25	0.95	**3.51**
SHEN	Soil ($\mu g/m^3$)	0.332	0.205	**0.781**	0.233	0.644	0.475	**0.824**	0.461	0.669
	Al/Ca	NaN	2.89	NaN	NaN	2.18	1.10	1.53	1.26	0.62
SHRO	Soil ($\mu g/m^3$)	ND	ND	ND	ND	0.465	0.458	**0.796**	0.410	**1.085**
	Al/Ca	ND	ND	ND	ND	NaN	1.51	NaN	2.54	3.86
SIPS	Soil ($\mu g/m^3$)	**6.253**	0.904	**1.190**	0.689	**1.524**	0.464	**3.299**	0.565	ND
	Al/Ca	**4.95**	NaN	**3.41**	NaN	**4.31**	NaN	**7.78**	NaN	ND
UPBU	Soil ($\mu g/m^3$)	0.522	**2.533**	**7.524**	**2.878**	0.449	0.802	**2.574**	0.819	**6.798**
	Al/Ca	NaN	**4.72**	**5.87**	**7.00**	NaN	NaN	**5.30**	**3.12**	**7.20**

The first day with Saharan dust impact was 13-June. GRSM, SHRO and UPBU all exceeded the two-part criterion and the fine soil concentrations at MACA and SIPS exceeded their soil criteria. All parks not passing the Al/Ca ratio part of the criterion had Al concentrations below the minimum detection limit. Transport to all parks was primarily from the Gulf of Mexico, which is consistent with the finding of Saharan dust impact at GRSM, SHRO and UPBU and the high soil concentrations at MACA and SIPS (Figures 6.4.1a and 6.4.1b). The EDAS trajectories for MACA differ from the FNL trajectories in that EDAS has a front passing during the first half of the day while FNL indicates frontal passage near the end of the day.

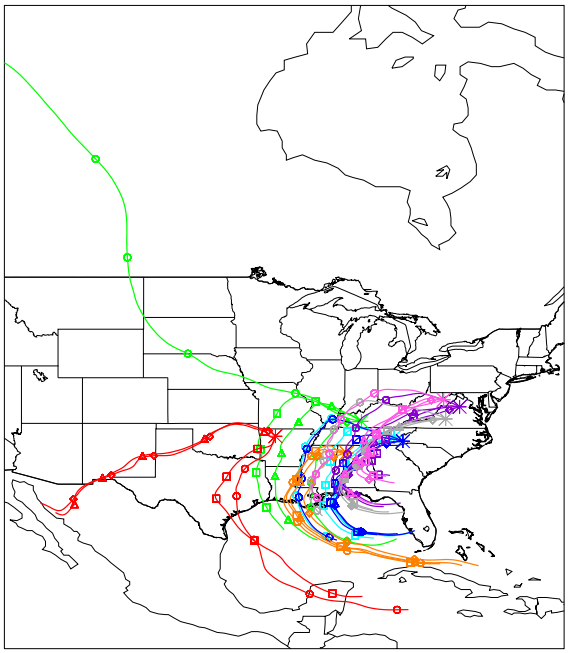

Figure 6.4.1a 13-June trajectories calculated using FNL data.

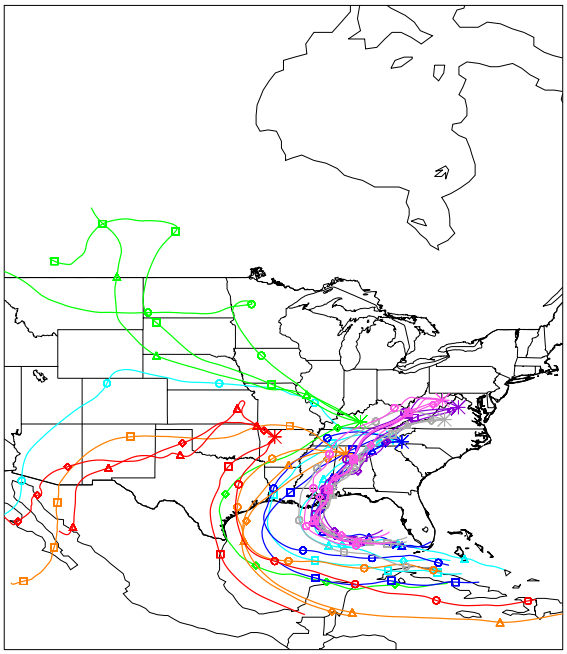

Figure 6.4.1b 13-June trajectories calculated using EDAS data.

All parks had soil concentrations passing the fine soil criterion on 27-June. UPBU, SIPS, SHEN and MACA also exceeded the criterion for the Al/Ca ratio. GRSM was very close to passing the Al/Ca = 3.5 criterion with a ratio of 3.47. The Al concentration was below the minimum detection limit at DOSO. Transport patterns support the finding of North African dust impact at UPBU, SIPS, SHEN and MACA and the high soil concentrations at all parks (Figure 6.4.2).

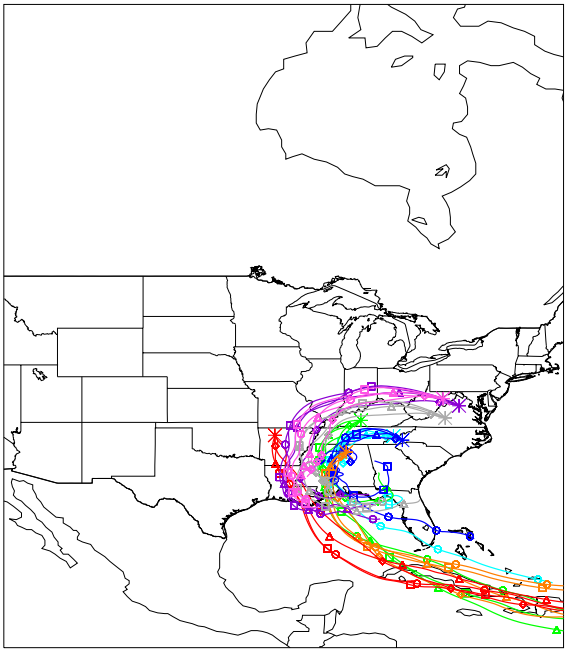

Figure 6.4.2 27-June trajectories calculated using FNL data.

Again, on 8-July soil concentrations were high at all parks except SHRO, which was missing data. GRSM, JEFF, MACA, SIPS and UPBU passed both parts of the criterion and DOSO and SHEN had Al concentrations less than the minimum detection limit. The trajectories for MACA, SIPS and UPBU on this day are consistent with North African dust transport (Figure 6.4.3). JEFF and GRSM did not have transport patterns consistent with North African dust transport; however, trajectories indicate these parks were under the influence of high pressure, which could explain the high soil concentrations.

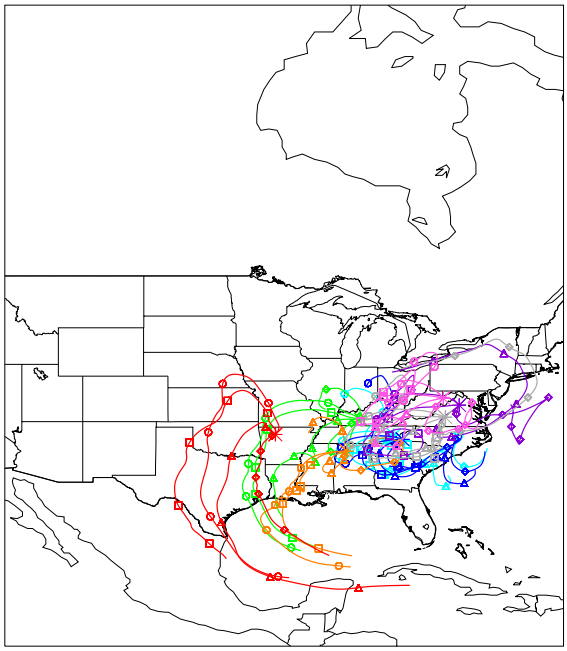

Figure 6.4.3 8-July trajectories calculated using FNL data.

Figures 6.4.4 and 6.4.5 are the trajectories for 22-July and 29-July. On 22-July GRSM, SIPS and UPBU passed and on 29-July UPBU and MACA passed the criterion. Transport patterns for 22-July are consistent with the findings of North African dust impact at GRSM, SIPS and UPBU, and with no Saharan dust impact at DOSO, JEFF and SHEN. Transport to SHRO was from the same region as GRSM, but the Al concentration was below the minimum detection limit. On the 29th transport to UPBU was consistent with the finding of Saharan dust impact in the aerosol sample and SIPS was missing data. Transport to MACA was not from a region that would indicate Saharan dust transport and does not agree with the finding of Saharan dust impact on the aerosol sample for 29-July.

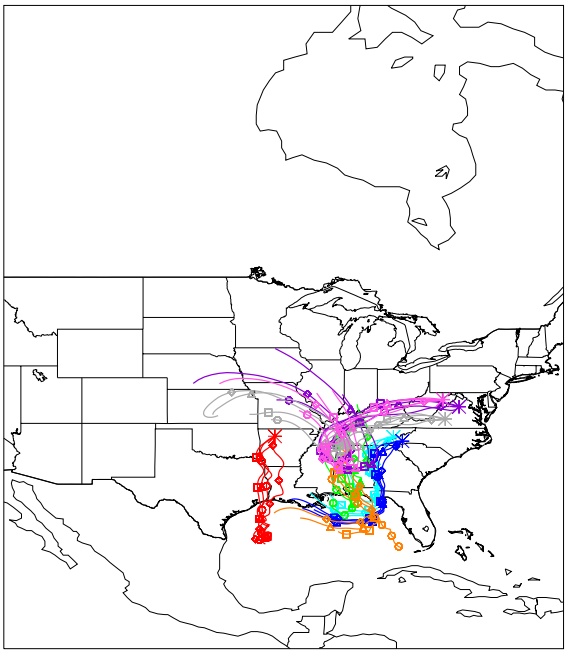

Figure 6.4.4 22-July trajectories calculated using FNL data.

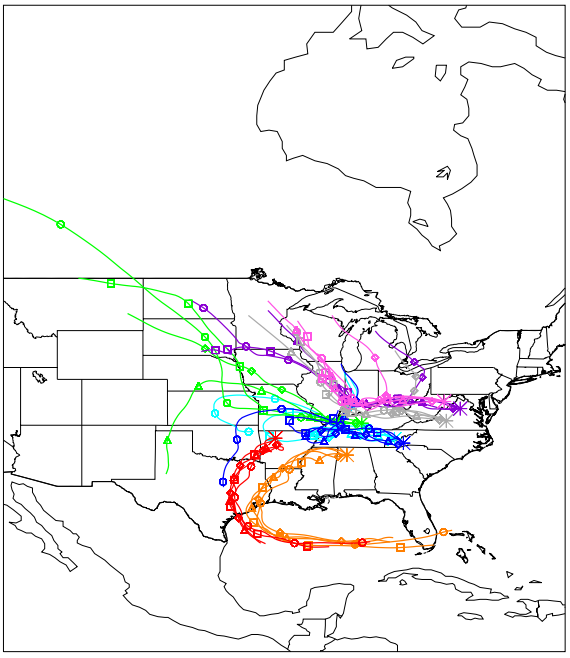

Figure 6.4.5 29-July trajectories calculated using FNL data.

6.5 Discussion of the Al/Ca Ratio Criterion

As discussed previously, the elemental composition of soils varies globally. The assumption made when using the Al/Ca ratio is that there are distinct differences between the ratio of Al to Ca in U.S. soils and North African dust. To illustrate this, Figures 6.5.1 through 6.5.8 plot aluminum versus calcium over all years of available data at each park. Included on each plot is the Al/Ca criterion value calculated in this study and Perry et al.'s (1997) 3.8 criterion. The important aspect of these plots is that, at higher soil concentrations, two populations are expected to emerge: one population with a higher Al/Ca ratio that is representative of North African dust, and another with lower Al/Ca ratio that is representative of local soils. These populations are likely to overlap with samples having ratios in between the local soil and Saharan dust ratios because many of the samples will contain a mix of the two sources.

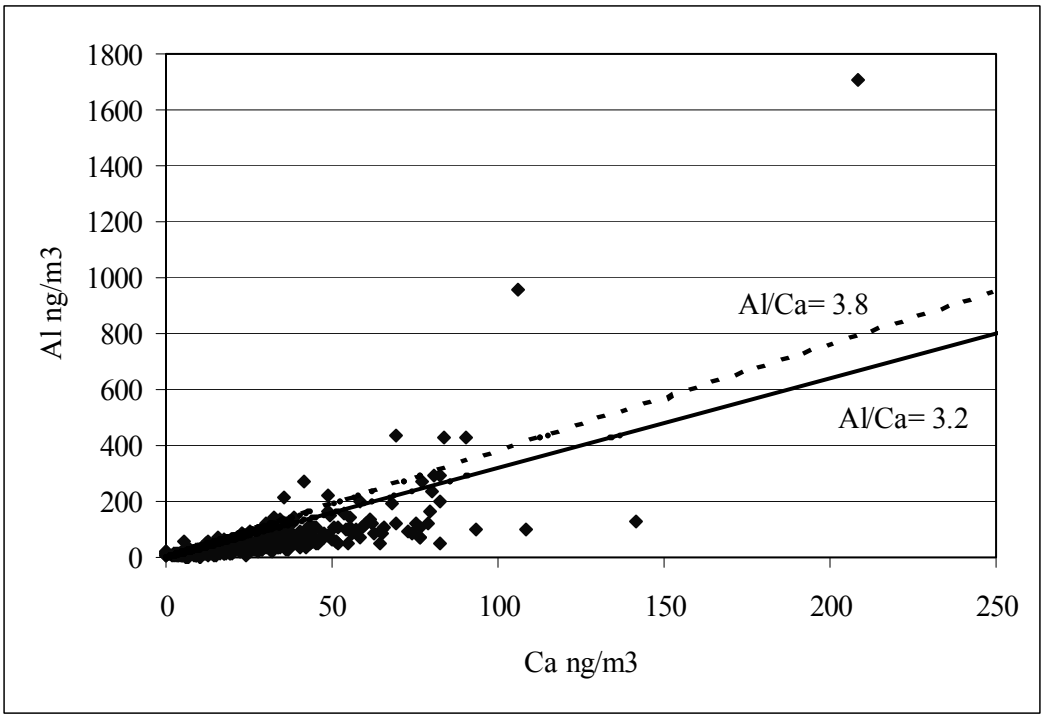

Figure 6.5.1 Aluminum versus Calcium concentrations at DOSO over all years. Dotted line is Al/Ca = 3.8 and solid line is the Al/Ca criterion used in this study.

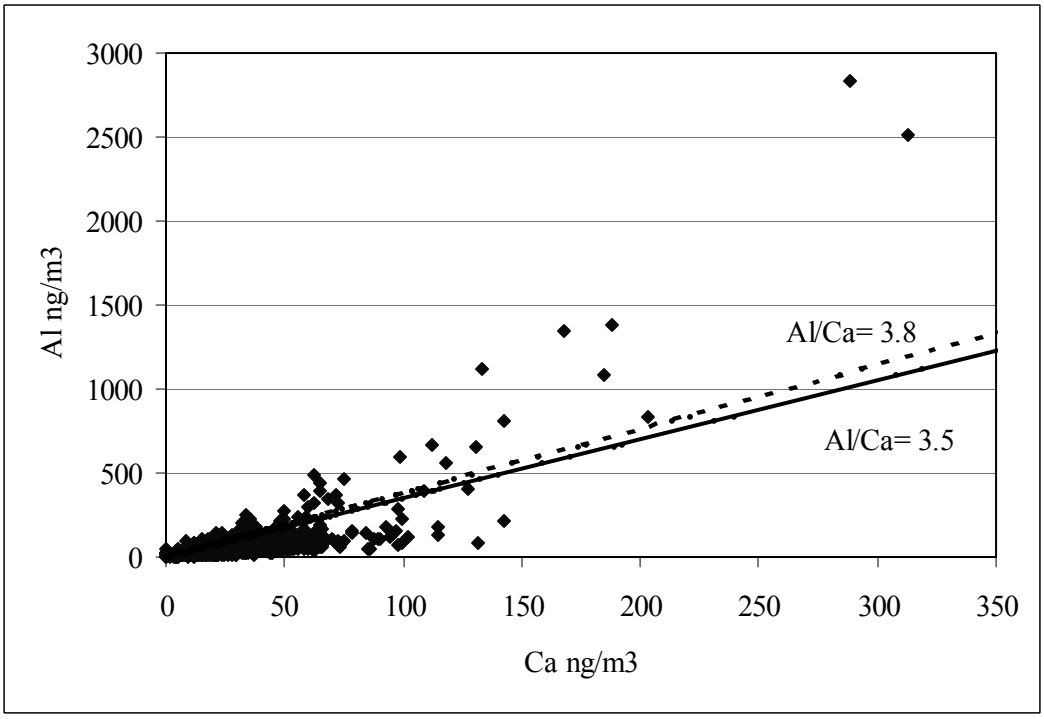

Figure 6.5.2 Aluminum versus Calcium concentrations at GRSM over all years. Dotted line is Al/Ca = 3.8 and solid line is the Al/Ca criterion used.

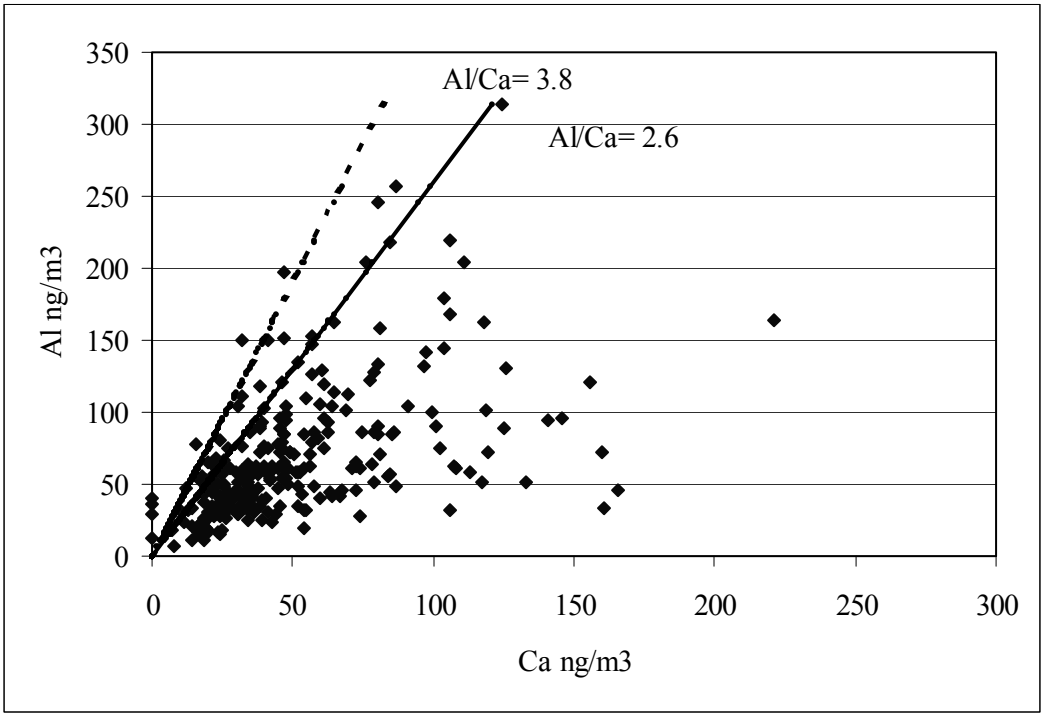

Figure 6.5.3 Aluminum versus Calcium concentrations at JEFF over all years. Dotted line is Al/Ca = 3.8 and solid line is the Al/Ca criterion used.

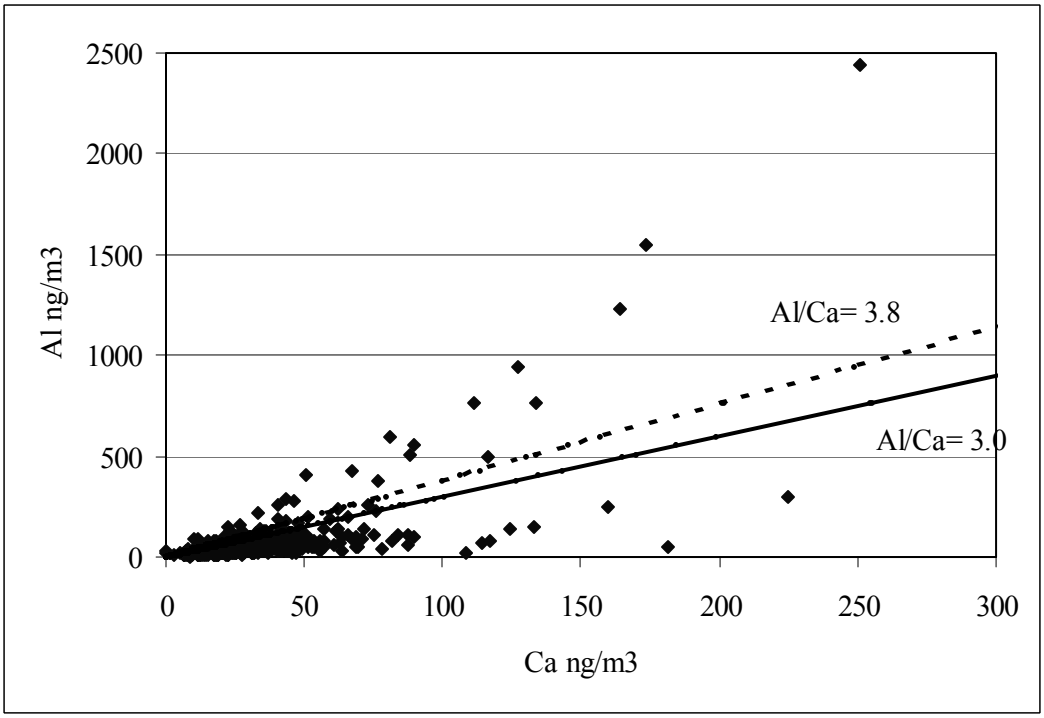

Figure 6.5.4 Aluminum versus Calcium concentrations at MACA over all years. Dotted line is Al/Ca = 3.8 and solid line is the Al/Ca criterion used.

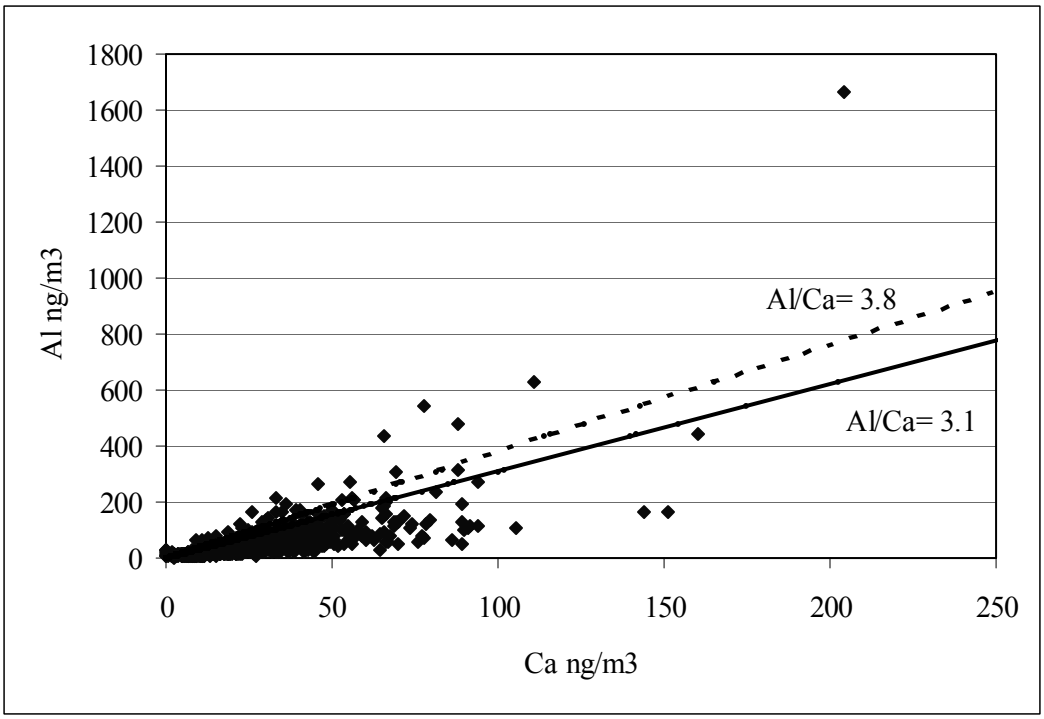

Figure 6.5.5 Aluminum versus Calcium concentrations at SHEN over all years. Dotted line is Al/Ca = 3.8 and solid line is the Al/Ca criterion used.

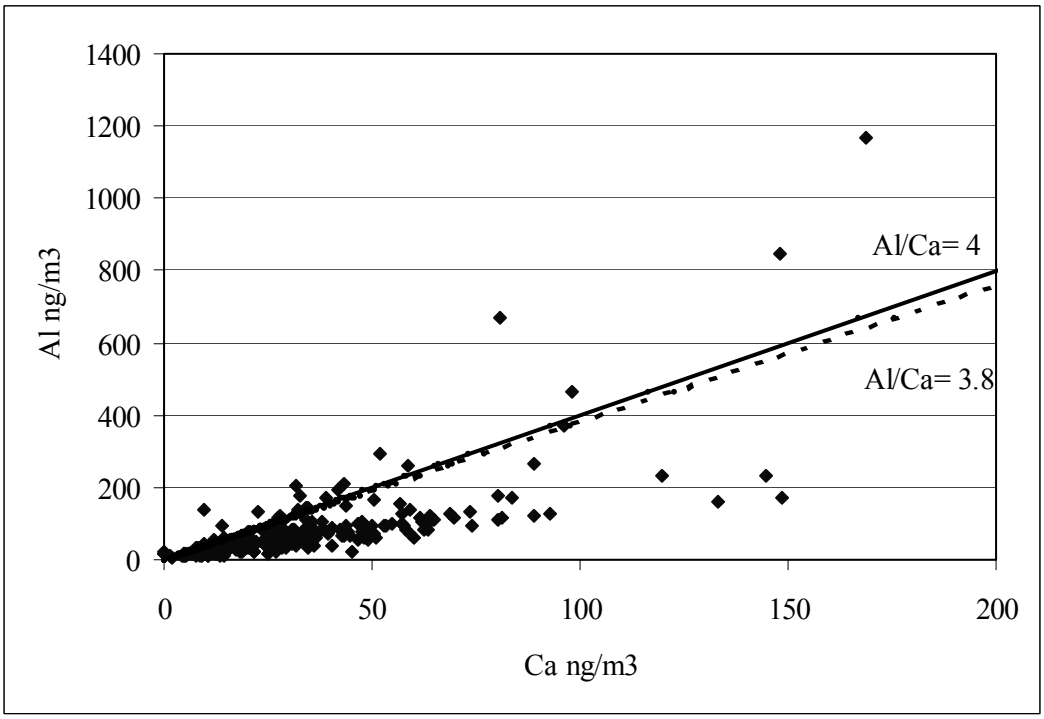

Figure 6.5.6 Aluminum versus Calcium concentrations at SHRO over all years. Dotted line is Al/Ca = 3.8 and solid line is the Al/Ca criterion used.

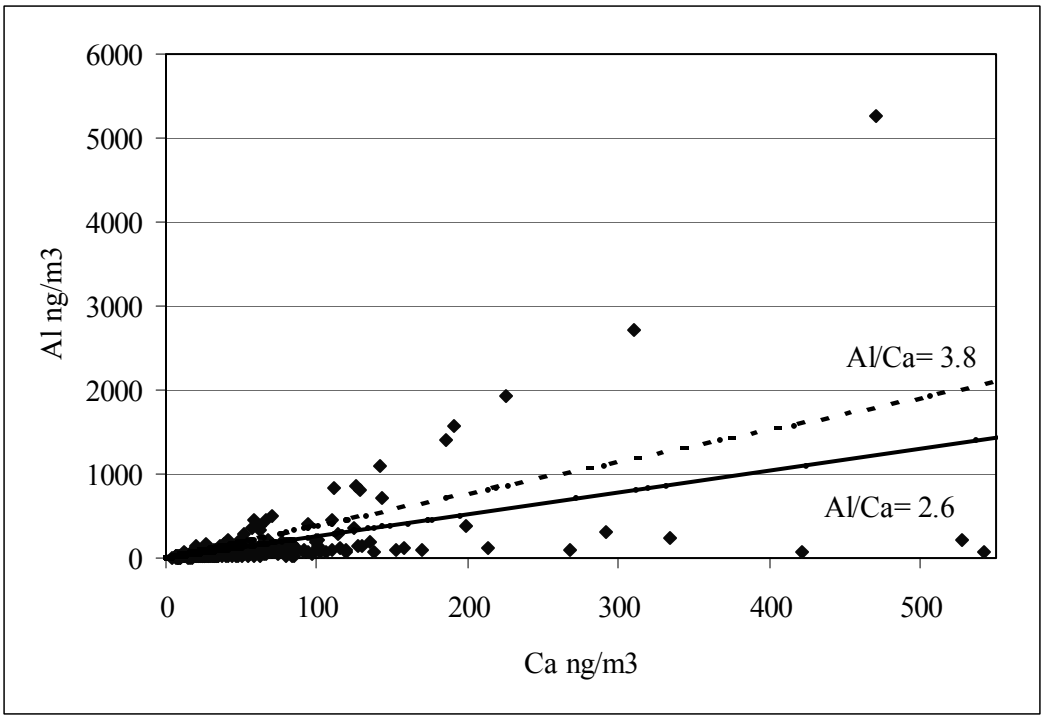

Figure 6.5.7 Aluminum versus Calcium concentrations at SIPS over all years. Dotted line is Al/Ca = 3.8 and solid line is the Al/Ca criterion used.

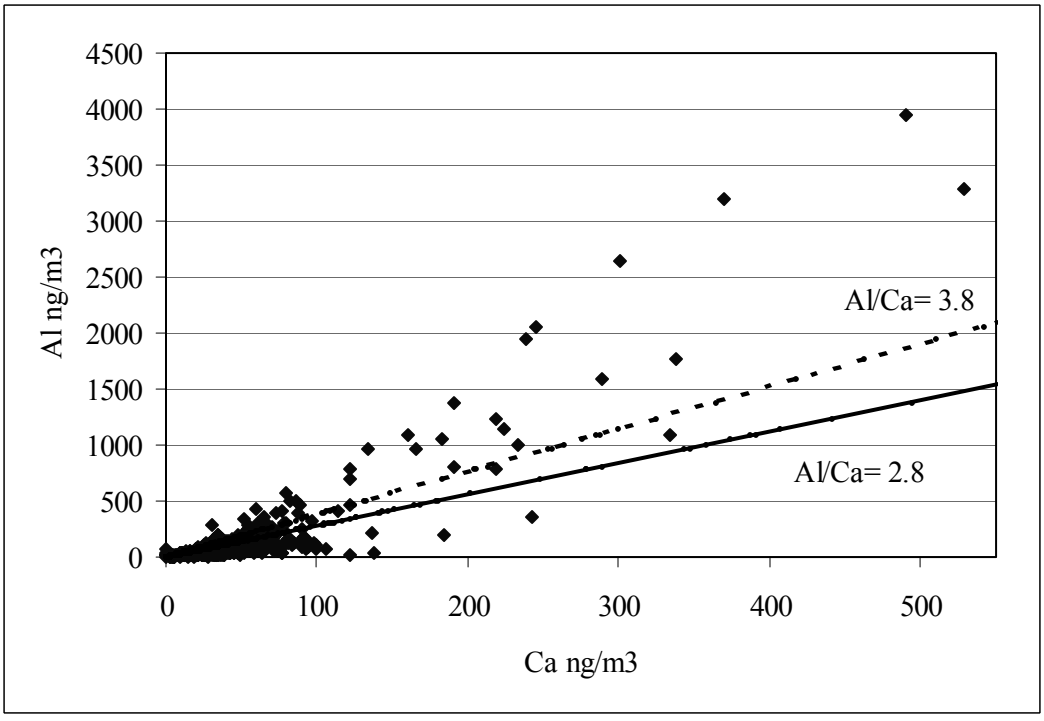

Figure 6.5.8 Aluminum versus Calcium concentrations at UPBU over all years. Dotted line is Al/Ca = 3.8 and solid line is the Al/Ca criterion used.

At DOSO, MACA, SHEN, SHRO and SIPS two populations do in fact emerge; one with high Al concentrations and another with lower Al concentrations. At JEFF, GRSM and UPBU two populations are not distinct. This reflects another important aspect, that the selection of a value to distinguish North African dust is not obvious. There is a wide range of values that would be useful indicators of dust from North Africa. The value separating North African dust from local soils is not distinct because "local" soils includes many different soil types from the U.S., Canada and Mexico and because the soil particles from North Africa can mix with soils from other regions resulting in different elemental composition. However, it is believed the values used in this study are adequate for distinguishing North African dust from other soil sources based on the results in Sections 6.3 and 6.4.

Chapter 7. K_{NON} Formula Modifications and Sensitivity to Assumptions

7.1 Modifications of the K_{NON} Formula

Modifications to the K_{NON} formula were made using 1995 as a test case. This year was chosen based on the findings of Wotawa and Trainer (2000), as discussed in Section 1.2.1. The goal was to minimize the number of false positives and false negatives for smoke impact by accounting for different soil types and sea salt in the calculation of K_{NON}.

The original formula for calculating K_{NON} was taken from the UC-Davis IMPROVE User's Guide (1995) (Eq. 7.1). It is based on the assumption that soil has a potassium to iron ratio of 0.6 as discussed in Chapter 2.

$$K_{NON} = K - 0.6*Fe \quad \text{(Eq. 7.1)}$$

The first modification to this equation was based on the knowledge that dust from North Africa is frequently transported to the southeastern U.S. (Perry et al., 1997). Two such events were identified in 1995 in the southeastern U.S. as discussed in Chapter 5. It was possible that smoke impacted days were left undetected using Eq. 7.1 due to a lower K/Fe ratio in Saharan dust. Thus, as discussed in Section 2.2.1, the ratio K/Fe=0.45 was used on days considered impacted by Saharan dust (Eq. 7.2).

$$K_{NON} = K - 0.45*Fe \quad \text{(Eq. 7.2)}$$

The next modification made was to account for aerosol potassium in sea salt. This was done because transport to the selected parks is often from the Gulf of Mexico or

the Atlantic Ocean. The ratio of K/Na=0.036 was calculated from the average composition of seawater in Seinfeld and Pandis (1998). Thus, the final equations used are Eq. 7.3 when samples were not impacted by dust from North Africa and Eq. 7.4 when samples were impacted by North African dust.

$$K_{NON} = K - 0.6*Fe - 0.036*Na \quad \text{(Eq. 7.3)}$$

$$K_{NON} = K - 0.45*Fe - 0.036*Na \quad \text{(Eq. 7.4)}$$

An alternative method for calculating K_{NON} uses Si to estimate the soil contribution to aerosol K. Silicon can be used rather than iron because the Si concentration in soils varies less than the Fe concentration globally (Eldred, 2002). The ratio assumed for this method is K/Si=0.11 (Eldred, 2002), which results in Eq. 7.5:

$$K_{NON} = K - 0.11*Si - 0.036*Na \quad \text{(Eq. 7.5)}$$

The results of the modifications to the K_{NON} equation and results using Si instead of Fe during 1995 are presented for each park individually (Figures 7.1.1 through 7.1.8). In addition, smoke days identified as discussed in Section 2.4 are presented. Each modification of the formula resulted in different medians, standard deviations and smoke criteria as well as K_{NON} values. The medians, standard deviations and smoke criteria from the various methods are presented in Table 7.1.1. The modification to account for dust from North Africa primarily affected the value used for the smoke criterion at each park. As discussed in Chapter 5, the months of maximum Saharan dust impact are June and July, and from Chapters 3 and 4, the peak of the fire season in Mexico, Central America and Cuba is in April and May. Thus, when dust impact is most likely, smoke impact from similar transport regions, Mexico, Central America and Cuba, is not as likely, so it is difficult to judge the overall importance of this modification.

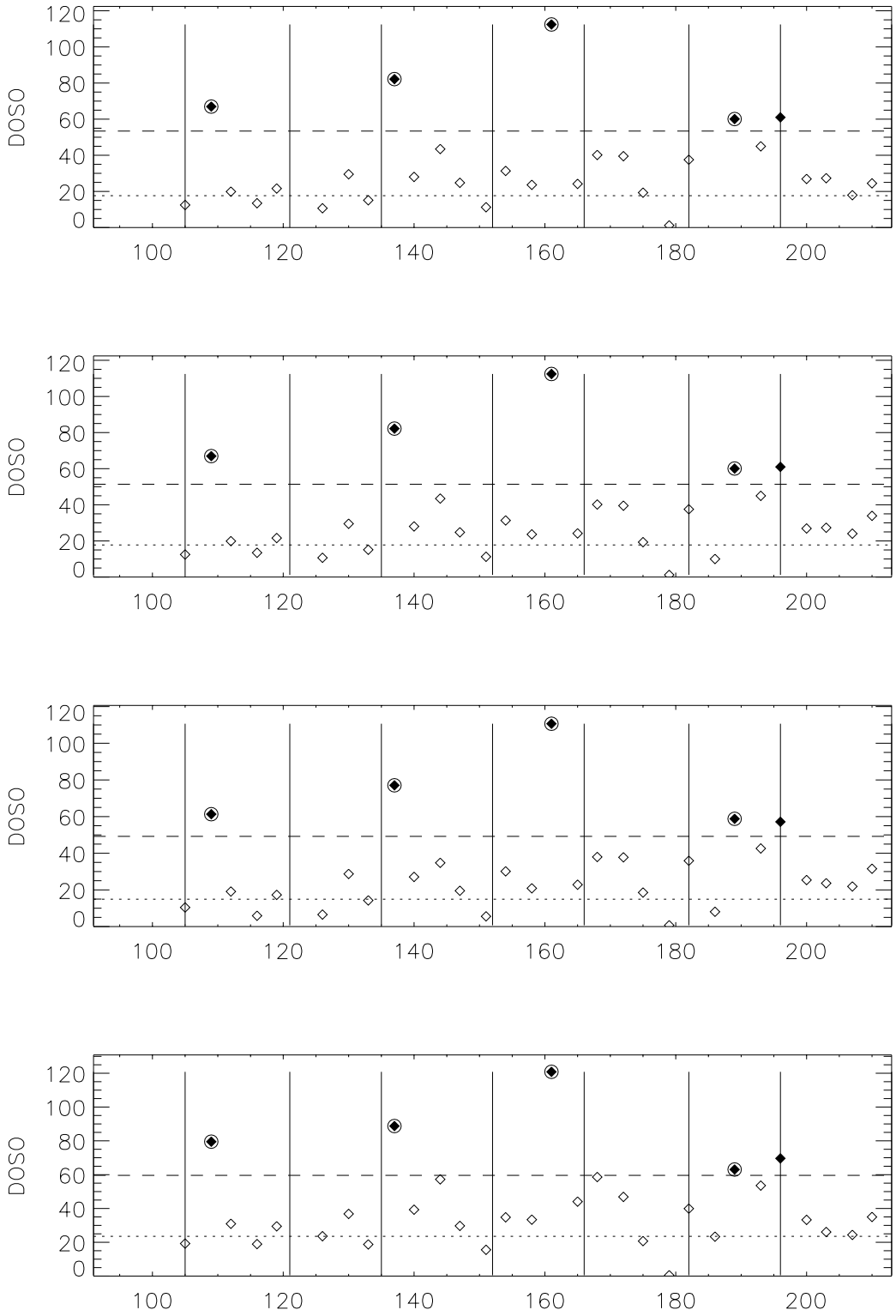

Figure 7.1.1 K_{NON} results at DOSO using various formulas for 15-April through 31-July 1995. Top--not accounting for North African dust or sea salt, second--accounting for North African dust and not sea salt, third--final equations used and bottom--silicon method. Filled symbols are days passing the criterion, circled symbols are smoke-impacted samples from trajectory analysis, x-axis is Julian day where 105 is 15-April and vertical lines mark the first and fifteenth of each month, April through July.

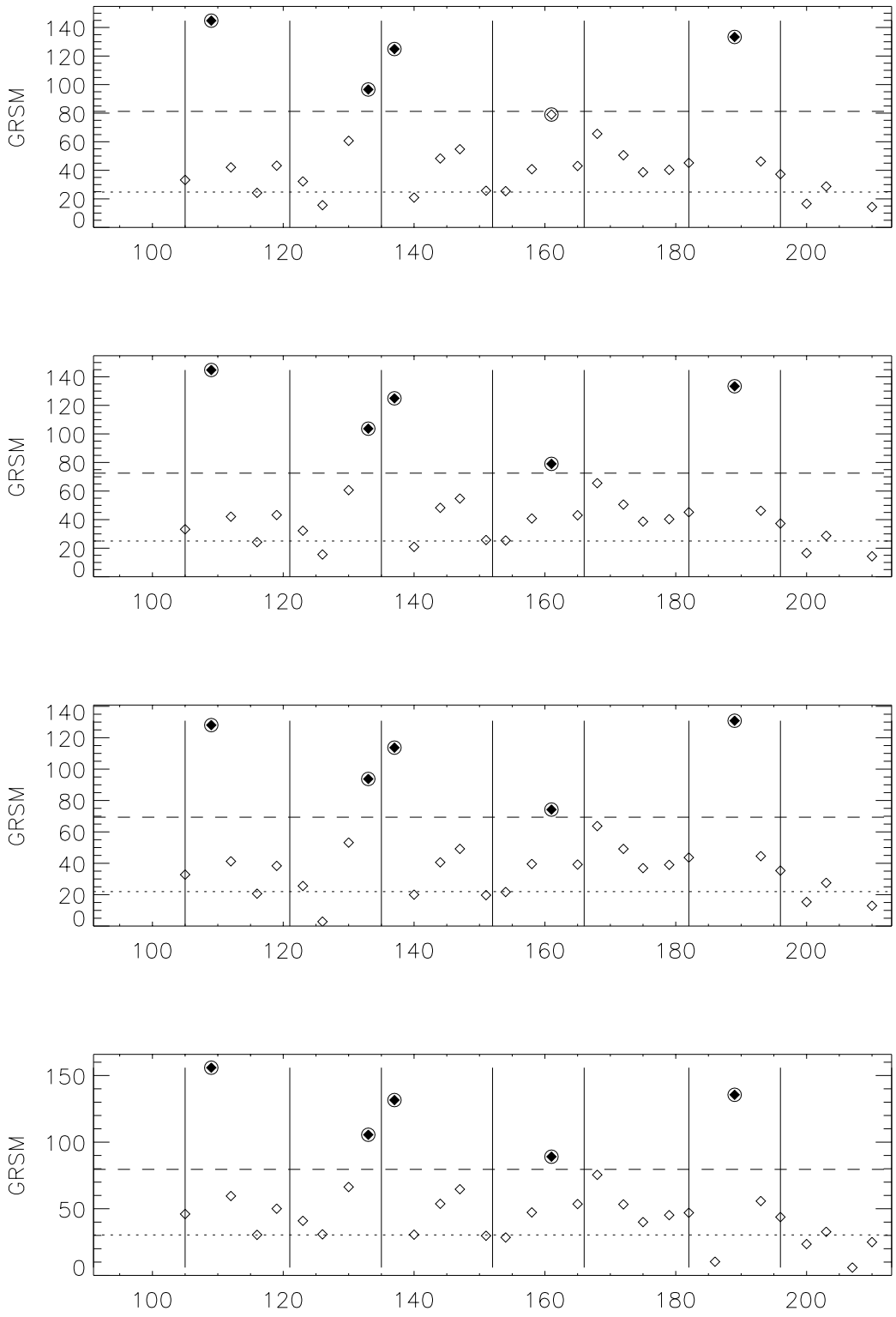

Figure 7.1.2 K_{NON} results at GRSM using various formulas for 15-April through 31-July 1995. Top--not accounting for North African dust or sea salt, second--accounting for North African dust and not sea salt, third--final equations used and bottom--silicon method. Filled symbols are days passing the criterion, circled symbols are smoke-impacted samples from trajectory analysis, x-axis is Julian day where 105 is 15-April and vertical lines mark the first and fifteenth of each month, April through July.

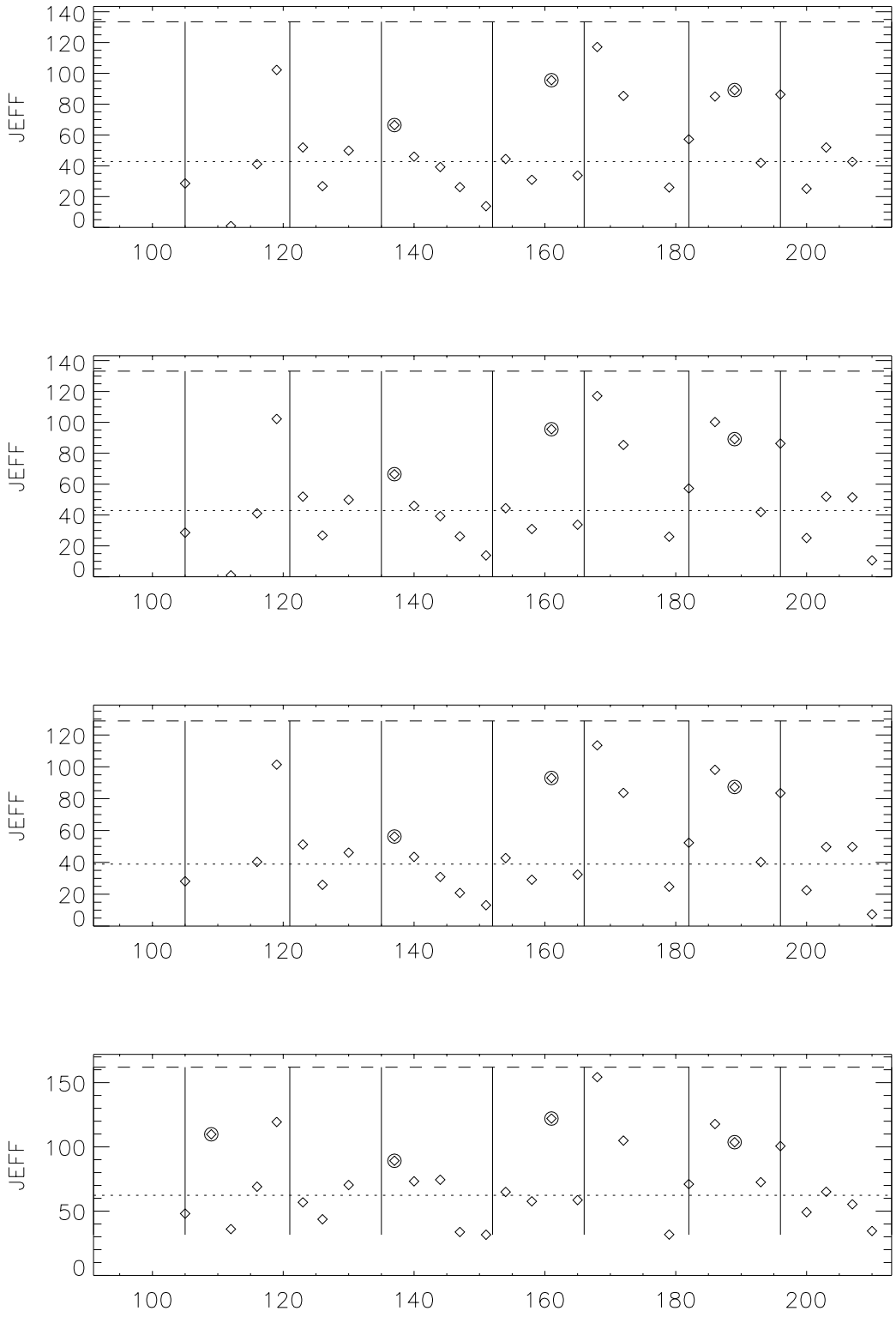

Figure 7.1.3 K_{NON} results at JEFF using various formulas for 15-April through 31-July 1995. Top--not accounting for North African dust or sea salt, second--accounting for North African dust and not sea salt, third--final equations used and bottom--silicon method. Filled symbols are days passing the criterion, circled symbols are smoke-impacted samples from trajectory analysis, x-axis is Julian day where 105 is 15-April and vertical lines mark the first and fifteenth of each month, April through July.

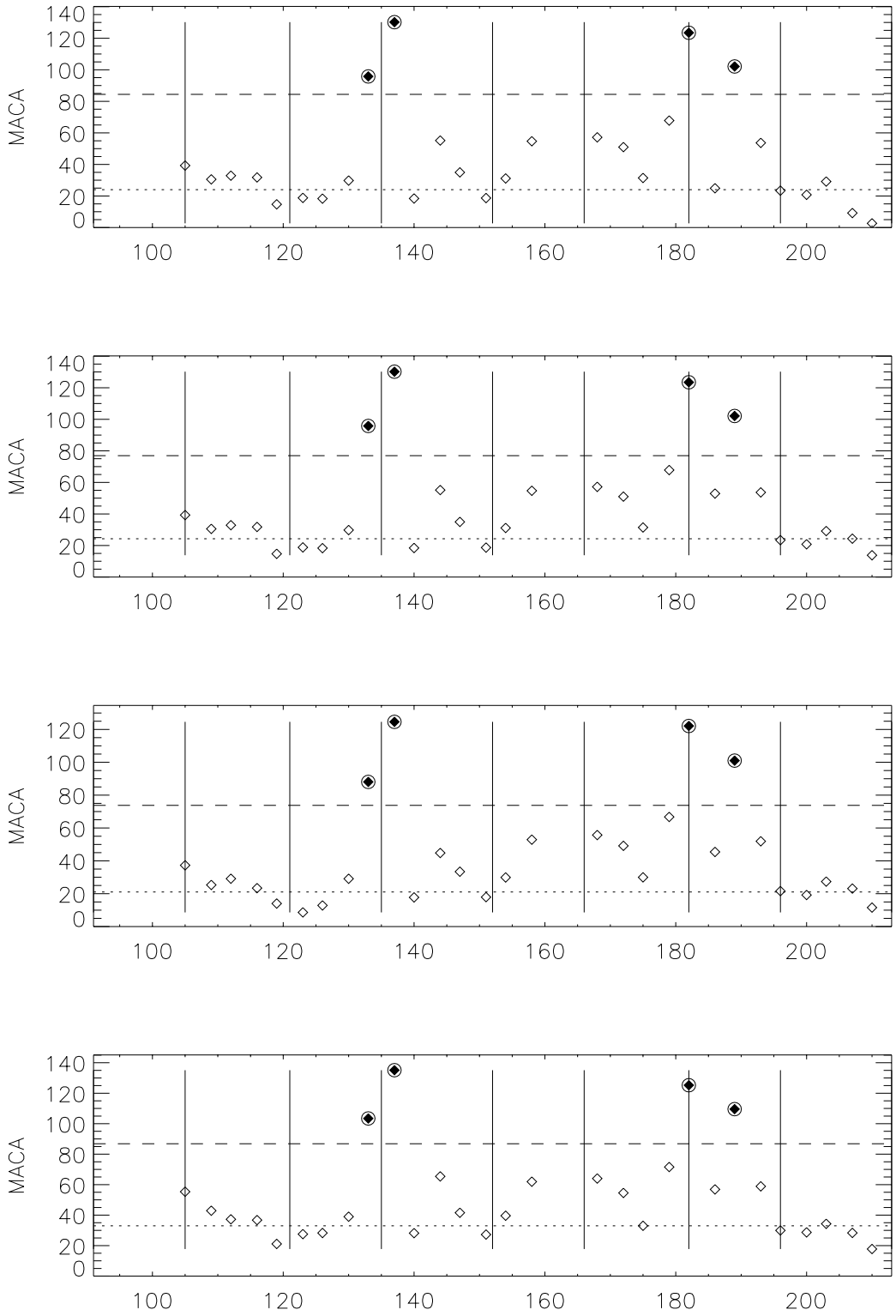

Figure 7.1.4 K_{NON} results at MACA using various formulas for 15-April through 31-July 1995. Top--not accounting for North African dust or sea salt, second--accounting for North African dust and not sea salt, third--final equations used and bottom--silicon method. Filled symbols are days passing the criterion, circled symbols are smoke-impacted samples from trajectory analysis, x-axis is Julian day where 105 is 15-April and vertical lines mark the first and fifteenth of each month, April through July.

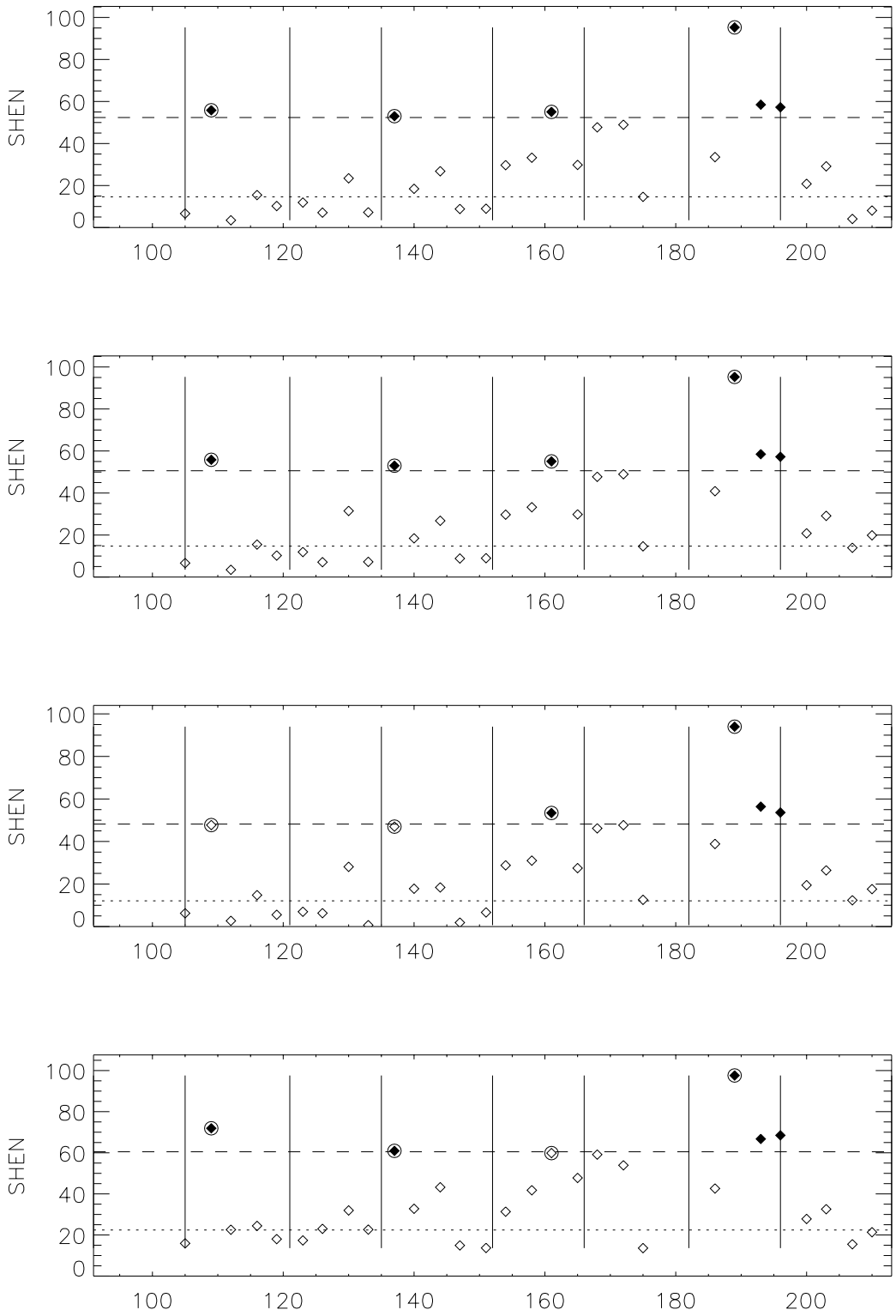

Figure 7.1.5 K_{NON} results at SHEN using various formulas for 15-April through 31-July 1995. Top--not accounting for North African dust or sea salt, second--accounting for North African dust and not sea salt, third--final equations used and bottom--silicon method. Filled symbols are days passing the criterion, circled symbols are smoke-impacted samples from trajectory analysis, x-axis is Julian day where 105 is 15-April and vertical lines mark the first and fifteenth of each month, April through July.

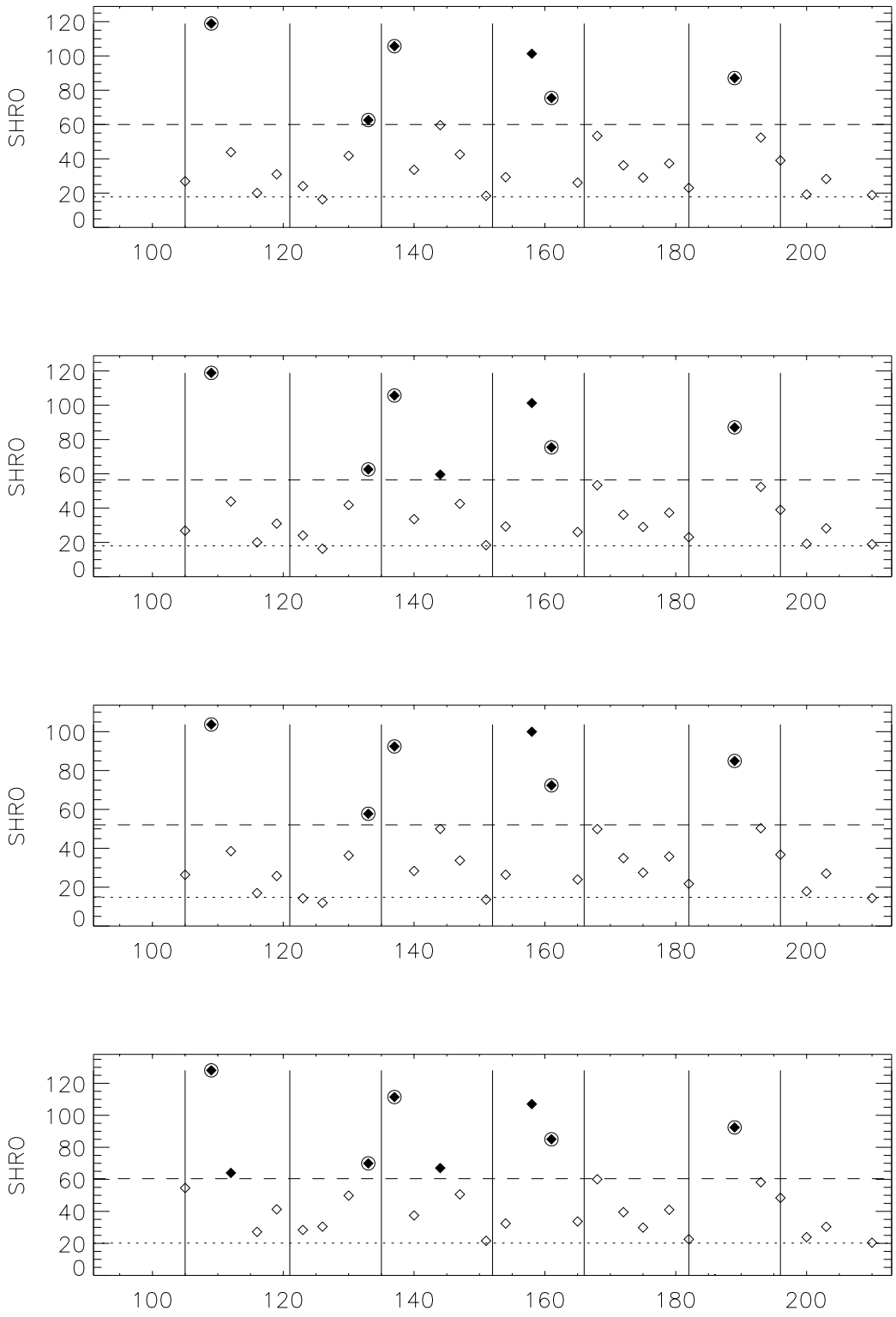

Figure 7.1.6 K_{NON} results at SHRO using various formulas for 15-April through 31-July 1995. Top--not accounting for North African dust or sea salt, second--accounting for North African dust and not sea salt, third--final equations used and bottom--silicon method. Filled symbols are days passing the criterion, circled symbols are smoke-impacted samples from trajectory analysis, x-axis is Julian day where 105 is 15-April and vertical lines mark the first and fifteenth of each month, April through July.

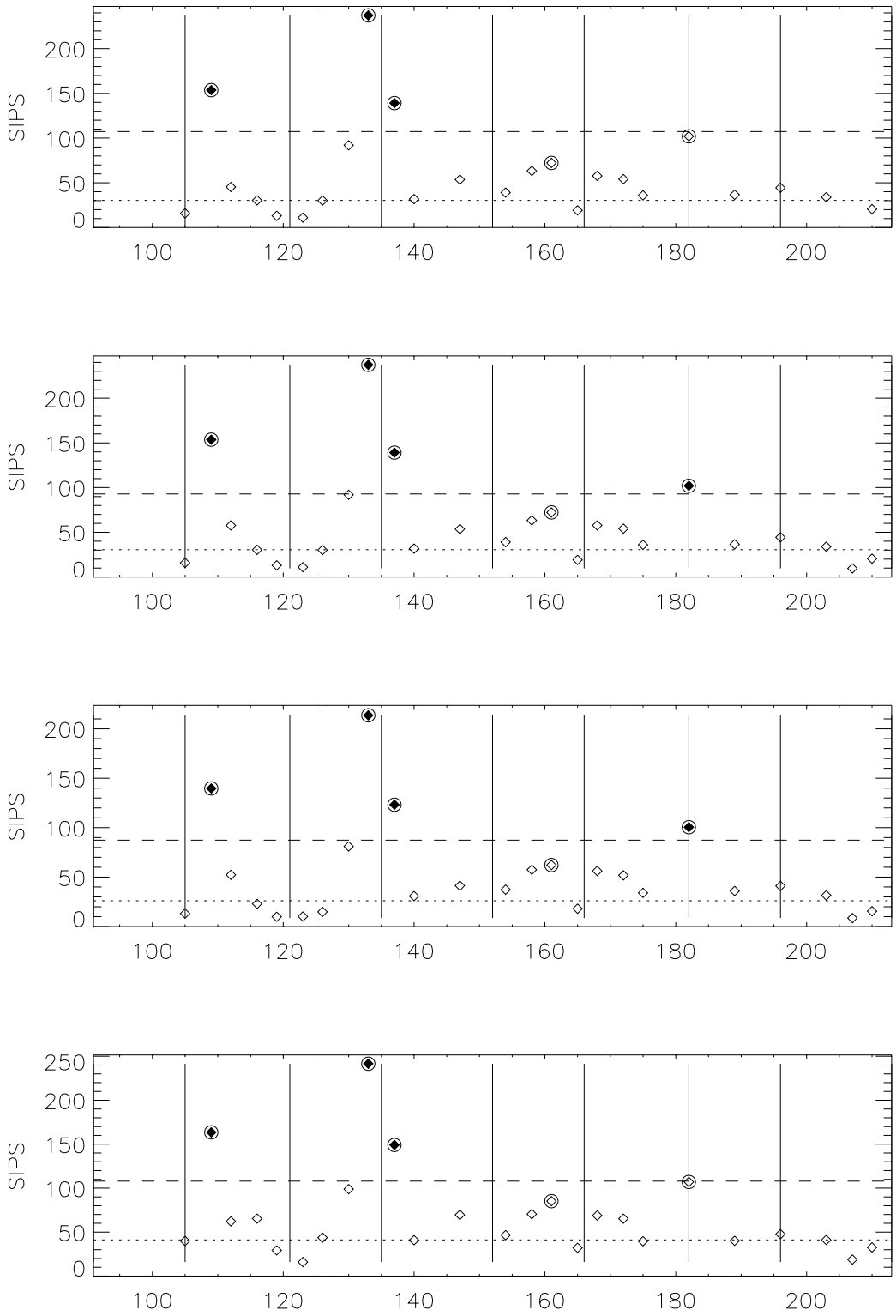

Figure 7.1.7 K_{NON} results at SIPS using various formulas for 15-April through 31-July 1995. Top--not accounting for North African dust or sea salt, second--accounting for North African dust and not sea salt, third--final equations used and bottom--silicon method. Filled symbols are days passing the criterion, circled symbols are smoke-impacted samples from trajectory analysis, x-axis is Julian day where 105 is 15-April and vertical lines mark the first and fifteenth of each month, April through July.

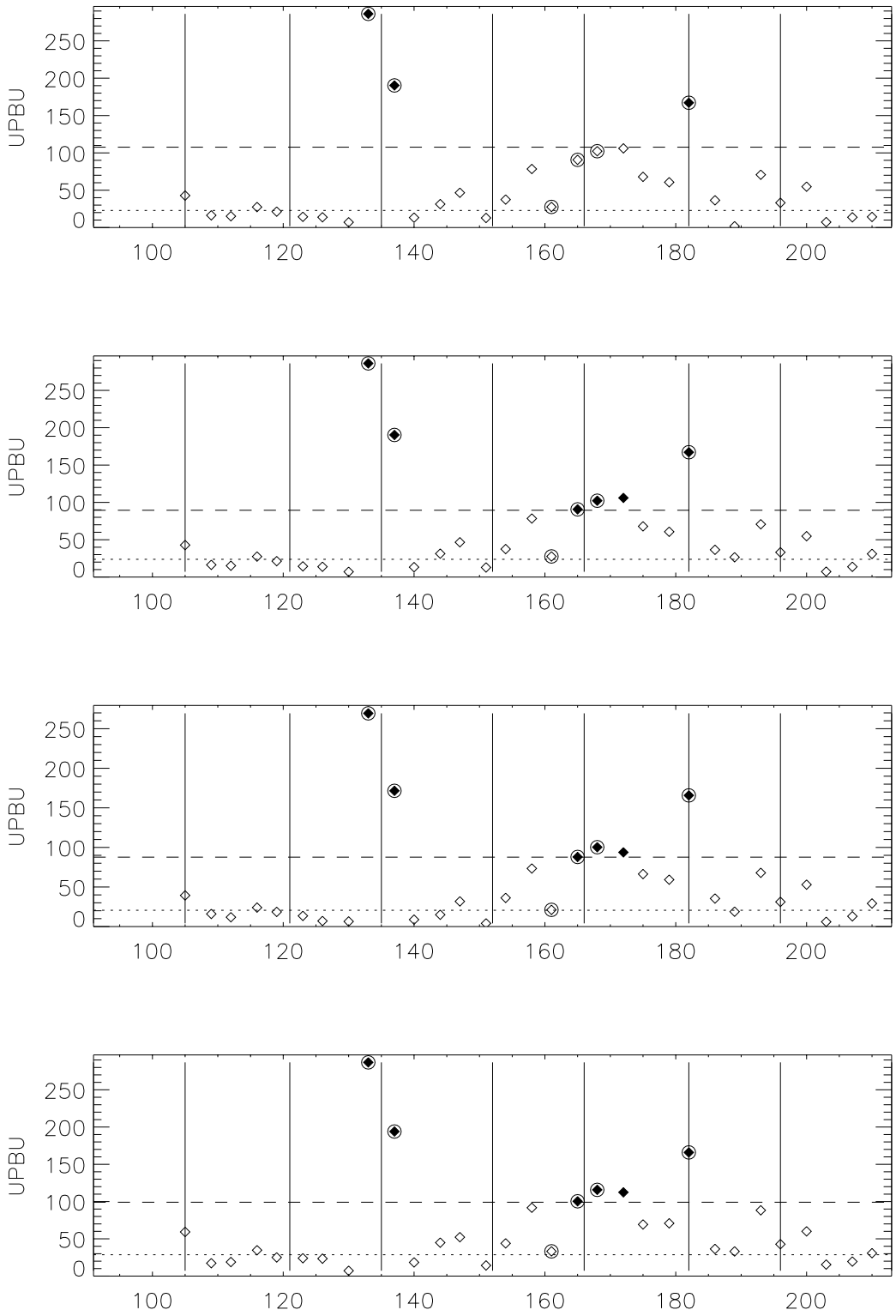

Figure 7.1.8 K_{NON} results at UPBU using various formulas for 15-April through 31-July 1995. Top--not accounting for North African dust or sea salt, second--accounting for North African dust and not sea salt, third--final equations used and bottom--silicon method. Filled symbols are days passing the criterion, circled symbols are smoke-impacted samples from trajectory analysis, x-axis is Julian day where 105 is 15-April and vertical lines mark the first and fifteenth of each month, April through July.

Table 7.1.1 K_{NON} (ng/m^3) statistics for the various equations used. 'Smoke Criterion' is the median plus two standard deviations.

No North African Dust or Sea Salt (Eq. 7.1)				No Sea Salt (Eq. 7.1 and Eq. 7.2)			
Park	Median	Standard Deviation	Smoke Criterion	Park	Median	Standard Deviation	Smoke Criterion
DOSO	17.65	17.89	53.42	DOSO	17.78	16.81	51.39
GRSM	24.76	28.25	81.26	GRSM	25.01	23.76	72.54
JEFF	42.75	45.36	133.47	JEFF	42.89	45.15	133.19
MACA	23.99	30.23	84.44	MACA	24.28	26.33	76.95
SHEN	14.60	18.89	52.38	SHEN	14.73	17.93	50.60
SHRO	17.79	21.11	60.01	SHRO	17.99	19.23	56.44
SIPS	30.29	38.52	107.32	SIPS	30.53	31.20	92.92
UPBU	22.90	42.37	107.65	UPBU	23.80	32.84	89.49
Final Equation Used (Eq. 7.3 and Eq. 7.4)				Silicon Method (Eq. 7.5)			
Park	Median	Standard Deviation	Smoke Criterion	Park	Median	Standard Deviation	Smoke Criterion
DOSO	14.92	17.15	49.22	DOSO	23.52	18.03	59.58
GRSM	21.94	23.72	69.38	GRSM	30.35	24.59	79.54
JEFF	38.90	44.95	128.81	JEFF	62.32	49.83	161.99
MACA	21.05	26.37	73.79	MACA	33.00	26.91	86.82
SHEN	12.10	18.05	48.20	SHEN	22.41	19.03	60.48
SHRO	14.77	18.65	52.07	SHRO	20.13	20.15	60.42
SIPS	26.04	30.66	87.35	SIPS	41.12	33.41	107.94
UPBU	20.56	33.58	87.71	UPBU	28.66	35.25	99.15

From Figures 7.1.1 through 7.1.8, the variations in the number of smoke-flagged days were minimal for the different assumptions. At JEFF, MACA and SIPS there were no differences in the days flagged smoke impacted when using the various equations. One false positive observation at SHRO was eliminated after accounting for the sea salt contribution to the fine aerosol potassium concentration. After accounting for Saharan dust, three days at UPBU passed the smoke criterion, 14-June, 17-June and 21-June, and one at GRSM, 10-June. One of the three days that passed after the Saharan dust modification was false positive, 21-June, and the other two were impacted from fires in Canada. At SHEN two days were false negative with the final formula, 19-April and 17-May. 17-May was also false negative with the silicon formula. The final formula also

resulted in one false positive at SHEN, 21-June, which was not smoke impacted with the other techniques.

The modifications to the iron based K_{NON} equations primarily affected days that were close to the smoke criterion. The K_{NON} medians at all parks were lowest with the final method using Eq. 7.3 and Eq. 7.4, which account for both North African dust and sea salt contributions to potassium. This method also resulted in the lowest value for the smoke criterion at all parks except UPBU. Based on the results from 1995 it is believed that Eq. 7.3 and Eq. 7.4 are the best indicators of smoke impact on the aerosol samples, although all false positives and negatives could not be eliminated with any of the equations investigated.

7.2 Sensitivity to Soil Ratio Assumptions

Similar to the Al/Ca ratio, discussed in Chapter 6, it is expected that a plot of potassium versus iron will result in three populations: local soil, North African dust, and smoke. As with the Al/Ca ratio there will be many samples containing a mix of two or three sources and thus the value of the observed ratio will reflect this.

Figure 7.2.1 is the potassium minus sea salt versus iron plot for GRSM over all years and all months of data available (1988 to 1999). Linear regressions were performed separately over all days impacted by North African dust and all days not impacted by North African dust. The intercepts were not forced to be zero in this case because potassium concentrations do not have to approach zero as iron concentrations approach zero, e.g. smoke is a source for potassium and not iron, and therefore potassium can be present in a sample with no iron present; however, it is not thought that the intercepts

hold any quantitative physical meaning. The two populations representing local soil (K/Fe=0.74) and Saharan dust (K/Fe=0.31) are evident in this figure, which further supports using a different K/Fe ratio on days strongly impacted by North African dust.

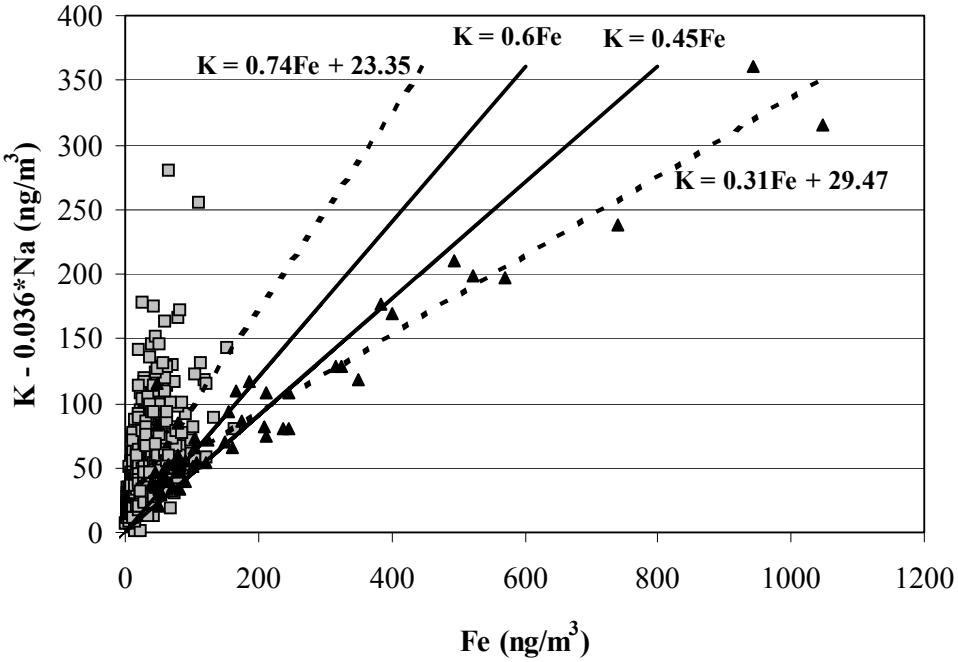

Figure 7.2.1 Potassium versus iron concentrations (ng/m^3) at GRSM over all months and all years (1988 – 1999). Triangles are samples impacted by North African dust and squares are samples not impacted by North African dust. Dotted lines are the results of the linear regressions and solid lines are the ratios used in the K_{NON} equations.

To test the robustness of the results using the final K_{NON} equations the local soil ratio K/Fe=0.74 and Saharan dust ratio K/Fe=0.31 from the linear regressions were then substituted for the ratios used in those equations (Eq. 7.3 and Eq. 7.4). Figure 7.2.2 shows the K_{NON} values, medians, and criteria at GRSM for 15-April through 31-July 1995 using the final equations in Section 7.1 (top), K/Fe=0.74 and K/Fe=0.31 (second), K/Fe=0.74 and K/Fe=0.45 (third), and K/Fe=0.6 and K/Fe=0.31 (bottom). These variations did not change the days flagged smoke impacted during 1995.

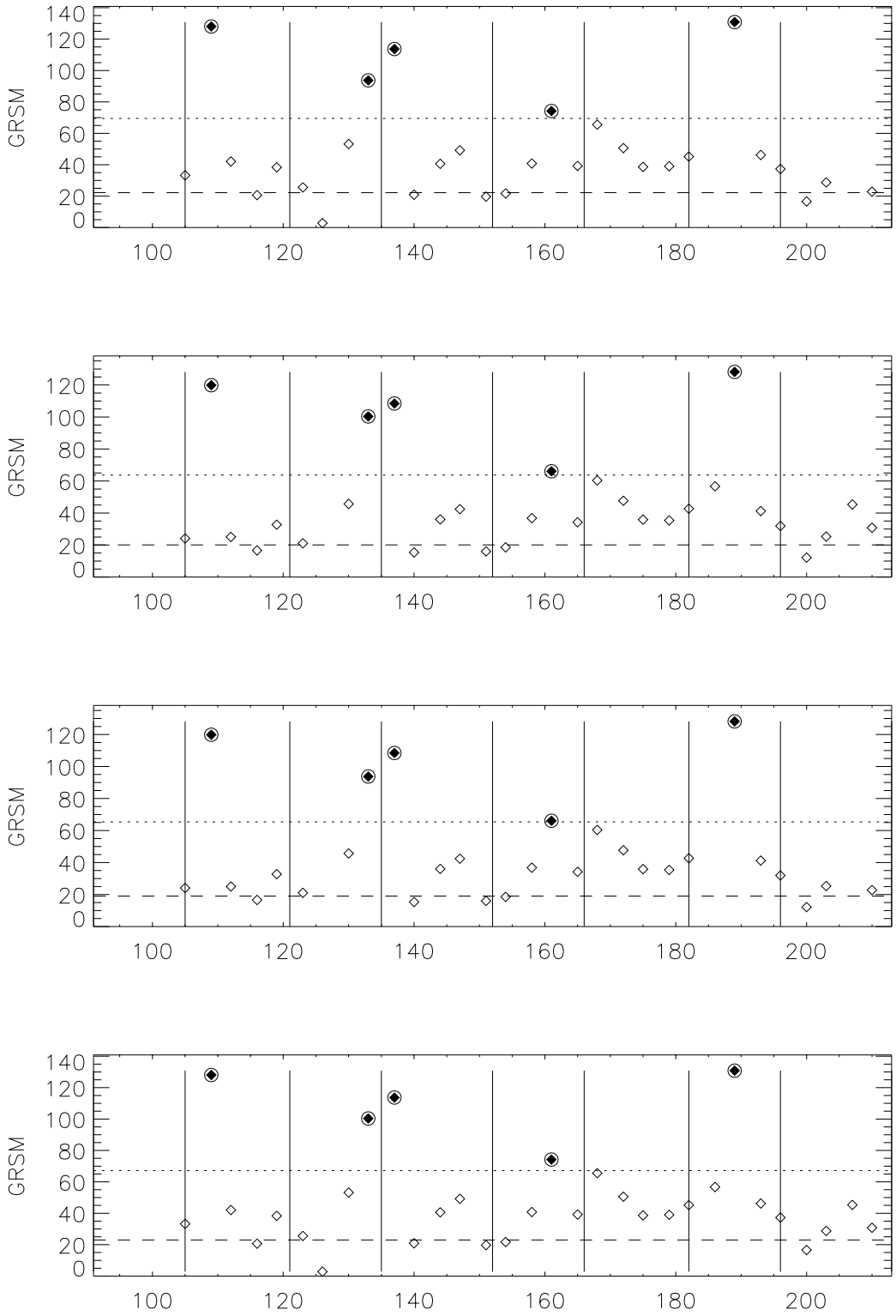

Figure 7.2.2 K_{NON} values, ng/m^3, (symbols), medians (dashed lines), and criteria (dotted lines) at GRSM for 15-April through 31-July 1995 using the final equations in Section 7.1 (top), K/Fe=0.74 and K/Fe=0.31 (second), K/Fe=0.74 and K/Fe=0.45 (third), and K/Fe=0.6 and K/Fe=0.31 (bottom). Numbers along x-axis indicate Julian day where 105 is 15-April and vertical lines are the first and fifteenth of every month, April through July. Filled diamonds are days flagged smoke impacted, circles are smoke impacted days based on trajectories and fire maps.

The next test performed used the mean (K – 0.36*Na)/Fe ratio over all months and years excluding June, July and August for the local soil ratio and the mean (K – 0.36*Na)/Fe ratio over all days identified as dust impacted, as discussed in Chapter 6, for the North African dust ratio. This resulted in a local soil ratio K/Fe=2.2 and a North African dust ratio K/Fe=0.62 at GRSM. The high local soil ratio resulted in mostly negative K_{NON} values that lack physical meaning (Figure 7.2.3). In addition, using the mean ratio is less appropriate than the ratio K/Fe=0.6 (K/Fe=0.45) because GRSM is impacted by smoke at times other than June, July and August and on those days a higher ratio of K/Fe would be present in the sample, skewing the resulting mean towards a higher value than appropriate for local soil (or Saharan dust).

When the ratio K/Fe=2.2 was assumed for local soil, using either 0.45 or 0.62 for the Saharan dust ratio, only two out of five days flagged smoke impacted remained. None of the five days originally flagged smoke impacted was found to be false positive and thus the ratio K/Fe=2.2 incorrectly eliminated three smoke impacted days. Assuming the mean ratio K/Fe=0.62 on days impacted by Saharan dust along with the assumed K/Fe=0.6 in local soil (Figure 7.2.3, bottom) is not appropriate because it does not account for the lower K/Fe ratio present in Saharan dust as seen in Figure 7.2.1.

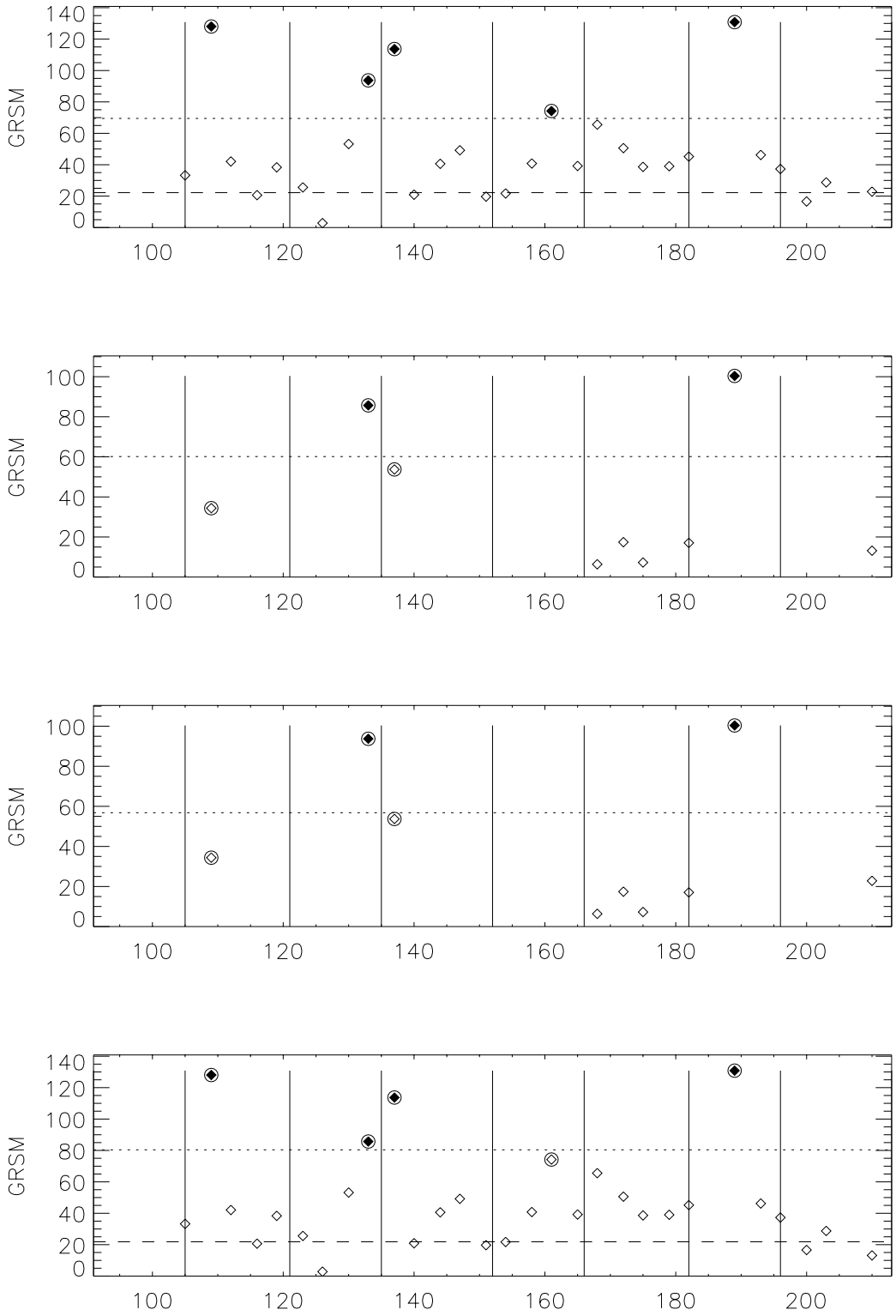

Figure 7.2.3 K_{NON} values, ng/m^3, (symbols), medians (dashed lines), and criteria (dotted lines) at GRSM for 15-April through 31-July 1995 using the final equations in Section 7.1 (top), K/Fe=2.2 and K/Fe=0.62 (second), K/Fe=2.2 and K/Fe=0.45 (third), and K/Fe=0.6 and K/Fe=0.62 (bottom). Numbers along x-axis indicate Julian day where 105 is 15-April and vertical lines are the first and fifteenth of every month, April through July. Filled diamonds are days flagged smoke impacted, circles are smoke impacted days based on trajectories and fire maps.

Based on the tests performed at GRSM it is believed that the K/Fe ratios used for local soil and North African dust, 0.6 and 0.45 respectively, are adequate for determining the non-soil potassium values in the southeastern U.S. The ratios resulting from the linear regressions did not change the days that were flagged smoke impacted for 1995. When the mean K/Fe over the non-summer months was used, most of the K_{NON} values became negative and only two of five smoke impacted days in 1995 were flagged as smoke impacted.

As mentioned previously, it was expected that three populations would emerge from the potassium (minus sea salt) versus iron plot. Based on the tests discussed, it was determined that the ratios used in the final K_{NON} equations are adequate for estimating the soil/dust contributions to fine aerosol potassium and were used to determine the smoke impacted days in Figure 7.2.4. From the figure, three populations are suggested; the lowest K/Fe ratios are in the samples impacted by North African dust and the highest K/Fe ratios are present in the samples impacted by smoke.

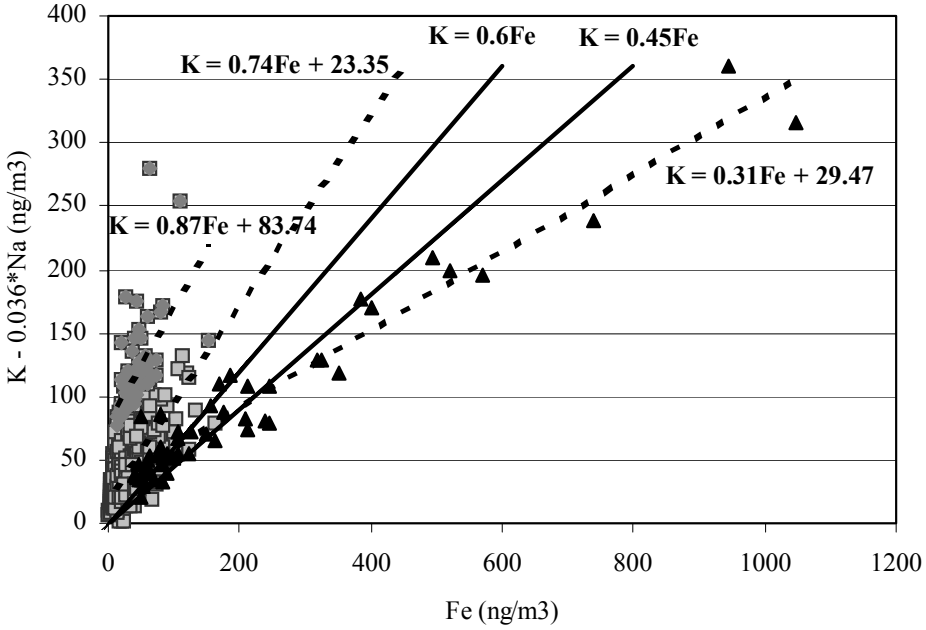

Figure 7.2.4 Potassium versus iron concentrations (ng/m^3) at GRSM over all months and all years (1988 – 1999). Triangles are samples impacted by North African dust, squares are samples not impacted by North African dust and diamonds are samples flagged smoke impacted using the final equations (7.3 and 7.4). Dotted lines are the results of the linear regressions and solid lines are the ratios used in the final K_{NON} equations.

Chapter 8. Conclusions and Future Work

8.1 Conclusions

Non-soil potassium was investigated as a tracer for smoke impact from biomass burning in aerosol samples from eight IMPROVE monitoring network sites in the eastern and southeastern U.S. Back trajectories were compared to maps of fire and hot spot locations in 1995 and 1998 to identify source regions and determine whether fires were within those regions. A criterion indicating significant smoke impact on aerosol samples was established, tested on two years of data (1995 and 1998) and then applied to all years of IMPROVE data (1988-1999).

The general utility of K_{NON} as a tracer for smoke from biomass burning was confirmed. K_{NON} was able to capture cases seen in gas phase data by Wotawa and Trainer (2000) during July 1995 in the aerosol data. In addition, smoke from the severe fires in Mexico and Central America during May 1998 was identified in the aerosol data. Based on the 1995 and 1998 results, 10/66 observations flagged as smoke impacted were assumed to be false positive for smoke impact and 14/409 observations not flagged as smoke impacted were assumed to be false negative for smoke impact. The number of observations flagged as false positive, especially in 1995, could be overestimated due to a lack of fire data. The National Fire Occurrence Database does not contain information on prescribed burns and was missing all data for Pennsylvania, South Carolina and Virginia

in 1995. Satellite detected hot spots are limited to cloud-free and nighttime detection. It was also shown that observations considered false negative could be inaccurately identified as such due to precipitation along the trajectory or an elevated smoke plume not sampled at the ground.

Modifications to the formula for calculating K_{NON} were necessary to account for contributions to aerosol potassium from sea salt and the lower K/Fe ratio present in North African dust. When adjusting the K/Fe ratio to account for North African dust it appeared that the two-part criterion used by Perry et al. (1997) was too strict for the parks investigated in this study. Due to particle deposition and mixing of North African dust with local soils the more northern sites rarely, if ever, passed the Perry et al. (1997) criterion and thus a specific North African dust criterion was developed for each park.

It was found that during 1995 and 1998 the southeastern U.S. was frequently impacted by smoke from fires in Canada, Mexico and Central America from 15-April through 31-July. Smoke impact from fires in Mexico and Central America primarily occurred in late spring and early summer. Smoke impact from fires in Canada occurred later, during late-June and July. These findings correspond with the average fire seasons for Mexico and Central America and Canada. Biomass burning tends to peak in April and May in Mexico and Central America whereas forest fires in Canada are most prevalent in June and July. In 1995 the number of observations impacted by smoke from fires in Canada exceeded the number impacted in 1998, which correlates with the larger acreage burned in 1995 than 1998. Similarly, the number of observations impacted by smoke from Mexico and Central America during the severe fire season of 1998 exceeded the number impacted in the nearly average 1995 fire season. The areas burned in the

U.S. during 1995 and 1998 were approximately equal and both were below the average annual area burned.

Overall source contributions and source contributions on days with high K_{NON} at GRSM, SHEN and UPBU were computed during 1995 and 1998 using the residence time weighted by an equal probability surface. Despite the different meteorological data used to calculate the trajectories similar source contributions were found in 1995 and 1998 at each park. In addition to high source contributions in the U.S., there were high source contributions from Canada, the Gulf of Mexico, Mexico and Central America at all three parks. Source contributions from Mexico in 1998 exceeded the 1995 contributions, correlating with the larger acreage burned in 1998. Correlating with the larger acreage burned in 1995, source contributions from Canada were higher in 1995 than 1998.

8.2 Future Work

It was necessary to assume the ratio K/Fe in soils in the southeastern U.S. was equivalent to the K/Fe ratio in soils from states in the western U.S. A better estimate of the soil contribution to aerosol potassium in the eastern U.S. might improve the K_{NON} results by reducing the number of false negatives and false positives.

This study was limited to late spring and early summer in the southeastern U.S. Applying the K_{NON} equations and Saharan dust criteria used in this study to the entire year could reveal more about the contributions of smoke to aerosol concentrations in the southeastern U.S. It would also be interesting to apply the techniques used here to sites in the western U.S. and compare the results to the results from the eastern U.S.

This study showed that long-range transport of smoke from fires in Canada and Mexico does impact the aerosol concentrations in the eastern and southeastern U.S. during late spring and summer, but in 1995 and 1998 there was no obvious effect on the fine mass concentrations on the smoke impacted days. In addition, K_{NON} is not a quantitative measure of smoke impact in an aerosol sample. From a policy-making point of view it would be useful, if not essential, to develop a technique for estimating the percentage of smoke in the total aerosol concentrations.

Source contributions could be interesting to investigate further in many respects. First, the overall source contributions and source contributions on high K_{NON} days could be calculated over more years and compared to the acreages burned each year in different regions. Also, other species such as crustal elements for Asian and Saharan dust could be investigated for the "high days" source contributions.

REFERENCES

ARL, NCEP/NCAR Reanalysis Data Archive, 2001. (Attained from: http://www.arl.noaa.gov/ready-bin/cdc.pl)

Ashbaugh, L., W. Malm, and W. Sadeh, A residence time probability analysis of sulfur concentrations at Grand Canyon National Park, *Atmospheric Environment*, *19*, 1263-1270, 1985.

Cahill, T.A., L.L. Ashbaugh, R.A. Eldred, P.J. Feeney, and B. Kusko, Comparisons between Size-Segregated Resuspended Soil Samples and Ambient Aerosols in the Western United-States, *Abstracts of Papers of the American Chemical Society*, *180* (AUG), 157-Nucl, 1980.

Canadian Forest Service, *The state of Canada's forests 1996-1997: learning from history,* 1997.

Canadian Forest Service and Canada Centre for Remote Sensing, Fire Monitoring Mapping and Modeling System, 2002. (Attained from: http://fms.nofc.cfs.nrcan.gc.ca/firem3)

Cooper, O.R., J.L. Moody, T.D. Thornberry, M.S. Town, and M.A. Carroll, PROPHET 1998 meteorological overview and air-mass classification, *Journal of Geophysical Research-Atmospheres*, *106* (D20), 24289-24299, 2001.

Draxler, R.R., The accuracy of trajectories during ANATEX calculated using dynamic model analyses versus rawinsonde observations, *Journal of Applied Meteorology, 30,* 1446-1467, 1991.

Draxler, R.R. and G.D. Hess, Description of the Hysplit_4 modeling system, NOAA Tech Memo ERL ARL-224, Dec. 1997. (Attained from: http://www.arl.noaa.gov/data/models/hysplit4/win95/arl-224.pdf)

Eldred, Bob. Personal Communication, 2002.

European Space Agency – ESA/ESRIN, *ATSR World Fire Atlas,* 2002. (Attained from: http://shark1.esrin.esa.it/ionia/FIRE/AF/ATSR/)

Finlayson-Pitts, Barbara J. and James N. Pitts, Jr., Chemistry of the Upper and Lower Atmosphere, Academic Press: San Diego, 2000.

Food and Agriculture Organization-Forestry (FAO), 2002. (Attained from: http://www.fao.org/forestry/Forestry.asp)

Forster, C., U. Wandinger, G. Wotawa, P. James, I. Mattis, D. Althausen, P. Simmonds, S. O'Doherty, S.G. Jennings, C. Kleefeld, J. Schneider, T. Trickl, S. Kreipl, H. Jager, and A. Stohl, Transport of boreal forest fire emissions from Canada to Europe, *Journal of Geophysical Research-Atmospheres*, *106* (D19), 22887-22906, 2001.

General Directorate for Forestry, Forest Protection Office, *México: Mexican Republic Wildfire Statistics Extract,* 2001. (Attained from: http://www.fire.uni-freiburg.de/inventory/stat/mx/mex2001_1.htm)

Hao, W.M., and M.-H. Liu, Spatial and temporal distribution of tropical biomass burning, *Global Biological Cycles, 8,* 495-503, 1994.

HYSPLIT4 (HYbrid Single-Particle Lagrangian Integrated Trajectory) Model, 1997. Web address: http://www.arl.noaa.gov/ready/hysplit4.html, NOAA Air Resources Laboratory, Silver Spring, MD.

Johnston, T., Canada: The 1995 Fire Season, *International Forest Fire News (IFFN), 14,* 15-18, 1996.

Kaufman, Y.J., et al., Smoke Clouds, and Radiation-Brazil (SCAR-B) Experiment, *Journal of Geophysical Research, 103,* 31783-31808, 1998.

Kreidenweis, S.M., L.A. Remer, R. Bruintjes, and O. Dubovik, Smoke Aerosol from Biomass Burning in Mexico: Hygroscopic Smoke Optical Model, *Journal of Geophysical Research*, *106*, 4831-4844, 2001.

Lavoue, D., C. Liousse, H. Cachier, B.J. Stocks, and J.G. Goldammer, Modeling of carbonaceous particles emitted by boreal and temperate wildfires at northern latitudes, *Journal of Geophysical Research-Atmospheres*, *105* (D22), 26871-26890, 2000.

National Interagency Fire Center (NIFC), *Prescribed Fire Statistics*, 2002. (Attained from: http://www.nifc.gov/stats/prescribedfirestats.html)

Peppler, R. A., et al., ARM Southern Grean Plains site observations of the smoke pall associated with the 1998 Central American fires, *Bulletin of the American Meteorological Society, 81,* 2563-2591, 2000.

Perry, K.D., T.A. Cahill, R.A. Eldred, and D.D. D., Long-Range Transport of North African Dust to the Eastern United States, *Journal of Geophysical Research*, *102*, 11225-11238, 1997.

Poirot, R.L., and P.R. Wishinski, Visibility, Sulfate and Air-Mass History Associated with the Summertime Aerosol in Northern Vermont, *Atmospheric Environment*, *20* (7), 1457-1469, 1986.

Prescribed Fire and Fire Effects Research Work Unit, Rocky Mountain Research Station (producer). *Course-scale Spatial Data for Wildland Fire and Fuel Management* [Online] 1999. (Attained from: www.fs.fed.us/fire/fuelman)

Prospero, J., Long-range transport of mineral dust in the global atmosphere: Impact of African dust on the environment of the southeastern United States, *Proceedings of the National Academy of Sciences of the United States of America, 96* (7)*,* 3396-3403, 1999.

Rolph, G.D., NGM Archive TD-6140 January 1991 – April 1997, 1997. (Attained from: http://www.arl.noaa.gov/ready-bin/ngm.pl)

Rolph, G.D., NCEP Model Output -- EDAS Archive TD-6141, 2002. (Attained from: http://www.arl.noaa.gov/ss/transport/edas.html)

Seinfeld, John H. and Spyros N. Pandis, Atmospheric Chemistry and Physics: From Air Pollution to Climate Change, John Wiley & Sons, Inc.: New York, 1998.

Stohl, A., and D.J. Thompson, A density correction for Lagrangian particle dispersion models, *Boundary-Layer Meteorology, 90,* 155-167, 1999.

Stohl, A., et al., *Journal of Applied Meteorology, 34,* 2149, 1995.

Stunder, B.J., NCEP Model Output – FNL Archive Data TD-6141, 1997. (Attained from: http://www.arl.noaa.gov/ready-bin/fnl.pl)

Turn, S.Q., B.M. Jenkins, J.C. Chow, L.C. Pritchett, D. Campbell, T. Cahill, and S.A. Whalen, Elemental characterization of particulate matter emitted from biomass burning: Wind-tunnel-derived source profiles for herbaceous and wood fuels, *Journal of Geophysical Research, 102,* 3683-3699, 1997.

United States Department of Agriculture (USDA) Forest Service, Effects of Fire on Air: A State-of-Knowledge Review, *USDA Forest Service General Technical Report WO-9,* Washington, D.C., 1979.

University of California, Davis (UC-Davis), *IMPROVE: A Guide to Interpret Data,* 1995. (Attained from: http://vista.cira.colostate.edu/improve/Publications)

Ward, D.E., and C.C. Hardy, Smoke Emissions from Wildland Fires, *Environment International*, *17* (2-3), 117-134, 1991.

Watson, J.G., J.C. Chow, and J.E. Houck, PM2.5 chemical source profiles for vehicle exhaust, vegetative burning, geological material, and coal burning in Northwestern Colorado during 1995, *Chemosphere*, *43* (8), 1141-1151, 2001.

Wotawa, G., P.C. Novelli, M. Trainer, and C. Granier, Inter-annual variability of summertime CO concentrations in the Northern Hemisphere explained by boreal forest fires in North America and Russia, *Geophysical Research Letters*, *28* (24), 4575-4578, 2001.

Wotawa, G., and M. Trainer, The influence of Canadian forest fires on pollutant concentrations in the United States, *Science*, *288* (5464), 324-328, 2000.

APPENDIX A. 1995 Back Trajectories

The following are all the back trajectory maps used in this study for 1995. NGM trajectories were used for all of 1995. Reanalysis trajectories were also used on days when the NGM trajectories reached the southern boundary of the model grid domain (Section 1.3.3) before reaching five days back. Trajectories are colored by park: red – UPBU, orange – SIPS, green – MACA, light blue – GRSM, dark blue – SHRO, gray – JEFF, pink – DOSO, purple – SHEN. Symbols mark the position of the air parcel at the end of each day for all five days back from the site. Four representative times are presented: 1 LST (diamonds), 7 LST (triangles), 13 LST (squares), and 19 LST (circles).

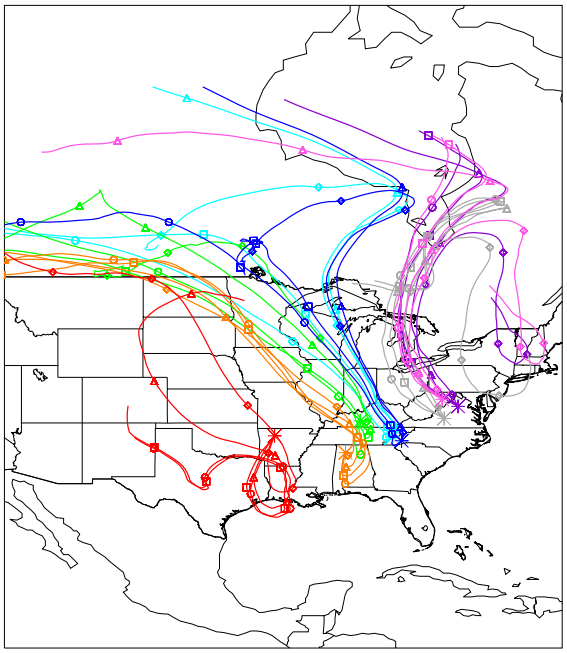

Figure A.1 15-April trajectories calculated using NGM data.

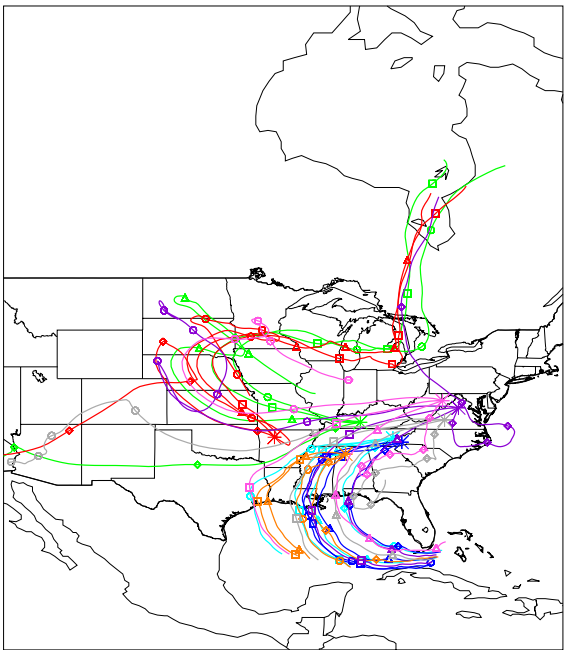

Figure A.2 19-April trajectories calculated using NGM data.

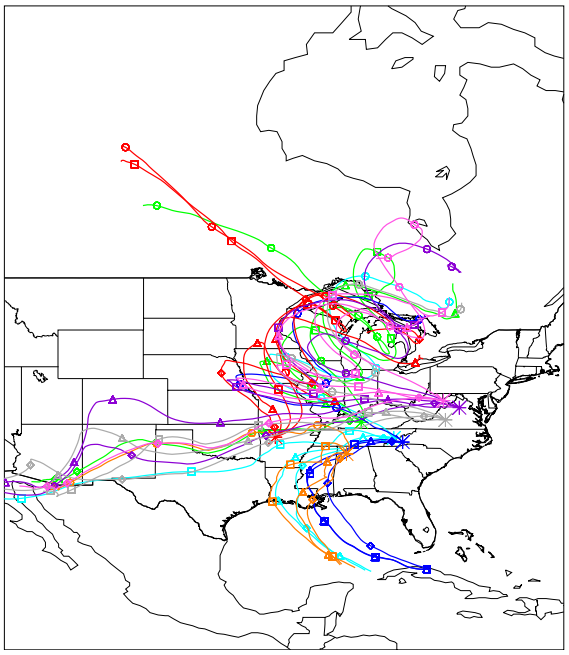

Figure A.3 22-April trajectories calculated using NGM data.

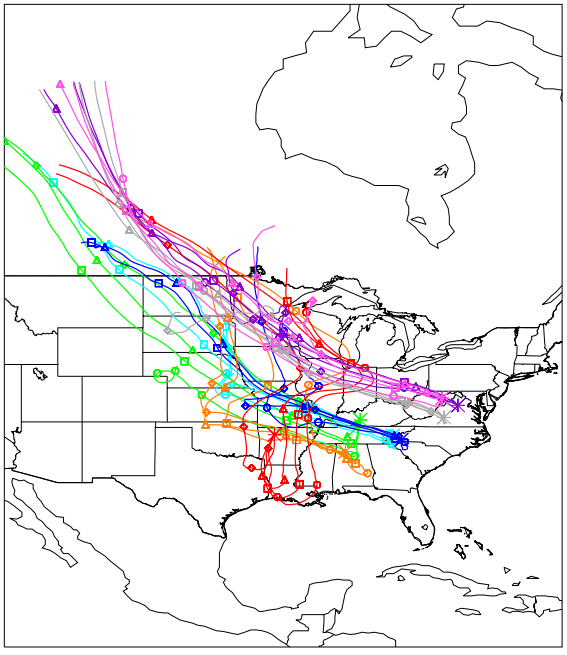

Figure A.4 26-April trajectories calculated using NGM data.

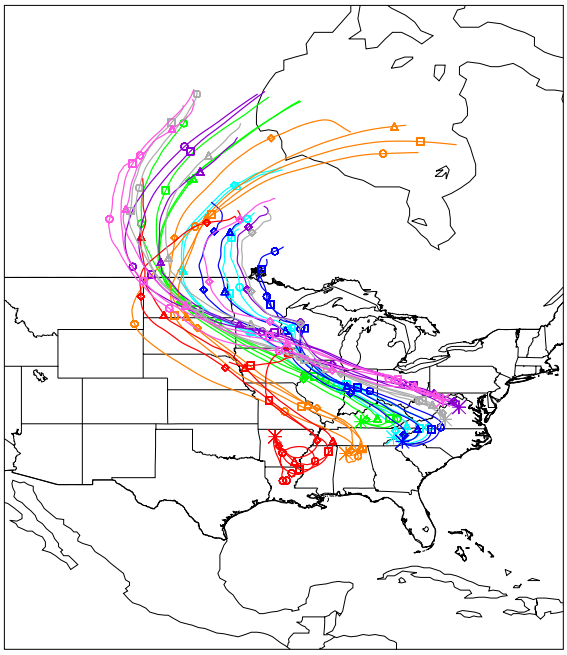

Figure A.5 29-April trajectories calculated using NGM data.

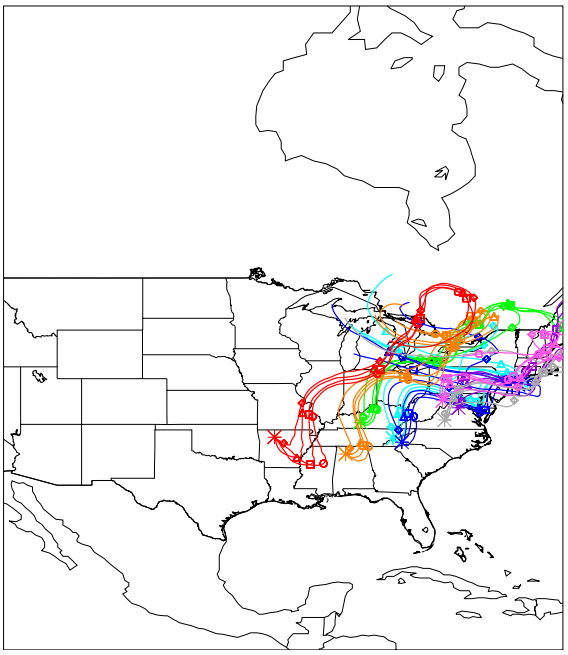

Figure A.6 3-May trajectories calculated using NGM data.

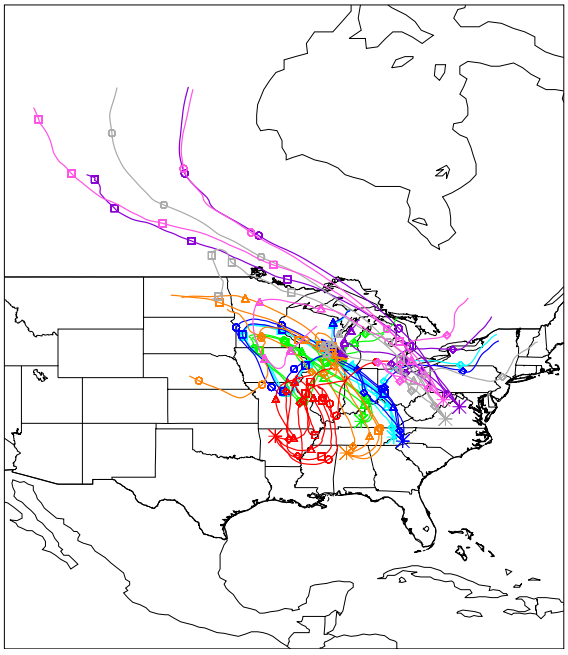

Figure A.7 6-May trajectories calculated using NGM data.

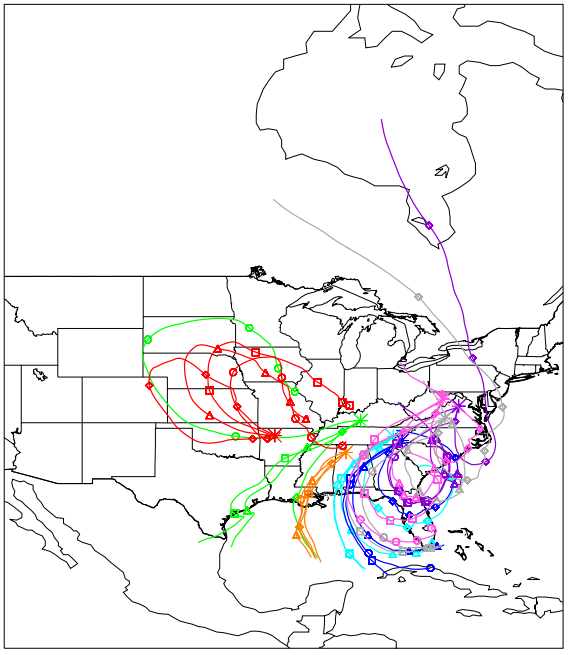

Figure A.8 10-May trajectories calculated using NGM data.

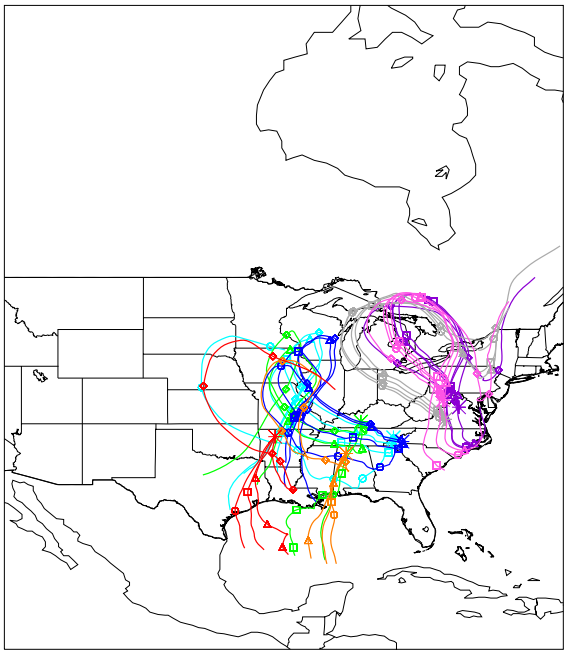

Figure A.9 13-May trajectories calculated using NGM data.

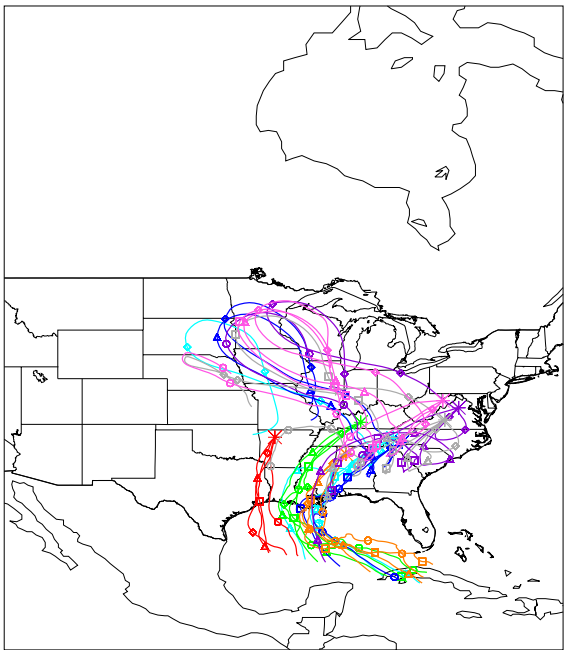

Figure A.10 17-May trajectories calculated using NGM data.

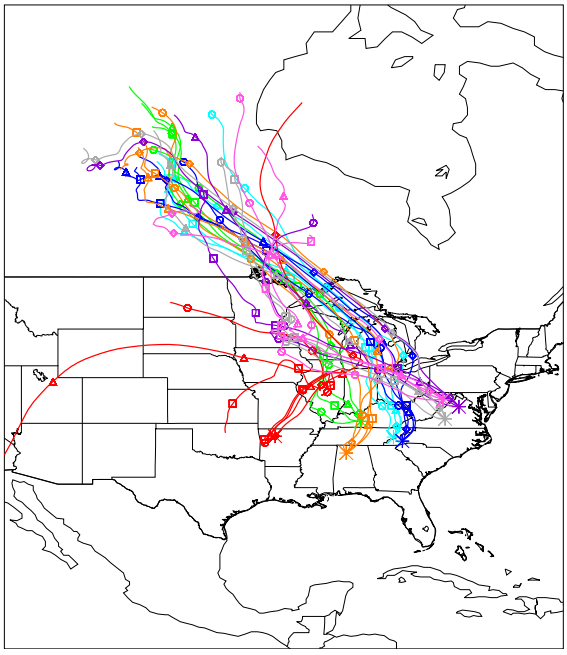

Figure A.11 20-May trajectories calculated using NGM data.

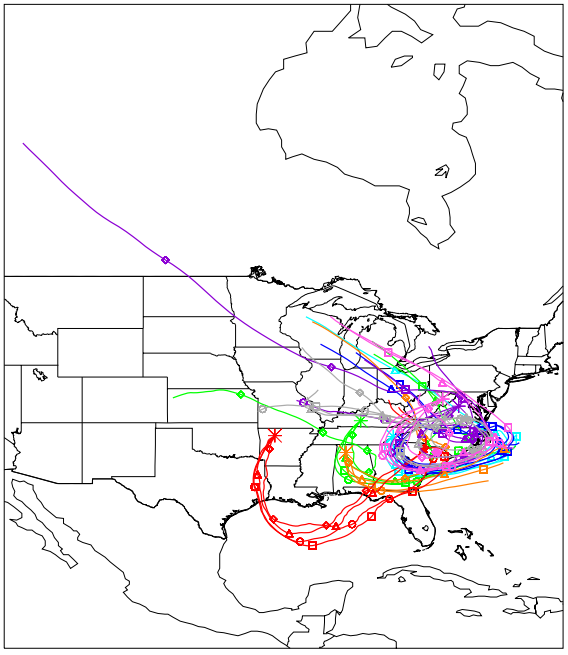

Figure A.12 24-May trajectories calculated using NGM data.

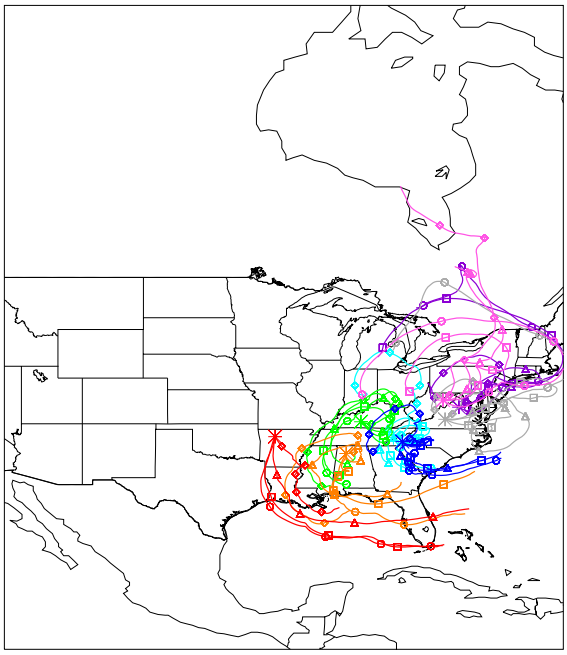

Figure A.13 27-May trajectories calculated using NGM data.

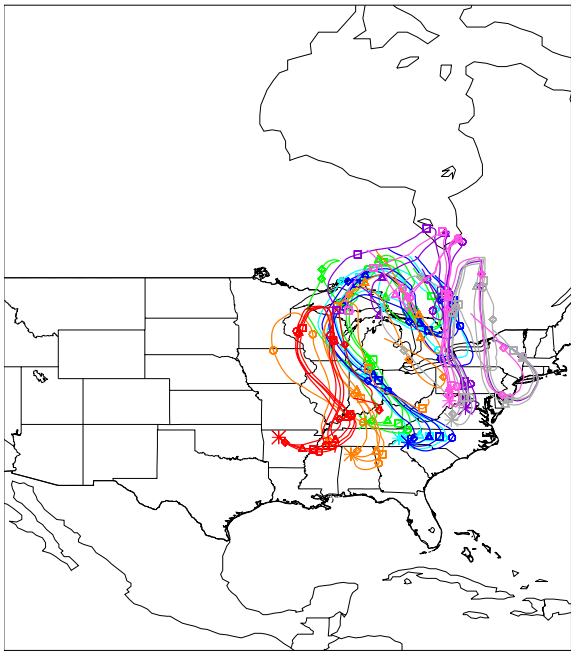

Figure A.14 31-May trajectories calculated using NGM data.

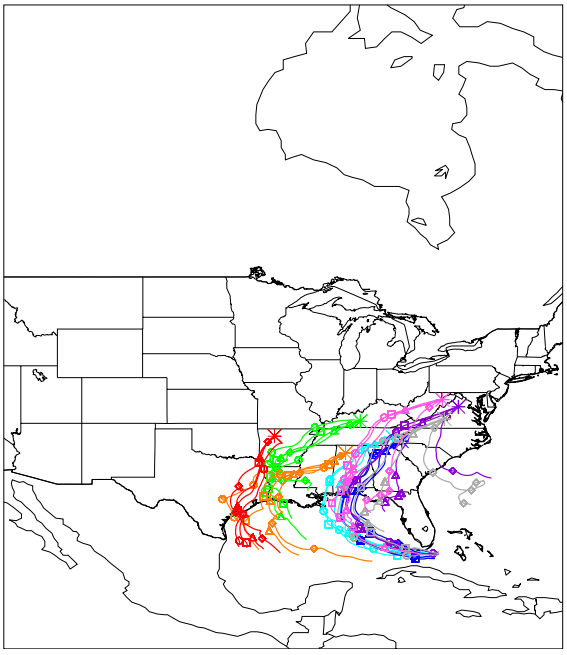

Figure A.15 3-June trajectories calculated using NGM data.

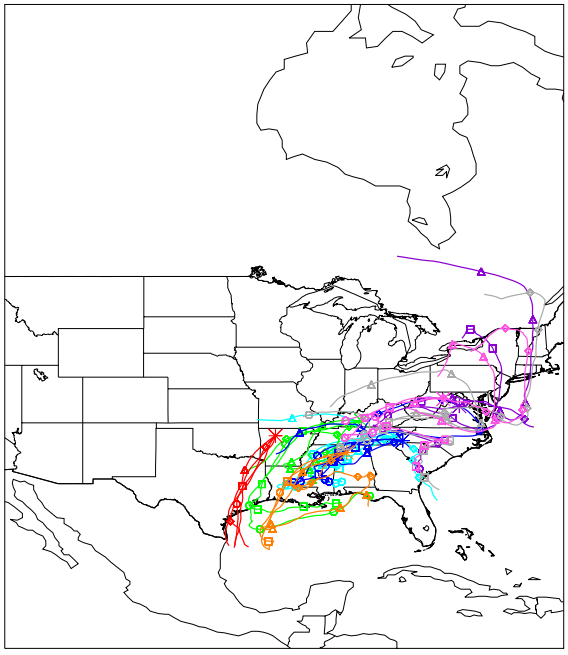

Figure A.16 7-June trajectories calculated using NGM data.

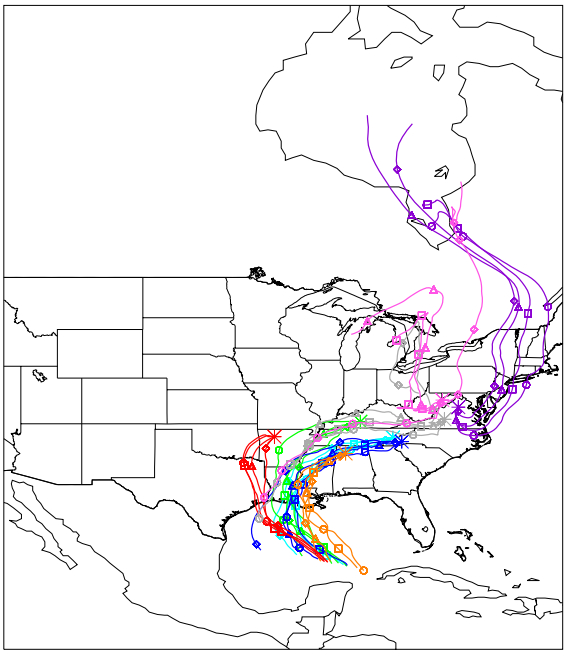

Figure A.17 10-June trajectories calculated using NGM data.

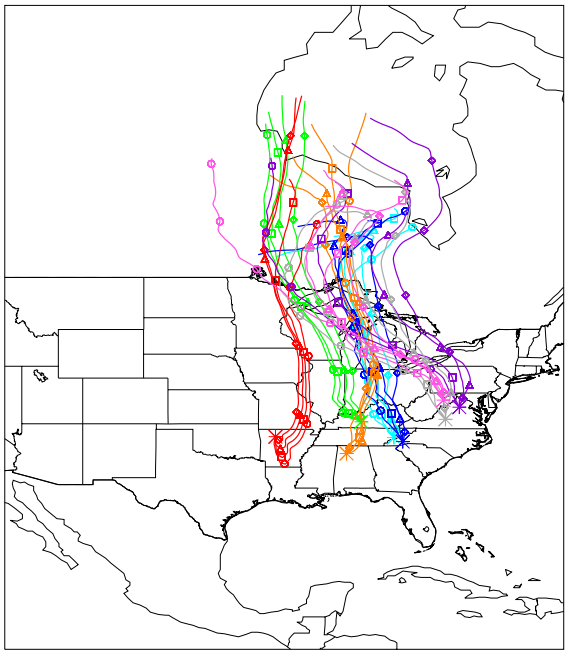

Figure A.18 14-June trajectories calculated using NGM data.

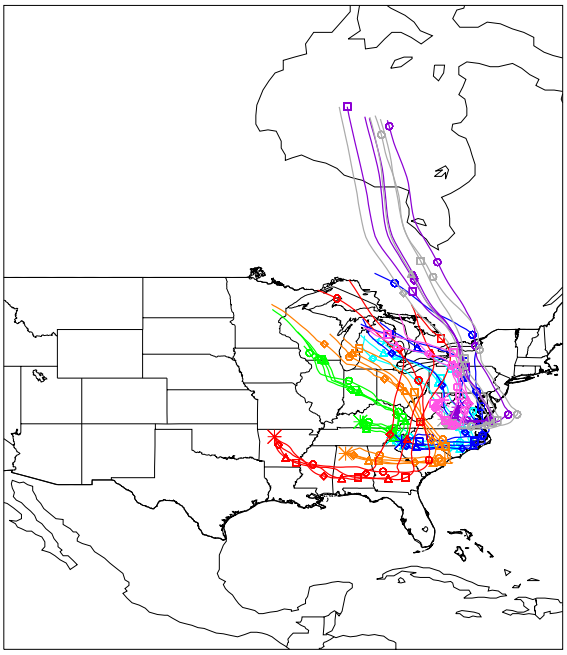

Figure A.19 17-June trajectories calculated using NGM data.

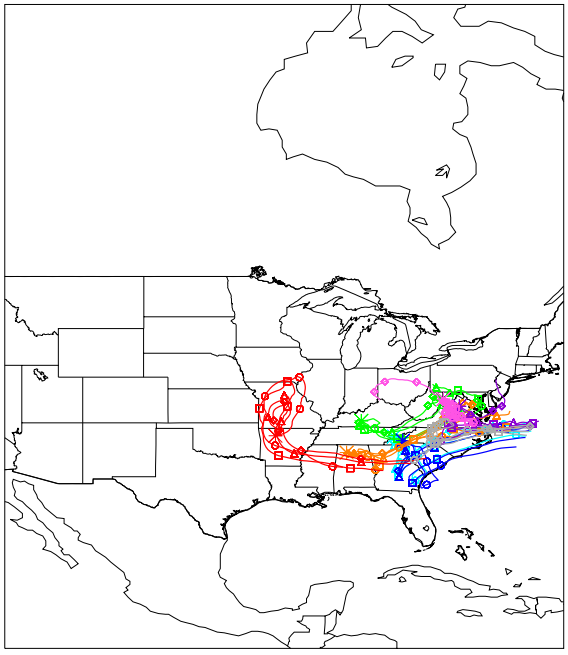

Figure A.20 21-June trajectories calculated using NGM data.

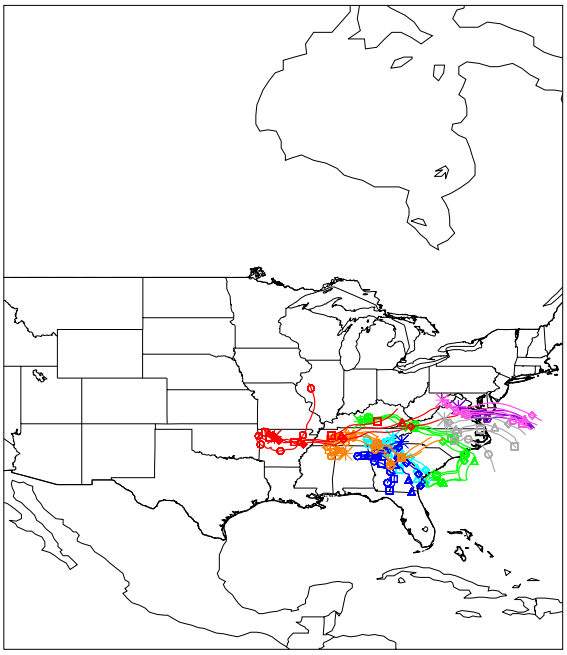

Figure A.21 24-June trajectories calculated using NGM data.

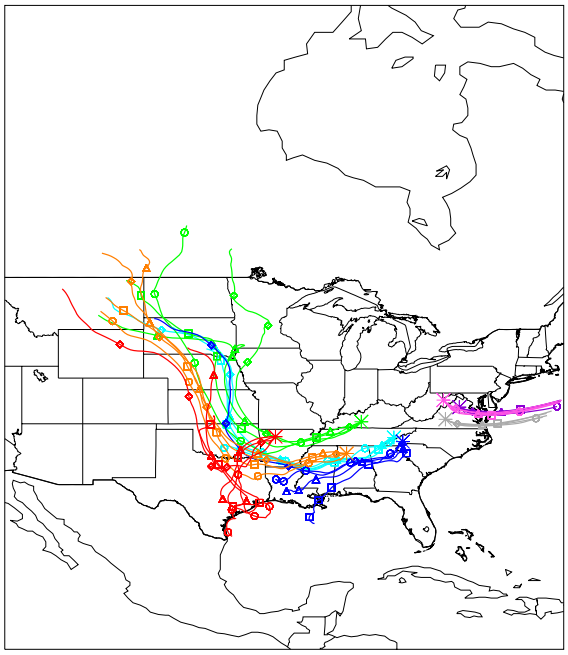

Figure A.22 28-June trajectories calculated using NGM data.

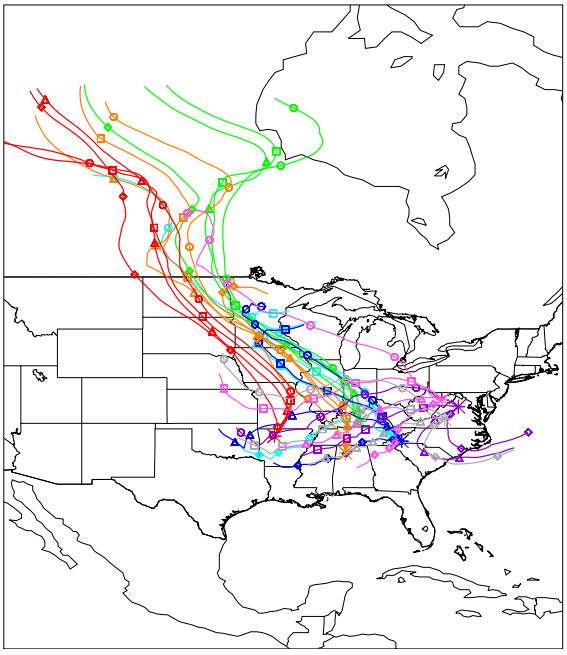

Figure A.23 1-July trajectories calculated using NGM data.

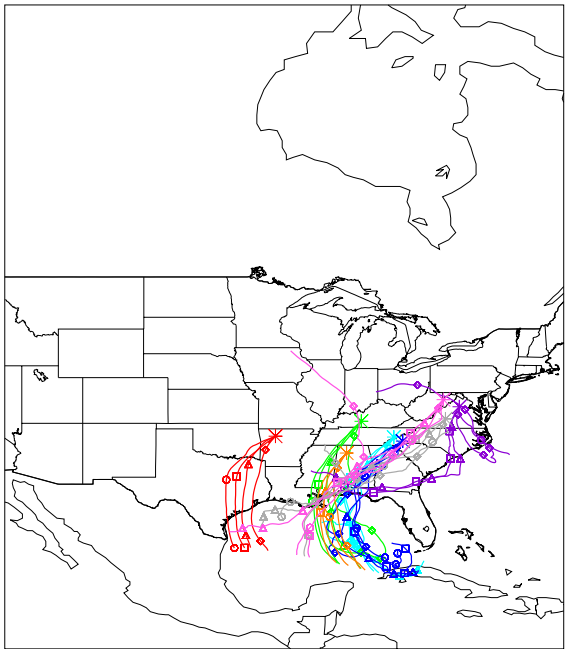

Figure A.24 5-July trajectories calculated using NGM data.

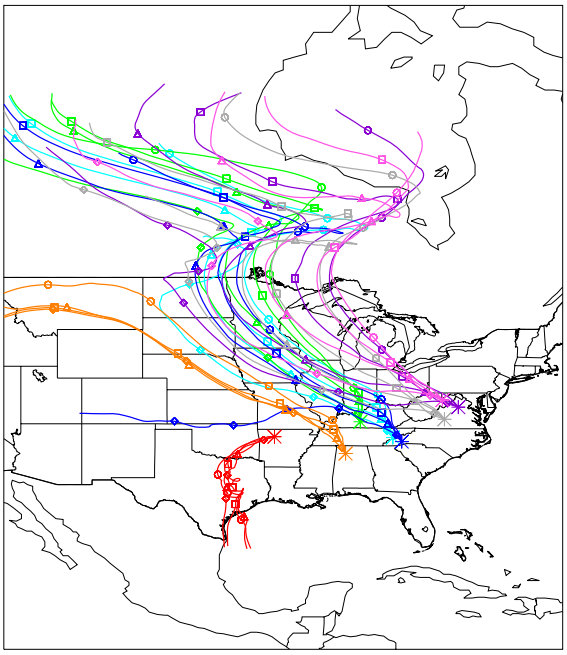

Figure A.25 8-July trajectories calculated using NGM data.

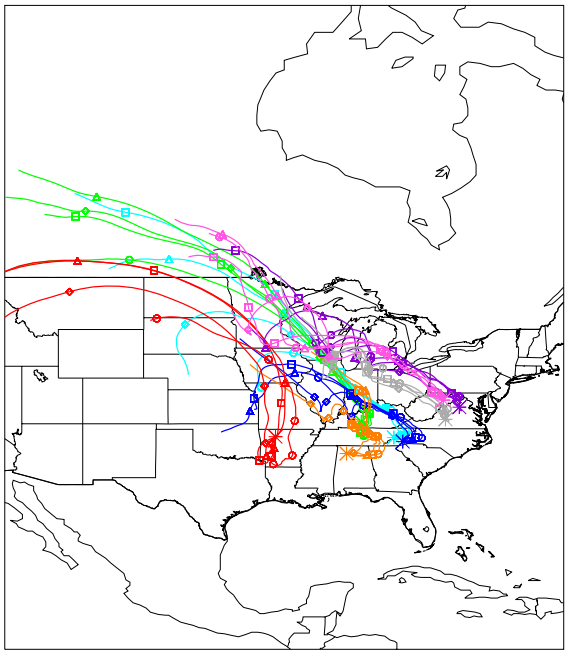

Figure A.26 12-July trajectories calculated using NGM data.

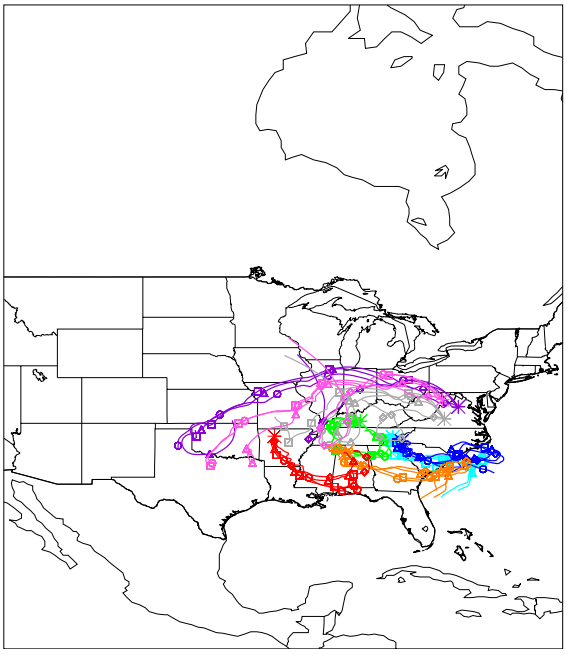

Figure A.27 15-July trajectories calculated using NGM data.

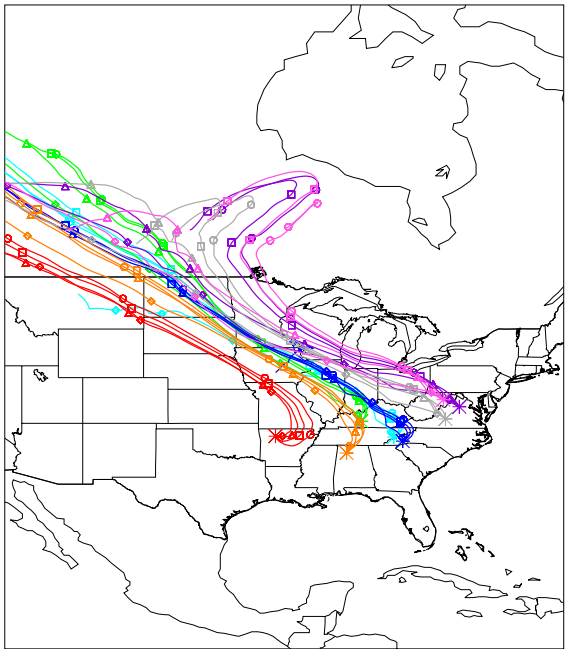

Figure A.28 19-July trajectories calculated using NGM data.

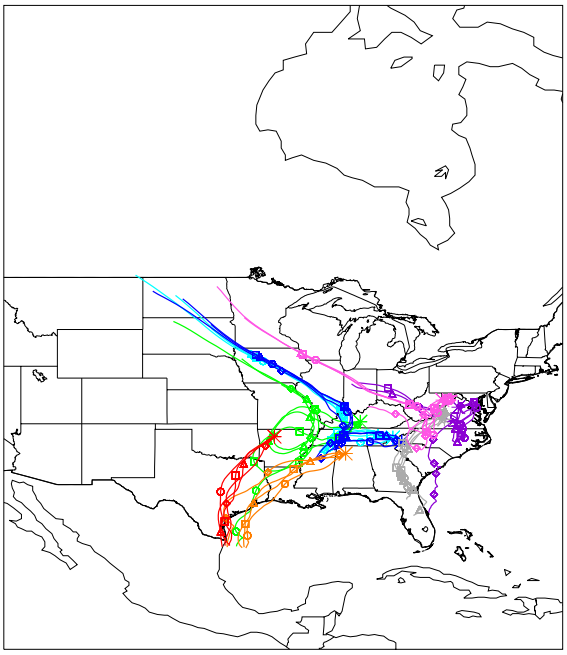

Figure A.29 22-July trajectories calculated using NGM data.

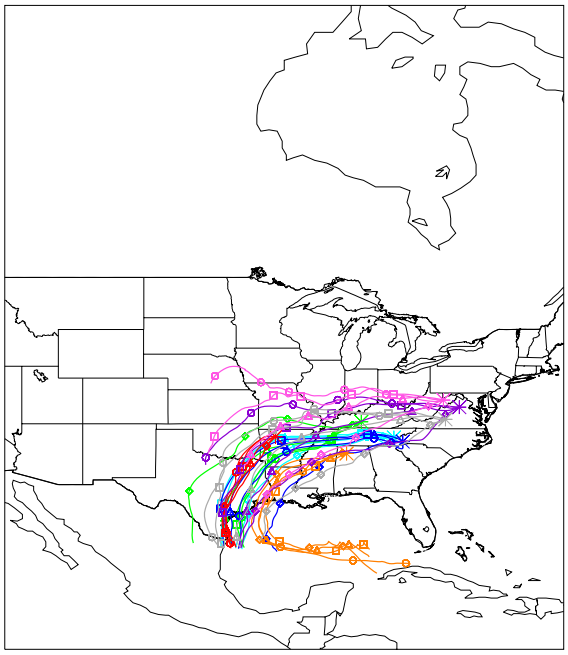

Figure A.30 26-July trajectories calculated using NGM data.

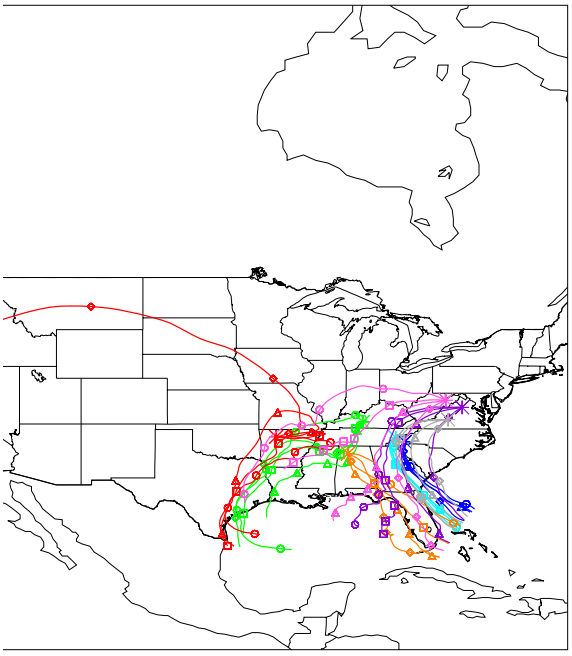

Figure A.31 29-July trajectories calculated using NGM data.

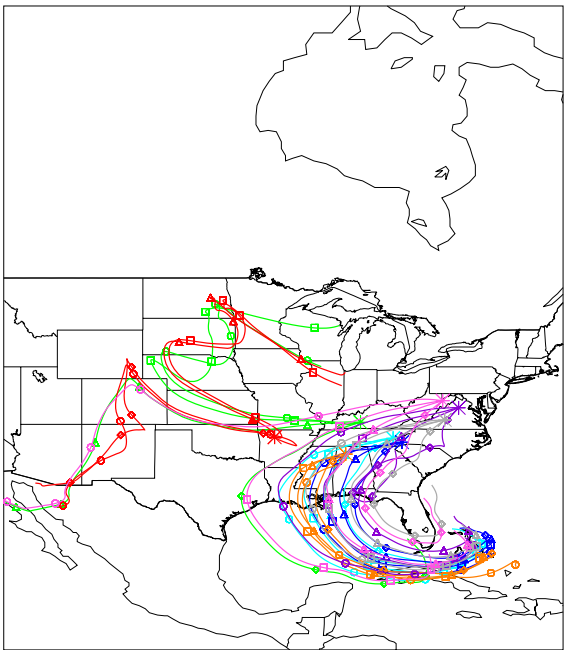

Figure A.32 19-April trajectories calculated using reanalysis data.

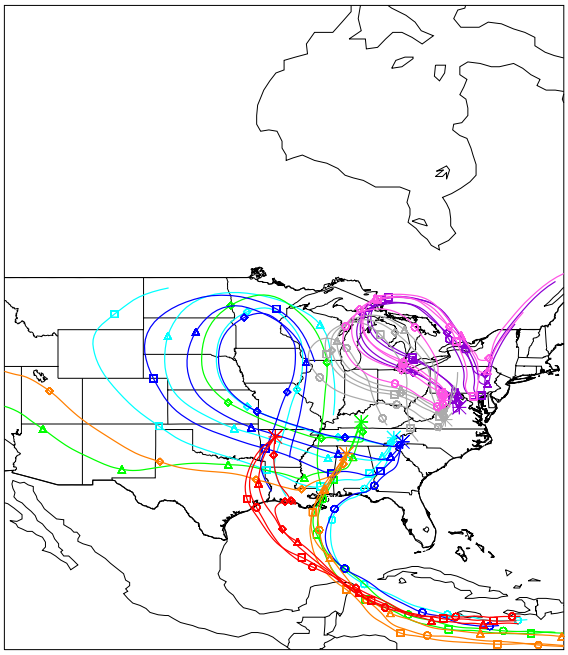

Figure A.33 13-May trajectories calculated using reanalysis data.

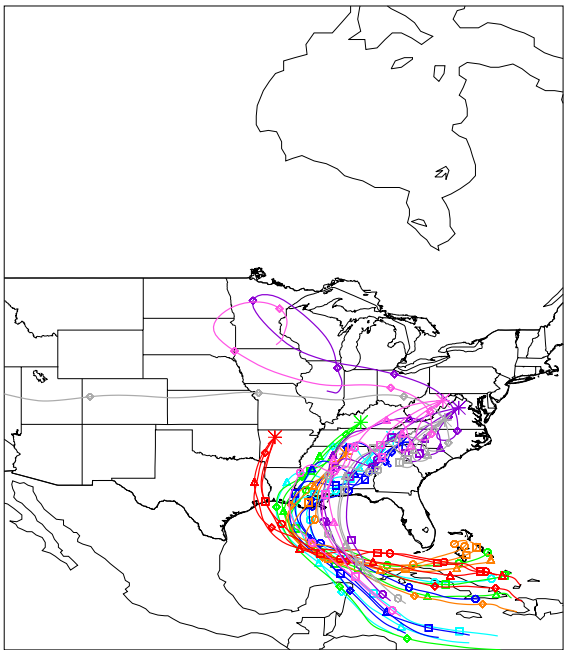

Figure A.34 17-May trajectories calculated using reanalysis data.

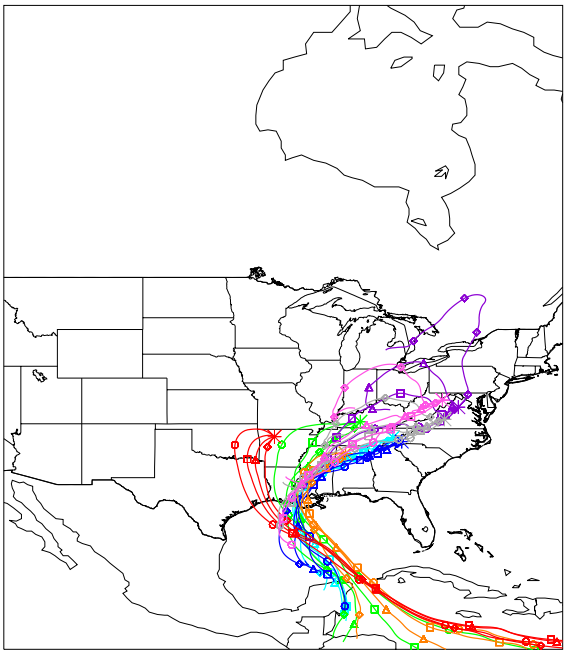

Figure A.35 10-June trajectories calculated using reanalysis data.

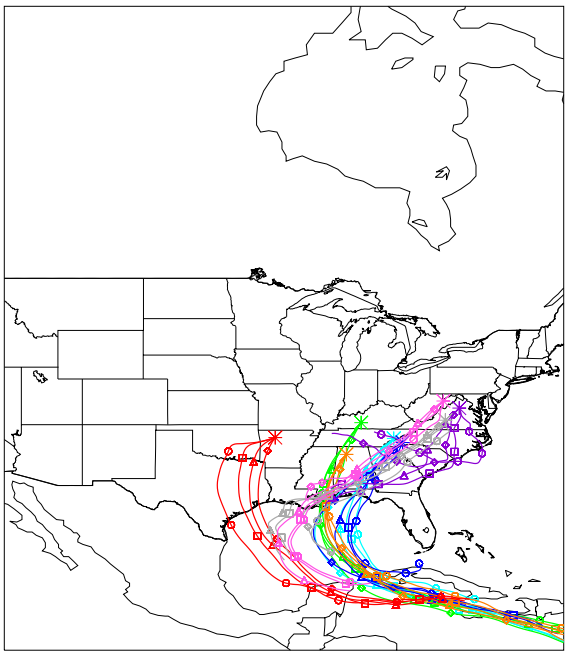

Figure A.36 5-July trajectories calculated using reanalysis data.

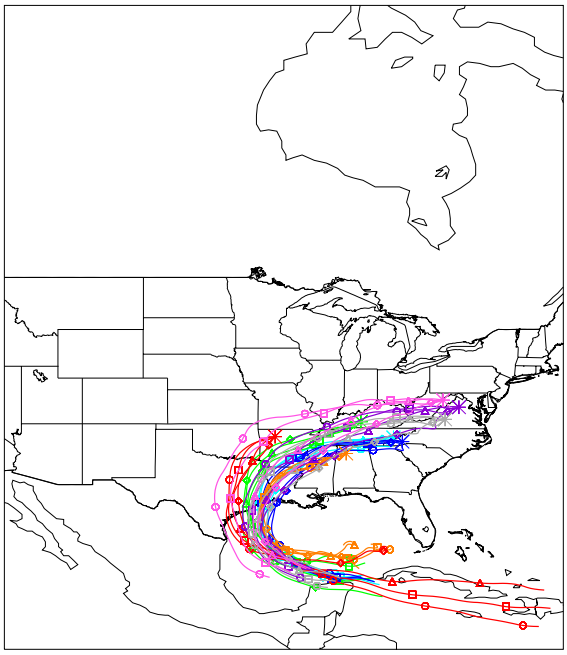

Figure A.37 26-July trajectories calculated using reanalysis data.

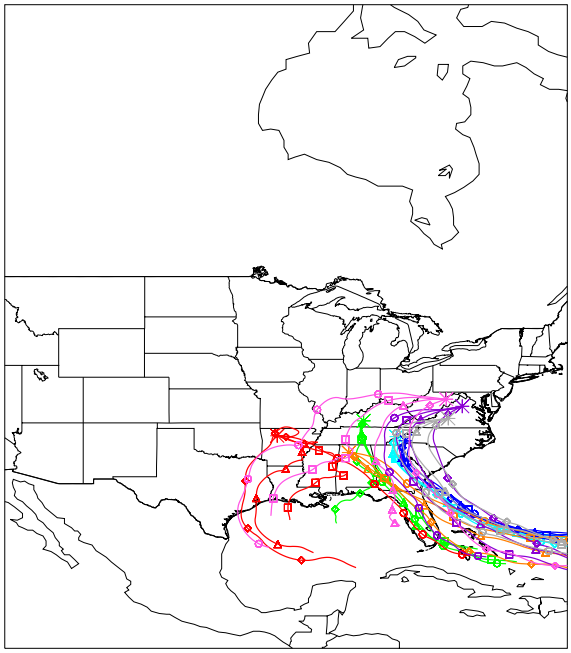

Figure A.38 29-July trajectories calculated using reanalysis data.

APPENDIX B. 1998 Back Trajectories

The following are all the back trajectory maps used in this study for 1998. FNL trajectories were used for all of 1998 and were supplemented with EDAS trajectories when available. Trajectories are colored by park: red – UPBU, orange – SIPS, green – MACA, light blue – GRSM, dark blue – SHRO, gray – JEFF, pink – DOSO, purple – SHEN. Symbols mark the position of the air parcel at the end of each day for all five days back from the site. Four representative times are presented: 1 LST (diamonds), 7 LST (triangles), 13 LST (squares), and 19 LST (circles).

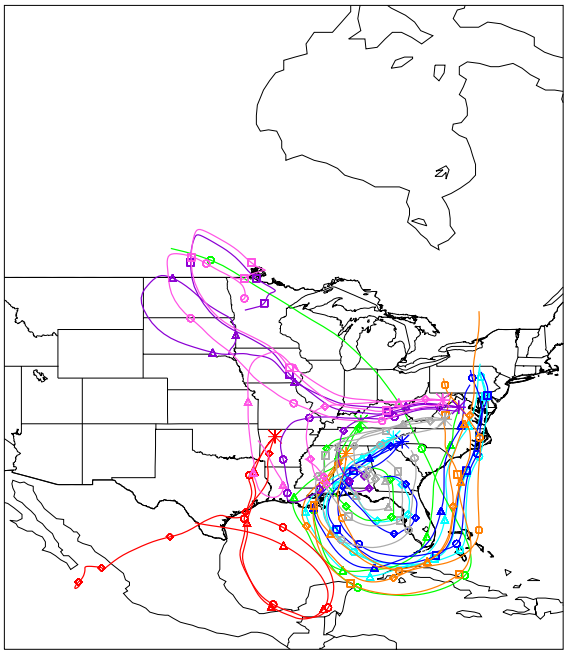

Figure B.1 15-April trajectories calculated using FNL data.

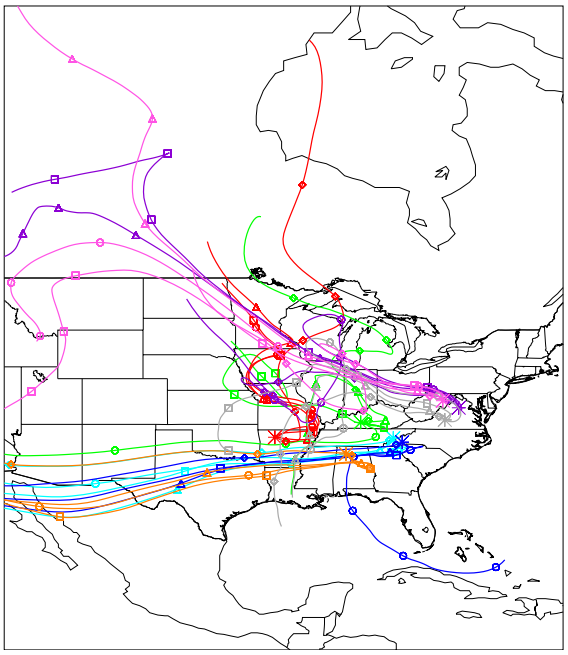

Figure B.2 18-April trajectories calculated using FNL data.

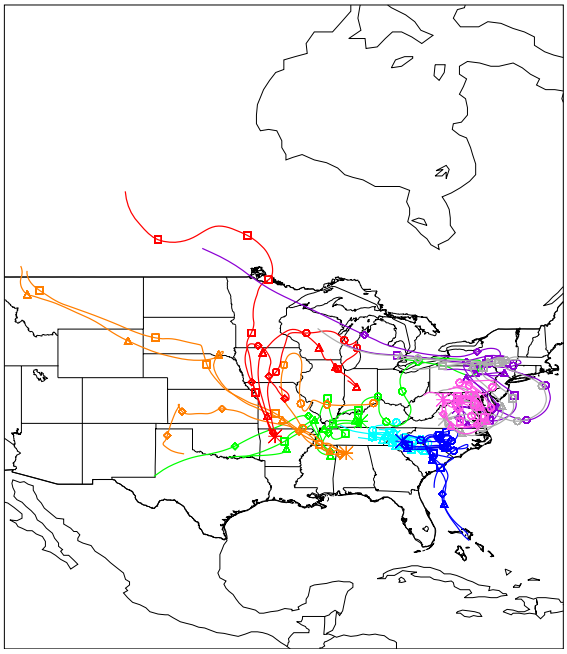

Figure B.3 22-April trajectories calculated using FNL data.

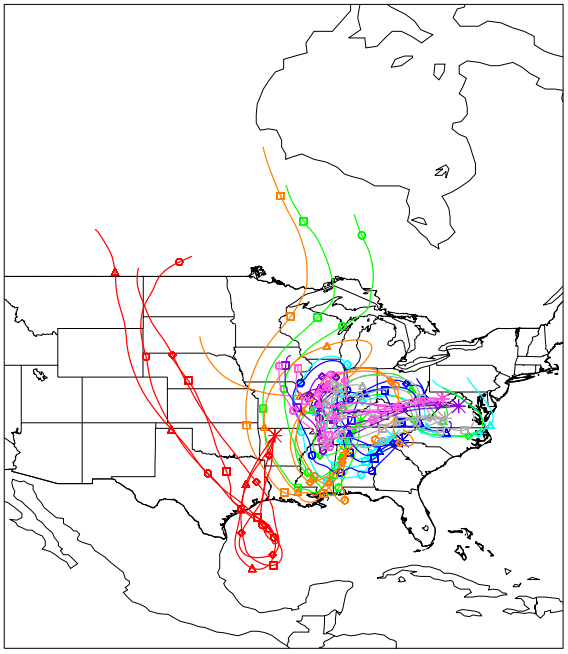

Figure B.4 25-April trajectories calculated using FNL data.

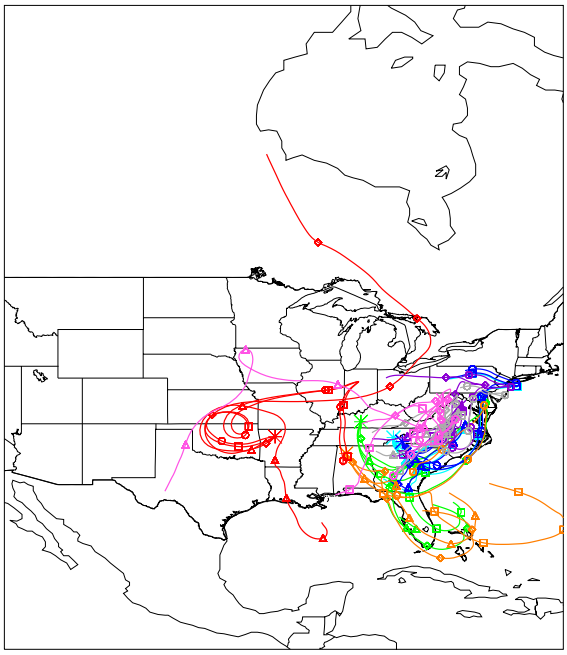

Figure B.5 29-April trajectories calculated using FNL data.

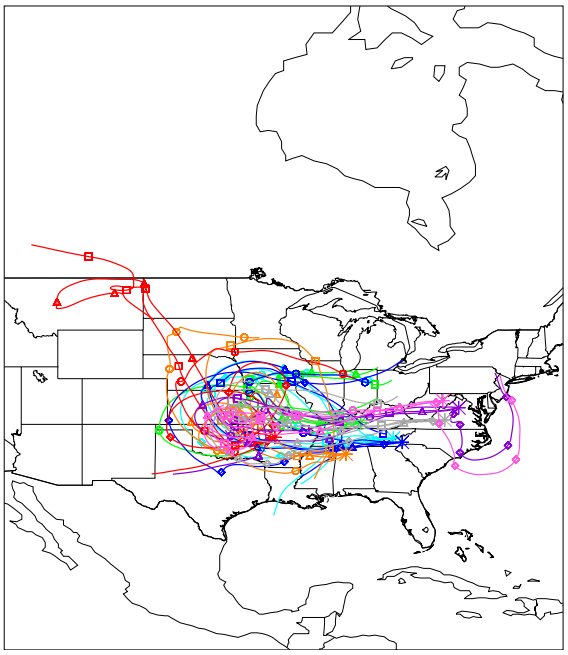

Figure B.6 2-May trajectories calculated using FNL data.

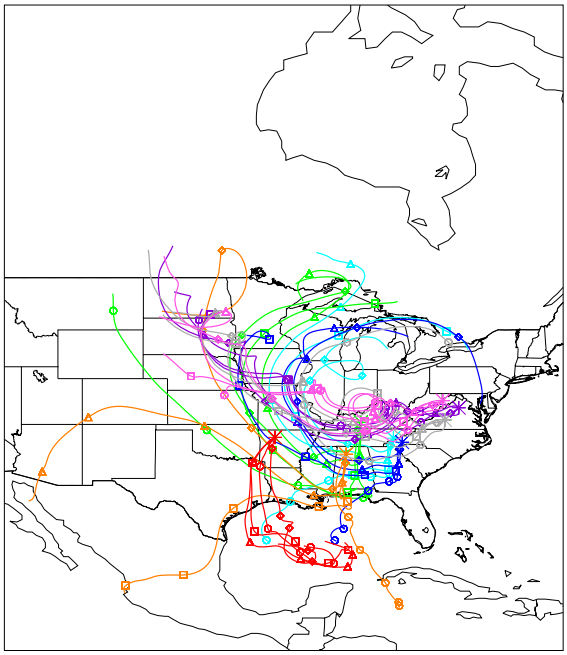

Figure B.7 6-May trajectories calculated using FNL data.

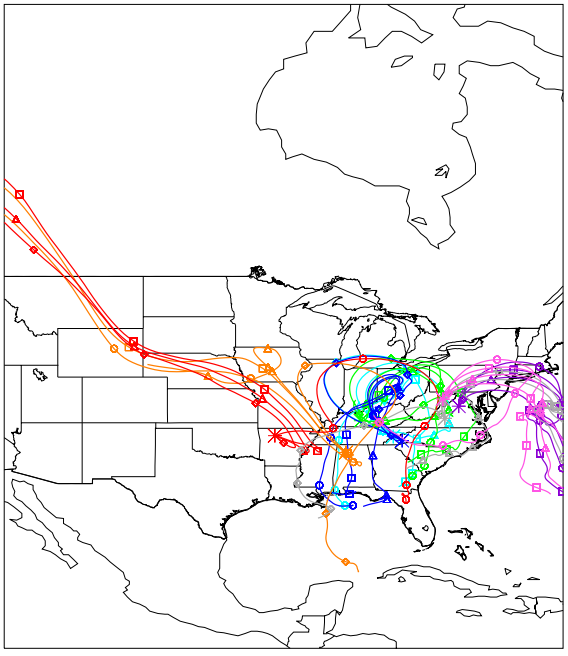

Figure B.8 9-May trajectories calculated using FNL data.

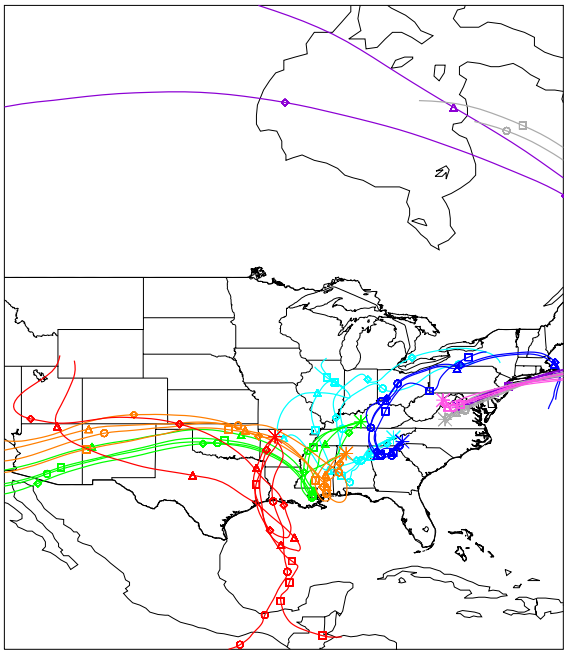

Figure B.9 13-May trajectories calculated using FNL data.

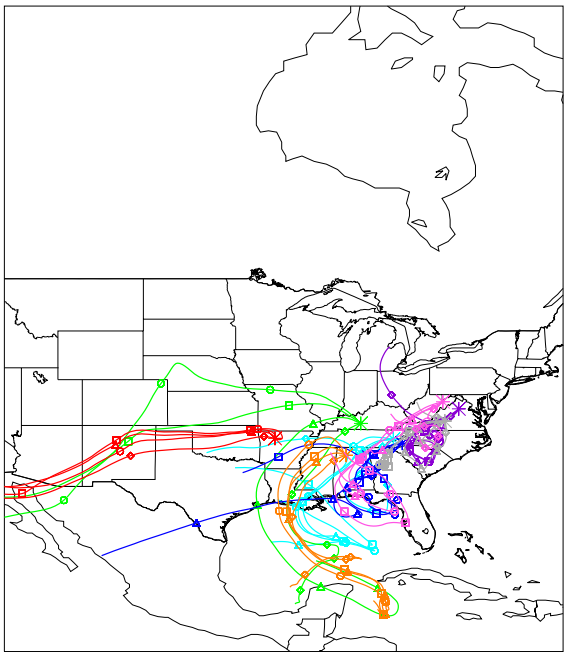

Figure B.10 16-May trajectories calculated using FNL data.

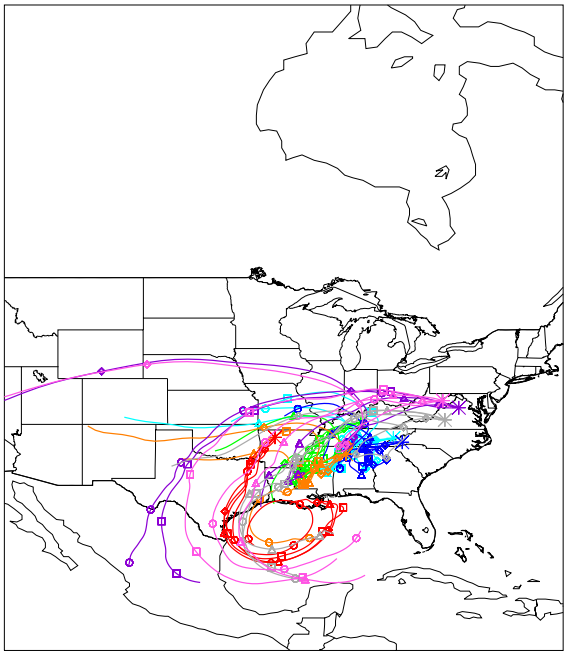

Figure B.11 20-May trajectories calculated using FNL data.

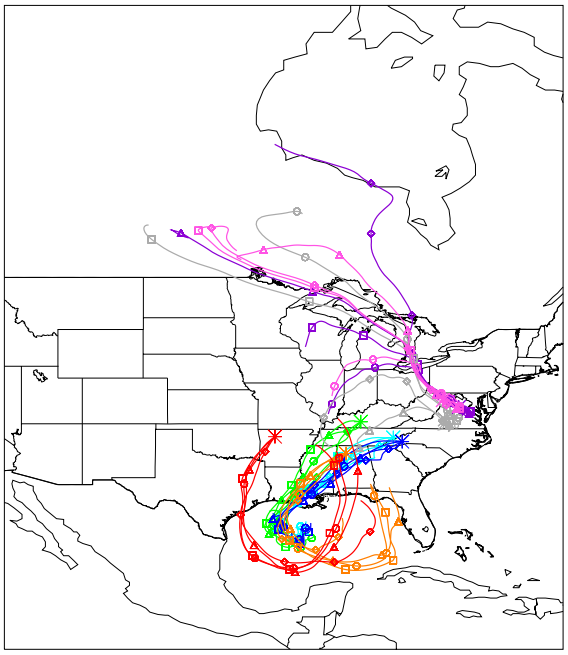

Figure B.12 23-May trajectories calculated using FNL data.

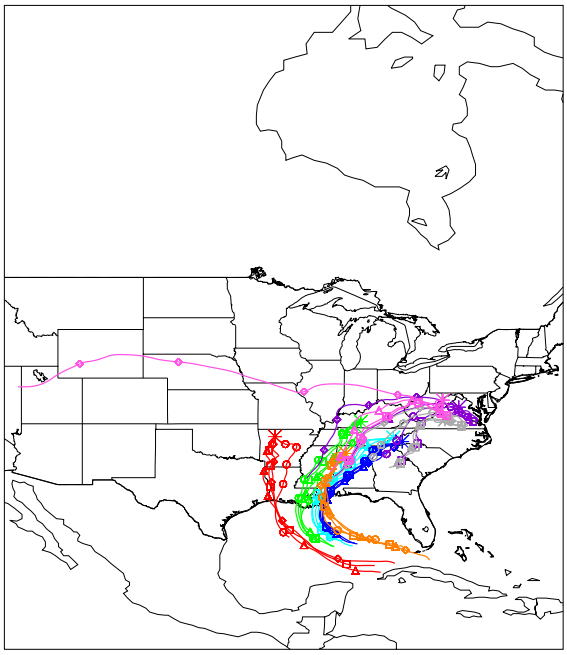

Figure B.13 27-May trajectories calculated using FNL data.

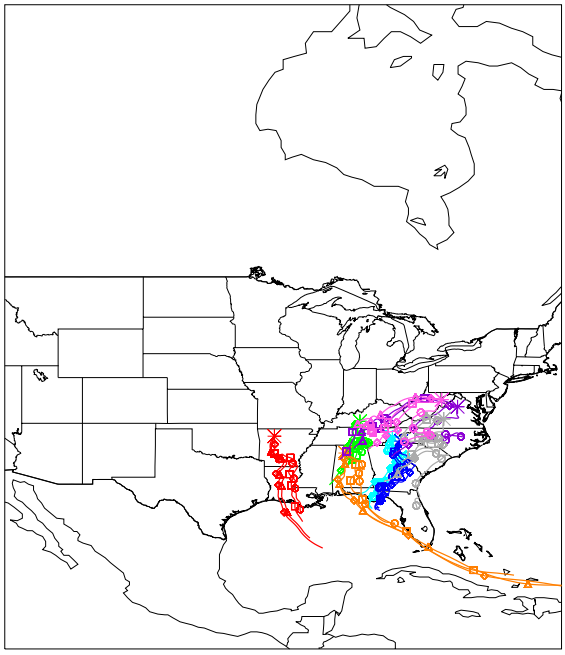

Figure B.14 30-May trajectories calculated using FNL data.

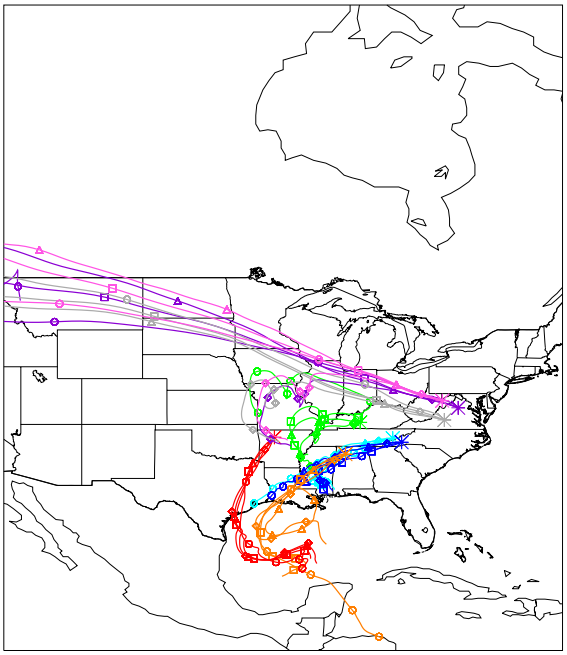

Figure B.15 3-June trajectories calculated using FNL data.

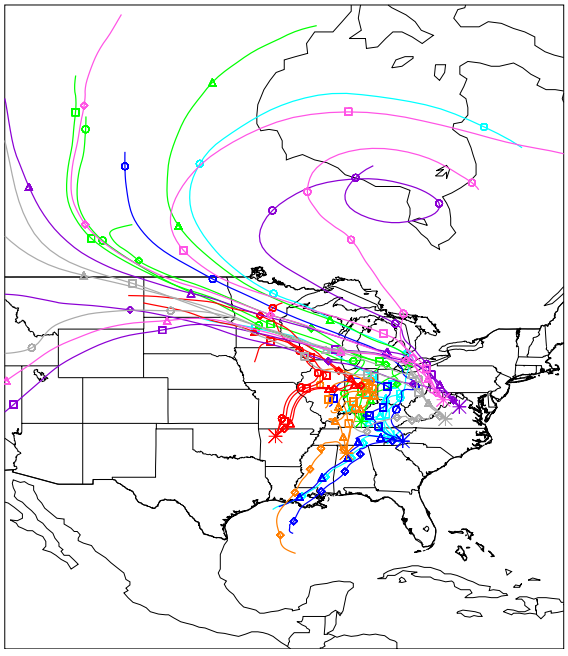

Figure B.16 6-June trajectories calculated using FNL data.

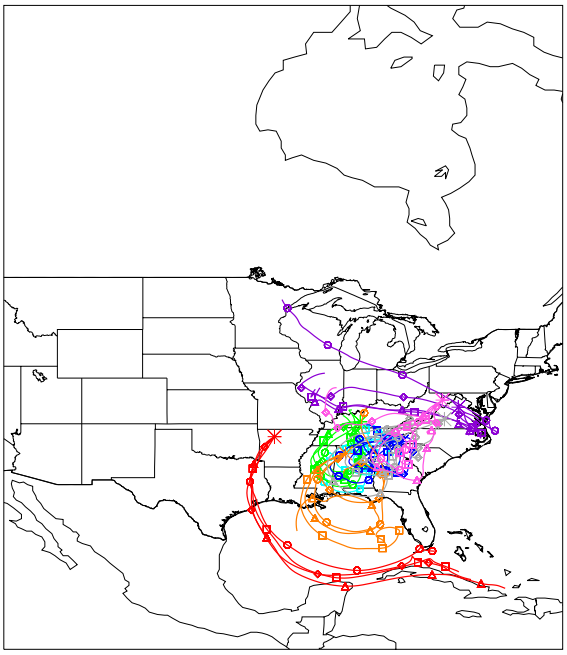

Figure B.17 10-June trajectories calculated using FNL data.

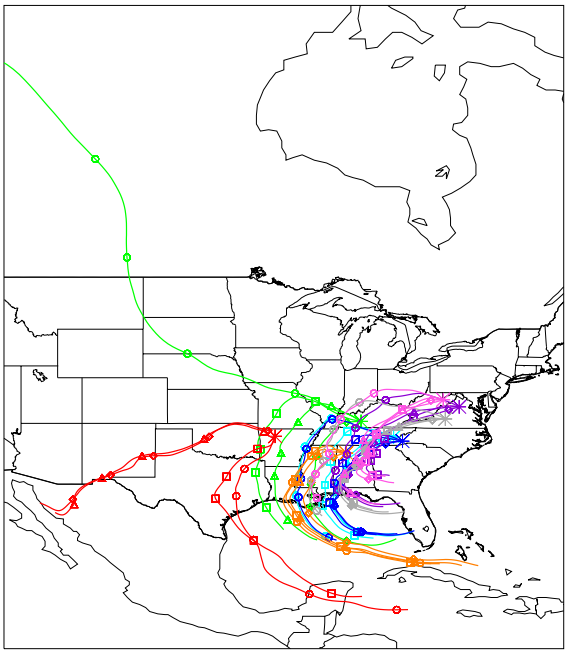

Figure B.18 13-June trajectories calculated using FNL data.

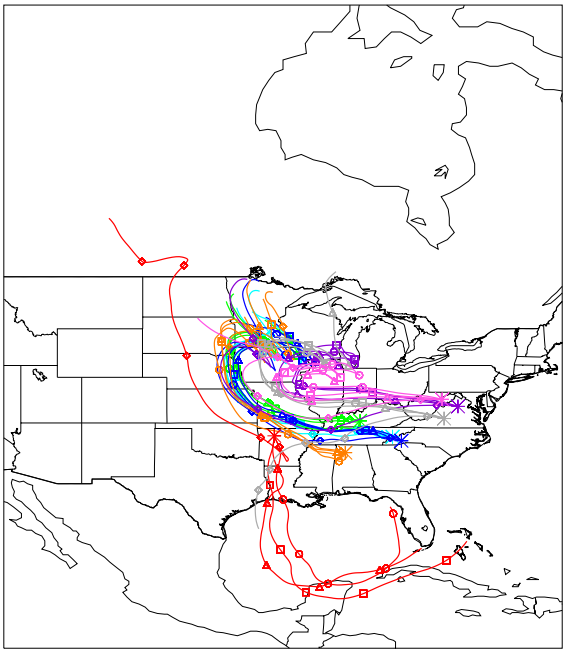

Figure B.19 17-June trajectories calculated using FNL data.

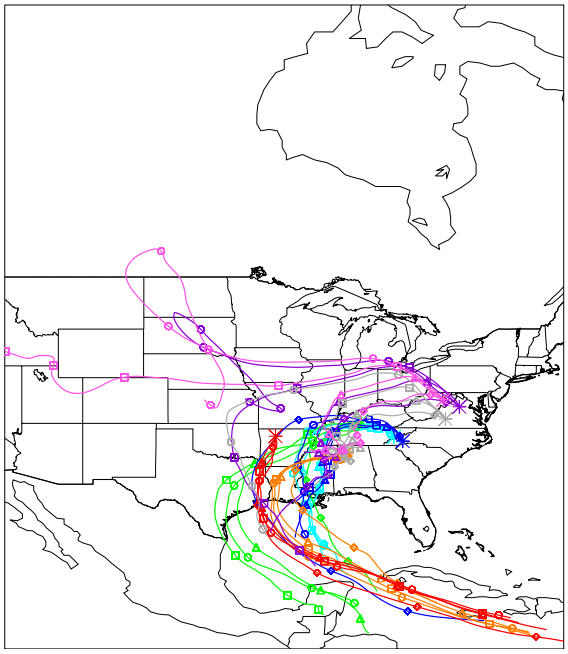

Figure B.20 20-June trajectories calculated using FNL data.

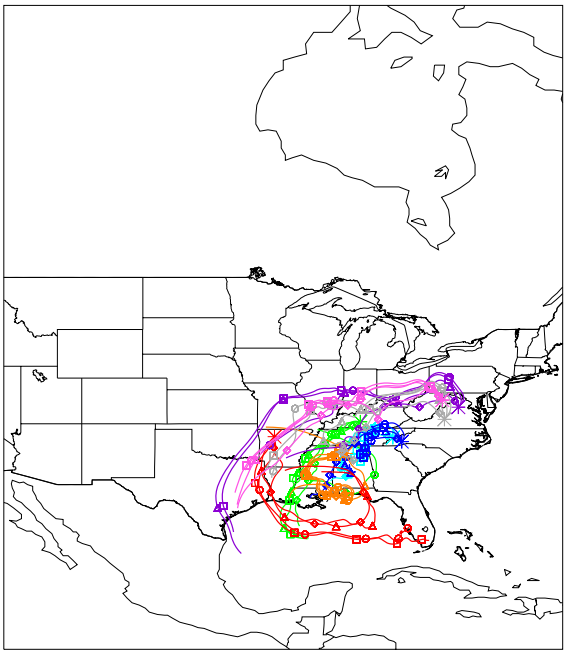

Figure B.21 24-June trajectories calculated using FNL data.

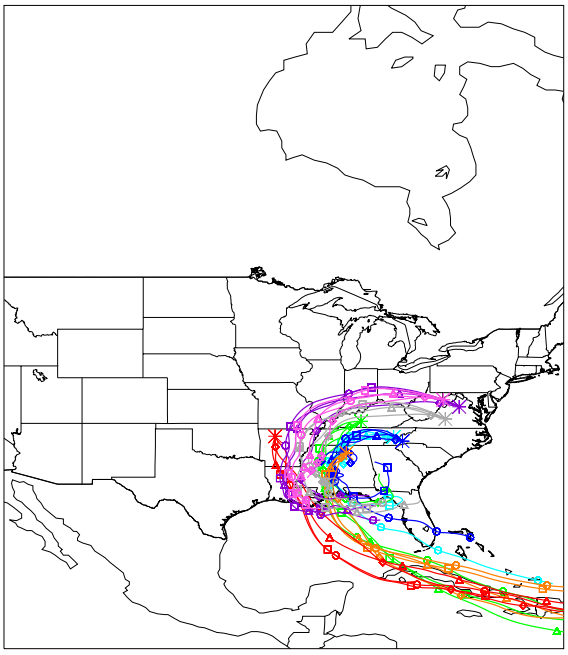

Figure B.22 27-June trajectories calculated using FNL data.

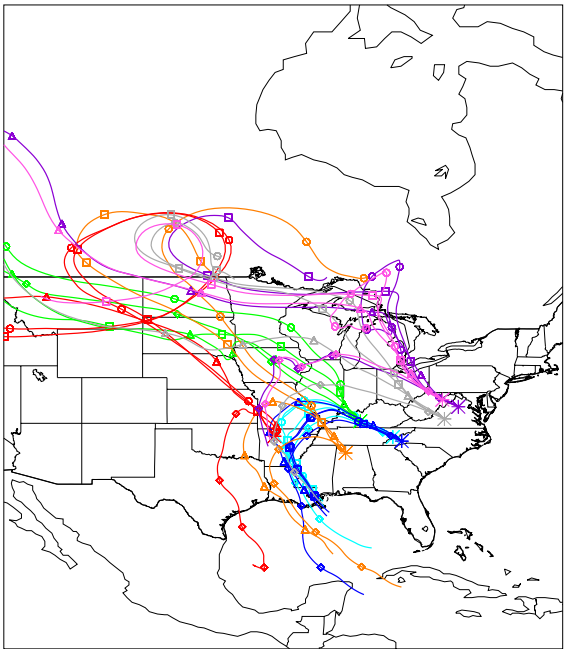

Figure B.23 1-July trajectories calculated using FNL data.

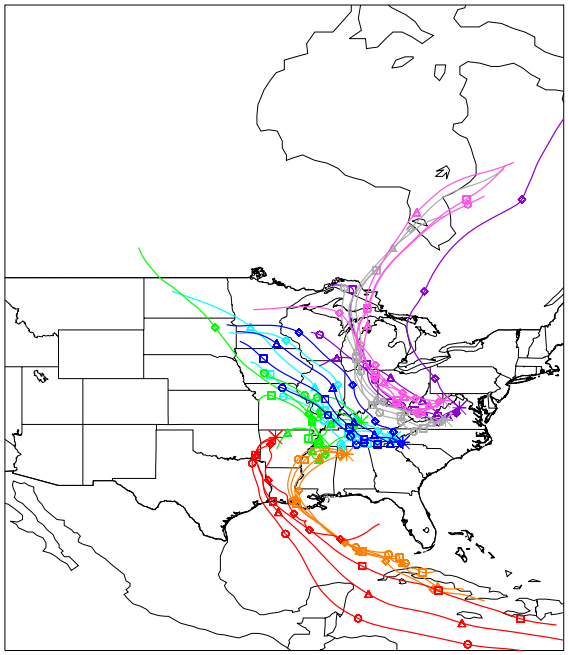

Figure B.24 4-July trajectories calculated using FNL data.

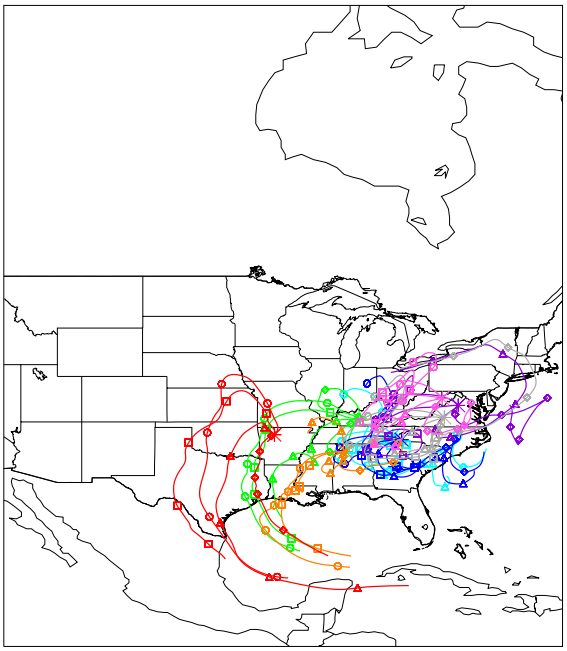

Figure B.25 8-July trajectories calculated using FNL data.

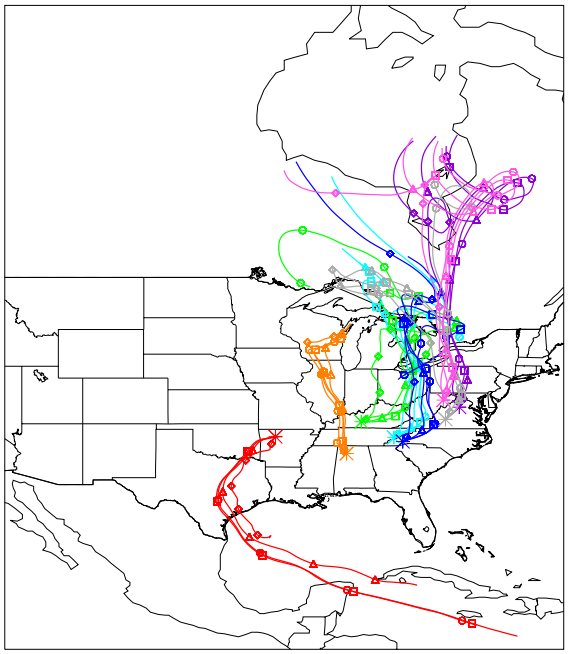

Figure B.26 11-July trajectories calculated using FNL data.

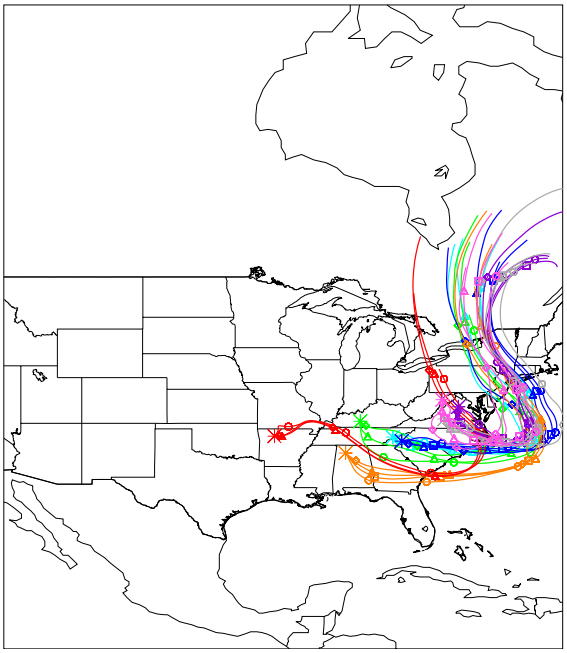

Figure B.27 15-July trajectories calculated using FNL data.

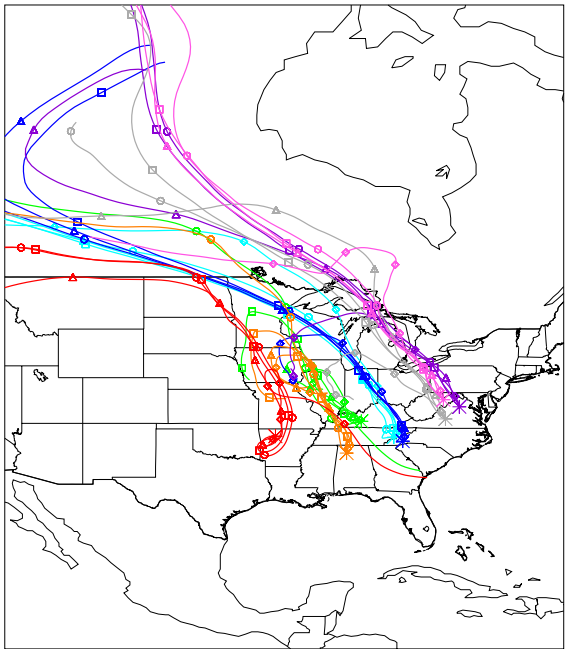

Figure B.28 18-July trajectories calculated using FNL data.

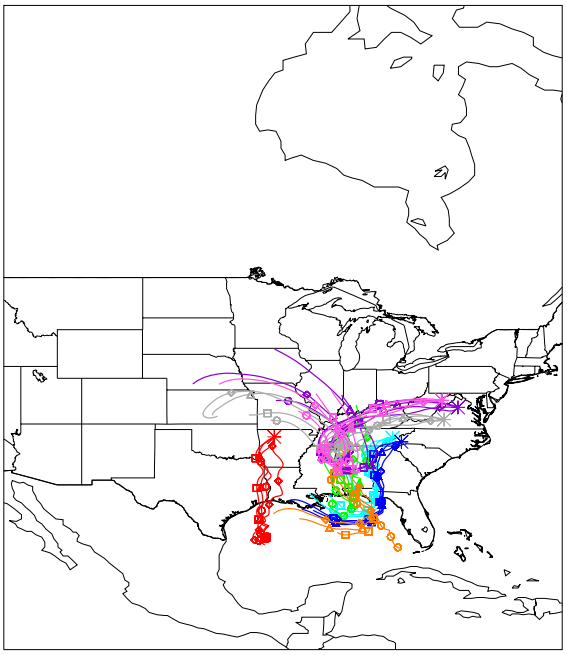

Figure B.29 22-July trajectories calculated using FNL data.

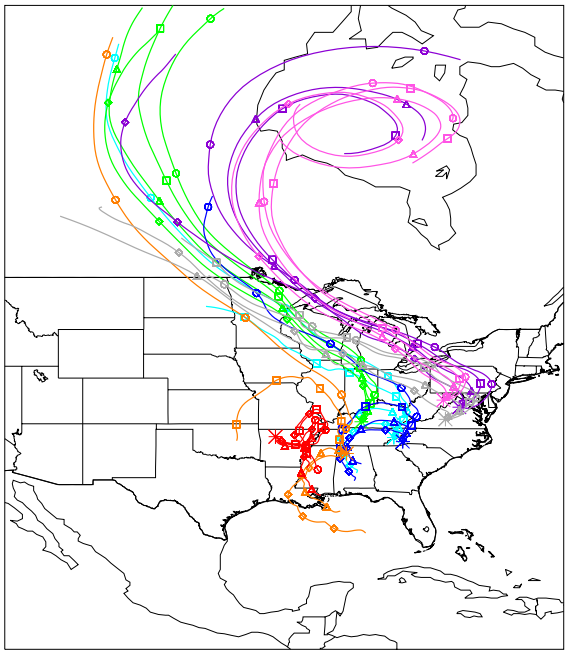

Figure B.30 25-July trajectories calculated using FNL data.

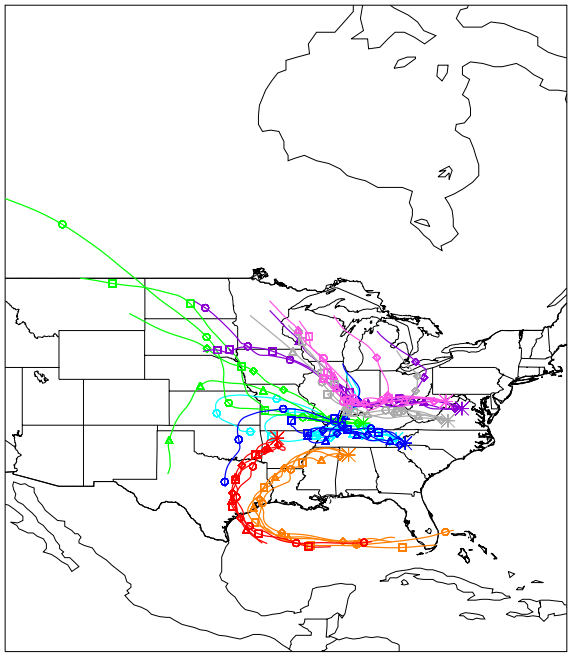

Figure B.31 29-July trajectories calculated using FNL data.

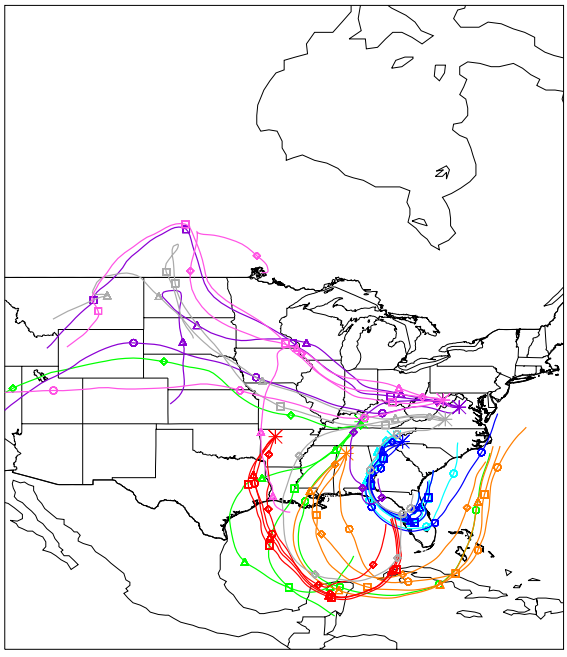

Figure B.32 15-April trajectories calculated using EDAS data.

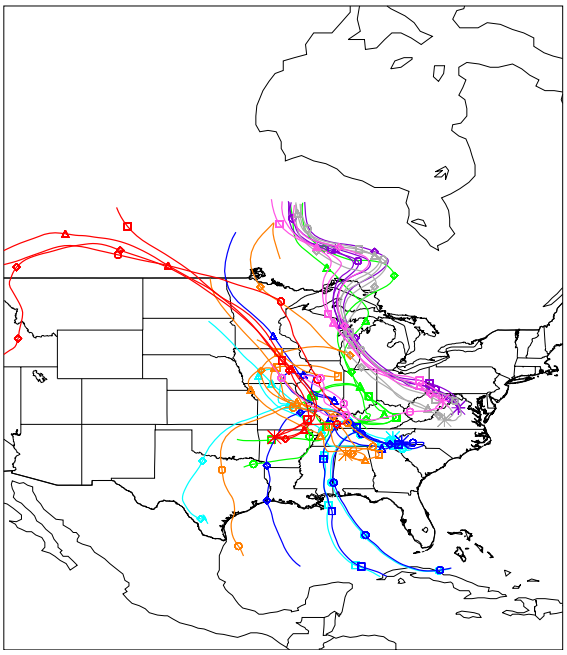

Figure B.33 18-April trajectories calculated using EDAS data.

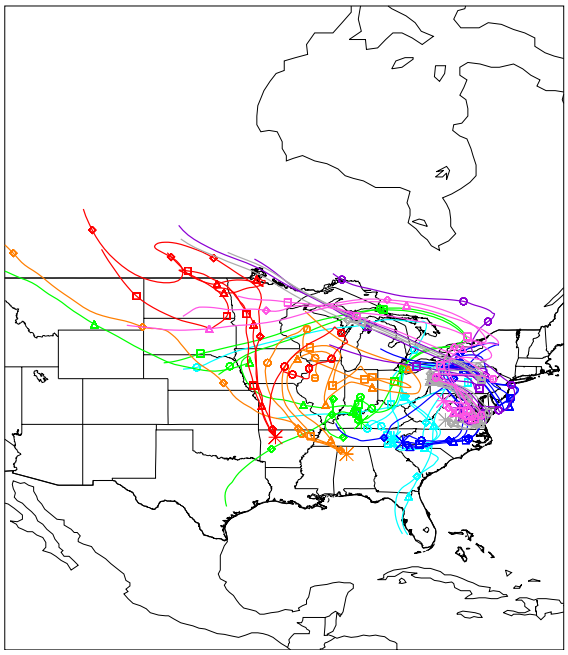

Figure B.34 22-April trajectories calculated using EDAS data.

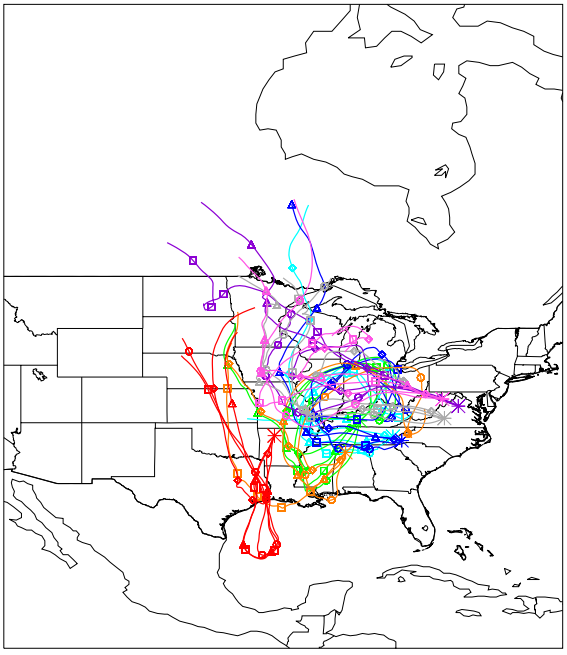

Figure B.35 25-April trajectories calculated using EDAS data.

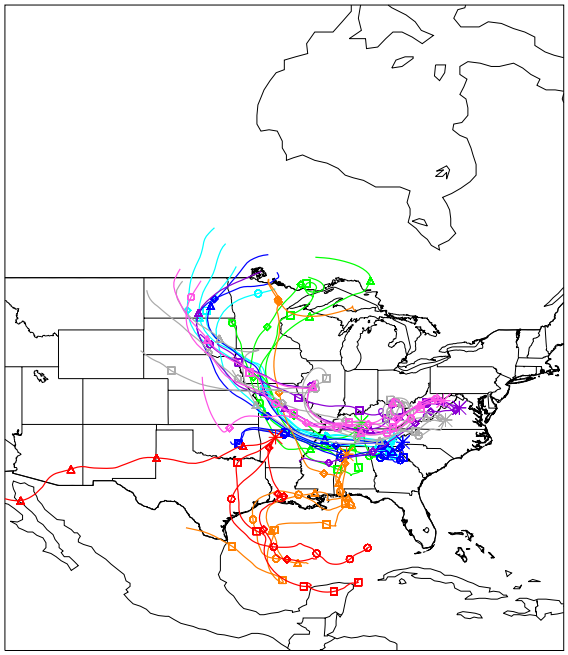

Figure B.36 6-May trajectories calculated using EDAS data.

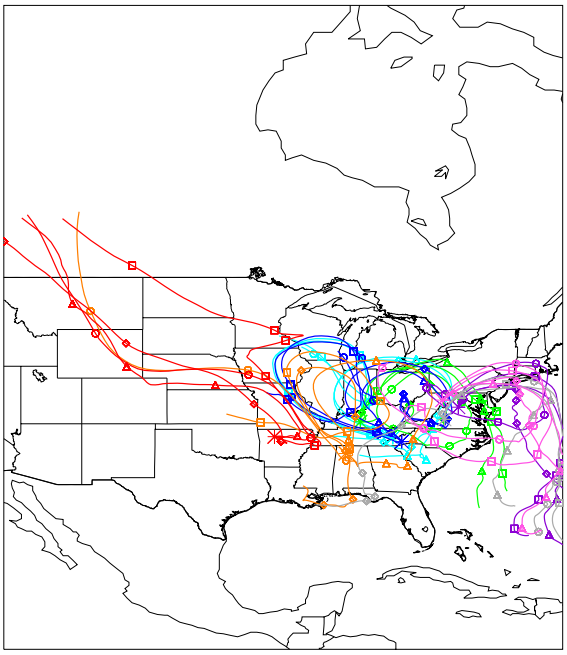

Figure B.37 9-May trajectories calculated using EDAS data.

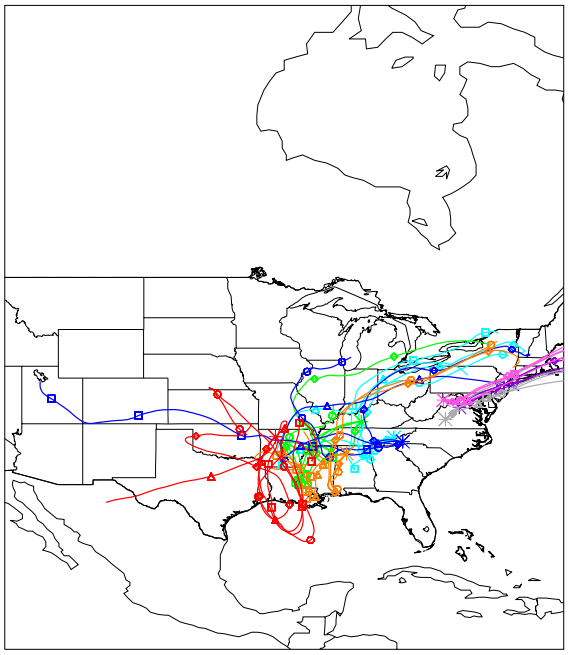

Figure B.38 13-May trajectories calculated using EDAS data.

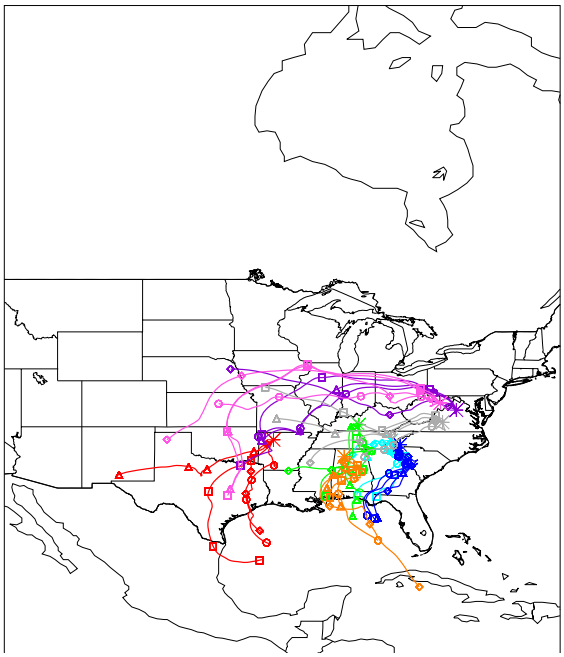

Figure B.39 30-May trajectories calculated using EDAS data.

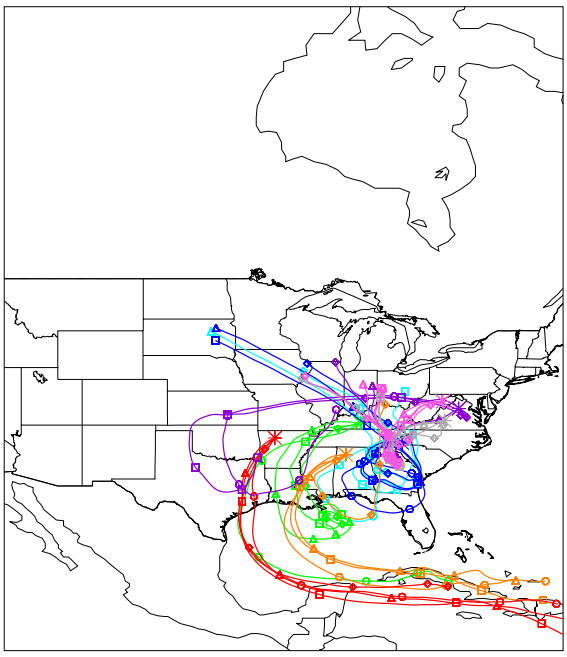

Figure B.40 10-June trajectories calculated using EDAS data.

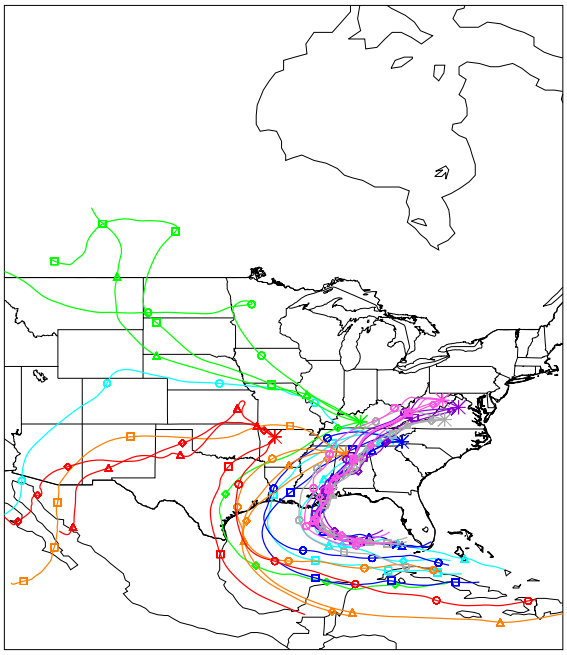

Figure B.41 13-June trajectories calculated using EDAS data.

APPENDIX C. 1995 U.S. Fire Maps

The following are maps of fire locations during 1995 from the National Fire Occurrence Database. Colored dots represent the acreage burned by each fire from day discovered through day contained: open purple circles – 0 or unknown acreage, gray filled dots – 0 to 1 acres, blue – 1 to 10 acres, green – 10 to 50 acres, yellow – 50 to 100 acres, orange – 100 to 1,000 acres, red – 1,000 to 10,000 acres.

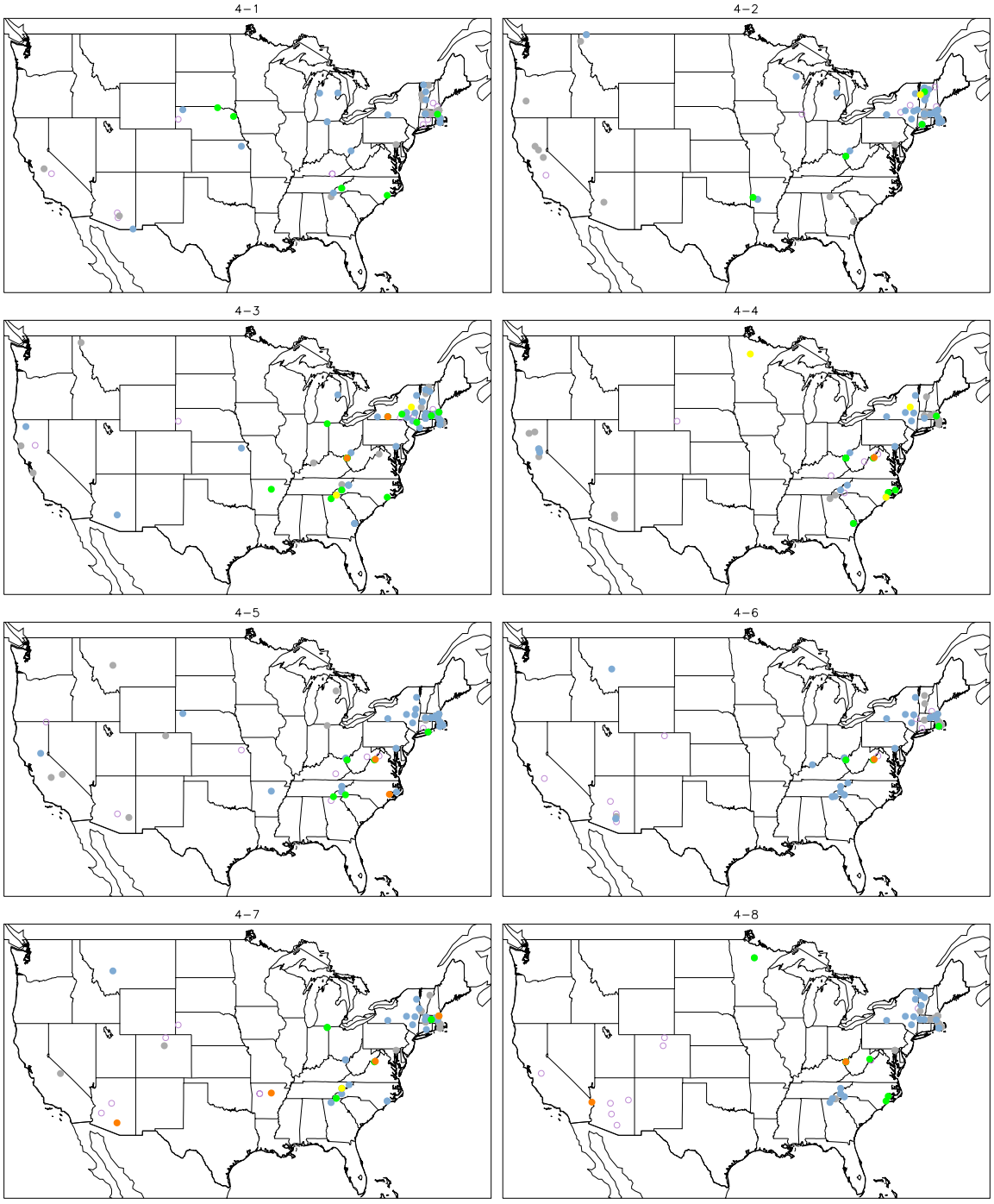

Figure C.1 Wildfire locations and acreages for 1-April through 8-April.

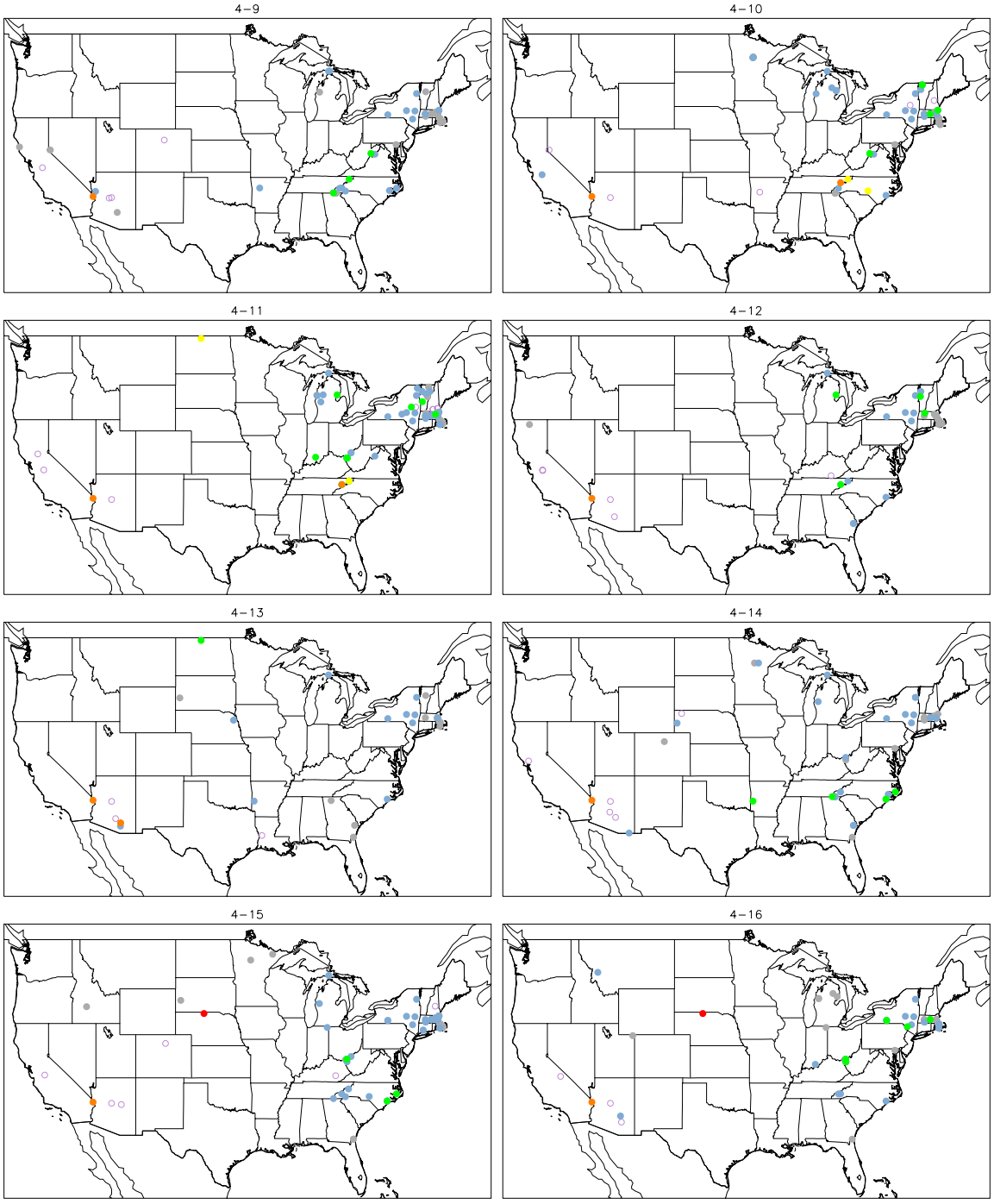

Figure C.2 Wildfire locations and acreages for 9-April through 16-April.

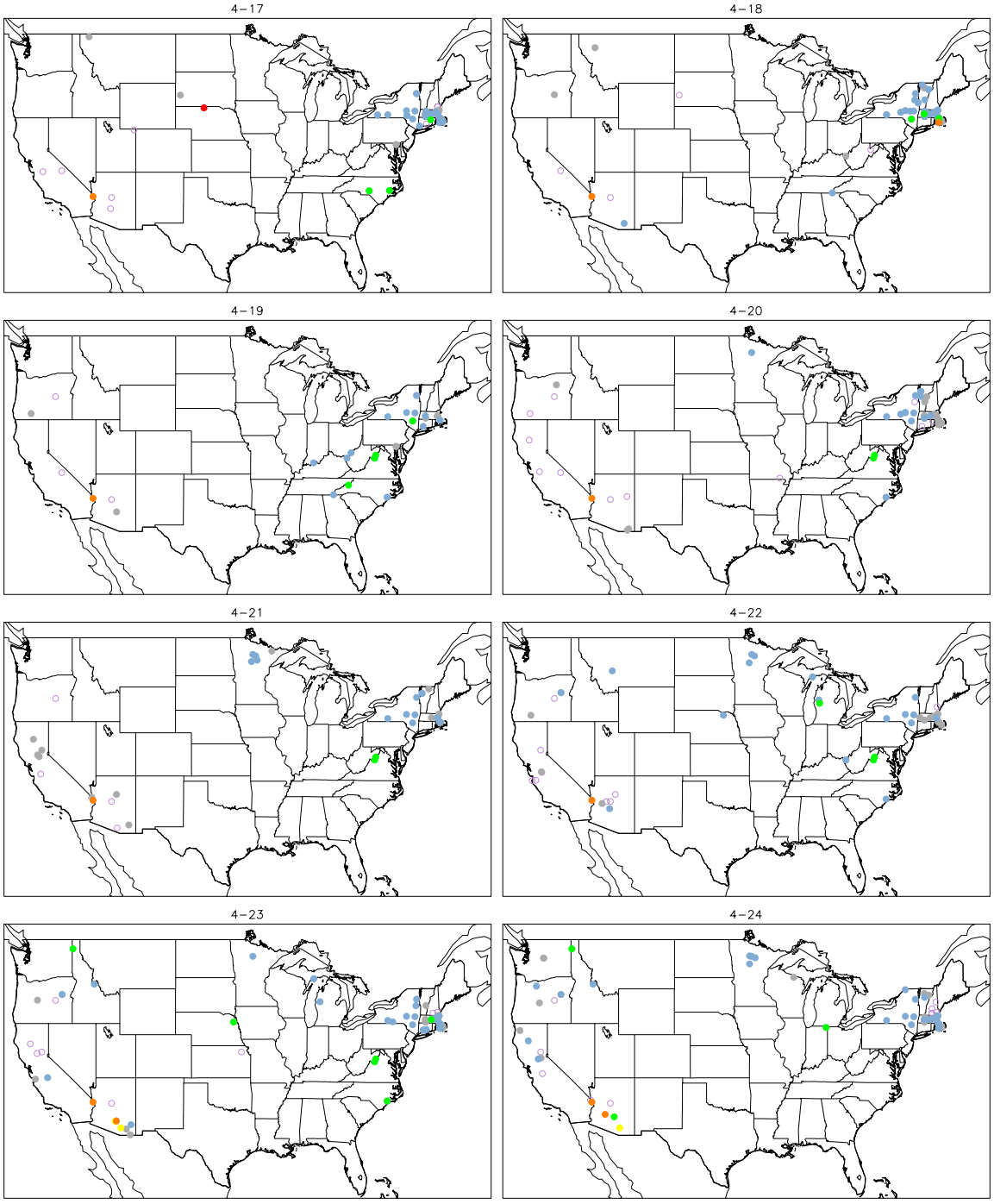

Figure C.3 Wildfire locations and acreages for 17-April through 24-April.

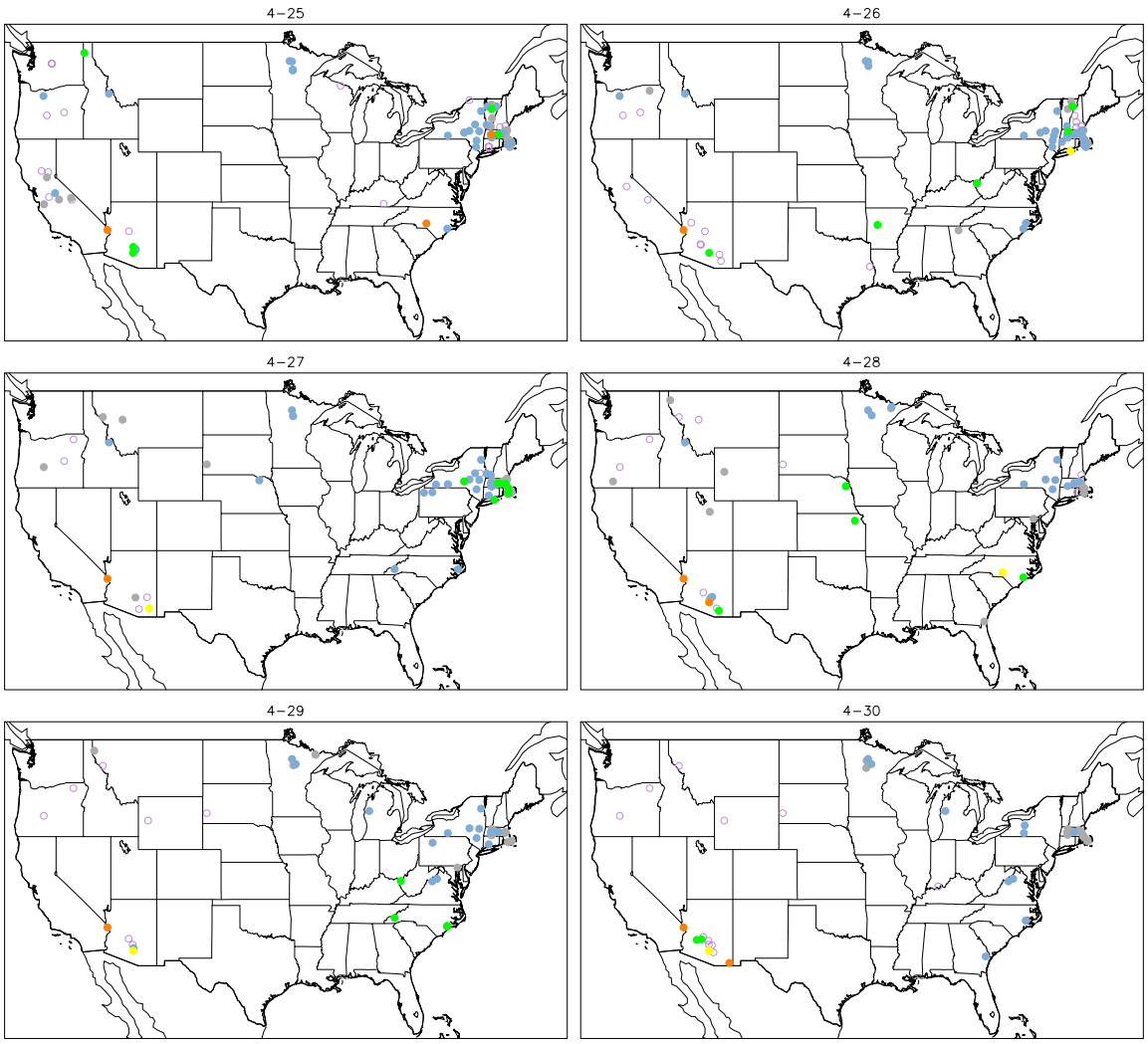

Figure C.4 Wildfire locations and acreages for 25-April through 30-April.

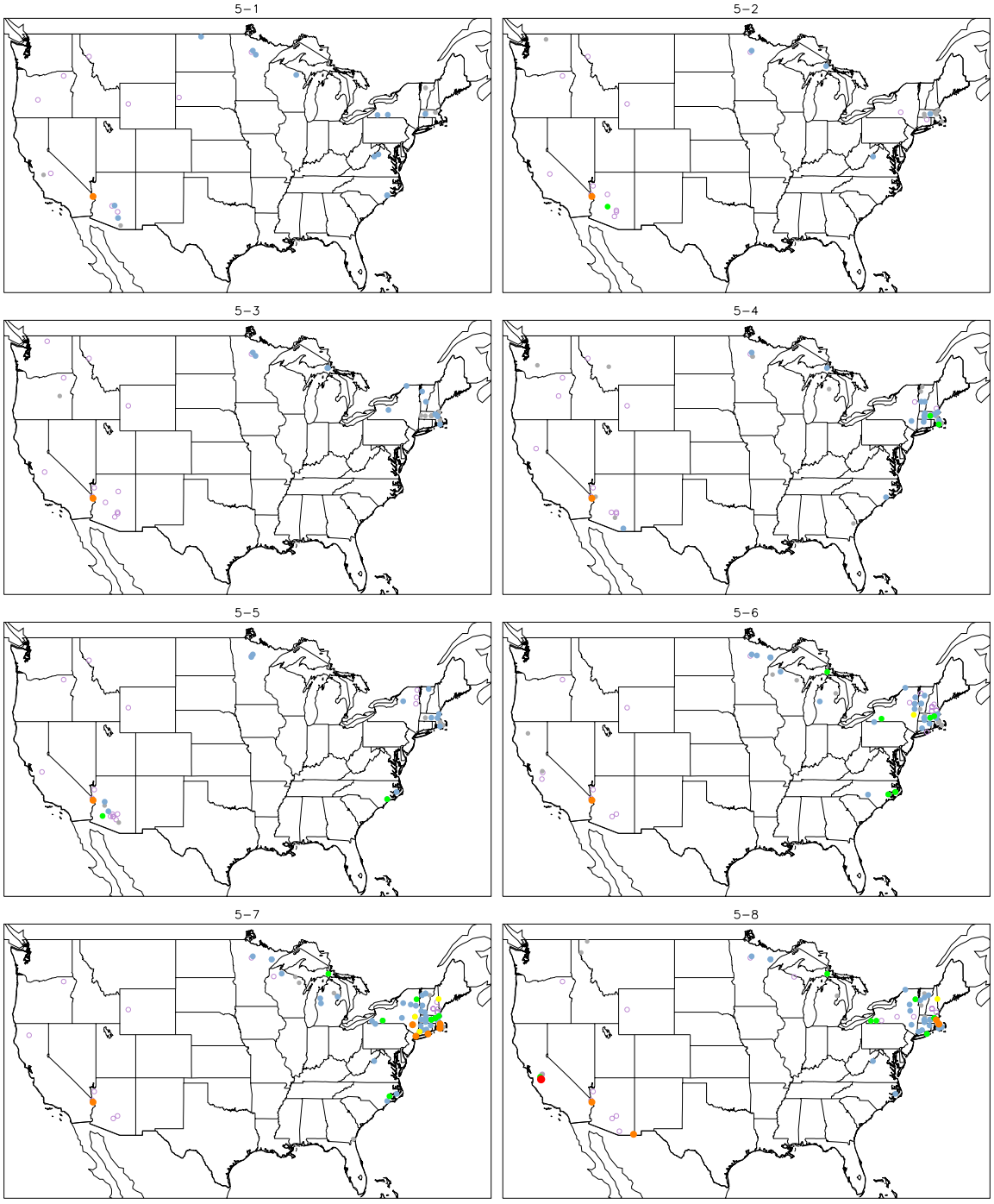

Figure C.5 Wildfire locations and acreages for 1-May through 8-May.

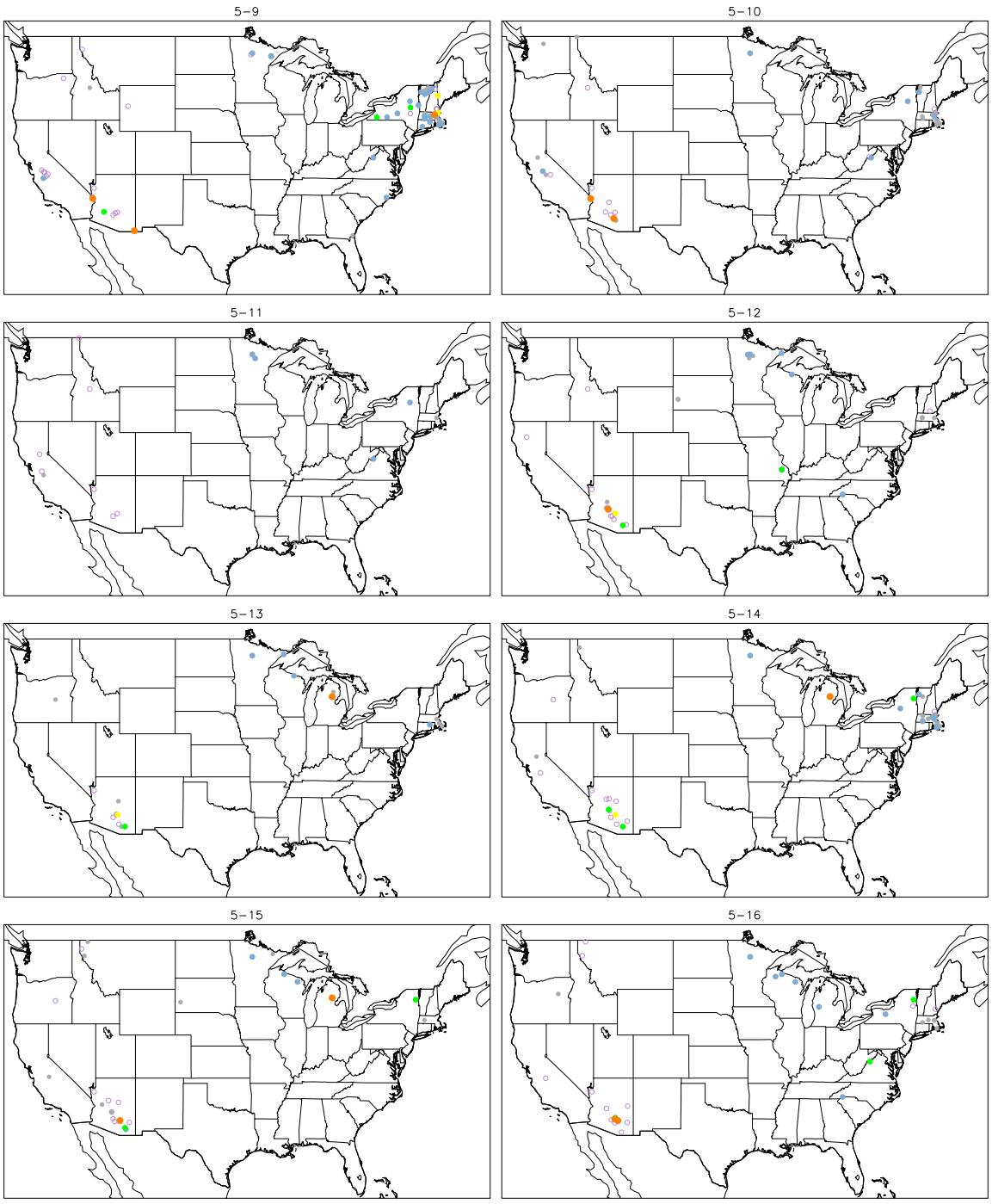

Figure C.6 Wildfire locations and acreages for 9-May through 16-May.

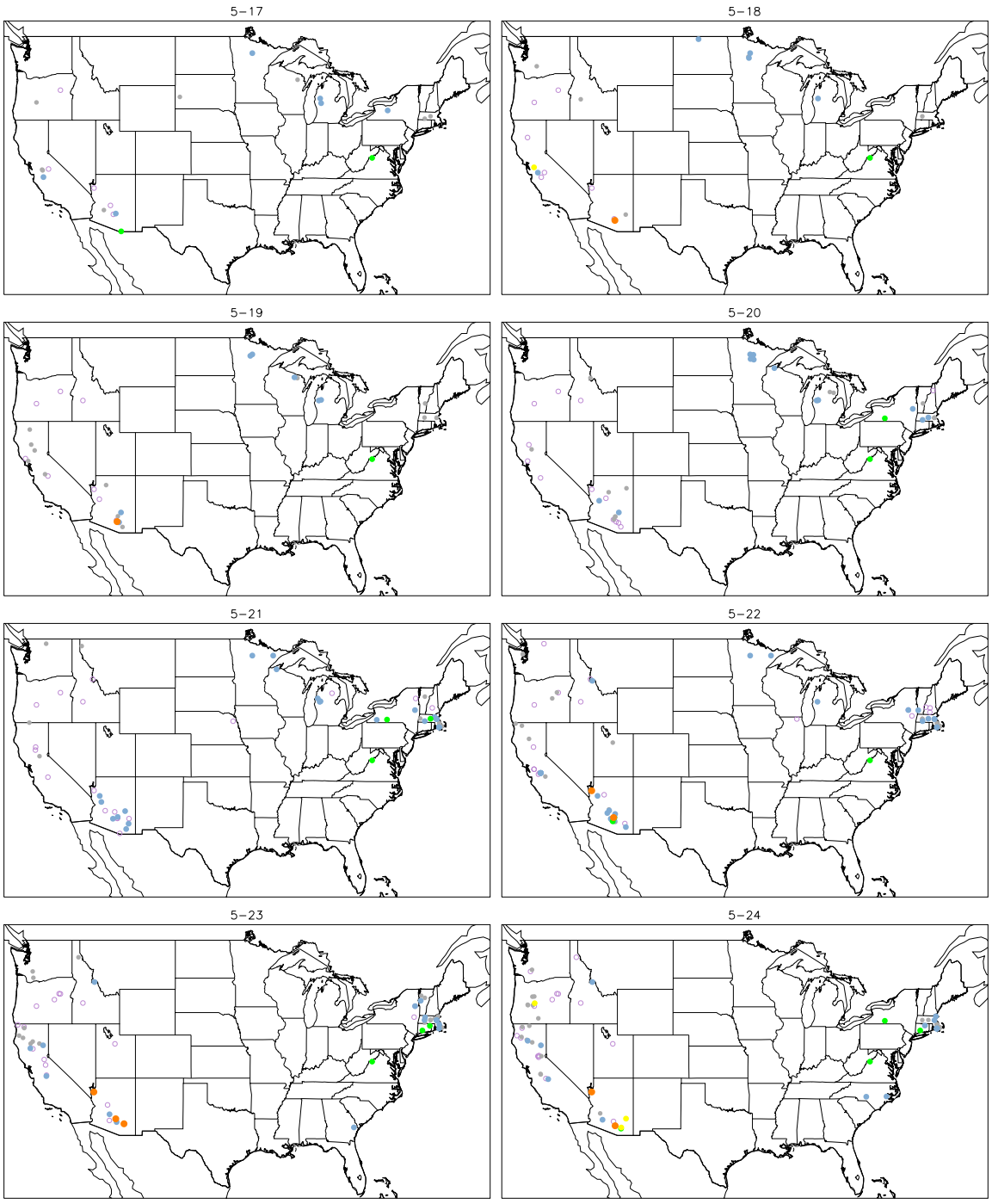

Figure C.7 Wildfire locations and acreages for 17-May through 24-May.

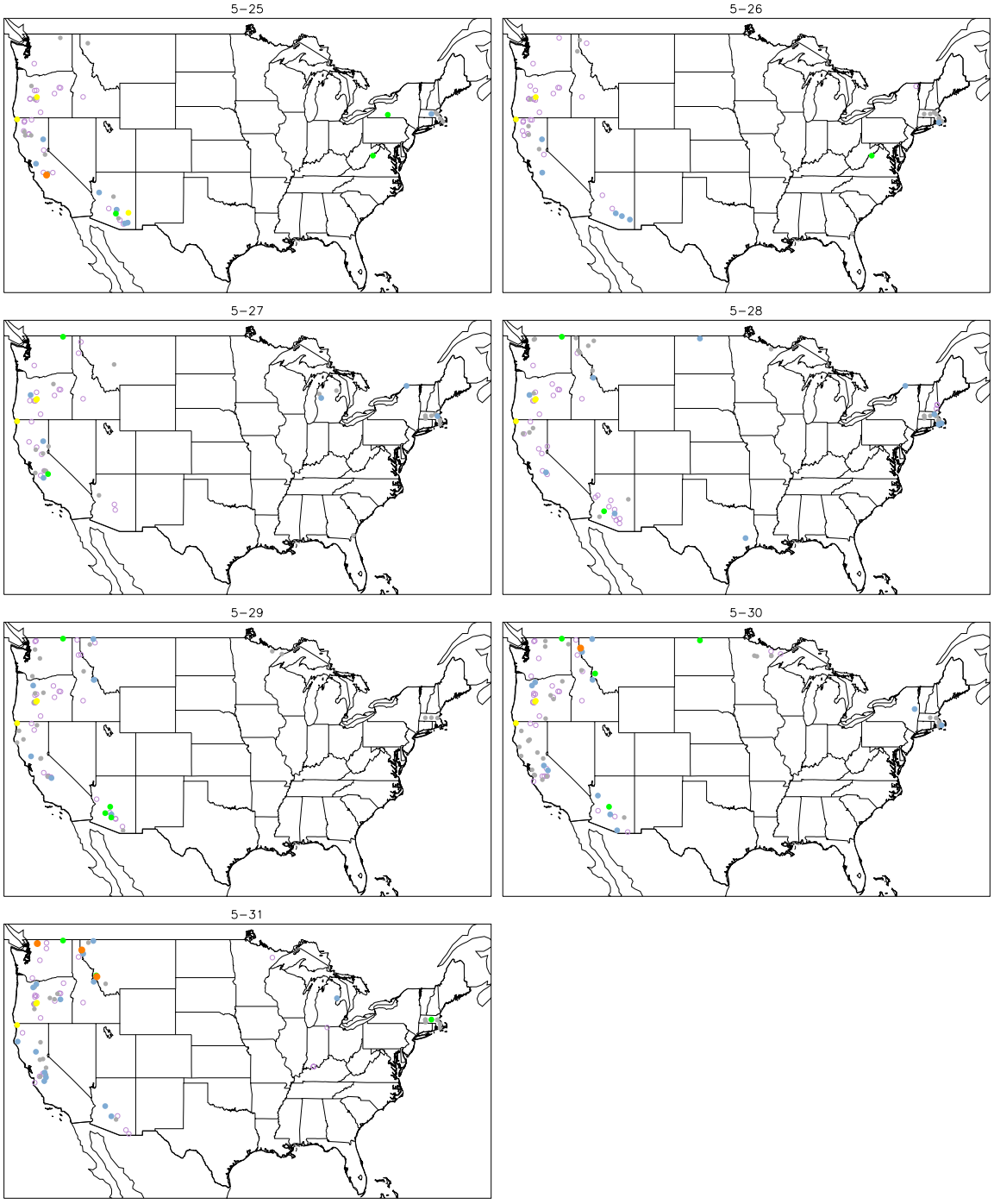

Figure C.8 Wildfire locations and acreages for 25-May through 31-May.

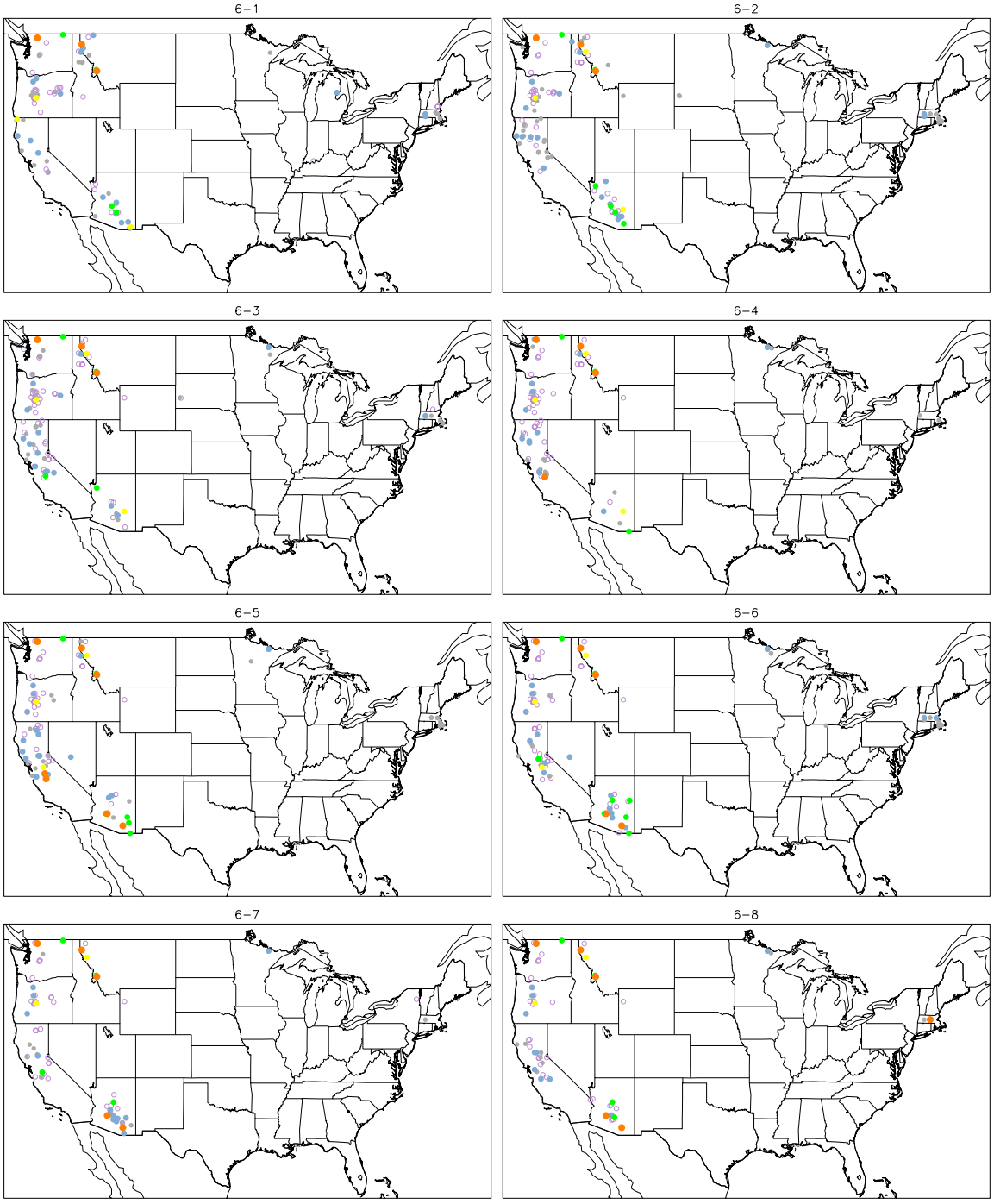

Figure C.9 Wildfire locations and acreages for 1-June through 8-June.

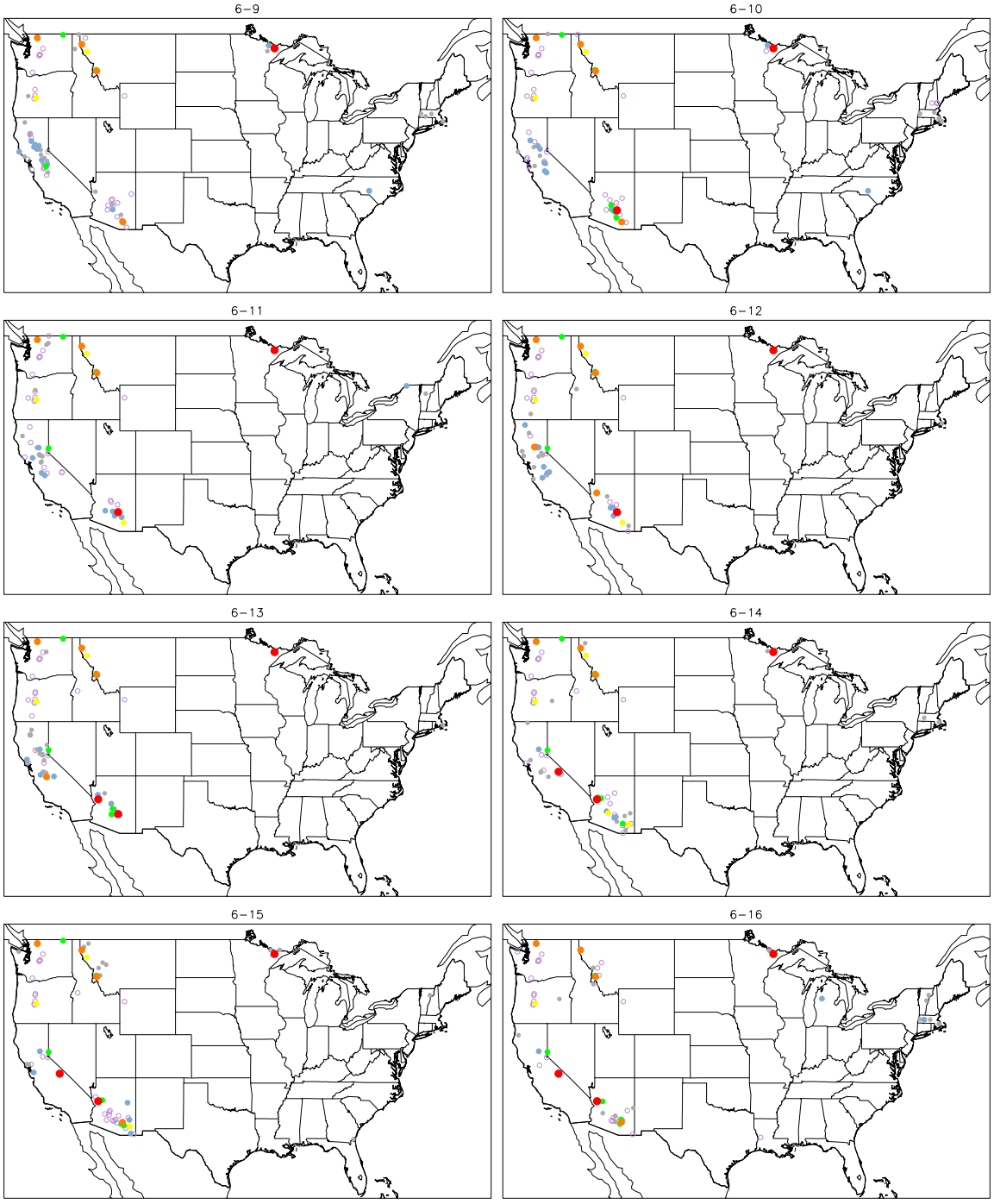

Figure C.10 Wildfire locations and acreages for 9-June through 16-June.

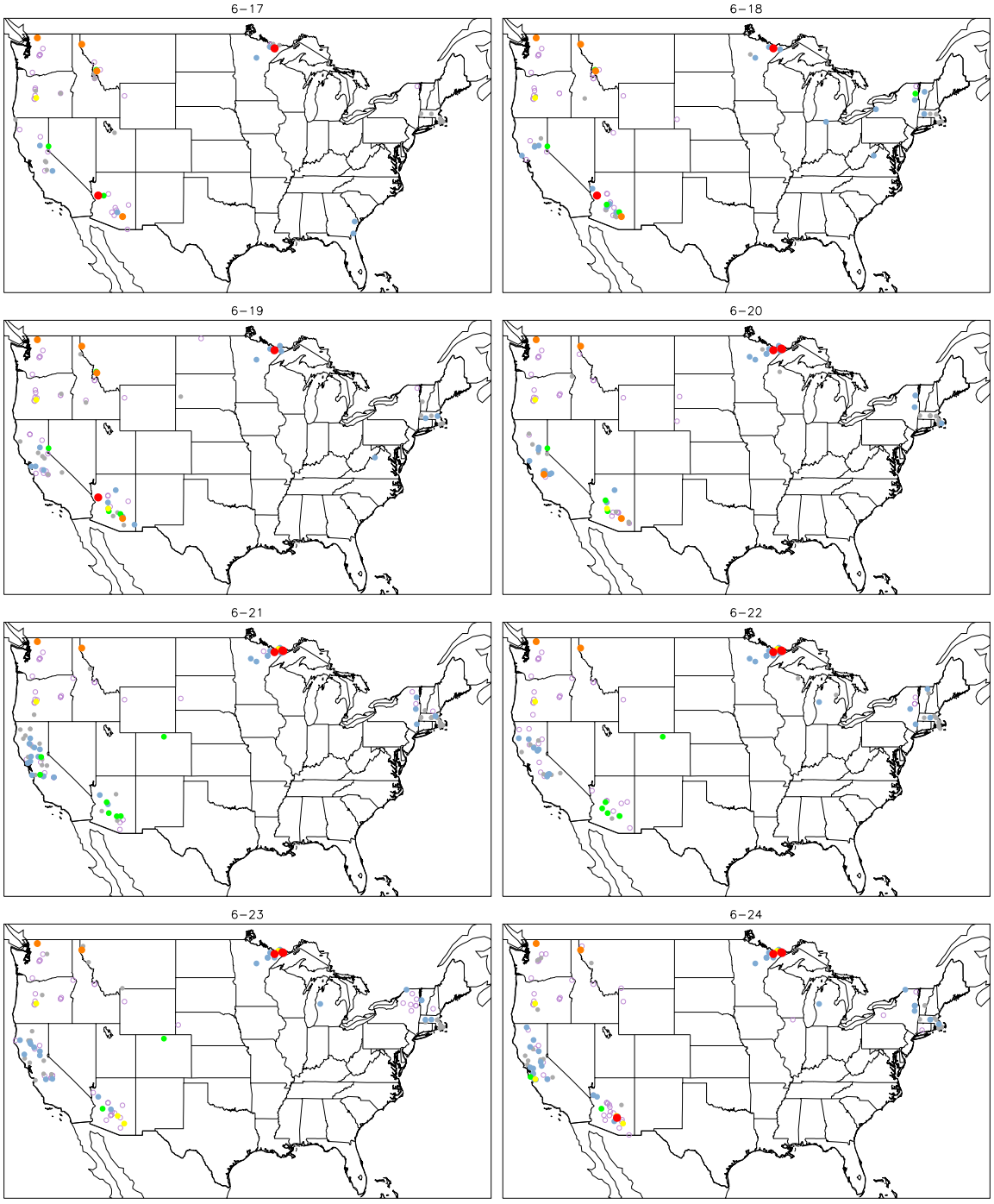

Figure C.11 Wildfire locations and acreages for 17-June through 24-June.

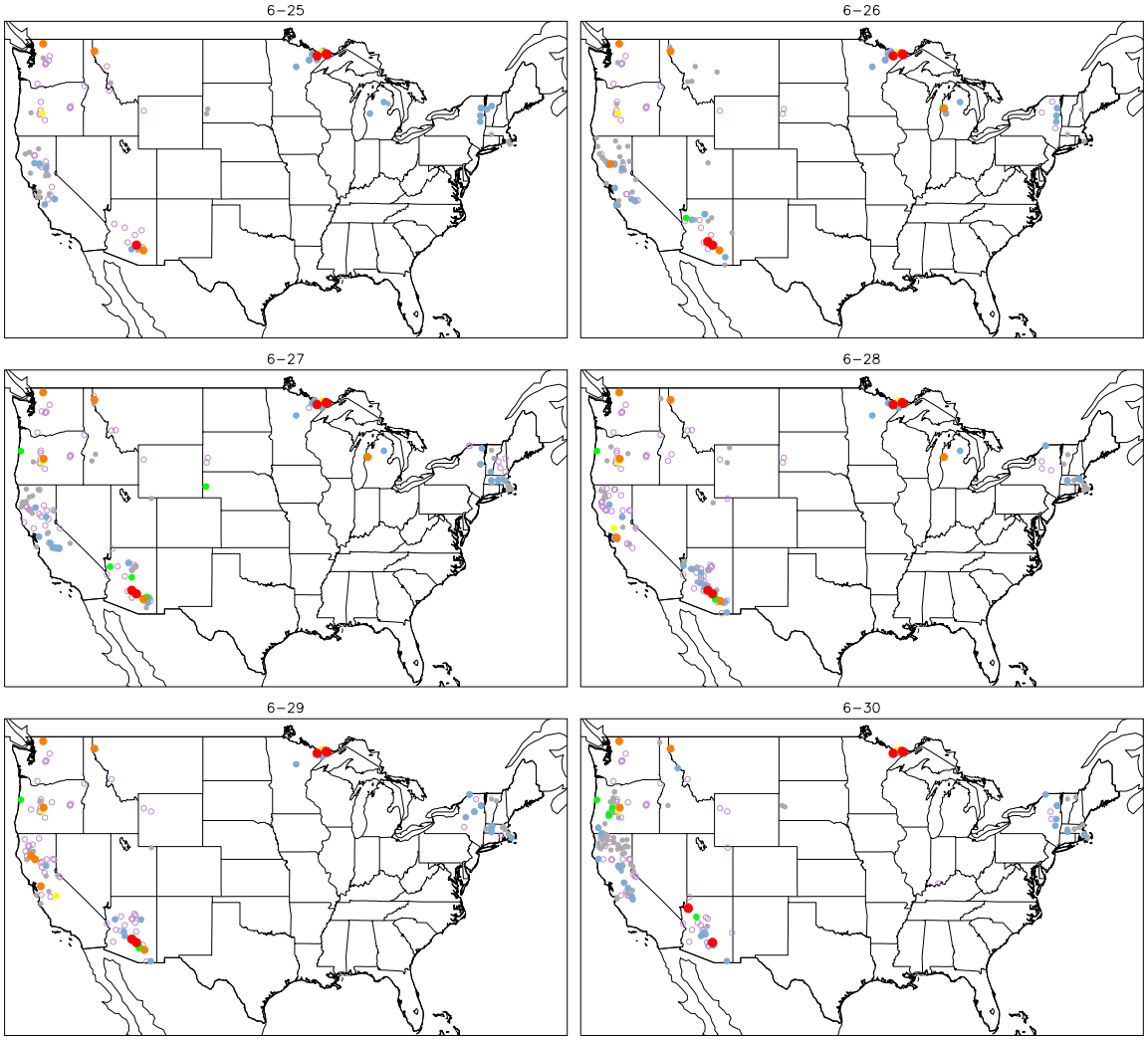

Figure C.12 Wildfire locations and acreages for 25-June through 30-June.

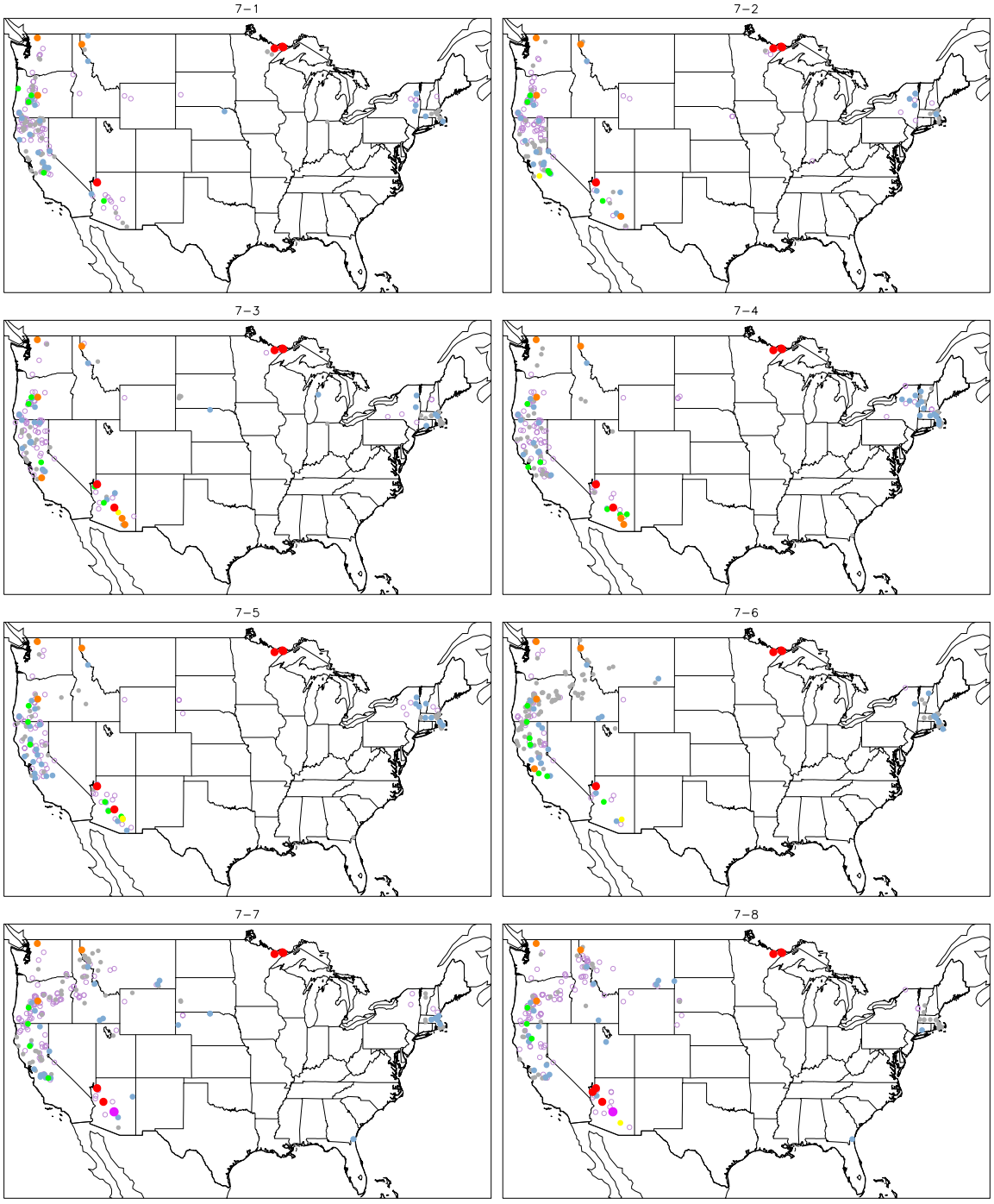

Figure C.13 Wildfire locations and acreages for 1-July through 8-July.

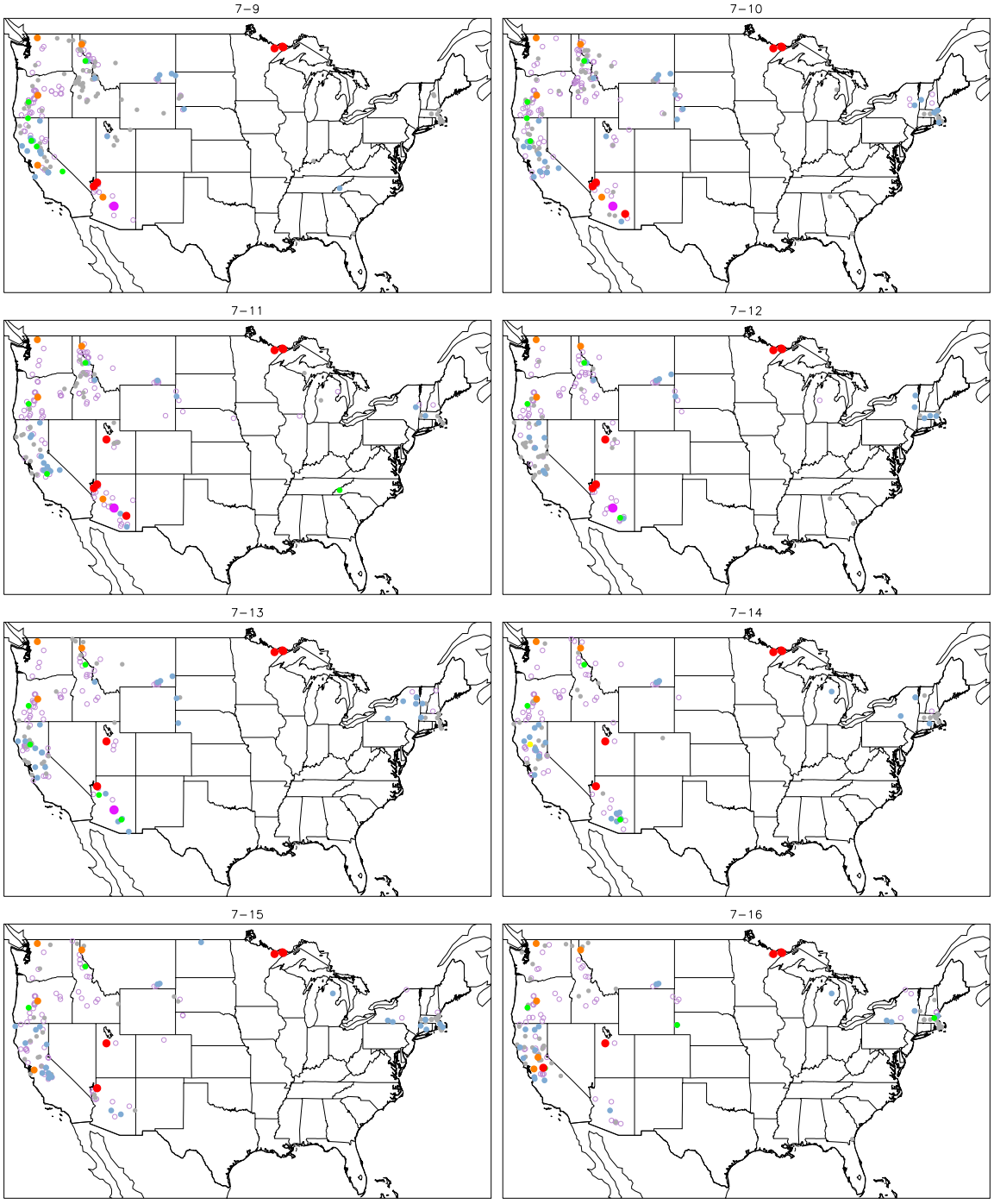

Figure C.14 Wildfire locations and acreages for 9-July through 16-July.

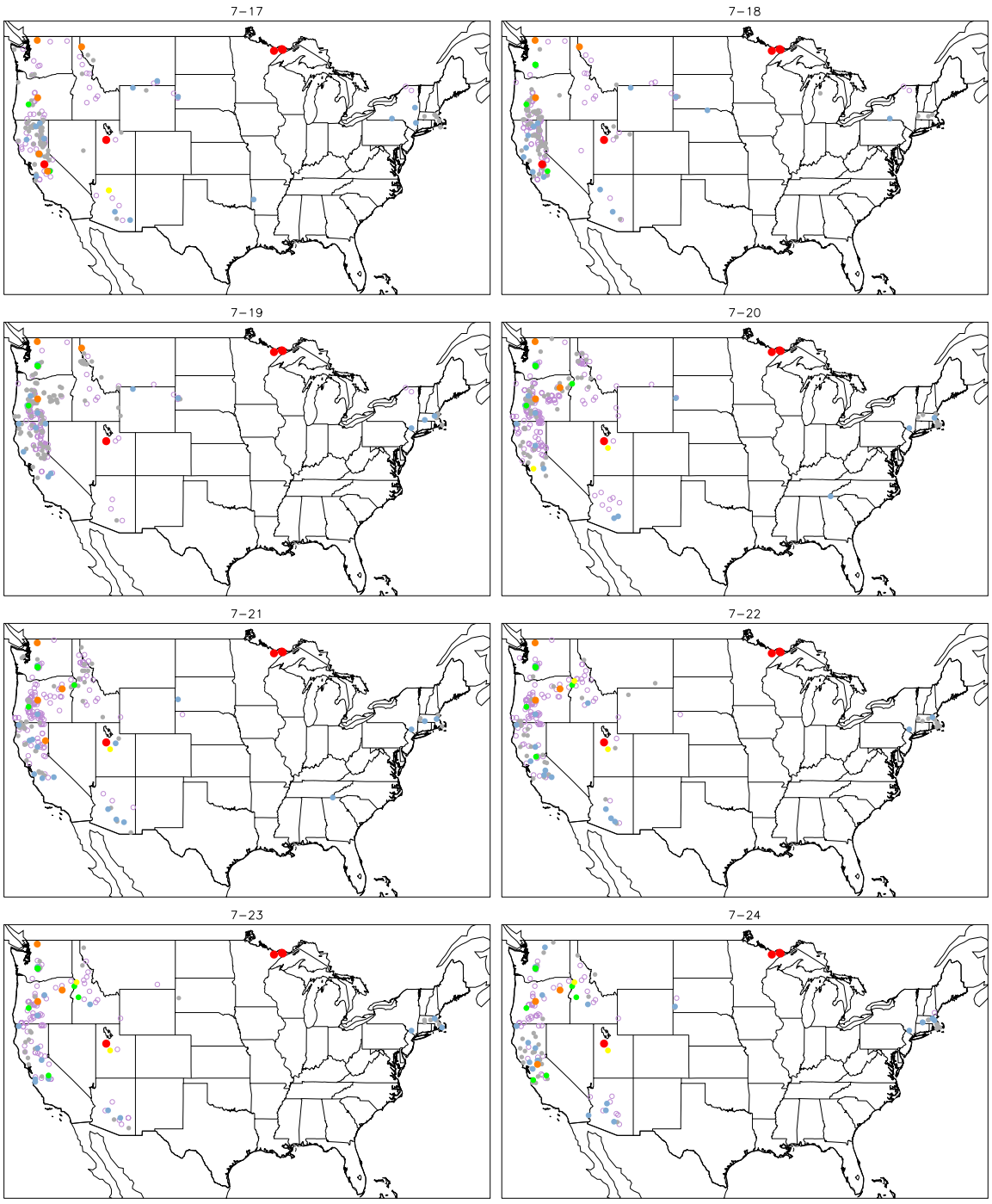

Figure C.15 Wildfire locations and acreages for 17-July through 24-July.

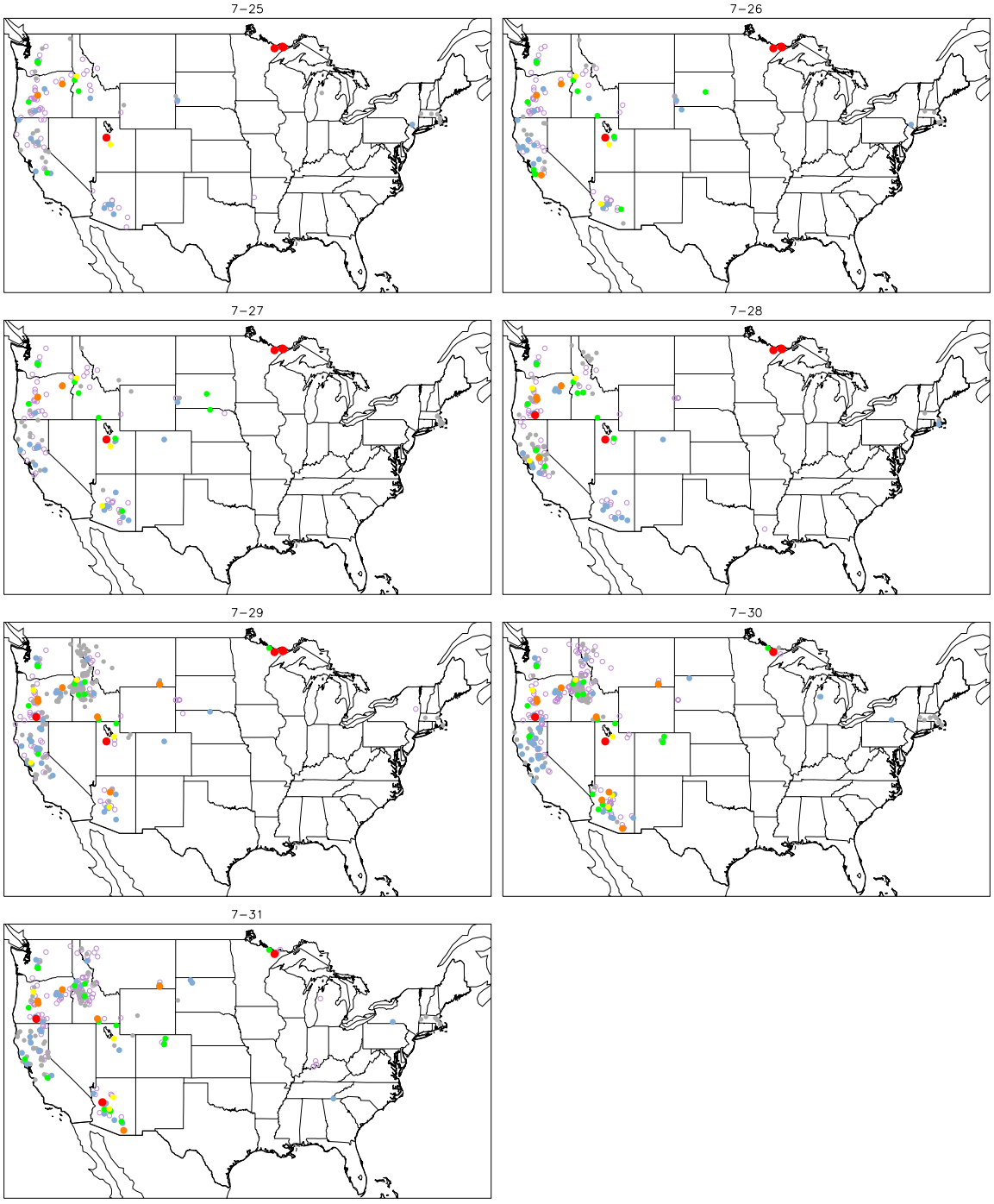

Figure C.16 Wildfire locations and acreages for 25-July through 31-July.

APPENDIX D. 1998 Hot Spot Maps

The following are the 1998 hot spot maps used in this study.

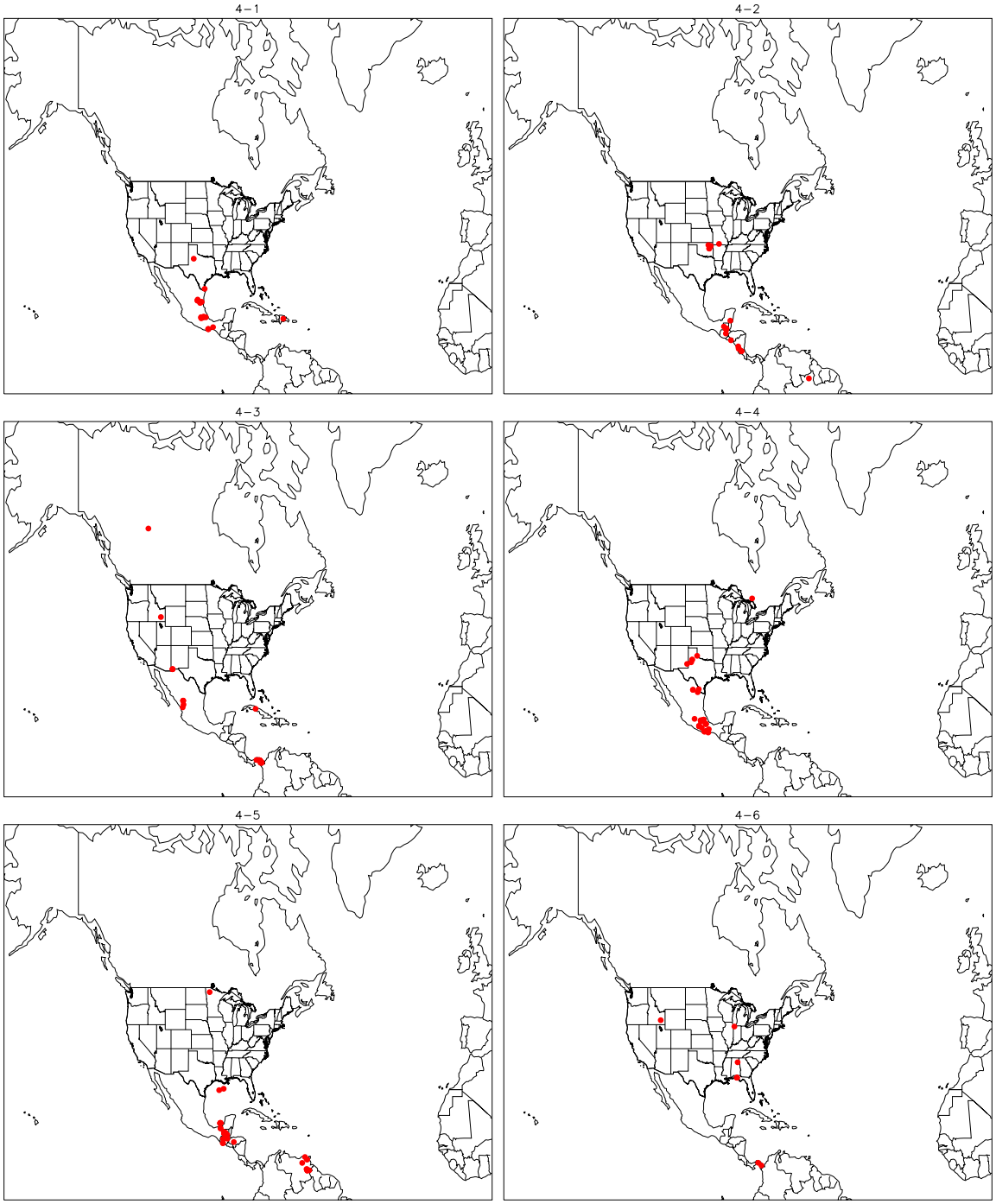

Figure D.1 Hot spots detected on 1-April through 6-April.

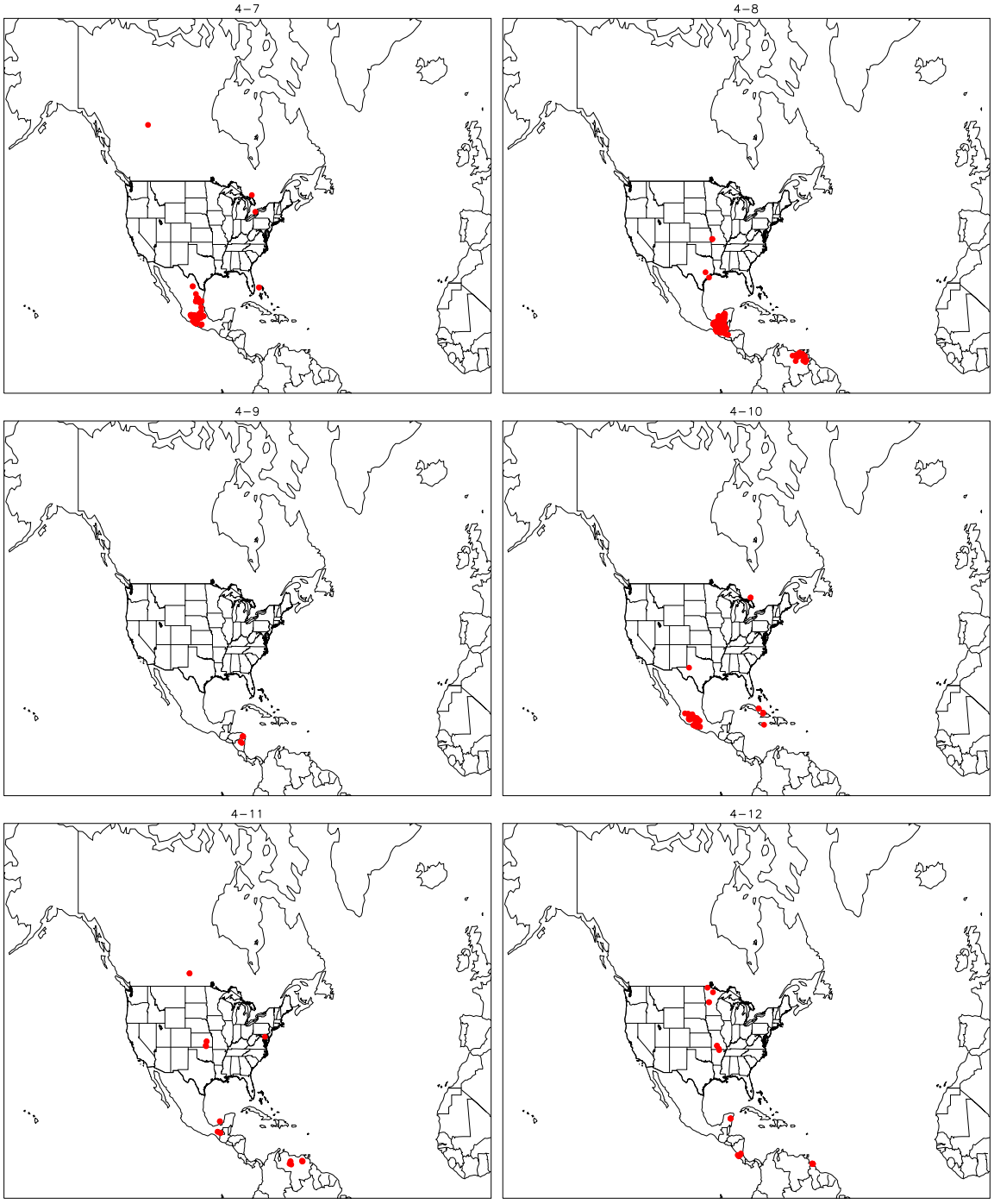

Figure D.2 Hot spots detected on 7-April through 12-April.

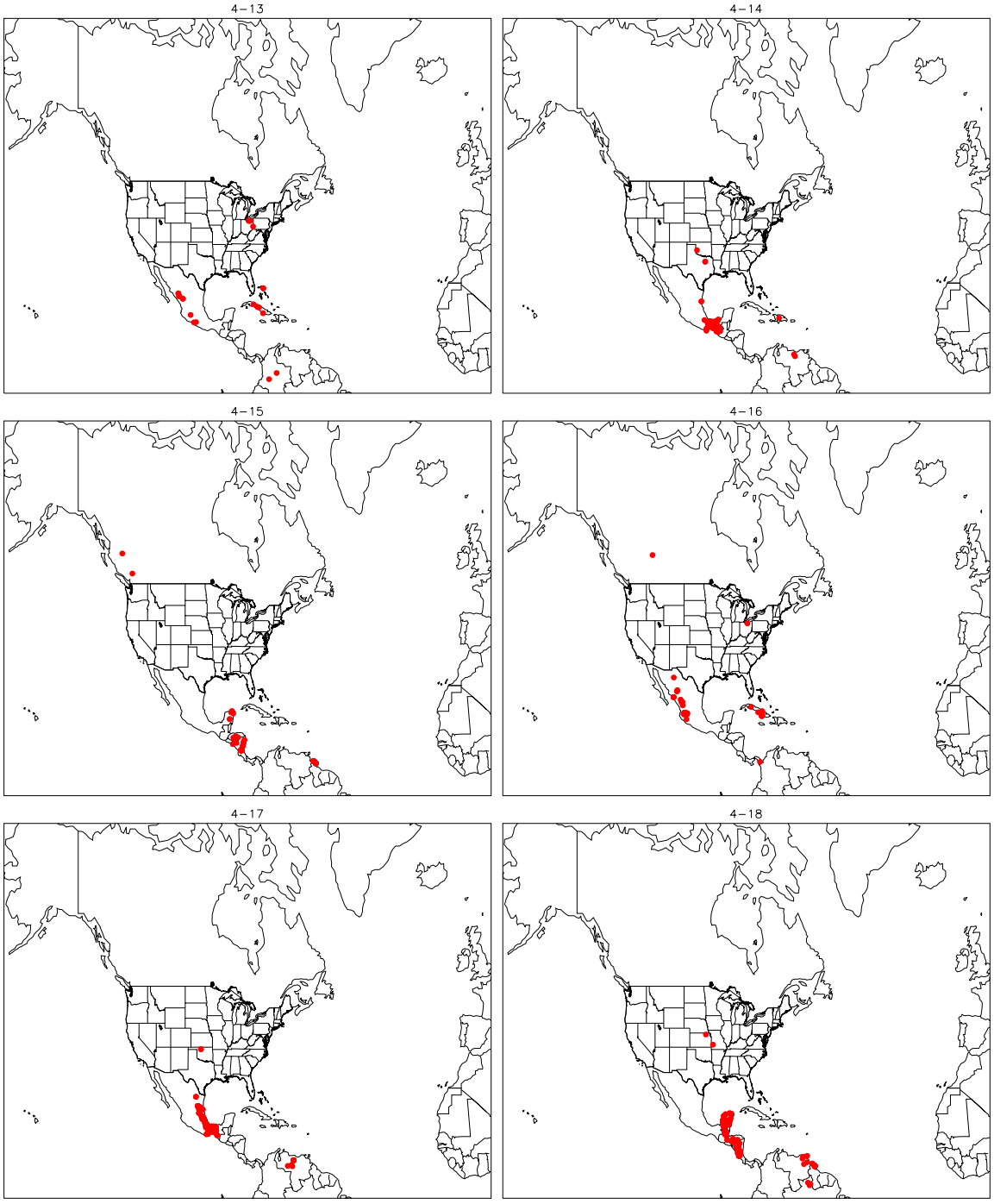

Figure D.3 Hot spots detected on 13-April through 18-April.

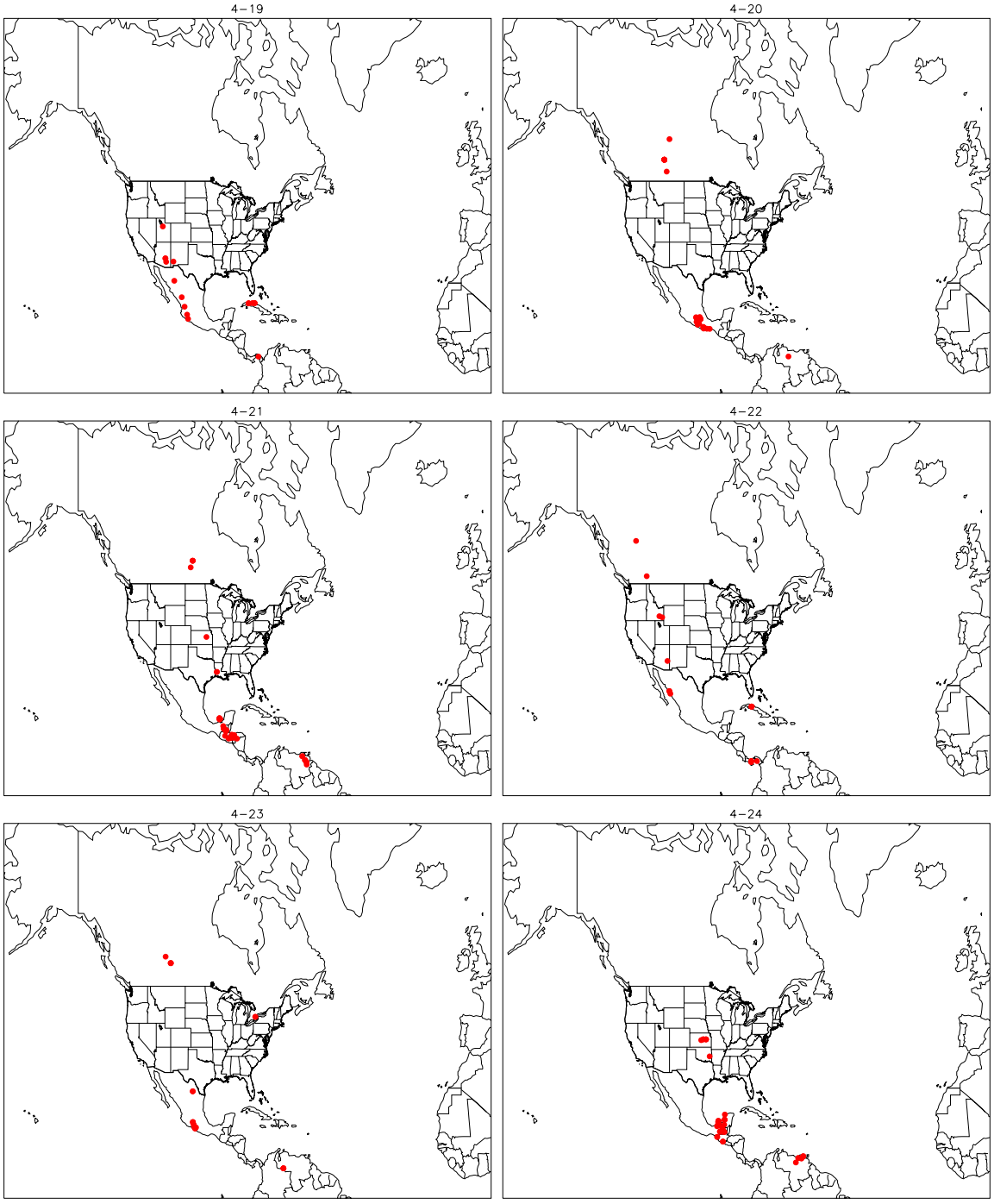

Figure D.4 Hot spots detected on 19-April through 24-April.

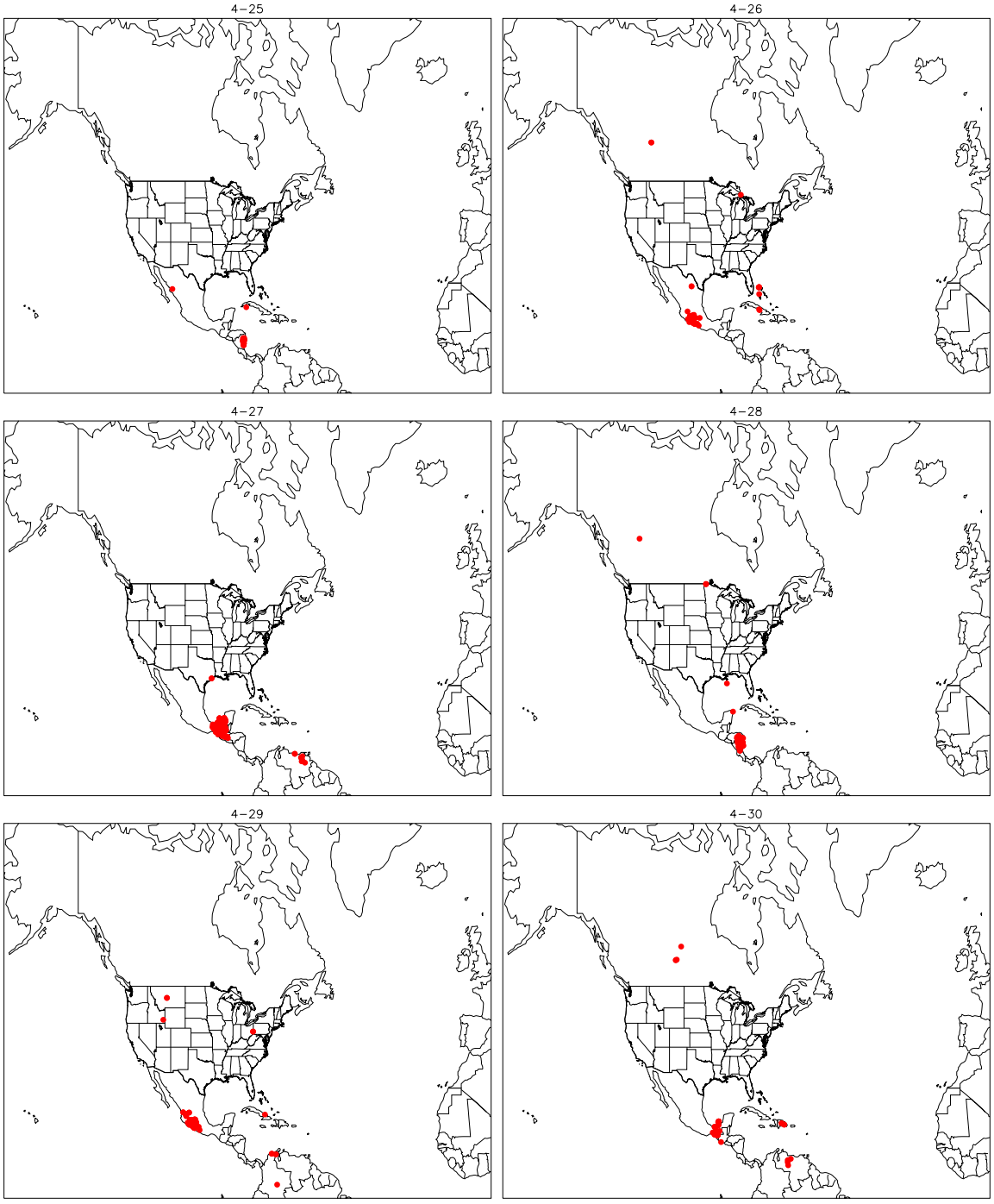

Figure D.5 Hot spots detected on 25-April through 30-April.

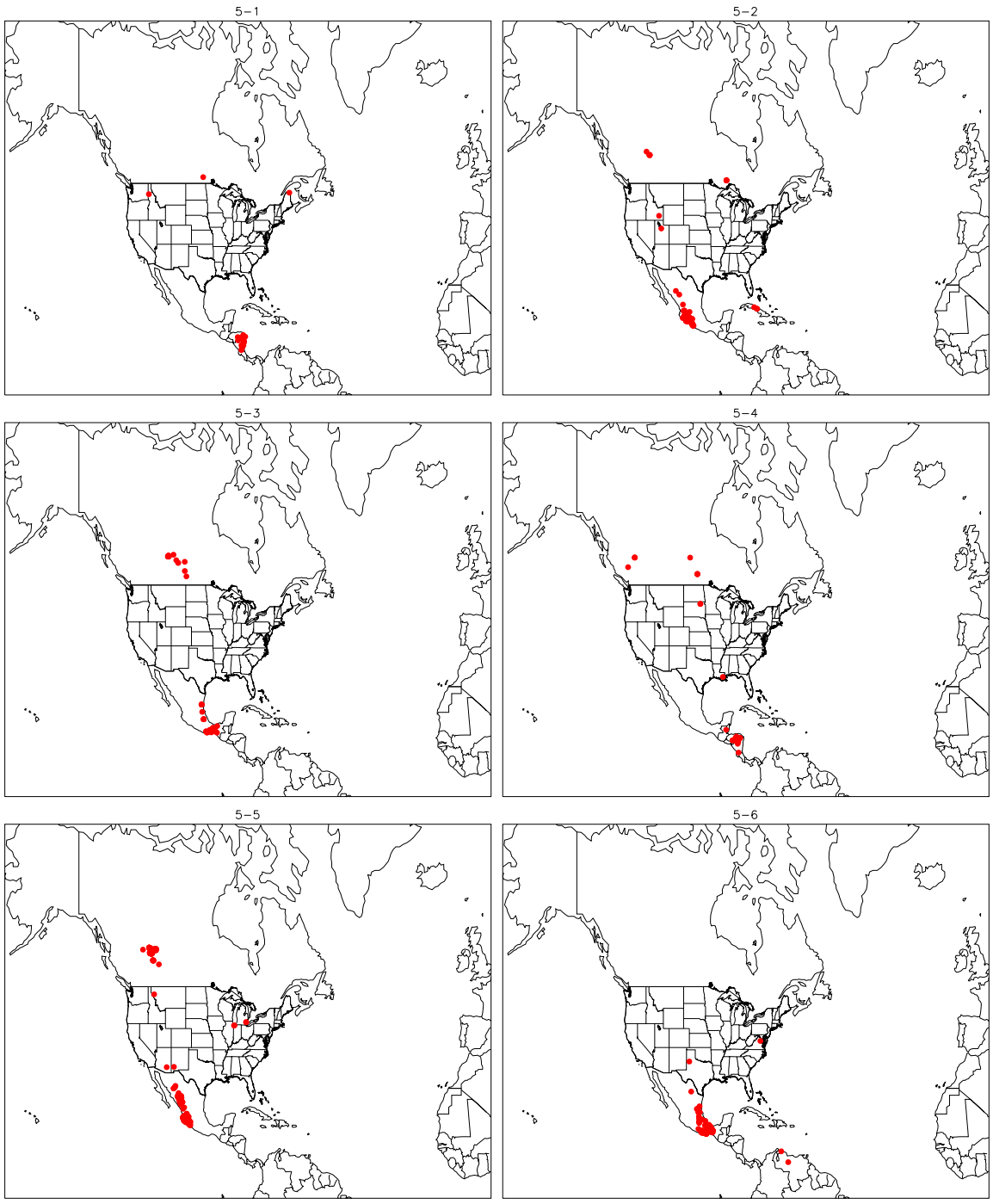

Figure D.6 Hot spots detected on 1-May through 6-May.

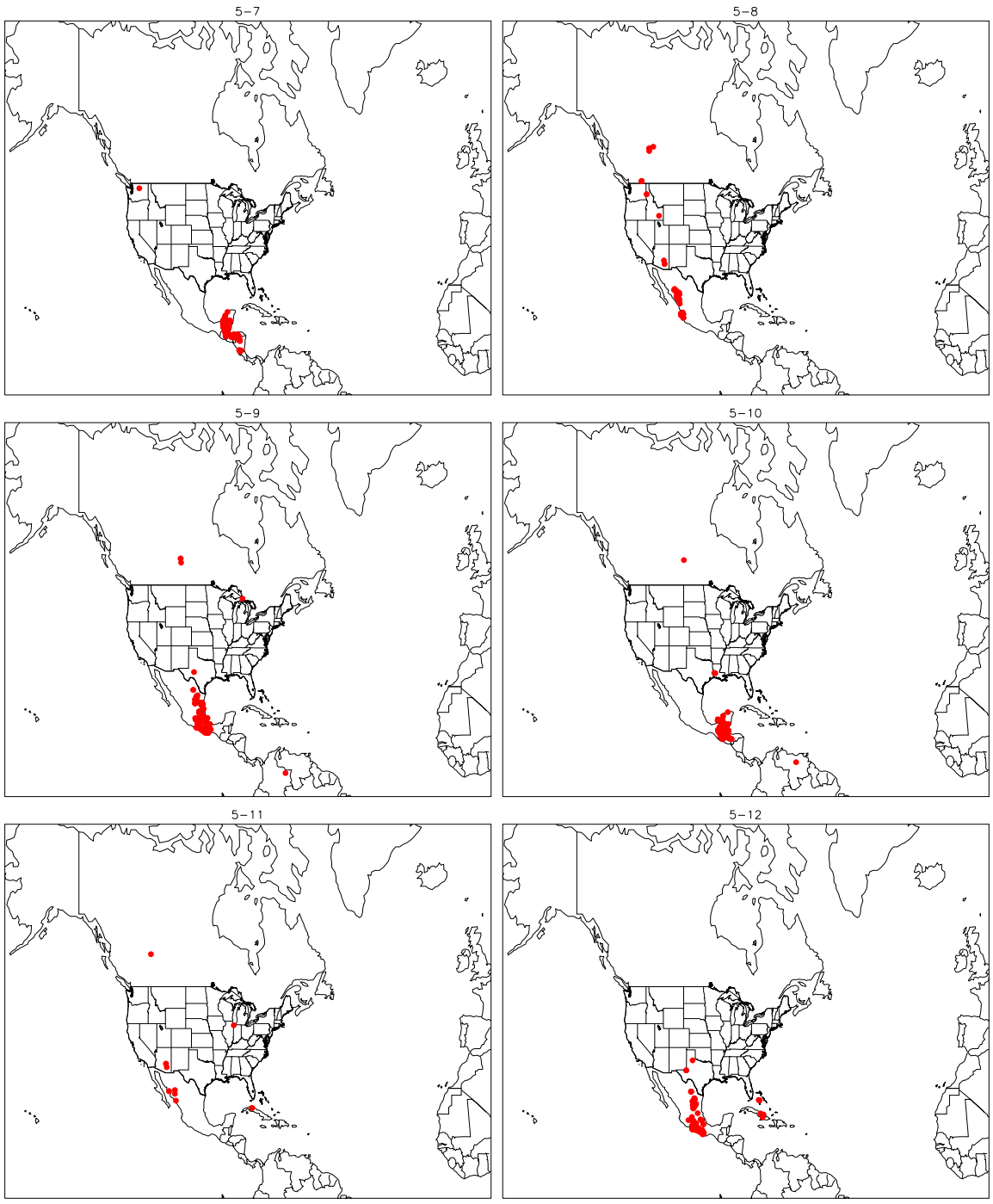

Figure D.7 Hot spots detected on 7-May through 12-May.

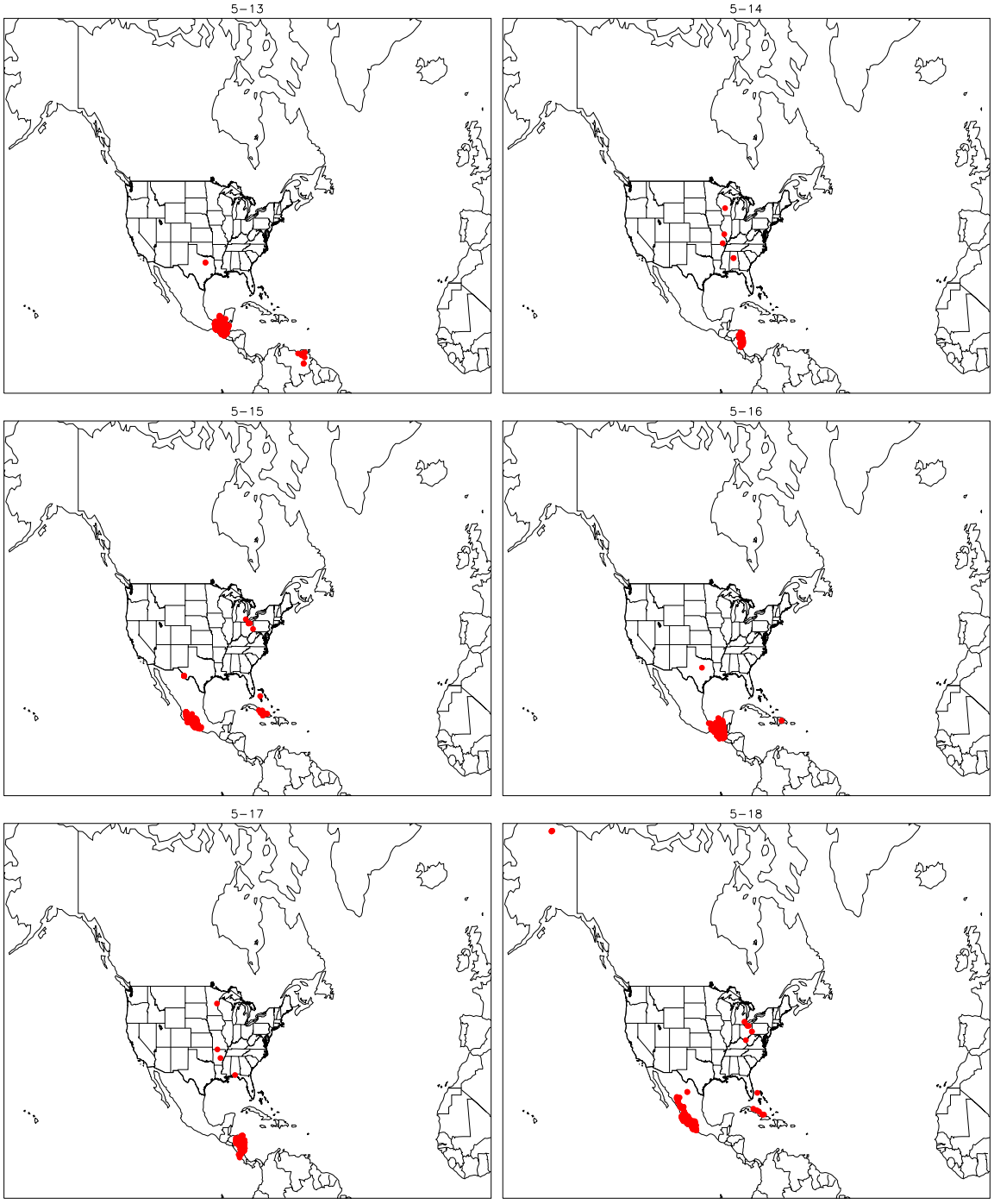

Figure D.8 Hot spots detected on 13-May through 18-May.

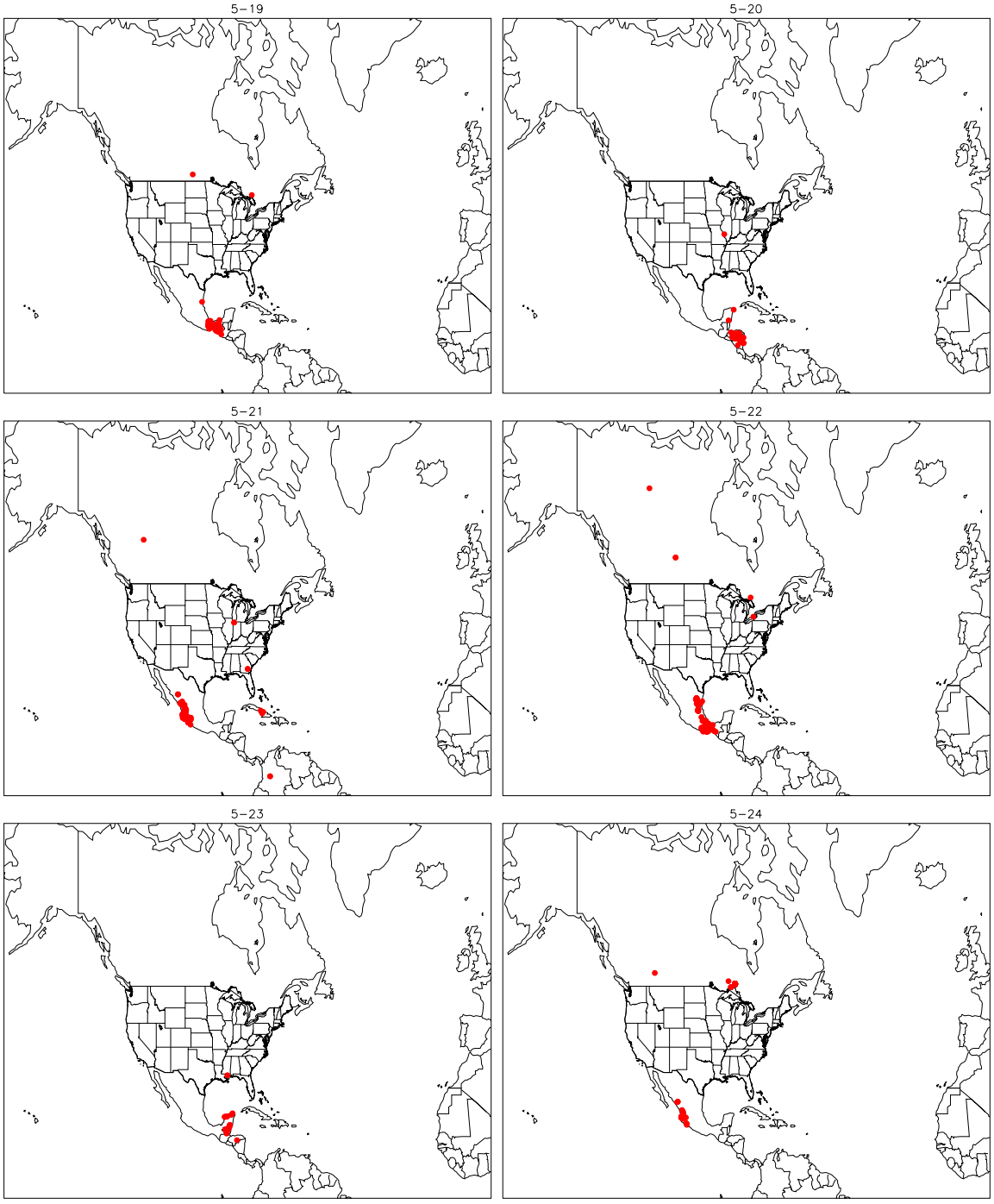

Figure D.9 Hot spots detected on 19-May through 24-May.

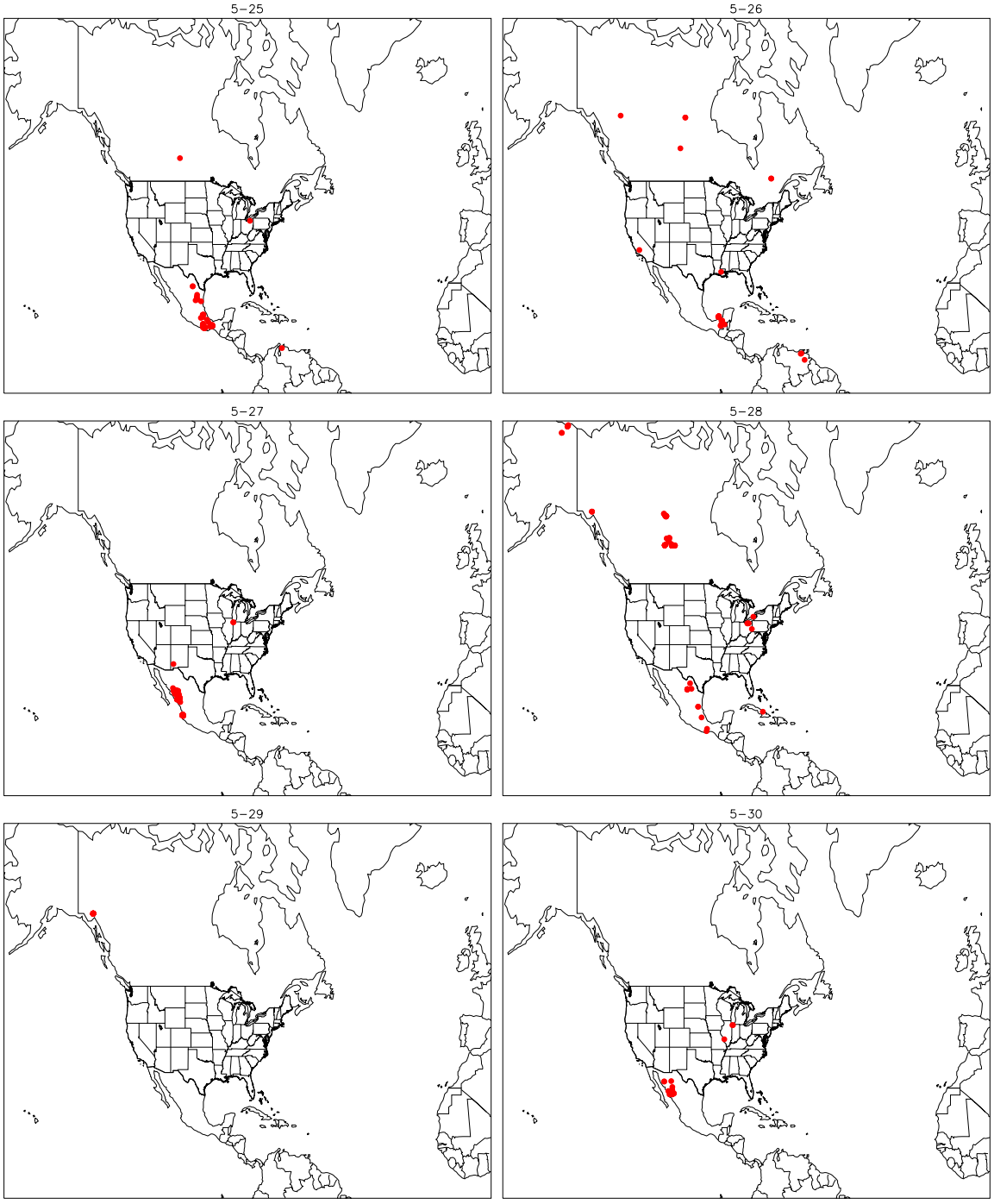

Figure D.10 Hot spots detected on 25-May through 30-May.

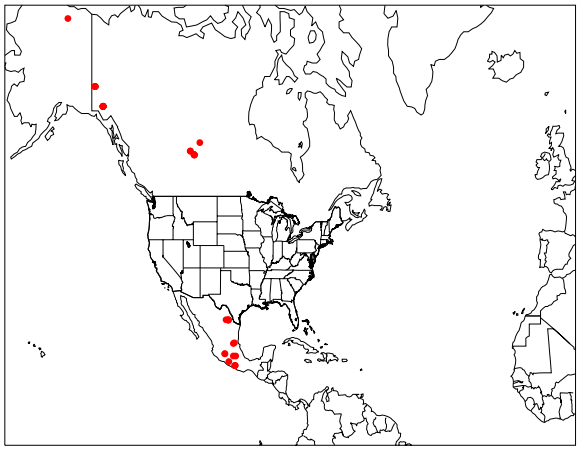

Figure D.11 Hot spots detected on 31-May.

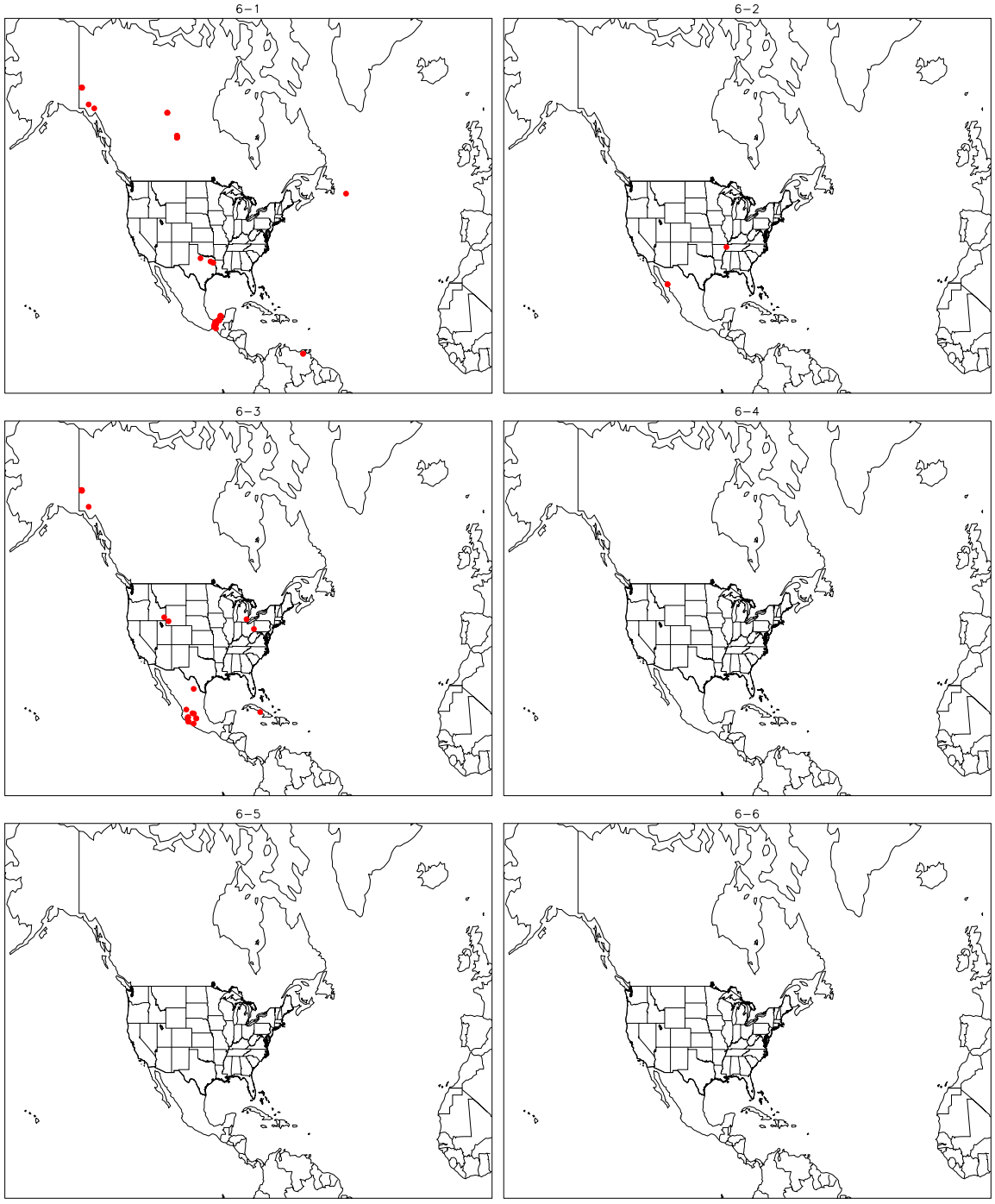

Figure D.12 Hot spots detected on 1-June through 6-June.

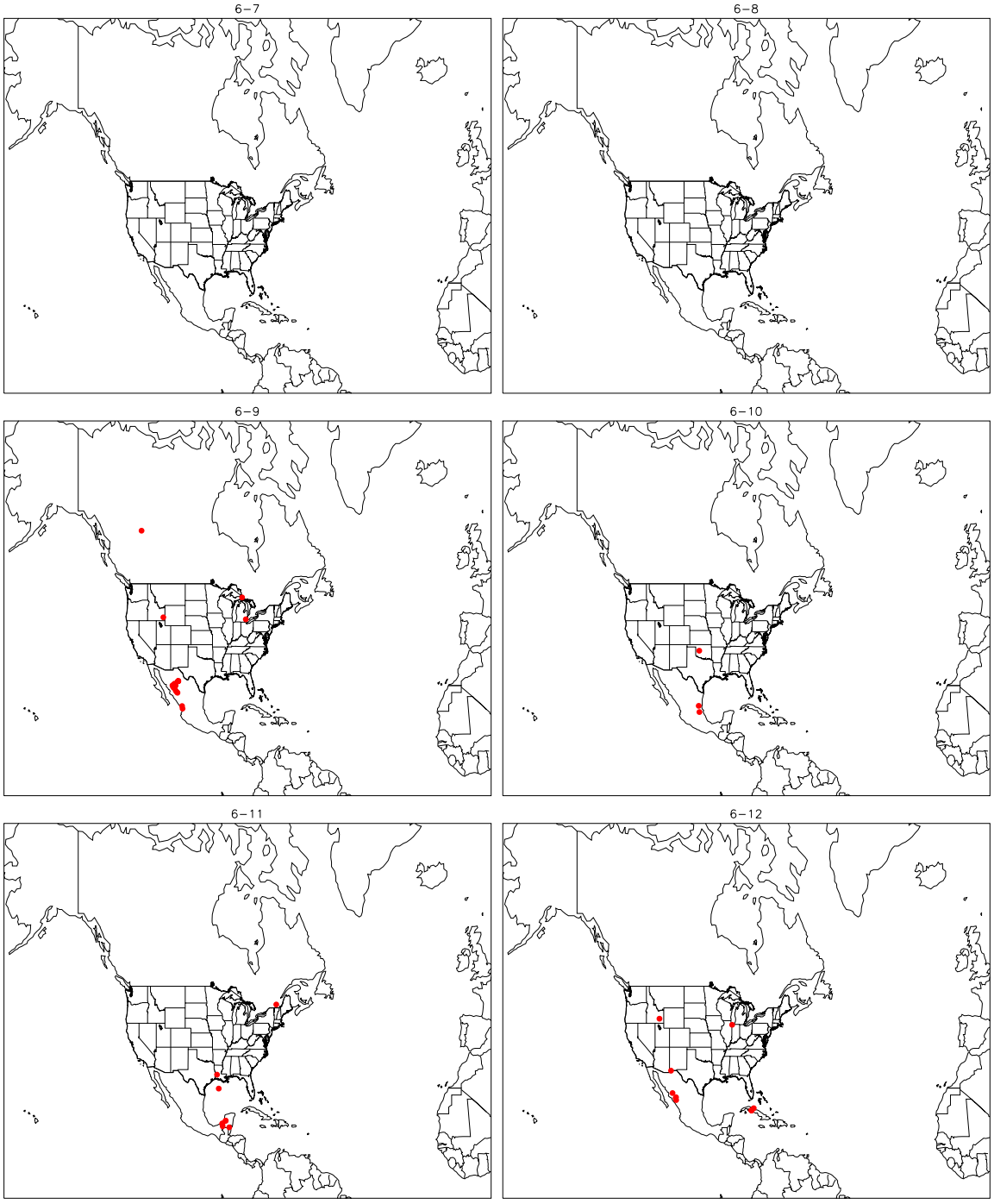

Figure D.13 Hot spots detected on 7-June through 12-June.

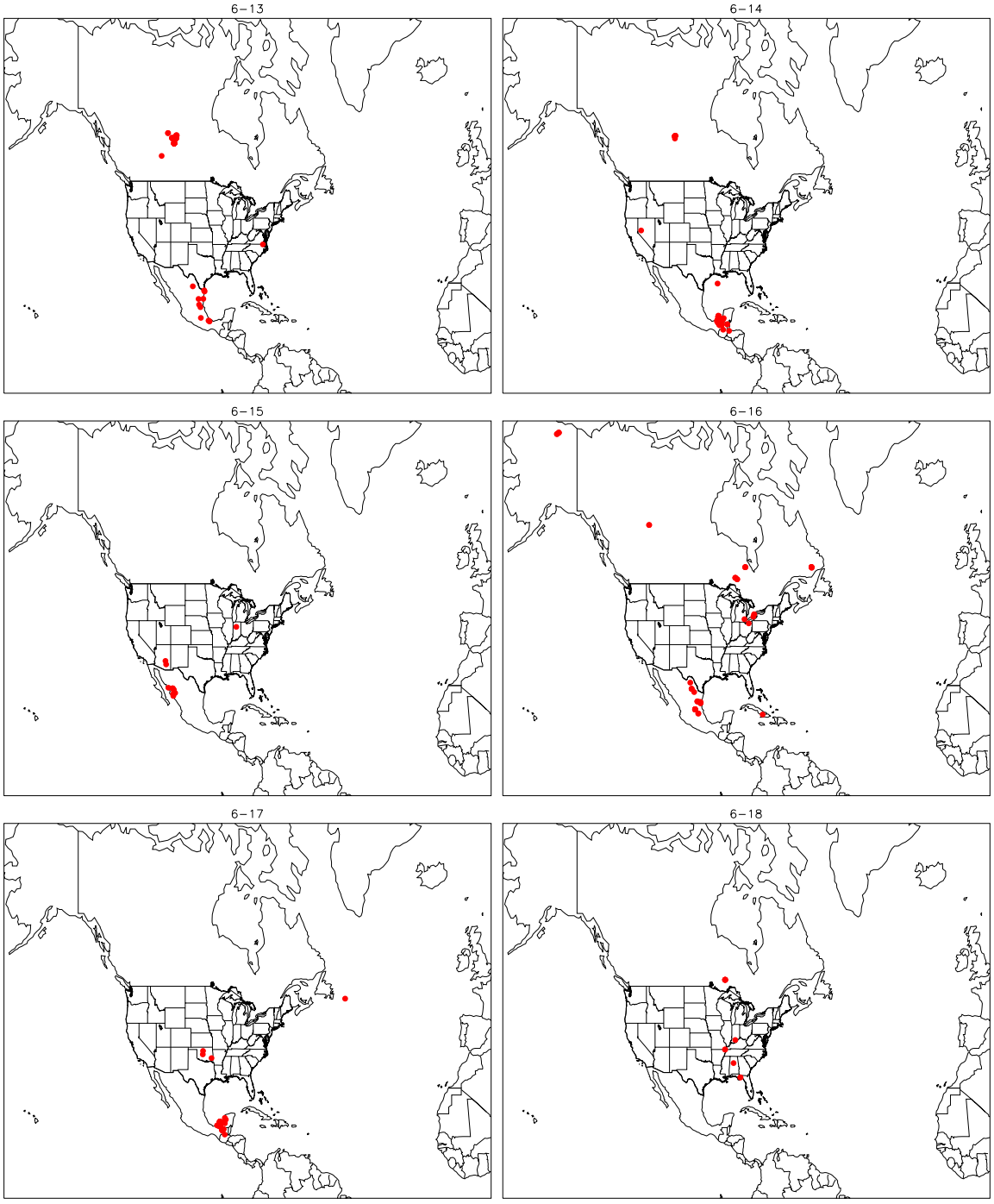

Figure D.14 Hot spots detected on 13-June through 18-June.

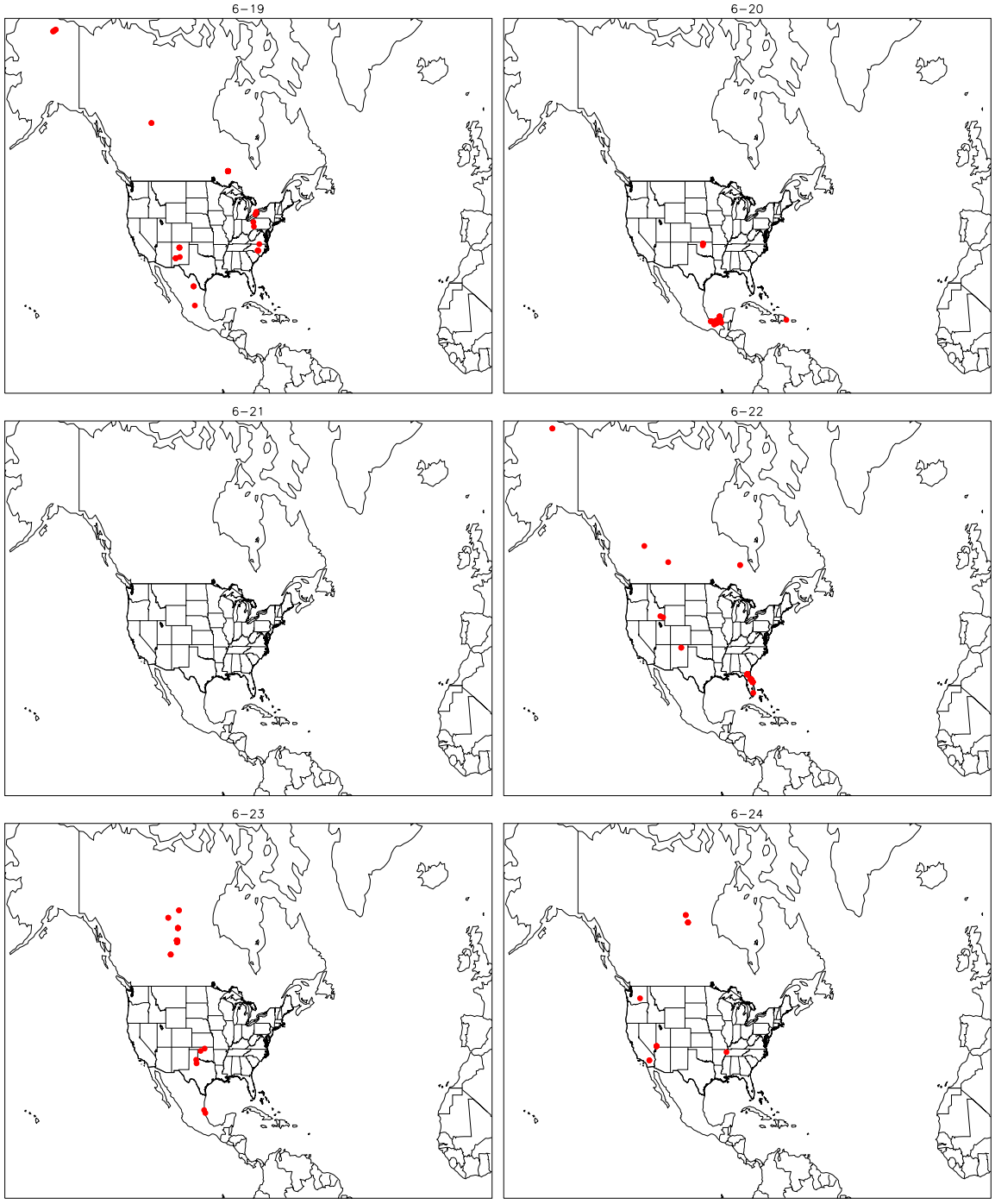

Figure D.15 Hot spots detected on 19-June through 24-June.

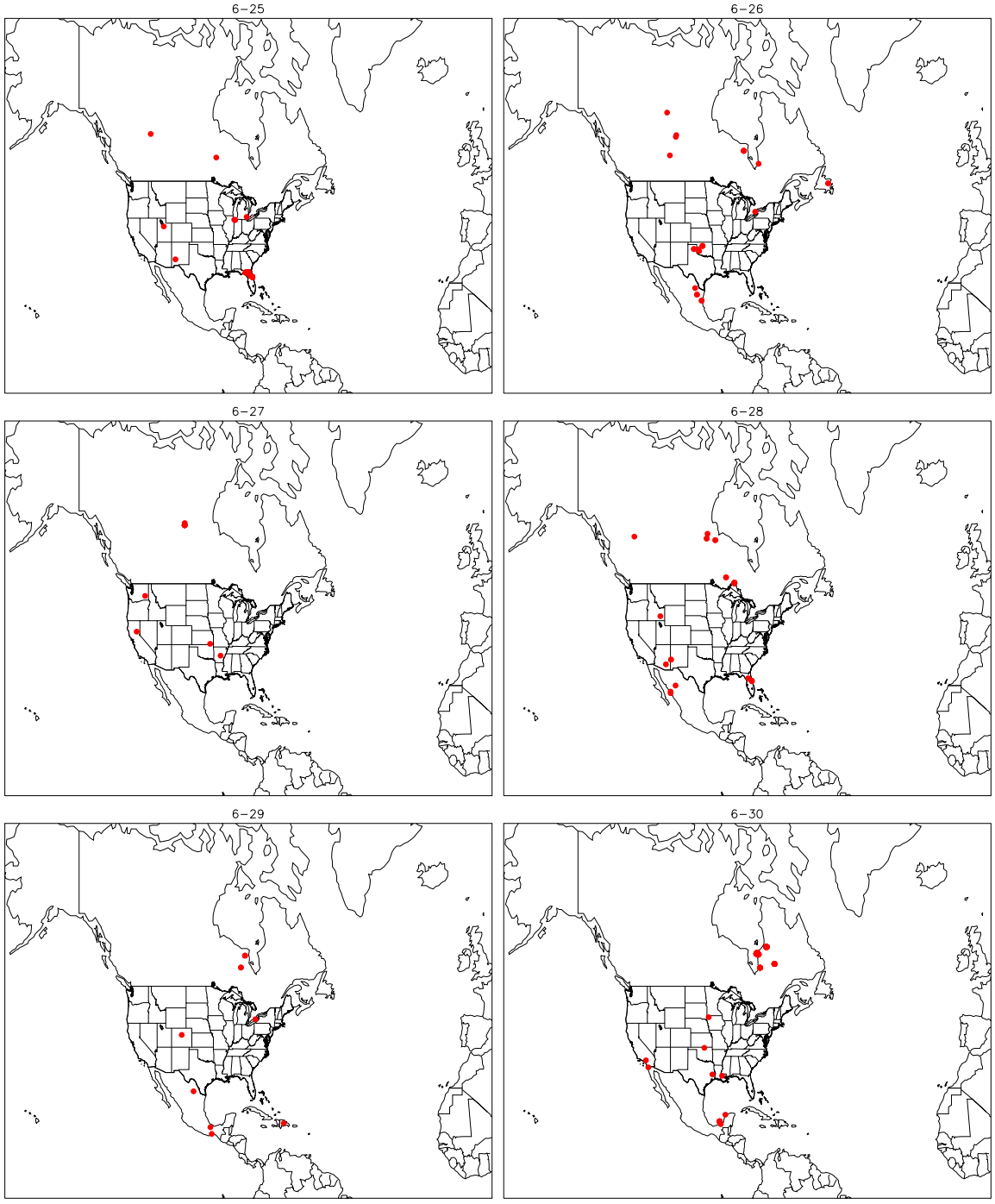

Figure D.16 Hot spots detected on 25-June through 30-June.

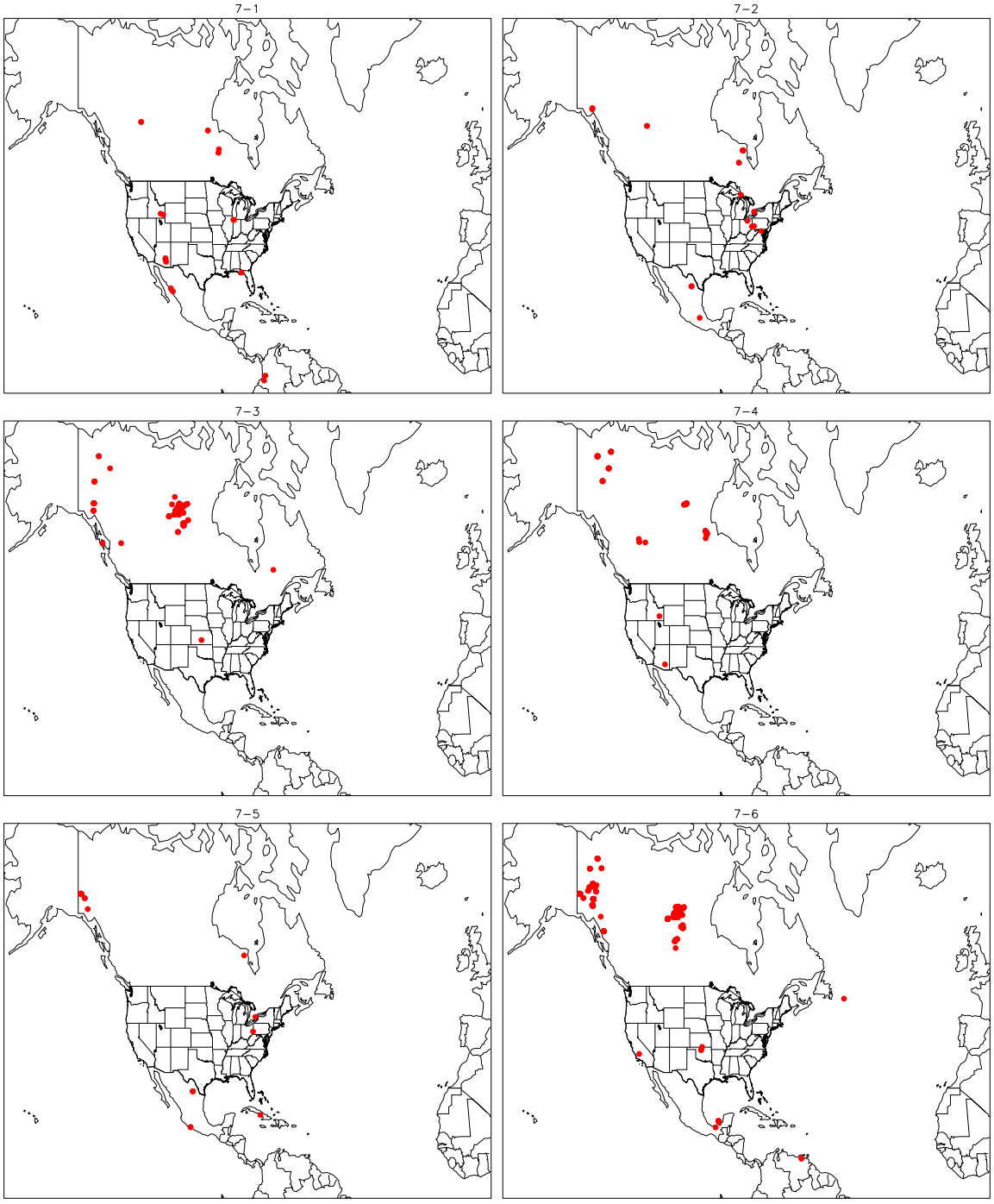

Figure D.17 Hot spots detected on 1-July through 6-July.

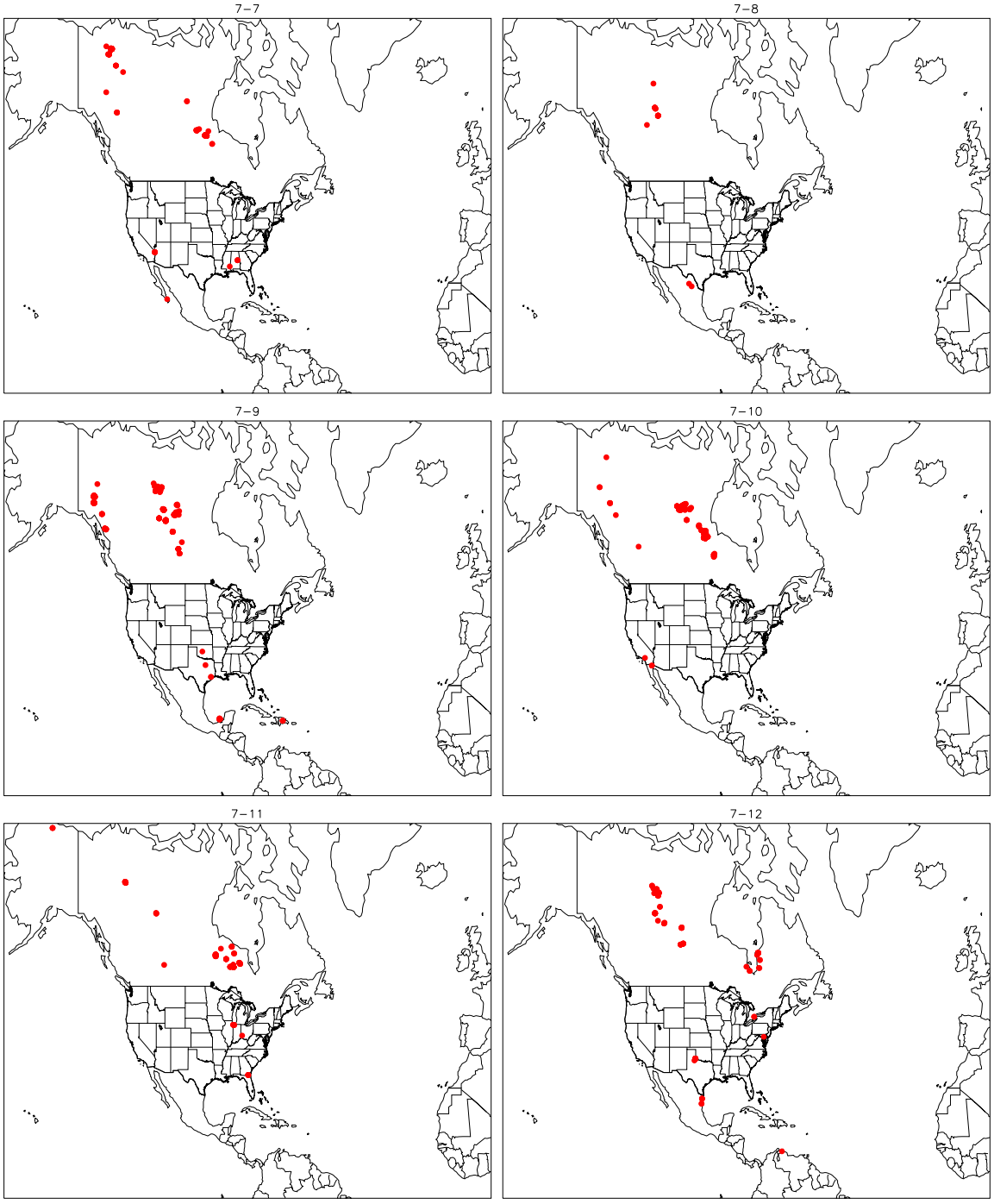

Figure D.18 Hot spots detected on 7-July through 12-July.

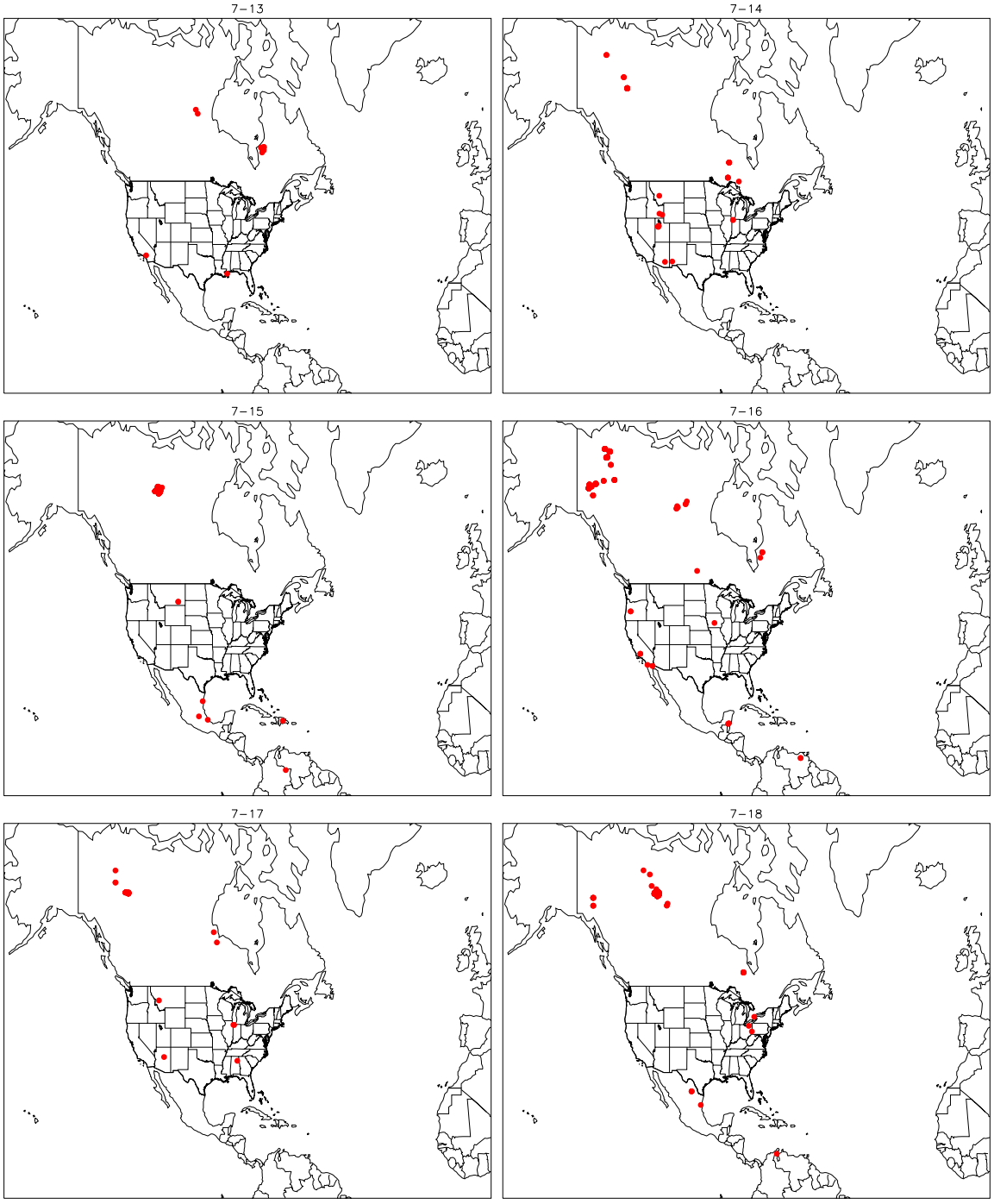

Figure D.19 Hot spots detected on 13-July through 18-July.

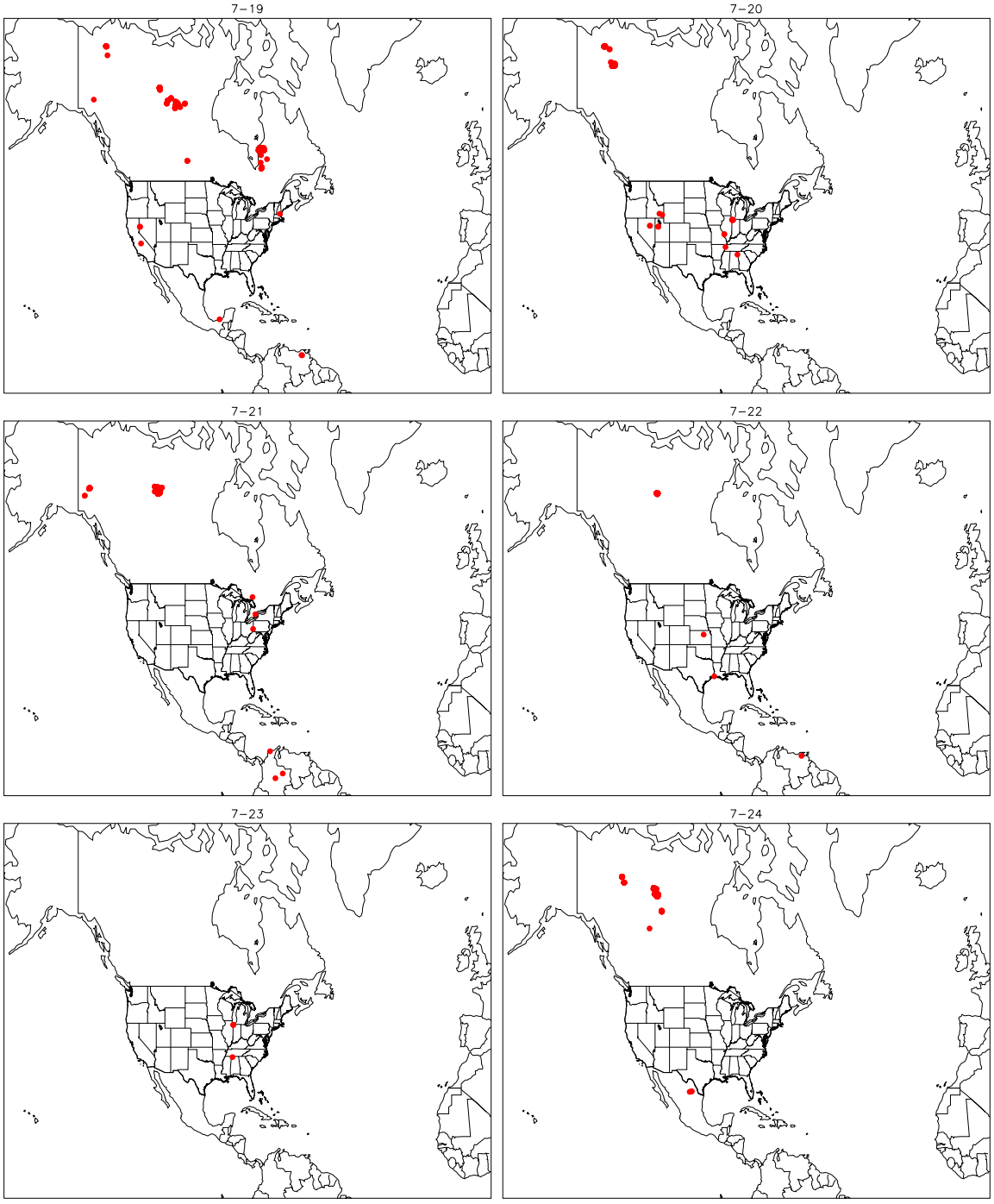

Figure D.20 Hot spots detected on 19-July through 24-July.

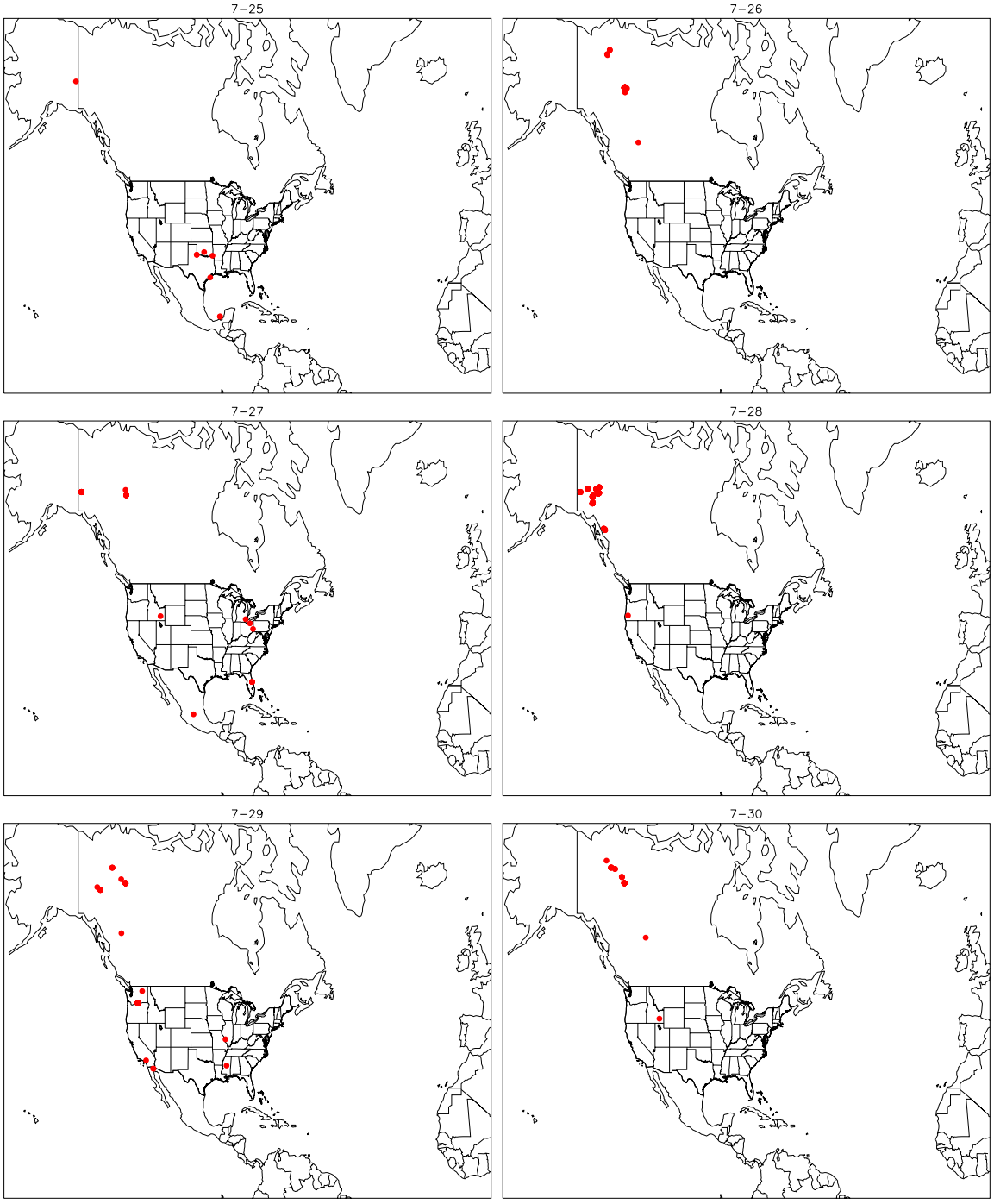

Figure D.21 Hot spots detected on 25-July through 30-July.